1988

Advances in molecular modeling: oriented orbitals, and a technique for improving data quality

Lance Leroy Miller
Iowa State University

INFORMATION TO USERS

The most advanced technology has been used to photograph and reproduce this manuscript from the microfilm master. UMI films the original text directly from the copy submitted. Thus, some dissertation copies are in typewriter face, while others may be from a computer printer.

In the unlikely event that the author did not send UMI a complete manuscript and there are missing pages, these will be noted. Also, if unauthorized copyrighted material had to be removed, a note will indicate the deletion.

Oversize materials (e.g., maps, drawings, charts) are reproduced by sectioning the original, beginning at the upper left-hand corner and continuing from left to right in equal sections with small overlaps. Each oversize page is available as one exposure on a standard 35 mm slide or as a 17″ × 23″ black and white photographic print for an additional charge.

Photographs included in the original manuscript have been reproduced xerographically in this copy. 35 mm slides or 6″ × 9″ black and white photographic prints are available for any photographs or illustrations appearing in this copy for an additional charge. Contact UMI directly to order.

Accessing the World's Information since 1938

300 North Zeeb Road, Ann Arbor, MI 48106-1346 USA

Order Number 8825422

Advances in molecular modeling: Oriented orbitals, and a technique for improving data quality

Miller, Lance Leroy, Ph.D.

Iowa State University, 1988

U·M·I
300 N. Zeeb Rd.
Ann Arbor, MI 48106

PLEASE NOTE:

In all cases this material has been filmed in the best possible way from the available copy. Problems encountered with this document have been identified here with a check mark ✓.

1. Glossy photographs or pages _____
2. Colored illustrations, paper or print _____
3. Photographs with dark background _____
4. Illustrations are poor copy _____
5. Pages with black marks, not original copy ✓
6. Print shows through as there is text on both sides of page _____
7. Indistinct, broken or small print on several pages ✓
8. Print exceeds margin requirements _____
9. Tightly bound copy with print lost in spine _____
10. Computer printout pages with indistinct print _____
11. Page(s) _____ lacking when material received, and not available from school or author.
12. Page(s) _____ seem to be missing in numbering only as text follows.
13. Two pages numbered _____. Text follows.
14. Curling and wrinkled pages _____
15. Dissertation contains pages with print at a slant, filmed as received _____
16. Other _____

_____

_____

Advances in molecular modeling: oriented orbitals, and a technique for improving data quality

by

Lance Leroy Miller

A Dissertation Submitted to the
Graduate Faculty in Partial Fulfillment of the
Requirements for the Degree of
DOCTOR OF PHILOSOPHY

Department: Chemistry
Major: Physical Chemistry

Approved:

Signature was redacted for privacy.

In Charge of Major Work

Signature was redacted for privacy.

For the Major Department

Signature was redacted for privacy.

For the Graduate College

Iowa State University
Ames, Iowa

1988

TABLE OF CONTENTS

CHAPTER I. INTRODUCTION

Foreword

The body of this thesis is not concerned with standard crystallography (i.e., the determination of the molecular conformation and the associated bond lengths and angles). Instead it is concerned with the extraction of information from x-ray data pertaining to the redistribution of electrons which occurs upon molecular formation.

Historical Perspective

The capability of transforming x-ray data into an electron density[1] function has been recognized since the early 1900s. While the potential[2,3,4] existed for extracting a large amount of information from x-ray data, there were a number of difficulties which had to be surmounted before this potential could be realized.

It was initially found that the data resolution and quality was very limited. It was determined[5] that only the grosses features of an observed electron density function could be modeled. The model consisted of spherically averaged ground-state atoms placed at the nuclear sites in the molecule. This type of model has come to be known as the promolecule[6] and is still widely used in standard crystallography. Information gained from the use of a

promolecule consists mainly of atomic positional and vibrational parameters.

With the advent of neutron diffraction in the early 1950s an unexpected shortcoming of the standard crystallographic approach was discovered. It was found that, since the promolecule represented only the free-atom state, the positions were influenced by the bonding and lone pair electron density (both of these are large contributors to what is known as the deformation density) which was not part of the promolecule model. A recent survey[7] comparing neutron results and x-ray results shows discrepancies in the magnitude of the interatomic distances of 0.003 to 0.010Å.

Aside from improving the quality and resolution of the data and developing various corrections for systematic errors[8], two methods were developed which attempt to correct for this shortcoming of standard crystallography. One involved improvement of the model[9] to account for the deformation density (DD) and the other consisted of an improved technique for obtaining the promolecule's parameters[10].

The model improvement consisted of fitting the entire observed electron density using a molecular model. This approach removes the bias due to the deformation density by accounting for it explicitly in the model. The second method, on the other hand, still uses the spherical-atom

promolecule, but refinement is carried out using only the high-order data where the DD does not contribute significantly. This technique eliminates bias due to the deformation density by effectively eliminating its contribution to the data used in the refinement process. The second method is called high-accuracy crystallography and its results differ from those of standard crystallography's only in the accuracy of the promolecules' parameters.

In addition to obtaining more accurate model parameters work has been, and still is being, devoted to obtaining information beyond that of positional and vibrational parameters. The additional information is gained by analysis of the DD or by using parameters from advanced models.

One method[11] of obtaining the DD subtracts the spherical-atom promolecule from the observed electron density function, the result being called the total difference density (TDD). The TDD function may be analyzed mathematically[12,13] by integrating over various functions of $\rho(r)$ or by comparing it with theoretical calculations[14].

Advanced models range from promolecules consisting of prepared-valence state atoms to the use of molecular models. The prepared-atom approach[15] is not usually acceptable since few atoms in molecules exist in the same ideal state to which the prepared atom belongs, thereby introducing experimenter bias. The molecular models are either prepared[16] or have so

many parameters[17] that the results are ambiguous. Many of the intermediate models suffer from a lack of proper chemical interpretation, even though they can model the electron density function well.

Recently it has been asserted[18,19] that the use of a spherical-atom promolecule in calculating the DD is not the most appropriate reference density. It has been shown theoretically that it is of greater utility to use a promolecule consisting of oriented ground-state atoms. Subtracting such a model from the observed electron density yields a chemical difference density[18] (CDD) map which does not exhibit artifacts due to the "selection" of a particular ground state configuration/orientation by an atom. These artifacts have often been misinterpreted in TDD maps as being due to some type of energy change which occurs during molecular formation.

Scope of This Research

This work involves the modeling of experimental data using the oriented-atom promolecule. Although this appeared feasible theoretically[18,19], it was not certain whether the available x-ray data would be of sufficient quality to determine meaningful promolecule parameters. There was also a question of whether the internal vibrations of the atoms would smear the electron density over space to such an extent

that the detailed orbital information obtainable in theory could not be realized in practice.

In order to answer these questions, the mathematical formalism had to be developed which could express oriented atom electron density in terms of atomic scattering functions which would lend themselves to refinement of their orientational attributes. Computer software then had to be developed before the approach could be tested on several molecules. The succeeding chapters describe this work and the results obtained.

The Promolecule

The promolecule developed in this work consists of atomic core electron density functions plus oriented valence orbitals. The core orbitals are described by unmodified, free-atom, SCF wavefunctions. The valence orbitals are based on similar wavefunctions, but they are no longer in their free-atom state. In the original development[18] the valence orbitals were to be in a configuration which was composed of a linear combination of the free-atom's ground-state configurations, a modification of the spherical free-atom which required virtually no energy change. Thus the oriented-orbital carbon atom would consist of some combination of $P_x^2+P_y^2$, $P_x^2+P_z^2$, and $P_y^2+P_z^2$ (the spherical ground-state is one third of their sum).

The requirement of no energy change has been relaxed in this work. The orbital constraints which are realized are that the orbitals remain orthonormal and that the electronic occupancies of the orbitals remain within the range [0,2] (as suggested by the Pauli principle). While there is no mathematical constraints that the atoms do not change their energy levels, results described in the succeeding chapters show that this constraint is nearly realized for most atoms.

A shortcoming of the molecular models was that they had so many parameters that the results became ambiguous. To avoid this the promolecule used here consists of only the most basic parameters necessary. In addition this will provide a firm foundation upon which future studies may be carried out and additional parameters added where necessary.

It was of considerable interest to be able to apply the oriented-atom promolecule concept to datasets which were not ideal. The main objective of such a study would not be to yield accurate positional and vibrational parameters, but rather to ascertain meaningful orbital information. This would permit one to study, and obtain valuable information from, a much larger set of molecules for which extensive datasets have not been collected. For this purpose a number of tests were carried out on the dataset for the 1,2,3-triazine molecule, the results of which are given in Chapter III.

CHAPTER II. EQUATIONS

Introduction

The standard crystallographic practice of using spherical atoms in promolecule models allows for approximations[20] which simplify the mathematics involved in such a way as to yield a few simple equations to describe the scattering of x-rays from atoms in a crystalline solid. However, the use of a superimposition-of-oriented-atoms promolecule model requires that the complete equations be used without these simplifications. Much of the mathematics needed for this approach is developed here and is based on the work of Ruedenberg[21]. Equations given later in this chapter pertain to the analysis and interpretation of the results.

While there are numerous equations which represent various corrections to the promolecule model, they lie outside the scope of this research. The approach taken here, as described in Chapter I, is to limit the number of parameters involved to the most basic thus producing a firm foundation for future work in which the correctness of the various additional parameters may be investigated.

Atomic Electron Density Functions and Their Fourier Transforms

The Fourier transform of the electron density of a crystalline solid is given by

$$F(k)=\int dV\ \rho(r)\ \exp(ik\cdot r) \qquad (II.1)$$

where $r=\Sigma_i\ x_i a_i$, $k=2\pi\ \Sigma_i\ h_i a^*_i$, and the integration is over the crystallographic unit cell. a_i and a^*_i are the real and reciprocal space lattice parameters and have the relationships $a^*_i\cdot a_j=\delta_{ij}$ for i=1,2,3.

By considering the electron density contribution from a finite set of origins, the structure factor (F(k)) can be rewritten as

$$F(k)=\Sigma_a\ f_a(k)\ \exp(ik\cdot r_a) \qquad (II.2)$$

where r_a is the location of the a^{th} origin. The scattering factor ($f_a(k)$) is thus given by

$$f_a(k)=\int dV\ \rho_a(r)\ \exp(ik\cdot r). \qquad (II.3)$$

This research involves the superimposition of the electron density contributions of individual atoms on the real molecule's atomic sites as a representation of that molecule. $\rho_a(r)$ is therefore taken to be the atomic electron density and $f_a(k)$ is the atomic scattering factor.

The electron density for an individual atom can be written as

$$\rho_a(r)=\Sigma_{\mu,\nu}\ P_{a\mu\nu}\ \chi_\mu(r)\ \chi_\nu(r) \qquad (II.4)$$

where $P_{a\mu\nu}$ is the electron density matrix, μ represent $n_\mu l_\mu m_\mu$, and $\chi_\mu(r)=R_{nl}(r)\ Y_{lm}(\Omega)$.

Substituting Equation (II.4) into Equation (II.3) yields

$$f_a(k)=\Sigma_{\mu,\nu}\ P_{a\mu\nu}\int dV\ \chi_\mu(r)\ \chi_\nu(r)\ \exp(ik\cdot r) \qquad (II.5)$$

which, by separation into even and odd functions, can be rewritten as

$$f_a(k)=f_a^g(k)+if_a^u(k) \qquad \text{(II.6)}$$

where

$$f_a^g(k)=\Sigma_{\mu,\nu}\ P_{a\mu\nu}^g\ f_{a\mu\nu}^g(k) \qquad \text{(II.7a)}$$

and

$$f_a^u(k)=\Sigma_{\mu,\nu}\ P_{a\mu\nu}^u\ f_{a\mu\nu}^u(k). \qquad \text{(II.7b)}$$

The even (^{g}) functions have $l_\mu+l_\nu=2n$ and the odd (^{u}) functions have $l_\mu+l_\nu=2n+1$. This originates from the parity of the atomic wavefunctions $\chi(r)$.

The orbital scattering factors ($f_{a\mu\nu}(k)$) are defined as

$$f_{a\mu\nu}(k)=\int dV\ \chi_\mu(k)\ \chi_\nu(k)\ \exp(ik\cdot r) \qquad \text{(II.8)}$$

which has both even and odd representations.

Utilizing the plane wave expansion[22], $\exp(ik\cdot r)=4\pi\ \Sigma_L\ i^L\ j_L(k\ r)\ [\Sigma_{M=-L}^{L}\ Y_{LM}(\Omega_k)\ Y_{LM}(\Omega)]$ where $j_L(k\ r)$ are the spherical Bessel functions[23], Equation (II.8) can be written as

$$f_{a\mu\nu}(k)=\Sigma_L\ (-1)^{L/2}\ \langle j_L(k)\rangle_{\mu\nu}\ Z_L(\mu,\nu) \qquad \text{(II.9)}$$

which also has both even and odd representations and where

$$\langle j_L(k)\rangle_{\mu\nu}=4\pi\int dr\ r^2\ j_L(k\ r)\ R_\mu(r)\ R_\nu(r) \qquad \text{(II.10)}$$

and

$$Z_L(\mu,\nu)=\Sigma_{M=-L}^{L}\langle Y_\mu(\Omega)|Y_{LM}(\Omega)|Y_\nu(\Omega)\rangle\ Y_{LM}(\Omega_k). \qquad \text{(II.11)}$$

Evaluation of Equation (II.9) involves the evaluation of two integrals, one over r and the other over Ω. The

integration in Equation (II.10) is unavoidable and is described in Appendix B. Evaluation of Equation (II.11) is facilitated by detailed analysis of the analytic functions involved.

The values[24] of $Y_\mu(\Omega)$ consist of a function of ϕ ($\Phi_m(\phi)$) and a function of θ ($\Theta_{lm}(\theta)$). The ϕ-integral in Equation (II.11) is zero unless $M=|m_\mu \pm m_\nu|$ (see Table II.1 for a listing of the results of the ϕ integration). Thus it can be separated into two parts corresponding to two possible values of M

$$V_L(\mu,\nu)=\sqrt{(1/2\pi)}\int d\theta\ P_\mu\ P_\nu\ P_L(|m\mu|+|m\nu|) \qquad \text{(II.12a)}$$

and

$$W_L(\mu,\nu)=\sqrt{(1/2\pi)}\int d\theta\ P_\mu\ P_\nu\ P_{L||m\mu|-|m\nu||} \qquad \text{(II.12b)}$$

where the P_μ are the normalized associated Legendre functions defined as $P_\mu(x)=\sqrt{\{[(2l+1)*(l-m)!]/[2(l+m)!]\}}\ (1-x^2)^{m/2}*(d/dx)^{l+m}\ [(x^2-1)^l/(2^l\ l!)]$.

The integral in Equation (II.11) is of the same form as the Clebsch-Gordon coefficients[25]. Due to some differences in form, Equations (II.12) have been reevaluated and are listed in Table II.3.

We are now in a position to rewrite Equation (II.9) as

$$f_{a\mu\nu}(k)=\Sigma_L\ \langle j_L(k)\rangle_{\mu\nu}\ Z_L(\mu,\nu) \qquad \text{(II.13)}$$

which has both even and odd representations and where M is in the range [0,L] and the following redefinitions have been

Table II.1. $Z_L(\mu,\nu)$ after integration over ϕ

m_1[a]	m_2	$Z_L(\mu,\nu)$		
0	0		$V_L(l_1m,l_20)$	Y_{L0}
m	0		$V_L(l_1m,l_20)$	Y_{Lm1}
0	m		$V_L(l_10,l_2m)$	Y_{Lm2}
-m	0		$V_L(l_1m,l_20)$	$Y_{L(-m)}$
0	-m		$V_L(l_10,l_2m)$	$Y_{L(-m)}$
m	m	$1/\sqrt{2}$	$V_L(l_1m,l_2m)$	$Y_{L(2m)}$
			$+W_L(l_1m,l_2m)$	Y_{L0}
-m	m	$-1/\sqrt{2}$	$V_L(l_1m,l_2m)$	$Y_{L(-2m)}$
m	-m	$1/\sqrt{2}$	$V_L(l_1m,l_2m)$	$Y_{L(-2m)}$
-m	-m		$V_L(l_1m,l_2m)$	$Y_{L(2m)}$
			$+W_L(l_1m,l_2m)$	Y_{L0}
m_1	m_2	$1/\sqrt{2}$	$V_L(l_1m_1,l_2m_2)$	$Y_{L(m1+m2)}$
		$+1/\sqrt{2}$	$W_L(l_1m_1,l_2m_2)$	$Y_{L\lvert m1-m2\rvert}$
$-m_1$	m_2	$1/\sqrt{2}$	$V_L(l_1m_1,l_2m_2)$	$Y_{L(-m1-m2)}$
		$+1/\sqrt{2}$	$W_L(l_1m_1,l_2m_2)$	$Y_{L(-\lvert m1-m2\rvert)}$ $\mathrm{sign}(m_1-m_2)$
m_1	$-m_2$	$1/\sqrt{2}$	$V_L(l_1m_1,l_2m_2)$	$Y_{L(-m1-m2)}$
		$-1/\sqrt{2}$	$W_L(l_1m_1,l_2m_2)$	$Y_{L(-\lvert m1-m2\rvert)}$ $\mathrm{sign}(m_1-m_2)$
$-m_1$	$-m_2$	$-1/\sqrt{2}$	$V_L(l_1m_1,l_2m_2)$	$Y_{L(m1+m2)}$
		$+1/\sqrt{2}$	$W_L(l_1m_1,l_2m_2)$	$Y_{L\lvert m1-m2\rvert}$

[a] m_i is a positive number, $-m_i$ is a negative number.

Table II.2. Listing of the $Y_{LM}(\Omega_k)$ functions

L M	$Y_{LM}(\Omega_k)$	L M	$Y_{LM}(\Omega_k)$
0 0	1	2-2	$\sqrt{(15/2)}\ h\,k/\lvert h\rvert^2$
		2-1	$\sqrt{30}\ k\,l/\lvert h\rvert^2$
1-1	$\sqrt{2}\ k/\lvert h\rvert$	2 0	$\sqrt{(5/2)}\ (3l^2-\lvert h\rvert^2)/\lvert h\rvert^2$
1 0	$l/\lvert h\rvert$	2 1	$\sqrt{30}\ h\,l/\lvert h\rvert^2$
1 1	$\sqrt{2}\ h/\lvert h\rvert$	2 2	$\sqrt{(15/2)}\ (h^2-k^2)/\lvert h\rvert^2$

Table II.3. Values of $V_L(\mu,\nu)$ and $W_L(\mu,\nu)$

$\langle l_1 m_1 \mid LM \mid l_2 m_2 \rangle$		$\langle l_1 m_1 \mid LM \mid l_2 m_2 \rangle$		$\langle l_1 m_1 \mid LM \mid l_2 m_2 \rangle$	
$\langle 00 \mid 00 \mid 00 \rangle$	1				
$\langle 00 \mid 11 \mid 11 \rangle$	1				
$\langle 00 \mid 10 \mid 10 \rangle$	1				
$\langle 11 \mid 00 \mid 11 \rangle$	1	$\langle 11 \mid 20 \mid 11 \rangle$	$-\sqrt{(1/5)}$		
$\langle 11 \mid 21 \mid 10 \rangle$	$\sqrt{(3/5)}$				
$\langle 11 \mid 22 \mid 11 \rangle$	$\sqrt{(6/5)}$				
$\langle 10 \mid 00 \mid 10 \rangle$	1	$\langle 10 \mid 20 \mid 10 \rangle$	$\sqrt{(4/5)}$		
$\langle 00 \mid 22 \mid 22 \rangle$	1				
$\langle 00 \mid 21 \mid 21 \rangle$	1				
$\langle 00 \mid 20 \mid 20 \rangle$	1				
$\langle 11 \mid 11 \mid 22 \rangle$	$\sqrt{(6/5)}$	$\langle 11 \mid 31 \mid 22 \rangle$	$-\sqrt{(9/245)}$		
$\langle 11 \mid 10 \mid 21 \rangle$	$\sqrt{(3/5)}$	$\langle 11 \mid 30 \mid 21 \rangle$	$-\sqrt{(27/245)}$		
$\langle 11 \mid 11 \mid 20 \rangle$	$-\sqrt{(1/5)}$	$\langle 11 \mid 31 \mid 20 \rangle$	$\sqrt{(54/245)}$		
$\langle 11 \mid 32 \mid 21 \rangle$	$\sqrt{(6/7)}$				
$\langle 11 \mid 33 \mid 22 \rangle$	$\sqrt{(9/7)}$				
$\langle 10 \mid 32 \mid 22 \rangle$	$\sqrt{(3/7)}$				
$\langle 10 \mid 11 \mid 21 \rangle$	$\sqrt{(3/5)}$	$\langle 10 \mid 31 \mid 21 \rangle$	$\sqrt{(24/35)}$		
$\langle 10 \mid 10 \mid 20 \rangle$	$\sqrt{(4/5)}$	$\langle 11 \mid 30 \mid 20 \rangle$	$\sqrt{(9/245)}$		
$\langle 22 \mid 00 \mid 22 \rangle$	1	$\langle 22 \mid 20 \mid 22 \rangle$	$-\sqrt{(20/49)}$	$\langle 22 \mid 40 \mid 22 \rangle$	1/7
$\langle 22 \mid 21 \mid 21 \rangle$	$\sqrt{(30/49)}$	$\langle 22 \mid 41 \mid 21 \rangle$	$-\sqrt{(5/49)}$		
$\langle 22 \mid 22 \mid 20 \rangle$	$-\sqrt{(20/7)}$	$\langle 22 \mid 42 \mid 20 \rangle$	$\sqrt{(15/49)}$		
$\langle 22 \mid 43 \mid 21 \rangle$	$\sqrt{(35/49)}$				
$\langle 22 \mid 44 \mid 22 \rangle$	$\sqrt{(10/7)}$				
$\langle 21 \mid 00 \mid 21 \rangle$	1	$\langle 21 \mid 20 \mid 21 \rangle$	$\sqrt{(5/49)}$	$\langle 21 \mid 21 \mid 40 \rangle$	-4/7
$\langle 21 \mid 21 \mid 20 \rangle$	$\sqrt{(5/49)}$	$\langle 21 \mid 20 \mid 41 \rangle$	$\sqrt{(30/49)}$		
$\langle 21 \mid 22 \mid 21 \rangle$	$\sqrt{(30/49)}$	$\langle 21 \mid 42 \mid 21 \rangle$	$\sqrt{(40/49)}$		
$\langle 20 \mid 00 \mid 20 \rangle$	1	$\langle 20 \mid 20 \mid 20 \rangle$	$\sqrt{(20/49)}$	$\langle 20 \mid 40 \mid 20 \rangle$	6/7

made; $\langle j_L(k)\rangle_{\mu\nu}$ has been divided by 4π, $\langle\mu|Y_{LM}|\nu\rangle$ has been multiplied by $\sqrt{[(2L+1)/4\pi]}$, and $Y_{LM}(\Omega_k)$ has been multiplied by either $(-1)^{L/2}*\sqrt{[4\pi/(2l+1)]}$ for L=2n or $(-1)^{(L-1)/2}*\sqrt{[4\pi/(2L+1)]}$ for L=2n+1. Table II.2 lists the functions $Y_{LM}(\Omega_k)$.

Interpretation of the electron density matrix (P_a) in terms of the classical chemistry concept embodied in the Pauli principle reveals that certain constraints should be placed on the coefficients. The Pauli principle states that no more than two electrons can have the same nlm quantum numbers.

As a first approximation this can be realized by constraining the $P_{a\mu\mu}$ values to the interval [0,2], although this does not strictly comply to the Pauli principle since it is the eigenvalues of P_a which need be constrained. Attempts to constrain $P_{a\mu\mu}$ alone failed to yield proper eigenvalues and thus a straightforward method of applying constraints to the entire P_a matrix was sought.

It was found that a simple way to achieve this was to diagonalize the density matrix, viz

$$N_a = U_a^+ P_a U_a \qquad \text{(II.14)}$$

where U_a is a unitary matrix which diagonalizes P_a and N_a is the eigenvalues or occupation numbers. Substituting the spectral representation of P_a into Equations (II.4) yields

$$\rho_a(r) = \Sigma_{\mu,\nu}\, U_{a\nu n}\, N_{an}\, U_{a\mu n}\, \chi_\mu(r)\, \chi_\nu(r) \qquad \text{(II.15)}$$

or, by rearranging,

$$\rho_a(r)=\Sigma_n \Sigma_{\mu,\nu} N_{an} U_{a\mu n} \chi_\mu(r) \chi_\nu(r) U_{a\nu n} \quad \text{(II.16a)}$$

$$=\Sigma_n N_{an} \Psi^2_{an}(r) \quad \text{(II.16b)}$$

where $\Psi_{an}(r)=\Sigma_\nu \chi_\nu(r) U_{a\nu n}$.

Further substitution of the spectral representation into Equations (II.7) yields an expression for the corresponding scattering factors

$$f_a(k)=\Sigma_n N_{an} f_{ann}(k) \quad \text{(II.17)}$$

where

$$f_{amn}(k)=\Sigma_{\mu,\nu} U_{a\mu m} f_{a\mu\nu}(k) U_{a\nu n} \quad \text{(II.18)}$$

which can also be split into even and odd functions ($f^g_{amn}(k)$ and $f^u_{amn}(k)$).

Additional parameters must now be added to the "ideal" atomic scattering factors described by Equation (II.3) (or equivalently by Equations (II.17) and (II.18)) to model the real molecule.

The first parameter is that of the temperature factor[26,27] ($T_a(k)$) which models the various motions of the atoms in the crystal. The functional form is

$$T_a(k)=\exp(-B \sin^2(\theta)/\lambda^2) \quad \text{(II.19a)}$$

for isotropic vibrations, and

$$T_a(k)=\exp(-\Sigma_{i,j} \beta_{ij} h_i h_j) \quad \text{(II.19b)}$$

for anisotropic vibrations. Both of these functions sharpen the atomic scattering factors and thus broaden the electron density distribution.

The rms amplitudes of vibration of the atoms are obtainable from the thermal parameters (B and β_{ij}). The

isotropic thermal parameter is related to the isotropic rms amplitude of vibration (u) by

$$u=\sqrt{[B/(8\pi^2)]} \qquad \text{(II.20a)}$$

and, for the anisotropic u_{ij},

$$u_{ij}=\sqrt{[\beta_{ij}/(2\pi^2\ a_i^*\cdot a_j^*)]}. \qquad \text{(II.20b)}$$

Another parameter which is often necessary is the atom site multiplicity factor (m_a). This value accounts for the multiplicity due to the site symmetry of an atomic site. A multiplicity factor is also used if an atom does not reside 100% of the time at a given site in the cell; in this case m_a represents the fraction of the time in which the atom is at the site.

The calculated structure factors (F(k)) must be placed on the same scale as the observed structure factors (E(k)) and a scale factor is therefore included.

Applying these additional parameters to Equation (II.2) yields

$$F(k)=\Sigma_a\ F_a(k) \qquad \text{(II.21)}$$

where the atomic structure factor ($F_a(k)$) is

$$F_a(k)=s\ m_a\ T_a(k)\ f_a(k)\ \exp(ik\cdot r_a) \qquad \text{(II.22)}$$

and represents the individual atom's contribution to the total scattering at k.

$F_a(k)$ may be split up into its real and imaginary parts, viz

$$F_a'(k)=s\ m_a\ T_a(k)\ [f_a^g(k)\ \cos(k\cdot r_a)- f_a^u(k)\ \sin(k\cdot r_a)] \qquad \text{(II.23a)}$$

and

$$F''_a(k)=s\ m_a\ T_a(k)\ [f^g_a(k)\ \sin(k\cdot r_a)+ f^u_a(k)\ \cos(k\cdot r_a)] \qquad \text{(II.23b)}$$

so that

$$F_a(k)=F'_a(k)+iF''_a(k). \qquad \text{(II.24)}$$

Up to now we have not considered the effect of the x-ray's frequency on the atomic scattering factors. When the x-ray frequency is on the same order of magnitude as that of the electron-nuclear dipole oscillation frequency, the x-rays are strongly absorbed. This occurs most strongly for core electrons since the coupling is strongest there. This also implies that 1) the magnitude is dependent on the radiation used, 2) there is little $\sin(\theta)/\lambda$ dependence, and 3) there is no contribution from the valence electrons which means there is no directional dependence.

The correction terms for this effect (called anomalous dispersion[28]) are added to the core scattering factors and have real and imaginary components ($f_{corr}(k)=f(k)+\Delta f'(k)+i*\Delta f''(k)$). The values of $\Delta f'$ and $\Delta f''$ are vanishingly small for atoms with atomic numbers less than 10.

Equation (II.24) can be written to explicitly include the components of the phase factor (α_k), i.e.,

$$F(k)=|F(k)|\ \cos(\alpha_k)+i|F(k)|\ \sin(\alpha_k) \qquad \text{(II.25)}$$

and illustrates the fact that the imaginary component cancels for light atom centrosymmetric structures (heavy atom data suffers from anomalous dispersion). Also we see that

$$\cos(\alpha_k)=F'(k)/|F(k)| \qquad \text{(II.26a)}$$

and

$$\sin(\alpha_k)=F''(k)/|F(k)|. \qquad \text{(II.26b)}$$

Orthogonalization

Use of the angular part of the spherical harmonics (listed in Table II.2) dictates the use of an orthogonal orbital scattering factor·reference system. As the equations are to be used in reciprocal space, an orthogonalization matrix (O^*) is needed which orthogonalizes reciprocal space. Since we often use an orthogonalization matrix (O) in real space, it would be beneficial to have them related in a simple manner.

The standard form[19] of O is

$$O=\begin{vmatrix} 1 & \cos(\gamma) & \cos(\beta) \\ 0 & \sin(\gamma) & -\sin(\beta)*\cos(\alpha^*) \\ 0 & 0 & \sin(\beta)*\sin(\alpha^*) \end{vmatrix} \qquad \text{(II.27a)}$$

which takes a_i to a_i' as shown in Figure II.1.

Using the relation between real and reciprocal space vectors ($a_i^*=(a_j\cdot a_k)/(a_i\cdot a_j\times a_k)$), it is clear that, in an orthogonal system, a_i^* and a_i are parallel and that $a_i^*=1/a_i$. Keeping this concept in an orthogonalized system one obtains

$$O^*=\begin{vmatrix} \sin(\beta^*)*\sin(\gamma) & 0 & 0 \\ -\sin(\beta^*)*\cos(\gamma) & \sin(\alpha^*) & 0 \\ \cos(\beta^*) & \cos(\alpha^*) & 1 \end{vmatrix} \qquad \text{(II.27b)}$$

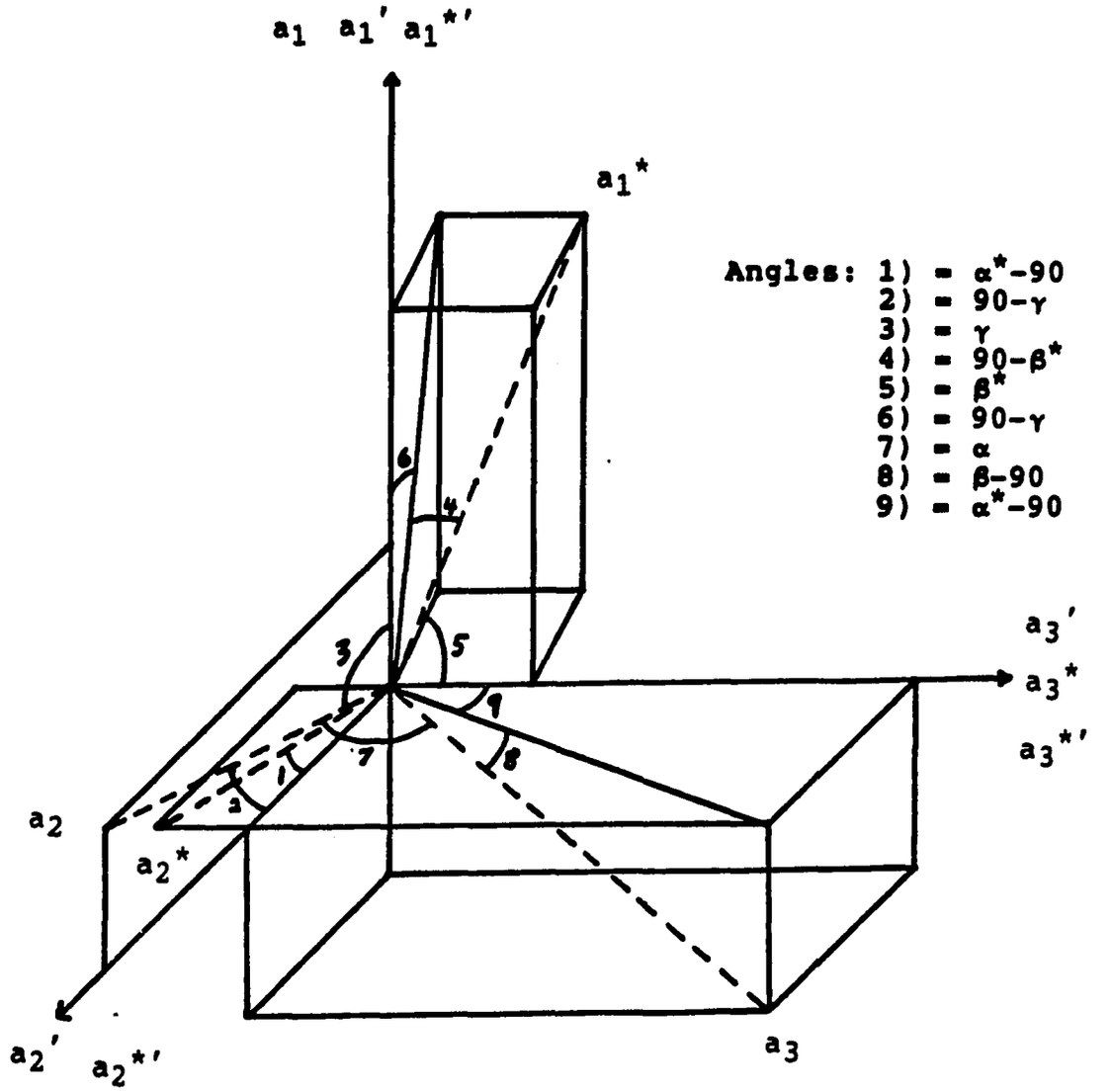

Figure II.1. Diagram of rotation angles for orthogonalization of real and reciprocal space lattices. α, β, and γ are real space lattice angles. α^*, β^*, and γ^* are the reciprocal space lattice angles

which will take the non-orthogonal a_i^* basis vectors and form the $a_i^{*\prime}$ which, as seen in Figure II.1, are parallel to the a_i' basis vectors.

As a check on the correctness of O and O^* one may make use of the relationships $O^\tau \cdot O = G$ and $O^* \cdot (O^*)^\tau = G^*$ where O^τ is the transpose of O, and G and G^* are the so-called metric tensors (inner product matrices) in real and reciprocal space respectively.

Model Refinement

Adjustment of the model's parameters for optimization of the agreement between the observed and calculated structure factors is performed in a weighted, least-mean-squares fashion.

There are two methods which are fundamentally different. The first (Method I) presumes that the phases are not known and thus does not rely on them. The second (Method II) assumes that the phases are known or will not change after adjustment of the model's parameters. The derivations for both methods are given Appendix A. The normal equation for Method I (Equation (A.5d)) is given again here for convenience

$$\Sigma_k \omega_k \Sigma_r \partial|F(k)|/\partial v \; \partial|F(k)|/\partial r \; \Delta r = \Sigma_k \omega_k [|E(k)| - |F(k)|] \partial|F(k)|/\partial v. \qquad \text{(II.28)}$$

Table II.4. Derivatives of the structure factors

Parameter	$\partial F'/\partial P$
s	$F'_a(k)/s$
m_a	$F'_a(k)/m_a$
x_{ai}	$-2\pi\ h_i\ F''_a(k)$
B_a	$-\sin^2(\theta)/\lambda^2\ F'_a(k)$
β_{aij} $(i\leq j)$	$(\delta_{ij}-2)\ h_i\ h_j\ F'_a(k)$
N_{an}	$s\ m_a\ T_a(k)\ [f^g_{an}(k)\ \cos(k\cdot r_a)-f^u_{an}(k)\ \sin(k\cdot r_a)]$
t_{amn} $(m<n)$	$2(N_{an}-N_{am})\ s\ m_a\ T_a(k)\ f_{amn}\ \cos(k\cdot r_a)$
$U_{\mu m}$	$s\ m_a\ T_a(k)\ 2\ N_{am}\ \{[f^g_{a\mu\mu}(k)\ U_{a\mu m}+(\Sigma_\nu\ f^g_{a\mu\nu}(k)\ U_{a\nu m})+(\Sigma_\nu\ f^g_{a\nu\mu}(k)\ U_{a\nu m})]\ \cos(k\cdot r_a)-[f^g_{a\mu\mu}(k)\ U_{a\mu m}+(\Sigma_\nu\ f^g_{a\mu\nu}(k)\ U_{a\nu m})+(\Sigma_\nu\ f^g_{a\nu\mu}(k)\ U_{a\nu m})]\ \sin(k\cdot r_a)\}$

Parameter	$\partial F''/\partial P$
s	$F''_a(k)/s$
m_a	$F''_a(k)/m_a$
x_{ai}	$2\pi\ h_i\ F'_a(k)$
B_a	$-\sin^2(\theta)/\lambda^2\ F''_a(k)$
β_{aij} $(i\leq j)$	$(\delta_{ij}-2)\ h_i\ h_j\ F''_a(k)$
N_{an}	$s\ m_a\ T_a(k)\ [f^g_{an}(k)\ \sin(k\cdot r_a)+f^u_{an}(k)\ \cos(k\cdot r_a)]$
t_{amn} $(m<n)$	$2(N_{an}-N_{am})\ s\ m_a\ T_a(k)\ f_{amn}\ \cos(k\cdot r_a)$
$U_{\mu m}$	$s\ m_a\ T_a(k)\ 2\ N_{am}\ \{[f^g_{a\mu\mu}(k)\ U_{a\mu m}+(\Sigma_\nu\ f^g_{a\mu\nu}(k)\ U_{a\nu m})+(\Sigma_\nu\ f^g_{a\nu\mu}(k)\ U_{a\nu m})]\ \sin(k\cdot r_a)-[f^g_{a\mu\mu}(k)\ U_{a\mu m}+(\Sigma_\nu\ f^g_{a\mu\nu}(k)\ U_{a\nu m})+(\Sigma_\nu\ f^g_{a\nu\mu}(k)\ U_{a\nu m})]\ \cos(k\cdot r_a)\}$

The derivatives for each parameter, except t_{amn}, are obtained in a straightforward manner from the Equations (II.17) through (II.24) and are listed in Table II.4. The t_{amn} parameters are discussed in the constraints section below.

The derivatives in Equation (II.28) are of |F(k)| and therefore the relationship

$$\partial|F(k)|/\partial P=\partial F'(k)/\partial P \cos(\alpha_k)+\partial F''(k)/\partial P \sin(\alpha_k) \quad \text{(II.29)}$$

is needed (as given in Equation A.6).

Constraints

There are numerous restrictions which must be applied to the parameters in the form of constraints. The restrictions in general keep the parameters from having non-physical values. Below, each of the parameters is discussed with respect to its appropriate range of values and the means used to keep the parameters in this range.

The scale factor (s) must be a positive number. To avoid a zero value for s it is standard procedure to define it as E(k)=s F(k). Defining s the the other way around often causes s to adjust to zero due to correlations between the multipliers, the temperature factors and the scale factor.

The atom site symmetry multiplier/occupancy factor (m_a)

lies in the range (0,1]. In the former case it is related to the site symmetry multiplicity divided by the number of space group symmetry operations and in the latter case it is defined as the fraction of the time an atom exists at a particular site. If m_a leaves the range indicated, manual action is required to reset it.

At times the occupancies of two or more different atoms are interrelated. In these cases the derivatives are also interrelated and thus, to apply the constraints, one must consider their interdependence via Equations (II.21) through (II.23). Suppose we have a case where two atoms share the same site in a random fashion so that $m_a+m_b=1$. The structure factor equation may be written as

$$F(k)=F_a(k)+F_b(k)+\Sigma_c\ F_c(k) \qquad \text{(II.30a)}$$

($c\neq a,b$) and the derivatives w.r.t. m_a and m_b are

$$\partial F(k)/\partial m_a=F(k)/m_a \qquad \text{(II.30b)}$$

and

$$\partial F(k)/\partial m_b=F(k)/m_b. \qquad \text{(II.30c)}$$

Since $m_b=1-m_a$ we may rewrite Equation (II.30a) as

$$F(k)=F_a(k)+(1-m_a)/m_b\ F_b(k)+\Sigma_c\ F_c(k) \qquad \text{(II.30d)}$$

and thus the derivatives become

$$\partial F(k)/\partial m_a=F(k)/m_a-F(k)/m_b \qquad \text{(II.30e)}$$

and

$$\partial F(k)/\partial m_b=0 \qquad \text{(II.30f)}$$

which is the same as subtracting Equation (II.30c) from that of (II.30b). The need for generality in programming dictates

that the derivatives in each variable are calculated as if unconstrained. One may constrain the derivatives by writing a special subroutine which forms Equations (II.30e) and (II.30f) from Equations (II.30b) and (II.30c). Another subroutine is written which applies the constraint $m_b=1-m_a$ to calculate m_b after the new m_a has been found.

The atomic coordinates are not constrained in general. Due to special crystallographic symmetry at an atom site, the value of one or more of the coordinates may have to be fixed at a particular value. Some cases exist where the values of the coordinates on either an individual atom or on different atoms are interrelated. If constraints such as these are needed, one must follow a procedure similar to that described for m_a.

The thermal parameters model the atomic vibrations and are related to the rms amplitude of vibration (u) of the atom. The isotropic temperature factors have the relation given in Equation (II.20a) and thus B must be non-negative to be physically meaningful. The anisotropic temperature factors have the relations given in Equation (II.20b) and thus the β tensor must be positive definite to describe physically meaningful vibrations.

Positive definiteness means that $x^T \beta x$ is positive for any real vector x. A practical test for positive definiteness is that the matrix and all its diagonal cofactor matrices must have non-negative determinants and the diagonal

elements themselves must be greater than zero. If a non-positive definite matrix would result from an adjustment, the shifts have to be either artificially damped or ignored.

A couple of useful definitions which relate B and β are

$$\beta = B/4 \quad G \tag{II.31a}$$

and

$$B_{ave} = 1/(6\pi^2)\ \mathrm{Tr}\{\beta\ G\}. \tag{II.31b}$$

There are cases in which the temperature factors are constrained either to zero or to one another[29] because of the symmetry of the site. Interrelations are solved in a manner similar to that described for m_a above.

The orbital occupation numbers (N_{ai}) are constrained to lie in the interval [0,2] by the Pauli principle. If a value attempts to shift out of this range, the shift must either be damped or ignored.

There are other constraints which are generally applied to the N_i, namely that the total number of electrons on an atom remains fixed at the free-atom value. To realize this restriction, Lagrange multipliers[30] must be used. The constraint which we wish to apply for all atoms is that $\Sigma_i\ \Delta N_{ai} = 0$, where ΔN_{ai} is the shift in N_{ai}. The quantity to be minimized (∇) (see Equation (A.1)) is thus modified as

$$\nabla = \nabla + \lambda_a\ \Sigma_i\ \Delta N_{ai} \tag{II.32a}$$

where λ_a is atom a's Lagrange multiplier. Henceforth the factor of 2 in Equation (A.1) is implicitly included in λ_a.

Using Equation (A.5e) for determination of the ΔN_i values

of a given atom and adding the constraint yields

$$\Sigma_m A_{nm} \Delta N_m = B_n + \lambda \qquad \text{(II.32b)}$$

whose solution for ΔN_m is

$$\Delta N_m = \Sigma_n (A^{-1})_{mn} B_n + \lambda \Sigma_n (A^{-1})_{mn}. \qquad \text{(II.32c)}$$

Summing Equations (II.32c) over m yields

$$0 = \Sigma_m \Sigma_n (A^{-1})_{mn} B_n + \Sigma_m \Sigma_n (A^{-1}) \qquad \text{(II.32d)}$$

from which the value of λ for the atom may be obtained. One might also formulate Equations (II.32) for calculating λ for all atoms simultaneously.

A different electronic constraint which can be applied is to keep the total number of electrons in the unit cell fixed at a particular value such as the free atom total. To do this m and n would now represent all atoms and all orbitals in Equations (II.32).

The spectral representation matrices (U_a) are orthogonal. Adjustment of the coefficients requires the introduction of the parameters t_{amn}. It is not necessary to define t_{amn} since it is the Δt_{amn}'s which are of interest.

The shifts in U for a given atom are ΔU so that

$$U = U^o + \Delta U. \qquad \text{(II.33a)}$$

Making the following definition

$$U = U^o (I + \Delta t) \qquad \text{(II.33b)}$$

we see that, to maintain the orthogonality of U, Δt must be an antisymmetric matrix and that it vanishes in the second order (since $U^t U \equiv I$).

Substituting Equation (II.33b) into Equation (II.17)

yields

$$f_a(k)=Tr\{U_a^o\ (I+\Delta t_a)\ N_a\ (I-\Delta t_a)\ U_a^{ot}\ f_a(k)\} \qquad (II.34a)$$

where $f_a(k)$ are composed from the new values of $f_{ann}(k)$.

This can be simplified and rewritten as

$$f_a(k)=f_a^o(k)+\Sigma_{m<n}\ \Delta t_{amn}\ 2(N_{an}-N_{am})\ f_{amn}^o(k) \qquad (II.34b)$$

where the factor of two originates in the number of independent parameters of U_a ($= n(n-1)/2$).

Now we want to consider the derivative of F(k) w.r.t. t_{amn} (n.b. not Δt_{amn}). One can visualize Equation (II.34b) as a first order Taylor series expansion in the variable t_{amn}, thus the derivative of Equation (II.22) w.r.t. t_{amn} is

$$\partial F_a(k)/\partial t_{amn}=s\ m_a\ T_a\ 2(N_{an}-N_{am})\ f_a(k)\ \exp(ik\cdot r). \qquad (II.35)$$

In general the antisymmetric Δt_a matrix is not strictly orthogonal. To force this one must use the approximation

$$(I+\Delta t_a)\simeq(I-\Delta t_a/2)^{-1}\ (I+\Delta t_a/2) \qquad (II.36)$$

which, again to first order, is orthogonal.

There are also crystallographic and chemical symmetry constraints on the orbitals to account for. This can be accomplished by relating the derivatives (as described for m_a) and the parameters. This is facilitated by use of rotation parameters (non-variable) which will orient the orbital reference system in any desired direction.

Using the standard electron density matrix (P) for a given atom, the relations due to symmetry are obtained from the character tables. For an orbital product ($\chi_i\chi_j$) to be non-zero the product must lie in the totally symmetric

representation (A_1) of the site symmetry.

When using the orbital occupancy numbers (N) and the spectral representation (U), as is used here, the relations are not as straightforward to obtain. The desired net result is that the total valence density has the symmetry of the site. Due to the way the equations are written and the definitions used, it is not possible to constrain the t_{ij} parameter shifts. Instead the derivatives of the U matrix are constrained as are the N parameters. To do this models are defined which consist of the different U and N combinations which cause the valence electron density matrix to follow the site symmetry. The parameters of the model are then defined and refined either by using the standard least squares procedure coupled with a specially written procedure or by using a specially prepared procedure to form the normal equations matrices, solve for the shifts, and apply the appropriate constraints. A few examples are described in Appendix D.

Electron Density Functions

The X-type (scale, atomic positional and thermal) parameters of the model are often the desired results from a crystallographic analysis. There is however other potentially useful information which may be obtained from either a qualitative or a quantitative interpretation of the electron density functions.

The experimental electron density function is calculated from a Fourier synthesis of the E(k) values

$$\rho_{exp}(r)=(1/V_{cell})\ \Sigma_k\ E(k)\ \exp(-ik\cdot r) \qquad (II.37)$$

and $\rho_{cal}(r)$ can be obtained from a similar expression involving F(k).

The resultant function is not very informative since the deformation density is approximately two orders of magnitude less than the core electron region which would therefore dominate this type of map as seen in Figure II.2.

There are literature examples[31] in which the region around the atomic core is set to zero in order to examine the relatively small deformation density. This procedure is ill-advised since the dataset is of finite resolution and the Fourier transform of a limited dataset produces ripples in the electron density. This, coupled with the fact that the core electrons are the main contributors at high angles (as seen in Figure B.1) and thus subject to the most severe truncation effects, produces results whereby the interpretation is of little value. An example of this is shown in Figures II.3. Figure II.3a contains only the calculated 1s orbitals and none of the fine details are seen at this level of contouring. Figure II.3b is of the same orbitals with a maximum contour value of 1. The Fourier ripples could, in the standard interpretation, be seen as deformation density. We know however that these details are actually ripples and due to the limited resolution of the

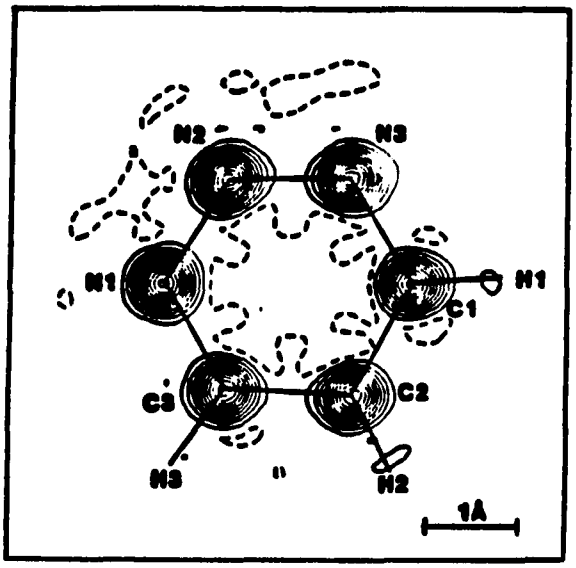

Figure II.2. Observed electron density[¶] for 1,2,3-triazine. Contour interval (CI) is 2.0e$^-$/Å^3. See Appendix E for an explanation of this and all other contour maps

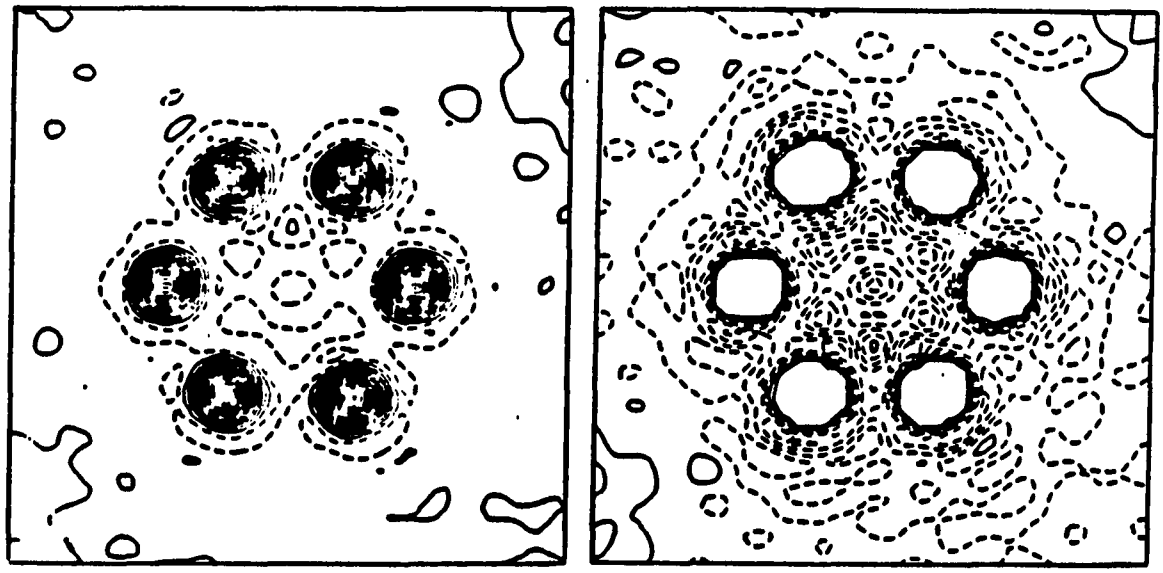

Figure II.3. Calculated electron density (left) for carbon and nitrogen 1s orbitals. Similar drawing (right), peaks truncated at 1.0e$^-$/Å^3. CI=0.1e$^-$/Å^3

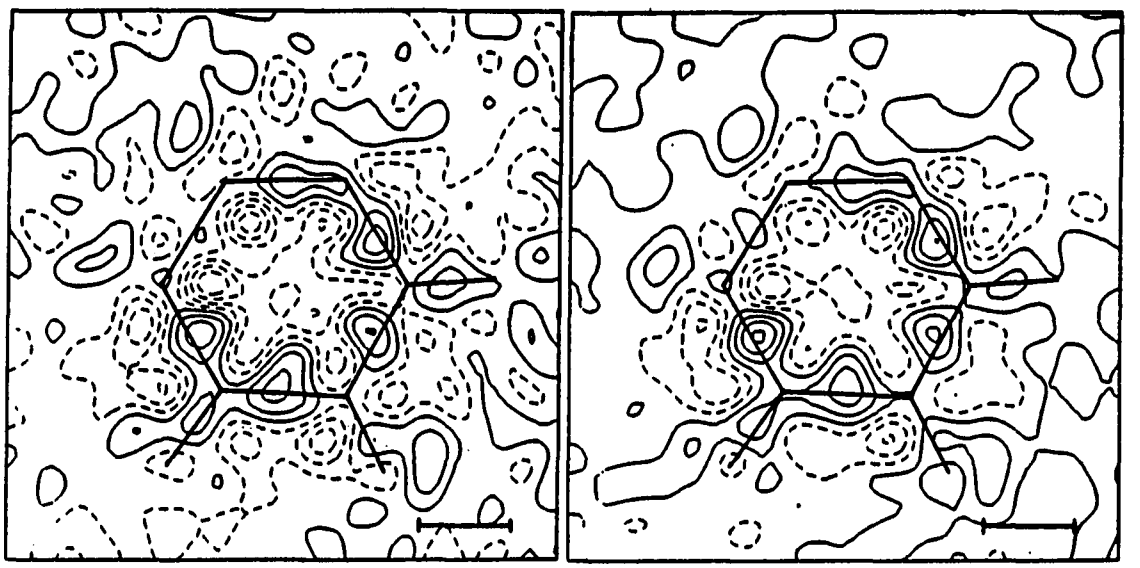

a b

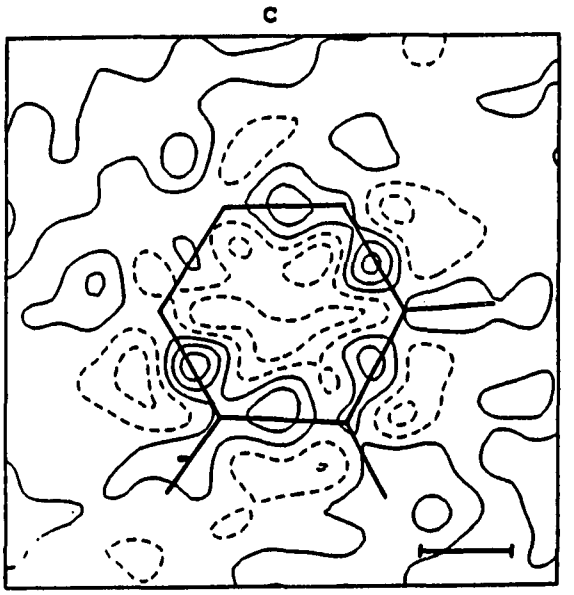

c

Figure II.4. Electron density difference maps with various signal to noise ratios. The $n\sigma(E(k))$ cutoff are 0, 3, and 20 for a, b, and c respectively

experiment.

A more useful function is

$$\Delta\rho_x = \rho_{exp}(r) - \rho_x(r) \qquad \text{(II.38a)}$$

$$= (1/V_{cell}) \Sigma_k (E(k) - F_x(k)) \exp(-ik\cdot r) \qquad \text{(II.38b)}$$

which is generally called a difference electron density function. The resultant function's interpretation depends on the definition of x. When $\rho_x(r)$ is the entire promolecule the result is called a deformation density and represents the electronic shifts which occur during molecular formation. Examples of $\rho_x(r)$ are given throughout the remaining chapters.

Aside from the definition of the promolecule there is another item which strongly affects the deformation density- that of the signal-to-noise ratio.

Generally a limit is set on the signal-to-noise ratio by selecting data for which $|E(k)| > n\sigma(E(k))$ where n is selected somewhat arbitrarily (sometimes as high as 20). While there is some merit to this, its effect on the interpretation has been ignored.

The Fourier series given in Equations (II.38) reveals that each reflection where E and F are not exactly equal will have some effect on the magnitude of $\Delta\rho_x$ and thus ignoring these data will flatten the resultant function. Nearly every author who has created $\Delta\rho_x$ maps points to the background and states that, since it is fairly flat, the dataset is good. This is a fallacy since their maps use some value of n

(usually greater than 2) which could readily throw-away a significant portion of the information. An example of the artificial improvement of the dataset is shown in Figures II.4 which reveals that the interpretation of maps (and the apparent data quality) in this manner is clearly biased by the experimenter. One should also note that the "bond peak heights" are also affected by the choice of n.

This dilemma cannot be solved in the above manner. It is necessary to return to the data collection procedure and measure reflections which have low signal-to-noise ratios in a manner which will improve the quality of these reflections. Reflections which are very weak do not contribute significantly in the Fourier synthesis and can be ignored.

Another possibility is to use a Fourier filtering technique which would transform the intensity data, smooth the intermolecular regions, and re-Fourier transform the data to give an "improved" dataset. It is not clear whether this procedure would introduce experimenter bias into the data but may well be worth a future study as it is untested at this time.

Statistical Analysis

Analysis of the results from any model fit to experimental data would be incomplete if statistical checks are not made. A summary of the more common tests is given here. For the purpose of this thesis only analysis

pertaining to the correctness of the resultant model and the electron density function are described.

For comparison of the experimentally determined (E(k)) and calculated (F(k)) structure factors there exist a number of approaches[32], none entirely satisfactory in themselves, which are useful in different ways.

The first is that of the least squares error (LSE)

$$LSE=\Sigma_k\ \omega\ (\Delta F)^2 \qquad (II.39)$$

where ω is the weight and ΔF is taken to be $||E(k)|-|F(k)||$. This function is the minimized quantity and should never increase during a given refinement cycle. It can also provide a comparison between models if used judiciously.

The error of fit (ERF) (a.k.a. goodness of fit) is the statistical standard deviation of a reflection of unit weight:

$$ERF=(LSE/DOF)^{1/2} \qquad (II.40)$$

where the degrees of freedom (DOF) of the system is defined as the number of observations minus the number of variables. The ERF is normalized and permits a comparison between different models as well as different structures.

The residuals are also normalized error functions,

$$R=(\Sigma_k\ |\Delta F|)/(\Sigma_k\ |E(k)|), \qquad (II.41a)$$

$$R_\omega=[(\Sigma_k\ \omega\ (\Delta F)^2/(\Sigma_k\ \omega\ |E(k)|^2]^{1/2}, \qquad (II.41b)$$

and

$$R_I=\Sigma_k\ |E(k)^2-F(k)^2|/(\Sigma_k\ E(k)^2 \qquad (II.41c)$$

which also allow comparisons between different structures and

models. Since R_ω is mostly closely related to the LSE it is the most meaningful, however comparisons against R and R_I provide a check against a faulty weighting scheme.

The residuals can be defined for all data or for subsets of the data. Reciprocal space zones and $\sin(\theta)/\lambda$ ranges are commonly the subsets of choice.

Counting the total number of reflections which have ΔF between $(n-1)\sigma(E(k))$ and $n\sigma(E(k))$ generally produces a Gaussian type distribution which can be analyzed for the appropriateness of the calculated standard deviations as well as how good the model fits the data. This function can also point out proper $n\sigma(E(k))$ cutoffs.

One type of $n\sigma(E(k))$ cutoff is used to define reflections for which the signal-to-noise ratio is too small for the reflection to be reliably used as discussed earlier. Another type of $n\sigma(E(k))$ cutoff is used to define reflections which are so poorly fit by the model's calculated structure factors that they are suspected to be "bad" reflections and hence that the reflections deserve a closer examination.

A check on serial correlation is obtained from the Durbin-Watson d statistic which is defined as

$$DWd=(\Sigma_{k=2}\ (\Delta F_k-\Delta F_{k-1})^2)/(\Sigma_k\ (\Delta F)^2). \qquad \text{(II.42)}$$

DWd should be 2 if no correlation exists and less than 2 if a positive correlation exists. The use of this function requires the data to be sorted according to the type of correlation to be checked (such as time or $\sin(\theta)/\lambda$).

The standard deviation of a variable ($\sigma(P_i)$) is obtained from

$$\sigma(P_i)=(b_{ii})^{1/2}\ \mathrm{ERF} \qquad \text{(II.43)}$$

where b_{ii} is the diagonal component of the inverse of the normal equations matrix A_{nm}.

The standard deviations are sometimes used in conjunction with the parameter shifts to check if the refinement process is finished. This is accomplished by assuming that if the parameter's shift divided by the parameter's standard deviation is less than 10, the structure is very close to its final position and further refinement will produce no significant change.

Calculation of the eigenvalues of the Hessian (second order derivative) matrix is necessary to test[33] whether or not the structure is at a saddle point on the least squares surface. More than a few negative eigenvalues imply that the structure is at a saddle point and should be perturbed and refinement continued.

Correlations between variables (δ_{ij}) are given by

$$\delta_{ij}=b_{ij}/(b_{ii}\ b_{jj})^{1/2} \qquad \text{(II.44)}$$

and lie in the interval [-1,1]. Correlations greater in magnitude than about 1/2 imply that a relation exists between the variables. If the magnitude approaches 1 the variables cannot be adjusted simultaneously and one must either find the relation between the variables and so constrain the system, or refine the variables on different least squares

cycles. If the magnitude of δ_{ij} is 1 then the normal equations matrix is singular and the least squares equations cannot be solved in the standard manner.

To obtain a feel for the quality of the electron density function one may use

$$\sigma(\rho_o)=1/V_{cell}\ [\Sigma_k\ (\Delta F)^2]^{1/2} \qquad \text{(II.45)}$$

which is an average standard deviation of the electron density.

It is of extreme importance to realize the downfalls of the functions described so far in terms of the superimposition-of-oriented-atoms approach.

The first is that none of these statistical functions (except for DWd) account for systematic errors (such as incorrect corrections or refining on $|F(k)|$ rather than $I(k)$) and thus they are really only a measure of the precision of the fit, not the accuracy. To check accuracy one must compare the results with other accurate experiments (such as neutron diffraction), with theoretical calculations (which may not actually be very realistic), or with a firm conceptual background (which introduces experimenter bias).

The second, and the most important item, is that the promolecule approach does not attempt to fit the deformation density (or rather we hope that it does not). This can be translated into meaning that the statistical analysis of low-order data must be treated with great care and is generally suspect. Analysis of the high-order data on the other hand

should produce very reliable results since the promolecule model does fit very well in this region.

A third point which should be mentioned is that, since these functions are statistical, there must be a sufficient data to obtain meaningful results. For most functions this usually translates into an observation to variable ratio of at least 8, with something approaching 30 being preferable.

CHAPTER III. 1,2,3-TRIAZINE

Introduction

An extensive study of compound 1,2,3-triazine is described in this chapter. In order to develop a procedure for obtaining highly accurate parameters and also valence orbital information, nine trial approaches are presented and comparisons between them made. These trials range from using the standard crystallographic approach to using a high-accuracy approach in which the valence orbitals are oriented and molecular ionization allowed. The feasibility of obtaining valence orbital information from various approaches is herein shown.

The general procedure used for refinement and the convergence criteria are described in Appendix E. As the approach taken here is to develop a rote method of obtaining the promolecule's parameters, all structure refinements followed similar procedures, allowing comparisons to be made. The electron density functions are shown as two-dimensional contour maps and in ORTEP-type illustrations. The features of the maps and drawings are discussed in Appendix E.

Preliminary Discussion

The compound itself is ideal in several ways. It involves light atoms and thus the relatively small deformation density is more readily seen. The molecule[34]

crystallizes in a centrosymmetric space group. The molecules have extended hydrogen bonding and thus rigid body motion is minimized. The molecule and the dataset are both small which helped expedite the testing of various approaches and analysis routines. The molecule is nearly planar which simplifies the understanding of difference density maps. The molecule also has a chemical symmetry (C_2) axis allowing for a check on the actual data quality and on the refinement results.

A summary of the pertinent data and crystal parameters is given in Table III.1. The carbon and nitrogen (SCF)

Table III.1. Summary of data and crystal parameters for 1,2,3-triazine

Chemical formula	$N_3C_3H_3$	
Crystal system	triclinic	
Space group symbol	$P\bar{1}$	
Lattice parameters[a]	a=5.7688(4)Å	α=110.080(6)°
	b=6.8732(6)Å	β=113.947(5)°
	c=5.6725(4)Å	γ= 95.302(6)°
Temperature of data collection	100K	
Total number of reflections	9046	
Number after averaging	2187	
Number observed	2032 (I>0)	
Internal agreement[b]	0.027	
Radiation	Mo k_α (λ=0.71Å)	
Sin(θ)/λ (min/max, $Å^{-1}$)	0.08/0.90	

[a]Estimated standard deviations in the least significant figures are given in parentheses in this and subsequent tables.

[b]Defined as $R_{Int}(<I>)= (\Sigma_k |<I>|-|I|)/(\Sigma_k |<I>|)$.

scattering factors used are described in Appendix B. Other carbon and nitrogen scattering factors (HF) values[35] were used in some cases as a comparison. Modified hydrogen scattering factors[36] were used in all cases.

The dataset[37,38] is not considered ideal. The data range is small. Generally data used in a high-order refinement should be above about $\sin(\theta)/\lambda=1.0\text{Å}^{-1}$. The implications of the low resolution are described below. Also, the quality of the data is questionable. In another study[39], data from the same source were found to be of lower quality. Other compounds obtained by this author from the same source are also of low quality. The chief criteria in both cases are that the thermal factors either do not agree well with other sources, or that the hydrogen thermal parameters do not refine to physically meaningful values. For this reason the hydrogens' parameters will not be discussed at any length.

Since the dataset is not ideal we cannot hope to obtain perfect results. On the other hand, if the valence orbital refinement does yield good qualitative information, it will be quite satisfactory to know that a very good (and rare) dataset is not required.

There are nine different trials (labeled 1 through 9) described in the remaining sections. A summary of the trial structures' refinement conditions are given in Table III.2.

Table III.2. Summary of refinement conditions for the trial structures

Trial	Scattering factors[a]	Adjustable parameters[b]	Refinement class[c]	Electronic constraints[d]
1	SCF	X	Std	Std
2	HF	X	Std	Std
3	SCF	X	Mix	Std
4	HF	X	Mix	Std
5	SCF	X,Ψ	Mix	Std
6	SCF	X,Ψ	Std	Std
7	SCF	X,Ψ	Mix	Ion
8	SCF	X,Ψ	Low	Std
9	SCF	X,Ψ	Mix	Tot

[a]SCF values are from this work (see Appendix B). HF are the Hartree-Fock values[34].

[b]X-type parameters are the scale and the atomic coordinates and thermal parameters of the carbon and nitrogen atoms. Ψ-type parameters are the valence orbital parameters and also the hydrogen atoms' parameters.

[c]"Std" implies that all data were used in the refinement. "Mix" implies that the high-order data was used for the X parameters and all data for the Ψ parameters. "Low" implies that all the parameters were refined against the low-order data ($\sin(\theta)/\lambda<0.6$) only.

[d]The standard constraints (Std) are that each atom maintains neutrality. Allowing the molecule to ionize (Ion) imply that there are no constraints on the valence electrons. Allowing electron transfer between the valence shells of different atoms implies that the total (Tot) molecular electronic charge is conserved.

Table III.3a. Atom coordinates[a] (fractional, 10^{-4}) for atoms in 1,2,3-triazine

x	1	2	3	4	5	6	7	8	9
N1	6772	6772	6777	6777	6776	6773	6776	6773	6776
N2	9072	9072	9068	9068	9068	9071	9068	9073	9068
N3	9715	9715	9710	9710	9710	9716	9710	9714	9710
C1	7996	7996	8000	8000	7999	7996	7999	7998	7999
C2	5558	5558	5557	5557	5557	5558	5557	5560	5557
C3	5038	5038	5040	5040	5040	5039	5040	5047	5040
H1	8588	8596	8569	8594	8618	8594	8591	8609	8614
H2	4298	4287	4265	4302	4270	4327	4330	4310	4274
H3	3382	3391	3313	3353	3355	3393	3373	3401	3345

y	1	2	3	4	5	6	7	8	9
N1	2965	2964	2964	2964	2964	2964	2964	2964	2964
N2	2578	2578	2576	2577	2577	2577	2577	2577	2577
N3	2135	2135	2137	2137	2137	2134	2137	2135	2137
C1	2063	2062	2060	2060	2061	2062	2061	2064	2061
C2	2433	2432	2431	2431	2430	2432	2430	2432	2430
C3	2900	2899	2900	2900	2900	2899	2900	2897	2900
H1	1765	1764	1532	1500	1800	1762	1807	1810	1804
H2	2460	2452	2131	2137	2390	2463	2426	2437	2395
H3	3288	3284	2990	3000	3245	3315	3237	3283	3230

z	1	2	3	4	5	6	7	8	9
N1	369	369	375	374	374	368	374	370	374
N2	1628	1628	1630	1630	1630	1627	1629	1627	1630
N3	3886	3886	3882	3882	3882	3886	3883	3884	3882
C1	4914	4913	4917	4917	4918	4914	4917	4909	4917
C2	3701	3700	3696	3696	3696	3701	3696	3697	3696
C3	1384	1384	1384	1384	1384	1384	1384	1383	1384
H1	6531	6537	6444	6408	6630	6559	6577	6563	6627
H2	4415	4407	4311	4286	4377	4423	4396	4433	4392
H3	384	400	231	239	362	423	381	363	360

[a]The standard deviations for carbon and nitrogen are ca. 10^{-4}. For hydrogen they are ca. $3*10^{-3}$.

Table III.3b. RMS amplitudes of vibration[a] (Å) for atoms in 1,2,3-triazine

Atom	1	2	3	4	5	6	7	8	9
N1	0.14	0.14	0.14	0.14	0.14	0.14	0.14	0.16	0.14
N2	0.14	0.14	0.14	0.14	0.14	0.14	0.14	0.16	0.14
N3	0.14	0.14	0.14	0.14	0.14	0.14	0.14	0.15	0.14
C1	0.13	0.14	0.14	0.14	0.14	0.13	0.14	0.15	0.14
C2	0.13	0.14	0.13	0.13	0.13	0.13	0.13	0.15	0.13
C3	0.13	0.14	0.14	0.13	0.14	0.13	0.14	0.15	0.14
H1	0.06	0.08	0.11	0.13	0.09	0.08	0.09	0.04	0.09
H2	0.05	0.08	0.08	0.11	0.04	0.04	0.05	0.05	0.04
H3	0.07	0.09	0.04	0.07	0.05	0.06	0.05	0.07	0.05

[a]Standard deviations for the hydrogens are ca. $6*10^{-2}$.

Table III.3c. Anisotropic thermal parameters[a] (Å, 10^{-3}) for atoms in 1,2,3-triazine

U_{11}	1	2	3	4	5	6	7	8	9
N1	18.8	19.0	18.3	18.1	18.0	18.2	18.0	26.1	18.0
N2	16.0	16.4	16.4	16.2	16.5	15.7	16.5	24.1	16.5
N3	13.2	13.6	12.7	12.5	12.4	11.9	12.5	16.5	12.4
C1	14.2	14.9	14.6	14.3	14.5	13.6	14.4	18.6	14.5
C2	12.8	13.5	13.2	12.9	13.1	12.2	13.2	15.7	13.1
C3	12.5	13.2	13.5	13.3	13.6	13.0	13.7	15.1	13.6

U_{22}	1	2	3	4	5	6	7	8	9
N1	24.7	25.0	24.8	24.6	26.0	25.0	25.8	20.4	26.1
N2	22.6	22.9	23.5	23.3	24.3	23.1	24.0	20.2	24.3
N3	25.3	25.6	25.8	25.6	26.8	25.7	26.6	23.0	26.8
C1	23.5	24.4	24.8	24.6	25.7	24.1	25.6	23.8	25.7
C2	19.3	20.2	19.8	19.5	20.4	18.8	20.2	18.0	20.5
C3	20.9	21.6	21.7	21.4	22.8	22.6	22.7	22.4	22.8

[a]$U=(1/2\pi^2)\ \beta\ G^*$, where the temperature factor is of the form $\exp[(k\ \beta\ k^T)/(4\pi^2)]$. [a]Standard deviations are ca. $3*10^{-3}$.

Table III.3c. Continued

U_{33}	1	2	3	4	5	6	7	8	9
N1	19.9	20.3	19.6	19.4	19.4	18.3	19.4	20.8	19.4
N2	21.1	21.5	21.7	21.5	22.2	22.0	22.2	26.9	22.2
N3	21.8	22.3	21.4	21.2	21.5	21.2	21.4	25.9	21.5
C1	18.1	19.0	18.7	18.5	18.8	18.0	18.8	21.3	18.7
C2	19.7	20.3	19.8	19.4	19.7	19.2	19.7	22.9	19.7
C3	19.7	20.3	19.9	19.6	19.8	18.7	19.9	22.1	19.8

U_{12}	1	2	3	4	5	6	7	8	9
N1	16.1	16.2	14.8	14.7	14.1	13.1	14.0	13.6	14.1
N2	16.9	17.0	17.8	17.7	18.5	18.2	18.4	23.4	18.5
N3	15.0	15.3	13.9	13.8	13.5	12.8	13.4	13.3	13.5
C1	13.4	14.1	13.6	13.4	13.6	13.2	13.5	15.6	13.6
C2	15.1	15.6	14.5	14.2	14.1	13.5	14.0	15.6	14.2
C3	10.4	10.8	11.3	11.1	11.4	11.2	11.4	10.4	11.3

U_{13}	1	2	3	4	5	6	7	8	9
N1	9.4	9.5	9.7	9.7	10.6	10.0	10.5	7.1	10.6
N2	8.1	8.2	8.8	8.7	9.5	8.8	9.3	6.6	9.5
N3	9.0	9.2	9.4	9.4	10.3	10.0	10.1	8.3	10.3
C1	8.9	9.2	9.4	9.3	9.8	9.1	9.7	8.7	9.8
C2	6.4	6.7	6.9	6.7	7.3	6.6	7.2	4.3	7.3
C3	7.6	7.8	8.2	8.1	8.9	8.5	8.8	6.6	8.9

U_{23}	1	2	3	4	5	6	7	8	9
N1	7.7	7.7	7.5	7.5	7.7	7.3	7.7	5.5	7.7
N2	6.7	6.8	6.9	6.9	7.3	6.9	7.1	7.3	7.2
N3	7.6	7.8	7.6	7.6	8.0	7.7	7.9	7.5	8.0
C1	7.5	7.7	7.7	7.6	7.9	7.7	7.9	7.3	7.9
C2	5.5	5.8	6.0	5.9	6.2	5.3	6.1	3.1	6.2
C3	6.5	6.6	7.1	7.0	7.4	6.9	7.3	5.4	7.4

Table III.4a. Comparisons between trials for 1,2,3-triazine. Percent differences[a] of the atomic coordinates

x	1:2	3:4	3:1	5:6	5:3	5:7	5:8	5:9
N1	0.00	0.00	0.07	0.04	-0.01	0.00	0.04	0.00
N2	0.00	0.00	-0.04	-0.03	0.00	0.00	-0.06	0.00
N3	0.00	0.00	-0.05	-0.06	0.00	0.00	-0.04	0.00
C1	0.00	0.00	0.05	0.04	-0.01	0.00	0.01	0.00
C2	0.00	0.00	-0.02	-0.02	0.00	0.00	-0.05	0.00
C3	0.00	0.00	0.04	0.02	0.00	0.00	-0.14	0.00
H1	-0.09	-0.29	-0.22	0.28	0.57	0.31	0.10	0.05
H2	0.26	-0.87	-0.77	-1.33	0.12	-1.41	-0.94	-0.09
H3	-0.27	-1.21	-2.08	-1.13	1.25	-0.54	-1.37	0.30
AVE	-0.01	-0.26	-0.34	-0.24	0.21	-0.18	-0.27	0.03

y	1:2	3:4	3:1	5:6	5:3	5:7	5:8	5:9
N1	0.03	0.00	-0.03	0.00	0.00	0.00	0.00	0.00
N2	0.00	-0.04	-0.08	0.00	0.04	0.00	0.00	0.00
N3	0.00	0.00	0.09	0.14	0.00	0.00	0.09	0.00
C1	0.05	0.00	-0.15	-0.05	0.05	0.00	-0.15	0.00
C2	0.04	0.00	-0.08	-0.08	-0.04	0.00	-0.08	0.00
C3	0.03	0.00	0.00	0.03	0.00	0.00	0.10	0.00
H1	0.06	2.09	-15.21	2.11	14.89	-0.39	-0.56	-0.22
H2	0.33	-0.28	-15.44	-3.05	10.84	-1.51	-1.97	-0.21
H3	0.12	-0.33	-9.97	-2.16	7.86	0.25	-1.17	0.46
AVE	0.07	0.16	-4.54	-0.34	3.74	-0.18	-0.41	0.00

z	1:2	3:4	3:1	5:6	5:3	5:7	5:8	5:9
N1	0.00	0.27	1.60	1.60	-0.27	0.00	1.07	0.00
N2	0.00	0.00	0.12	0.18	0.00	0.06	0.18	0.00
N3	0.00	0.00	-0.10	-0.10	0.00	-0.03	-0.05	0.00
C1	0.02	0.00	0.06	0.08	0.02	0.02	0.18	0.02
C2	0.03	0.00	-0.14	-0.14	0.00	0.00	-0.03	0.00
C3	0.00	0.00	0.00	0.00	0.00	0.00	0.07	0.00
H1	-0.09	0.56	-1.35	1.07	2.81	0.80	1.01	0.05
H2	0.18	0.58	-2.41	-1.05	1.51	-0.43	-1.28	-0.34
H3	-4.17	-3.46	-66.23	-16.85	36.19	-5.25	-0.28	0.55
AVE	-0.45	-0.23	-7.61	-1.69	4.47	-0.54	0.10	0.03

[a]Percent difference (A:B)=100*(A-B)/A.

Table III.4b. Comparisons of trials for 1,2,3-triazine. Percent differences of the rms amplitudes of vibration

Atom	1:2	3:4	3:1	5:6	5:3	5:7	5:8	5:9
N1	-0.82	0.58	-0.74	1.20	-0.02	0.07	-9.01	-0.01
N2	-0.85	0.55	1.00	1.29	0.44	-0.07	-10.57	-0.01
N3	-1.04	0.63	-0.52	1.50	-0.20	0.03	-7.89	0.01
C1	-2.41	0.83	2.14	2.79	0.21	-0.12	-6.94	-0.02
C2	-2.18	0.91	0.46	2.18	0.01	0.05	-9.63	0.01
C3	-2.11	0.86	1.11	1.60	0.23	-0.14	-8.18	-0.01
H1	-30.76	-14.96	45.97	15.51	-27.67	0.16	53.11	0.73
H2	-56.28	-35.69	30.81	-2.25	-75.30	-20.56	-21.29	2.85
H3	-23.30	-74.78	-81.96	-9.68	22.76	0.16	-40.54	10.76
N[a]	-0.90	0.59	-0.08	1.33	0.07	0.01	-9.16	0.00
C[a]	-2.23	0.86	1.24	2.19	0.15	-0.07	-8.25	0.00
H[a]	-36.78	-41.81	-1.73	1.20	-26.74	-6.75	-2.91	4.78

[a]Average percent difference for each atom type.

Table III.4c. Comparisons between trials for 1,2,3-triazine. Percent differences of the anisotropic thermal parameters

U_{11}	1:2	3:4	3:1	5:6	5:3	5:7	5:8	5:9
N1	-1.06	1.09	-2.73	-1.11	-1.67	0.00	-45.00	0.00
N2	-2.50	1.22	2.44	4.85	0.61	0.00	-46.06	0.00
N3	-3.03	1.57	-3.94	4.03	-2.42	-0.81	-33.06	0.00
C1	-4.93	2.05	2.74	6.21	-0.69	0.69	-28.28	0.00
C2	-5.47	2.27	3.03	6.87	-0.76	-0.76	-19.85	0.00
C3	-5.60	1.48	7.41	4.41	0.74	-0.74	-11.03	0.00
AVE	-3.77	1.62	1.49	4.21	-0.70	-0.27	-30.55	0.00

Table III.4c. Continued

U_{22}	1:2	3:4	3:1	5:6	5:3	5:7	5:8	5:9
N1	-1.21	0.81	0.40	3.85	4.62	0.77	21.54	-0.38
N2	-1.33	0.85	3.83	4.94	3.29	1.23	16.87	0.00
N3	-1.19	0.78	1.94	4.10	3.73	0.75	14.18	0.00
C1	-3.83	0.81	5.24	6.23	3.50	0.39	7.39	0.00
C2	-4.66	1.52	2.53	7.84	2.94	0.98	11.76	-0.49
C3	-3.35	1.38	3.69	0.88	4.82	0.44	1.75	0.00
AVE	-2.60	1.02	2.94	4.64	3.82	0.76	12.25	-0.15

U_{33}	1:2	3:4	3:1	5:6	5:3	5:7	5:8	5:9
N1	-2.01	1.02	-1.53	5.67	-1.03	0.00	-7.22	0.00
N2	-1.90	0.92	2.76	0.90	2.25	0.00	-21.17	0.00
N3	-2.29	0.93	-1.87	1.40	0.47	0.47	-20.47	0.00
C1	-4.97	1.07	3.21	4.26	0.53	0.00	-13.30	0.53
C2	-3.05	2.02	0.51	2.54	-0.51	0.00	-16.24	0.00
C3	-3.05	1.51	1.01	5.56	-0.51	-0.51	-11.62	0.00
AVE	-2.88	1.25	0.68	3.39	0.20	-0.01	-15.00	0.09

U_{12}	1:2	3:4	3:1	5:6	5:3	5:7	5:8	5:9
N1	-0.62	0.68	-8.78	7.09	-4.96	0.71	3.55	0.00
N2	-0.59	0.56	5.06	1.62	3.78	0.54	-26.49	0.00
N3	-2.00	0.72	-7.91	5.19	-2.96	0.74	1.48	0.00
C1	-5.22	1.47	1.47	2.94	0.00	0.74	-14.71	0.00
C2	-3.31	2.07	-4.14	4.26	-2.84	0.71	-10.64	-0.71
C3	-3.85	1.77	7.96	1.75	0.88	0.00	8.77	0.88
AVE	-2.60	1.21	-1.06	3.81	-1.02	0.57	-6.34	0.03

U_{13}	1:2	3:4	3:1	5:6	5:3	5:7	5:8	5:9
N1	-1.06	0.00	3.09	5.66	8.49	0.94	33.02	0.00
N2	-1.23	1.14	7.95	7.37	7.37	2.11	30.53	0.00
N3	-2.22	0.00	4.26	2.91	8.74	1.94	19.42	0.00
C1	-3.37	1.06	5.32	7.14	4.08	1.02	11.22	0.00
C2	-4.69	2.90	7.25	9.59	5.48	1.37	41.10	0.00
C3	-2.63	1.22	7.32	4.49	7.87	1.12	25.84	0.00
AVE	-2.54	1.05	5.86	6.19	7.00	1.42	26.85	0.00

Table III.4c. Continued

U_{23}	1:2	3:4	3:1	5:6	5:3	5:7	5:8	5:9
N1	0.00	0.00	-2.67	5.19	2.60	0.00	28.57	0.00
N2	-1.49	0.00	2.90	5.48	5.48	2.74	0.00	1.37
N3	-2.63	0.00	0.00	3.75	5.00	1.25	6.25	0.00
C1	-2.67	1.30	2.60	2.53	2.53	0.00	7.59	0.00
C2	-5.45	1.67	8.33	14.52	3.23	1.61	50.00	0.00
C3	-1.54	1.41	8.45	6.76	4.05	1.35	27.03	0.00
AVE	-2.30	0.73	3.27	6.37	3.81	1.16	19.91	0.23

Initial Structure Refinement

The first stage of any refinement process is to obtain the approximate structure from a standard refinement. The initial atomic positions were obtained from a direct methods approach[40]. The results from the standard crystallographic refinement (Trial 2) are given in Tables III.3, the bond distances and angles are listed in Tables III.5, and the pertinent statistical analysis results are given in Tables III.7 and III.8.

The refinement proceeded without difficulty. The hydrogen atoms (as well as bond peaks) were found from electron density difference calculations. The hydrogen positions and isotropic thermal parameters refined well. A drawing[41] of the promolecule is shown in Figure III.1a. Figure III.1d shows the hydrogen bonding and the molecular stacking arrangement. Figures III.1b and III.1c are maps of the observed electron density.

Table III.5a. Interatomic distances[a] (Å) for 1,2,3-triazine

	1	2	3	4	5	6	7	8	9
N1-N2	1.329	1.329	1.325	1.325	1.325	1.329	1.329	1.329	1.325
N2-N3	1.332	1.332	1.328	1.328	1.328	1.332	1.328	1.331	1.328
N3-C1	1.344	1.344	1.342	1.342	1.343	1.344	1.343	1.341	1.343
C1-C2	1.385	1.385	1.388	1.388	1.387	1.385	1.387	1.384	1.387
N1-C3	1.345	1.345	1.345	1.345	1.345	1.346	1.345	1.341	1.345
C2-C3	1.382	1.381	1.380	1.380	1.380	1.381	1.380	1.379	1.380
C1-H1	0.942	0.946	0.998	0.997	0.976	0.957	0.947	0.944	0.973
C2-H2	0.964	0.967	0.976	0.945	0.968	0.951	0.942	0.969	0.972
C3-H3	1.008	1.001	0.967	0.951	1.008	1.009	0.995	1.006	1.008

[a]The standard deviations for bonds not involving hydrogen are ca. 10^{-3}. Bonds involving hydrogen are ca. 10^{-2}.

Table III.5b. Bond angles[a] (°) for 1,2,3-triazine

	1	2	3	4	5	6	7	8	9
$N_2N_1C_3$	119.5	119.5	119.6	119.6	119.6	119.4	119.6	119.4	119.6
$N_1N_2N_3$	121.6	121.6	121.7	121.7	121.7	121.7	121.7	121.5	121.7
$N_2N_3C_1$	119.4	119.4	119.7	119.7	119.7	119.4	119.7	119.4	119.7
$N_3C_1C_2$	122.2	122.2	121.8	121.8	121.8	122.2	121.8	122.3	121.8
$N_3C_1H_1$	115.0	114.8	113.3	111.7	115.8	115.2	116.1	115.1	115.9
$C_2C_1H_1$	122.8	123.0	124.5	125.9	122.3	122.7	122.1	122.6	122.2
$C_1C_2C_3$	115.2	115.1	115.3	115.3	115.3	115.1	115.3	115.0	115.3
$C_1C_2H_2$	125.0	125.1	119.0	119.1	124.3	124.5	124.0	123.9	124.1
$C_3C_2H_2$	119.8	119.7	124.9	124.8	120.4	120.3	120.7	121.1	120.6
$N_1C_3C_2$	122.2	122.2	122.0	122.0	122.0	122.2	122.0	122.4	122.0
$N_1C_3H_3$	114.8	115.2	115.8	115.1	115.5	115.3	115.8	113.9	115.9
$C_2C_3H_3$	122.9	122.6	121.5	122.3	122.4	122.3	122.1	123.6	122.0

[a]The standard deviations for angles not involving hydrogen are ca. $7*10^{-2}$. For angles involving hydrogen they are ca. $8*10^{-1}$.

Table III.6a. Comparisons of trials for 1,2,3-triazine. Percent differences of the interatomic distances

	1:2	3:4	3:1	5:6	5:3	5:7	5:8	5:9
N1-N2	-0.02	-0.01	-0.32	-0.26	0.02	0.00	-0.29	0.00
N2-N3	-0.02	0.00	-0.29	-0.28	0.02	-0.02	-0.23	0.00
N3-C1	0.03	0.00	-0.11	-0.11	0.01	0.00	0.14	0.00
C1-C2	-0.01	0.01	0.22	0.14	-0.04	-0.01	0.24	-0.01
N1-C3	0.00	0.00	-0.06	-0.10	0.00	0.00	0.27	0.00
C2-C3	0.04	0.01	-0.10	-0.07	0.02	0.02	0.09	0.00
C1-H1	-0.34	0.17	5.61	1.96	-2.27	3.02	3.32	0.33
C2-H2	-0.31	3.15	1.23	1.78	-0.77	2.72	-0.06	-0.35
C3-H3	0.68	1.66	-4.29	-0.04	4.13	1.33	0.19	0.07
AVE	0.01	0.55	0.21	0.33	0.12	0.79	0.41	0.00

Table III.6b. Comparisons of trials for 1,2,3-triazine. Percent differences of the bond angles

	1:2	3:4	3:1	5:6	5:3	5:7	5:8	5:9
N2-N1-C3	0.00	0.00	0.08	0.13	0.01	0.00	0.12	0.00
N1-N2-N3	0.01	0.01	0.03	-0.02	-0.01	0.01	0.11	0.01
N2-N3-C1	0.02	-0.01	0.24	0.23	-0.01	0.00	0.22	0.00
N3-C1-C2	-0.03	0.01	-0.34	-0.30	0.02	0.01	-0.39	0.00
N3-C1-H1	0.17	1.36	-1.48	0.58	2.19	-0.21	0.66	-0.10
C2-C1-H1	-0.14	-1.11	1.32	-0.29	-1.77	0.18	-0.25	0.10
C1-C2-C3	0.02	-0.01	0.11	0.12	0.00	-0.01	0.26	0.00
C1-C2-H2	-0.11	-0.06	-5.00	-0.14	4.25	0.26	0.36	0.19
C3-C2-H2	0.08	0.09	4.15	0.11	-3.79	-0.23	-0.58	-0.20
N1-C3-C2	-0.02	0.00	-0.11	-0.14	0.00	0.00	-0.29	0.00
N1-C3-H3	-0.29	0.66	0.88	0.16	-0.27	-0.28	1.40	-0.35
C2-C3-H3	0.28	-0.67	-1.19	0.09	0.75	0.26	-1.00	0.32
AVE	0.00	0.02	-0.11	0.04	0.11	0.00	0.05	0.00

Table III.7a. R_w (10^{-3}) in reciprocal space zones

		ALL[a]	h00	0k0	00l	0kl	h0l	hk0
	#1[b]	2032	9	7	7	128	106	133
	#2	644	6	5	5	54	47	58
	#3	1027	2	2	1	48	41	53
1	#1	61	67	171	52	72	62	61
2	#1	61	64	163	57	75	63	59
3	#1	76	63	398	80	97	68	69
3	#2	46	32	178	2636	42	49	44
4	#1	72	58	391	78	97	73	63
4	#2	46	30	171	2681	41	48	44
5	#1	62	52	208	61	81	60	84
5	#2	46	26	111	2730	38	49	44
6	#1	56	79	175	52	68	60	63
7	#1	60	55	197	57	84	61	68
7	#2	46	26	107	2782	38	49	44
8	#3	48	57	159	49	51	52	55
9	#1	63	52	208	64	82	60	84
9	#2	46	26	108	2730	38	49	44

[a]ALL implies that all reflections were used.

[b]Number of reflections in each zone. They are dependent on the range of $\sin(\theta)/\lambda$ and correspond to total, high-order, low-order data respectively.

In any standard crystallographic refinement the entire dataset is used. Since we are using a promolecule model it is not meaningful to place much significance on the statistical analysis or the atomic parameters in an absolute sense.

The first test of the standard refinement is to compare the results using HF scattering factors (as in Trial 2) and the results using SCF scattering factors (as in Trial 1). In

Table III.7b. R_w[a] (10^{-3}) in sin(θ)/λ ranges

n	#[b] 2	16	60	112	183	271	361	463	559	5
	0.1	0.2	0.3	0.4	0.5	0.6	0.7	0.8	0.9	1.0
1	269	64	62	68	67	63	50	49	63	27
2	254	59	62	68	66	65	48	47	64	37
3	628	52	76	81	92	92	49	40	54	21
4	614	63	84	85	78	80	47	40	54	22
5	297	42	70	61	72	76	52	40	54	30
6	279	56	62	59	58	55	48	45	57	30
7	281	49	68	63	63	72	50	40	53	29
8	252	42	46	46	47	48				
9	302	50	69	61	72	76	52	40	53	31

[a] R_w is calculated for the range [n-0.1, n) where n=sin(θ)/λ.

[b] Number of reflections in the range [n-0.1, n).

Table III.7c. Number of reflections with (|E|-|F|) in the range ((n-1)σ(E), nσ(E)]

n=	1	2	3	4	5	6	7	8	9	≥10
1	1493	383	79	44	14	7	2	5	1	4
2	1503	383	72	36	17	9	3	5	1	3
3	1477	351	95	42	30	10	12	7	3	5
3[a]	912	108	7							
4[a]	916	104	7							
5	1475	371	107	46	18	6	2	3	1	3
5[a]	920	100	7							
6	1540	350	80	31	15	8	5	3		
7	1514	356	88	35	16	13	4	3	2	1
7[a]	923	98	6							
8[b]	411	156	45	20	4	6	0	2		
9	1473	375	104	47	16	6	3	4	1	3
9[a]	921	99	7							

[a] High-order data only.

[b] Low-order data only.

Table III.8. Refinement results for 1,2,3-triazine

Trial	LSE	ERF	σ(p)	Scale
1	3428	1.3207	0.2651	5.05(1)
2	3407	1.3167	0.2659	5.33(1)
3[a]	429	0.6647	0.1461	5.19(5)
3	5208	1.6279	0.2883	
4[a]	425	0.6613	0.1459	5.29(5)
4	4774	1.5587	0.2831	
5[a]	429	0.6643	0.1456	5.22(5)
5	3572	1.3544	0.2847	
6	2818	1.1829	0.2703	5.01(1)
7[a]	425	0.6612	0.1453	5.22(5)
7	3296	1.2912	0.2845	
8[b]	1291	1.4362	0.1649	5.27(2)
9[a]	429	0.6643	0.1455	5.22(5)
9	3549	1.3399	0.2860	

[a]High-order data only.

[b]Low-order data only.

Tables III.4 we find little difference in the atomic coordinates and a general decrease (SCF values are smaller) in the vibrational parameters.

Examination of Figure B.1 shows that the SCF scattering factor is a more diffuse function than the HF scattering factor. In real space, this translates into the SCF carbon atom being more localized which would indicate that larger vibrations for the SCF atoms are expected so that their electron density will match the electron density calculated by the HF atoms.

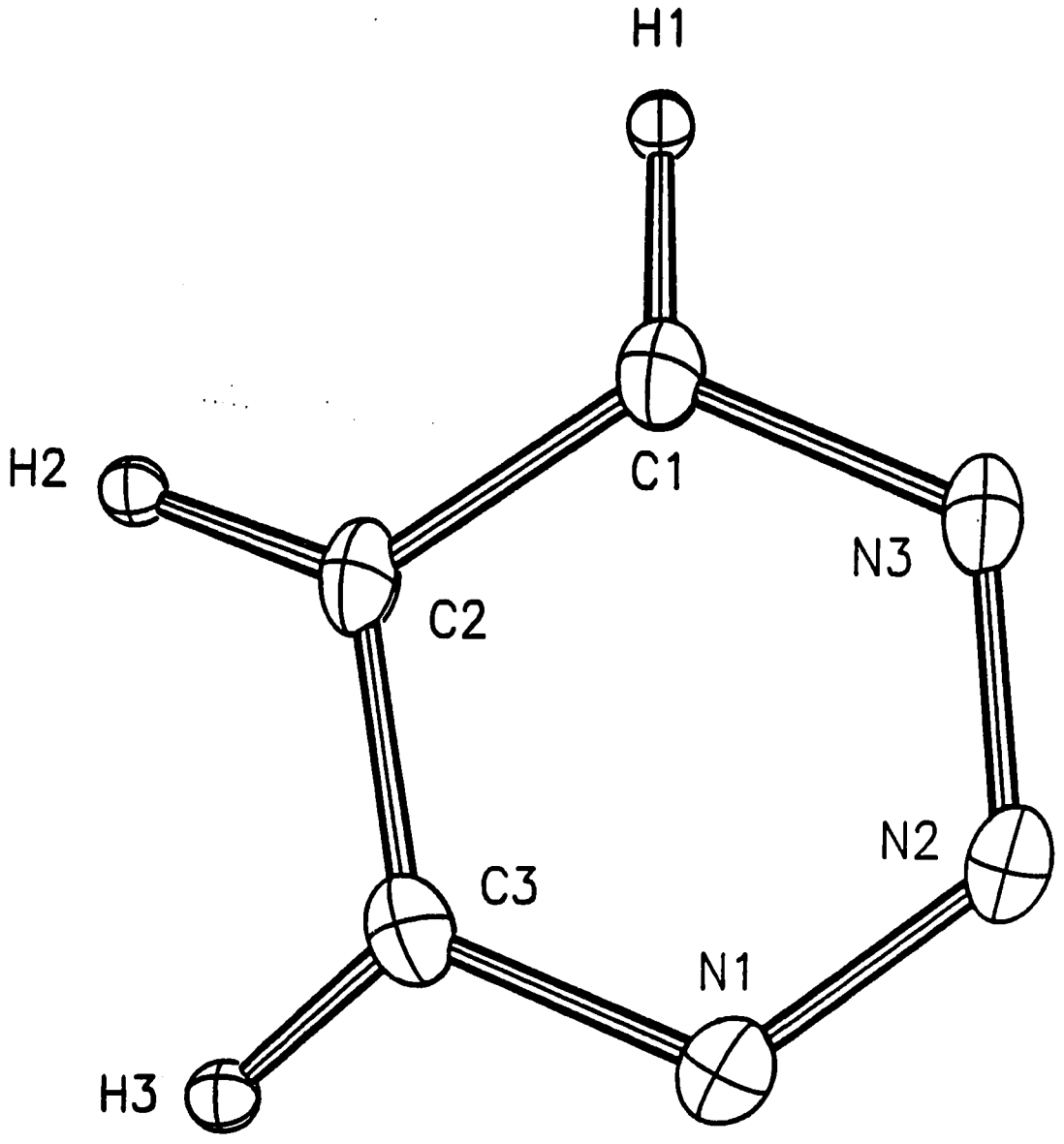

Figure III.1a. Drawing of the 1,2,3-triazine promolecule

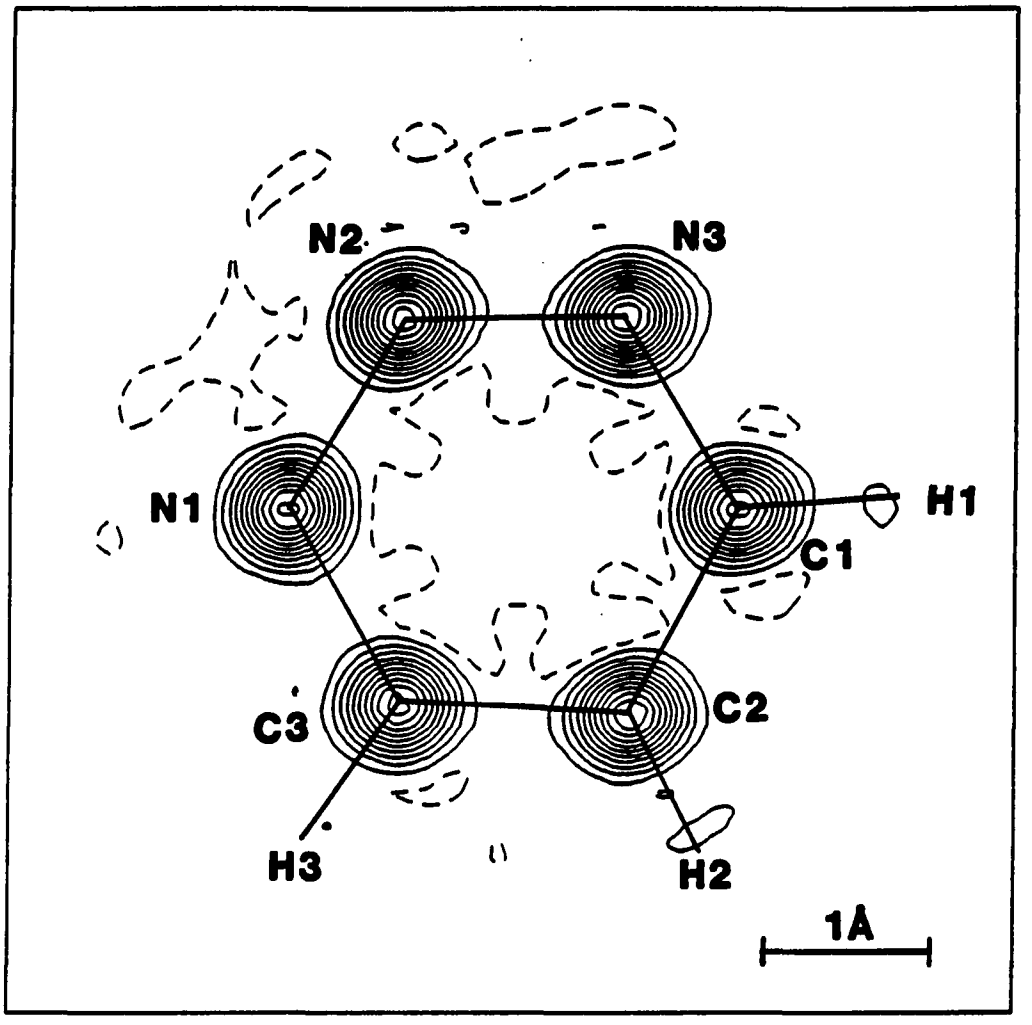

Figure III.1b. Contour map of observed electron density for 1,2,3-triazine. CI=2.0$e^-/Å^3$. See Appendix E for explanation of map features for this and all other contour maps

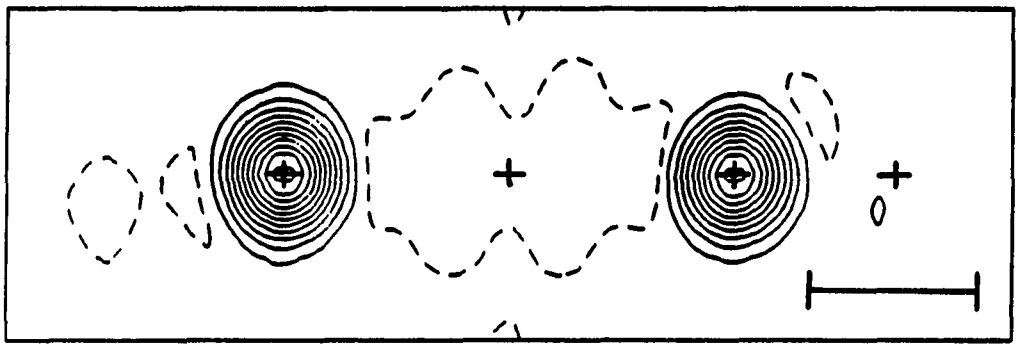

Figure III.1c. Horizontal cross-section of Figure III.1b. Crosses represent, from left to right, N1, map center, C1, and H1. CI=2.0$e^-/Å^3$

The scale factor can however raise the average of the scattering factor curve for the HF atoms above the SCF average. This then is compensated for by an increase in the HF vibrational parameters which essentially flattens the scattering factor curves. The hydrogen atoms' thermal factor decrease can be explained as a compensation for errors and thus are not meaningful. As might be expected, no significant differences in bond distances or angles are seen in Tables III.6.

In light of these results, it is expected that the scale factor and the vibrational parameters will be the main difference between structures refined using SCF and those using HF scattering factors. While the LSE is lower when using the HF values, it is not proper to speculate that they

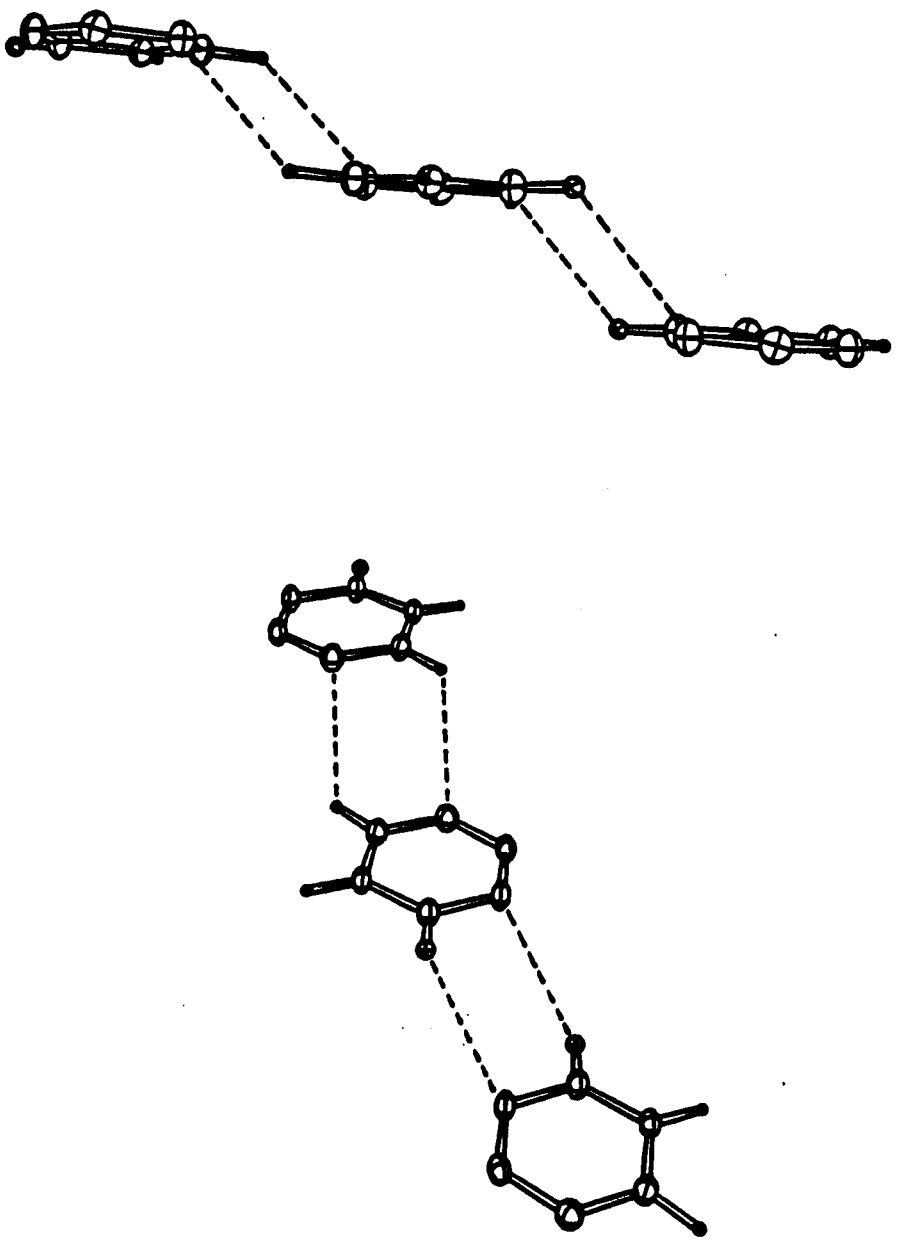

Figure III.1d. View of hydrogen bonding for 1,2,3-triazine

are the correct ones to use. This is unique to the promolecule model used and stems from the HF atoms being more diffuse. Upon chemical bonding the electron density itself becomes more delocalized over the molecular region and thus an atom which is more diffuse will be able to model the chemical bonding better. This argument is born out by Table III.7b where R_w in the high-order (core electron) regions are actually lower for the Trial 1 promolecule.

High-Order Cutoff

The next step is to determine the high-order data cutoff. This may be done using the Trial 1 structure. The procedure calls for the bond and lone pair electron density peak heights to be plotted versus the $\sin(\theta)/\lambda$ maximum. The peaks heights for all peaks (including atoms) should increase as one increases the cutoff. By finding a point on the plot above which the bond or lone pair electron density peak height is not changing, one locates the lower $\sin(\theta)/\lambda$ value for a high-order refinement. In this high-order data region only the core electrons contribute significantly to the structure factors (this is approximately true for both the experimental structure and the promolecule model).

As shown Figure III.2 there is no such point for this dataset. This means that the resolution is too low and a decoupling of the core electrons from the none-core electrons is not completely possible. In this work a high-order cutoff

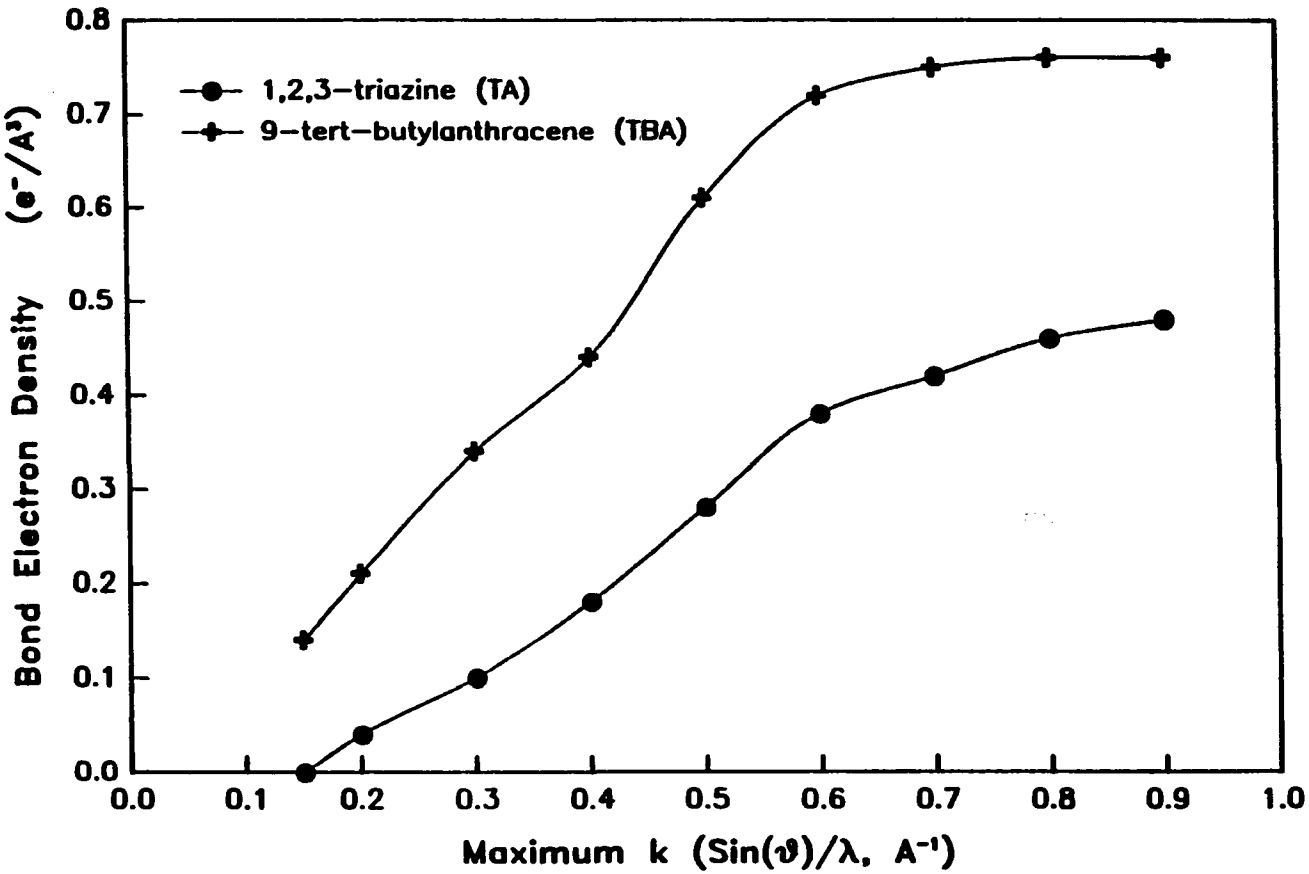

Figure III.2. Plot of bond peak height versus sin(θ)/λ maximum for 1,2,3-triazine and 9-tert-butylanthracene

was chosen as being $\sin(\theta)/\lambda=0.70\text{Å}^{-1}$ and it is assumed that the bonding and lone pair electron density will not greatly influence the X-type parameters obtained from a high-order refinement. This cutoff yielded a data/variable ratio of 73 for the high-order refinement of the X-type parameters.

High-Order Refinement

Trials 3 and 4 are the structures resulting from a high-order, spherical-atom refinement using SCF and HF values respectively. The hydrogen parameters were obtained from a refinement against all data. This was necessary since the thermal parameters became negative when only high-order data were used (this is generally true, independent of the data quality, since the hydrogen atoms' loosely bound electron will not contribute significantly to the total scattering at high angles in any structure).

Comparing the results of Trials 3 and 4 one sees little differences in the positional parameters, the interatomic distances, and the bond angles. The thermal parameters however decreased for the carbons and nitrogens and increased for the hydrogens. The hydrogen atoms may again be explained as a compensation for errors.

The carbon and nitrogen atoms' thermal factor increase is explained by examining the combination of the scale factor and the thermal parameters. Taking the high-order range to be from 0.7 to 0.9 with an average of 0.8 we find that the

the ratio of the scattering factor values for carbon at 0.8 is 1.367(SCF)/1.323(HF)=1.03. From the scale factor ratio (5.29(HF)/5.19(SCF)=1.02) we see that the scale factor difference is a compensation for the difference of the scattering factors in this range. Taking the slopes of the scattering factors in this range we find -0.985 for the SCF carbon scattering factors and -1.036 for the HF scattering factors. Thus the temperature factors are expected to be larger. One might also argue that, since the SCF atoms' core regions are more localized, they would be expected to have larger vibrations.

High-Order Versus Standard Refinement

Trials 1 and 3 permit a comparison of parameters obtained by standard refinement with those from a high-order refinement. As seen in Tables III.4a and III.4b there are few systematic differences in the positional and average vibrational parameters. Table III.4c shows that the SCF atoms have larger values of U_{22}, U_{13}, and U_{23}. The off-diagonal components are mainly directional in nature. The larger U_{22} term indicates that the vibrations are greater in the b^* direction, which is approximately perpendicular to the molecular plane.

The bond distances are slightly shorter for the SCF values and no tendencies are noted for the bond angles. One of the main reasons behind a high-order refinement is to

obtain more accurate parameters. Table III.6a reveals little change which reflects the fact that the electronic environment around the atomic positions is fairly symmetric. The p-π orbitals balance themselves above and below the molecular plane, and the bonding and lone pair electrons balance each other within the molecular plane. Thus the standard refinement does produce reasonably accurate positional information in this case.

The average rms amplitudes of vibration for Trial 1 are similar to those for Trial 3; this is unexpected but can again be attributed to the scale factor compensating for errors in the Trial 1 structure.

Analysis of the residuals in Tables III.7 points out the problem of indiscriminate use of the residuals. The R_w(ALL) value being lower for Trial 1 has no meaning since it is from a conceptually incorrect model. A more accurate measure of the model's quality can be obtained by comparing R_w in the high-order range. It is seen in Table III.7b that R_w in the $\sin(\theta)/\lambda$ range of [0.7,0.9) is lower for Trial 3. This indicates that Trial 3 has more accurate X-type parameters (which are the main contributors at high angles).

Valence Orbital Refinement

Using the structure from Trial 3 as a starting point, the valence (p) orbitals were refined in Trial 5. The refinement procedure alternated between high-order refinement of the X-type parameters and refinement of the Y-type parameters using all the data. Valence information includes the orbital occupancies and the "orientation" of the p-orbitals. A summary of the valence orbital information is given in Tables III.9.

Figures III.3 reveal the directions to which the orbitals refine. The valence shells tend to have a single orientation relative to the atoms. One orbital type is tangential to the ring and models the ring σ-bonding. The sum of this type of orbital has roughly the same shape as that of the ring. The second type is radially oriented to the ring and models the lone pair or hydrogen bond electron density. The third orbital models the p-π orbital and lies perpendicular to the molecular plane. Maps of these three orbital types, weighted by their electron occupancies, as well as there sum are given in Figures III.4.

An examination of these maps reveals that the individual valence orbitals as well as their sum roughly approximate the chemical C_2 axis. This, and the fact that at least one of the lobes on each orbital accounts for parts of the bonding or lone pair density, indicates that the results from this fit are physically meaningful.

In Tables III.9 the three orbital types correspond to: 1) Y_1(N1), Y_1(N2), Y_3(N3), Y_2(C1), Y_2(C2), and Y_2(C3), 2) Y_2(N1), Y_3(N2), Y_2(N3), Y_3(C1), Y_3(C2), and Y_3(C3), 3) Y_3(N1), Y_2(N2), Y_1(N3), Y_1(C1), Y_1(C2), and Y_1(C3). Table III.9f shows the Trial 5 orbitals rotated to a local atomic coordinate systems. It is interesting to note that the type 3 orbitals (modeling the p-π) have lower occupancies than do the other types, the type 2 carbons are consistently lower than the type 2 nitrogen orbitals, and all type 1 orbitals are approximately equal. This internal consistency is an indication of the reasonable quality of the results.

Since the core electron scattering can not be totally disassociated from the deformation density scattering in this case, the X-type parameters were refined again after the orbitals were oriented. This allows one to account for as much of the deformation density (the valence part) as possible without going to a molecular model (a quick check indicated that the valence electrons contributed about 2% of the total scattering in the $\sin(\theta)/\lambda$ range [0.7,0.8)).

Comparing the new high-order refinement X-type parameters with those of Trial 4 (whose structure consisted of spherically averaged atoms) shows little difference between the non-hydrogen coordinates and the rms amplitudes of vibration. The U_{22}, U_{13}, and U_{23} components of the anisotropic thermal parameters are systematically larger for Trial 5. This again indicates a larger vibrational motion

Table III.9a. Trial 5 orbital parameters[a] for 1,2,3-triazine

Atom	i	λ_i[b]	$U(p_x,i)$	$U(p_y,i)$	$U(p_z,i)$	Δe_i[c]
N1	1	1.088	0.853	0.490	0.179	0.09
	2	1.463	0.166	-0.580	0.798	0.46
	3	0.449	0.494	-0.651	-0.576	-0.55
N2	1	1.034	-0.757	0.415	-0.506	0.03
	2	0.595	-0.109	0.683	0.722	-0.40
	3	1.371	0.645	0.601	-0.472	0.37
N3	1	0.546	-0.189	0.697	0.691	-0.45
	2	1.442	0.370	-0.602	0.708	0.44
	3	1.012	0.910	0.389	-0.144	0.01
C1	1	0.309	-0.133	0.779	0.612	-0.36
	2	0.954	0.414	-0.517	0.749	0.29
	3	0.737	0.900	0.353	-0.254	0.07
C2	1	0.309	-0.275	0.688	0.672	-0.36
	2	1.103	0.325	-0.591	0.738	0.44
	3	0.589	0.905	0.421	-0.061	-0.08
C3	1	0.108	-0.184	0.812	0.553	-0.56
	2	1.185	-0.201	-0.582	0.788	0.52
	3	0.707	0.962	0.034	0.270	0.04

[a] $\Psi_i = U(p_x,i)*(p_x) + U(p_y,i)*(p_y) + U(p_z,i)*(p_z)$ and $\rho(\text{valence}) = \Sigma_i \lambda_i \Psi_i^2$.

[b] Standard deviations for the orbital occupancies are ca. $5*10^{-2}$.

[c] Number of electrons gained relative to the spherical atom's orbitals.

Table III.9b. Trial 6 orbital parameters for 1,2,3-triazine

Atom	i	λ_i	$U(p_x,i)$	$U(p_y,i)$	$U(p_z,i)$	Δe_i
N1	1	1.000	0.532	0.796	0.290	0.00
	2	1.478	0.280	-0.488	0.827	0.48
	3	0.522	0.799	-0.358	-0.483	-0.48
N2	1	0.987	-0.611	0.497	-0.617	-0.01
	2	0.737	-0.232	0.632	0.739	-0.26
	3	1.276	0.757	0.595	-0.271	0.28
N3	1	0.974	0.707	0.687	0.167	-0.03
	2	1.410	0.380	-0.568	0.730	0.41
	3	0.616	0.596	-0.453	-0.663	-0.38
C1	1	0.448	0.029	0.859	0.512	-0.22
	2	0.633	-0.761	-0.313	0.569	-0.03
	3	0.919	0.648	-0.406	0.644	0.25
C2	1	0.940	-0.407	0.580	-0.705	0.27
	2	0.715	0.474	0.794	0.379	0.05
	3	0.345	0.780	-0.180	-0.599	-0.32
C3	1	0.165	-0.428	0.817	0.386	-0.50
	2	1.176	-0.388	-0.552	0.738	0.51
	3	0.659	0.816	0.166	0.553	-0.01

Table III.9c. Trial 7 orbital parameters for 1,2,3-triazine

Atom	i	λ_i	$U(p_x,i)$	$U(p_y,i)$	$U(p_z,i)$	Net[a]	Δe_i^-
N1	1	0.897	0.808	0.576	0.128	-0.31	-0.10
	2	1.360	0.267	-0.550	0.791		0.36
	3	0.437	0.526	-0.605	-0.598		-0.56
N2	1	0.846	-0.665	0.404	-0.629	-0.31	-0.15
	2	0.595	-0.237	0.684	0.690		-0.41
	3	1.251	0.708	0.608	-0.359		0.25
N3	1	0.489	-0.339	0.646	0.684	-0.42	-0.51
	2	1.273	0.344	-0.592	0.729		0.27
	3	0.822	0.876	0.482	-0.022		-0.18
C1	1	0.212	-0.157	0.788	0.595	-0.51	-0.45
	2	0.768	0.628	-0.385	0.676		0.10
	3	0.515	0.762	0.480	-0.434		-0.15
C2	1	0.267	-0.507	0.524	0.684	-0.24	-0.40
	2	1.053	0.339	-0.609	0.717		0.39
	3	0.443	0.793	0.596	0.131		-0.22
C3	1	0.000	-0.255	0.797	0.548	-0.59	-0.67
	2	0.939	-0.207	-0.598	0.774		0.27
	3	0.472	0.944	0.084	0.318		-0.19

[a]Net number of electrons gained from neutral atom's number of electrons.

Table III.9d. Trial 8 orbital parameters for 1,2,3-triazine

Atom	i	λ_i	$U(p_x,i)$	$U(p_y,i)$	$U(p_z,i)$	Δe_i^-
N1	1	1.489	0.203	0.837	0.508	0.49
	2	1.281	0.137	-0.538	0.832	0.28
	3	0.229	0.969	-0.099	-0.224	-0.77
N2	1	1.337	-0.178	0.876	0.448	0.34
	2	0.636	0.590	-0.270	0.761	-0.36
	3	1.027	0.788	0.400	-0.468	0.03
N3	1	0.426	-0.790	-0.243	0.562	-0.57
	2	1.338	0.280	-0.960	-0.021	0.34
	3	1.236	0.545	0.141	0.827	0.24
C1	1	0.568	-0.733	0.490	0.472	-0.10
	2	0.683	0.113	-0.596	0.795	0.02
	3	0.749	0.671	0.636	0.381	0.08
C2	1	0.344	-0.811	0.567	0.143	-0.32
	2	0.640	-0.171	-0.463	0.870	-0.03
	3	1.016	0.559	0.681	0.473	0.35
C3	1	0.289	-0.627	0.752	0.204	-0.38
	2	0.894	0.021	-0.245	0.969	0.23
	3	0.817	0.778	0.612	0.138	0.15

Table III.9e. Trial 9 orbital parameters for 1,2,3-triazine

Atom	i	λ_i	$U(p_x,i)$	$U(p_y,i)$	$U(p_z,i)$	Net	Δe_i^-
N1	1	1.124	0.876	0.445	0.185	0.07	0.12
	2	1.492	0.133	-0.592	0.795		0.49
	3	0.450	0.463	-0.672	-0.578		-0.55
N2	1	1.014	-0.737	0.403	-0.542	0.02	0.01
	2	0.598	-0.136	0.697	0.704		-0.40
	3	1.406	0.662	0.593	-0.459		0.41
N3	1	0.536	-0.192	0.697	0.691	-0.02	-0.46
	2	1.435	0.373	-0.599	0.708		0.43
	3	1.011	0.908	0.394	-0.145		0.01
C1	1	0.299	-0.143	0.787	0.600	-0.03	-0.37
	2	0.936	0.372	-0.519	0.769		0.27
	3	0.736	0.917	0.333	-0.218		0.07
C2	1	0.307	-0.185	0.727	0.661	0.05	-0.36
	2	1.142	0.309	-0.596	0.741		0.48
	3	0.603	0.933	0.341	-0.115		-0.06
C3	1	0.117	-0.166	0.806	0.568	-0.09	-0.55
	2	1.125	-0.131	-0.589	0.797		0.46
	3	0.670	0.977	0.058	0.203		0.00

Table III.9f. Trial 5 orbital parameters for 1,2,3-triazine. Rotated[a] to local coordinate system and sorted according to type

Atom	i	λ_i	a[b]	b	c
N1	1	1.088	0.552	0.252	-0.795
	2	1.463	0.034	-0.959	-0.281
	3	0.449	-0.833	0.128	-0.538
N2	1	1.034	-0.026	-0.413	0.910
	2	1.371	0.240	0.882	0.407
	3	0.595	0.971	-0.229	-0.076
N3	1	1.012	0.278	0.525	0.805
	2	1.442	-0.033	0.842	-0.538
	3	0.546	0.960	-0.123	-0.251
C1	1	0.954	0.061	0.881	0.470
	2	0.737	0.183	-0.473	0.862
	3	0.309	0.981	0.033	-0.190
C2	1	1.103	-0.002	0.044	0.999
	2	0.589	0.344	-0.938	0.042
	3	0.309	0.939	0.344	-0.013
C3	1	1.185	0.007	-0.420	0.907
	2	0.707	0.256	-0.876	-0.408
	3	0.108	0.967	0.235	0.102

[a]The actual signs of the orbital direction vectors may be changed without affecting the interpretation.

[b]The local reference system consists of a) perpendicular to the molecular plane, b) radially outward from the center, and c) tangential to the ring.

Table III.10. Comparisons of trials for 1,2,3-triazine. Angles between wavefunctions (Ψ_i)

Atom	i	5:6	5:7	5:8	5:9
N1	1	26.45	6.30	47.61	2.89
	2	8.57	6.06	3.47	2.01
	3	25.00	3.45	47.70	2.15
N2	1	11.52	8.82	74.26	2.46
	2	7.74	7.62	72.43	2.08
	3	13.22	7.44	14.19	1.30
N3	1	62.55	9.09	68.38	0.11
	2	2.36	1.98	48.20	0.13
	3	62.49	9.03	64.46	0.30
C1	1	11.88	1.76	39.76	0.98
	2	74.17	15.02	18.09	2.69
	3	73.92	14.94	42.93	2.51
C2	1	87.87	16.35	44.85	5.66
	2	92.04	1.77	30.62	0.94
	3	48.18	16.25	40.18	5.73
C3	1	16.99	4.17	32.98	1.42
	2	11.26	1.26	25.57	4.04
	3	19.84	4.07	36.18	4.15

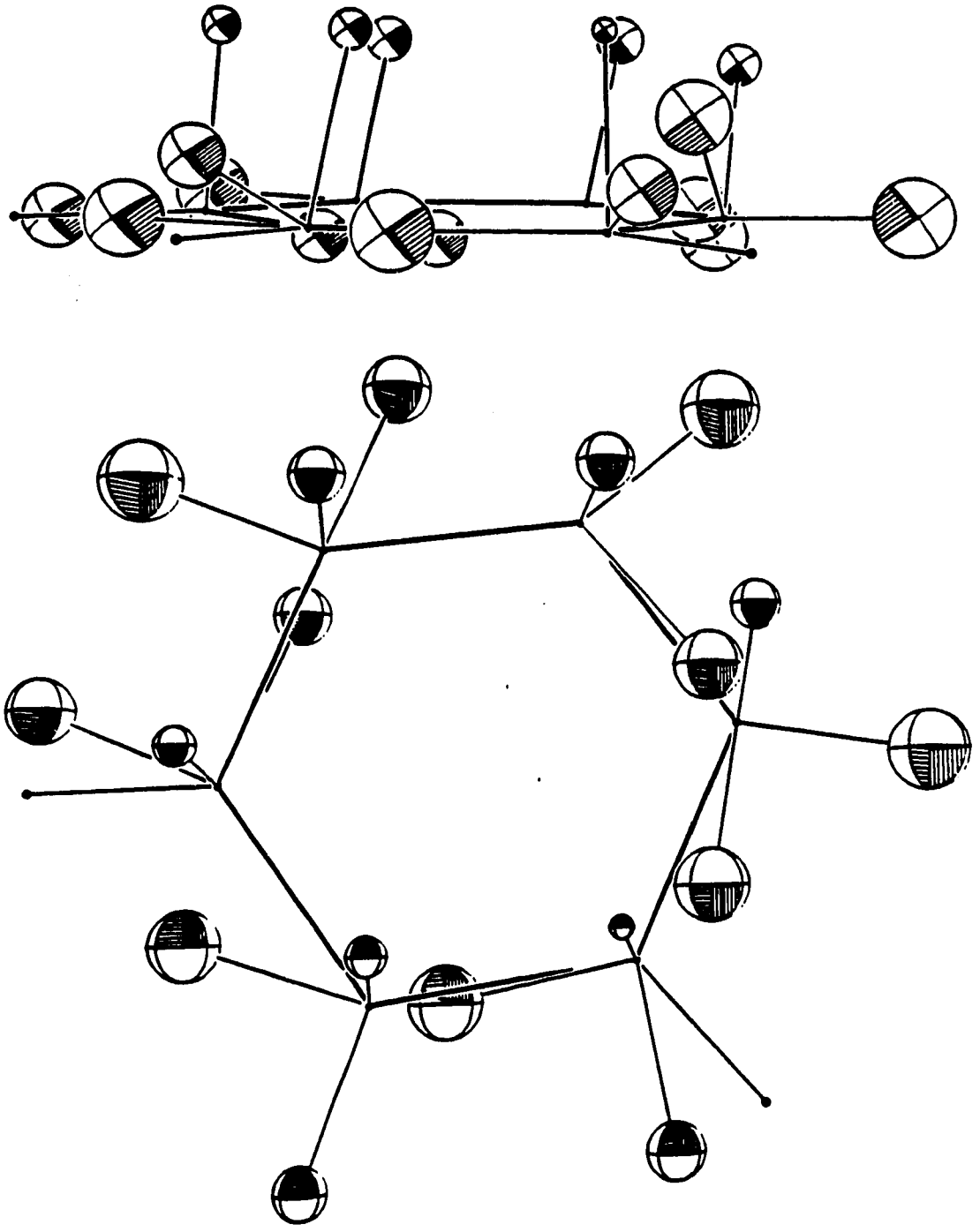

Figure III.3a. Orbital direction vectors superimposed on promolecule drawing. Cl is on the left

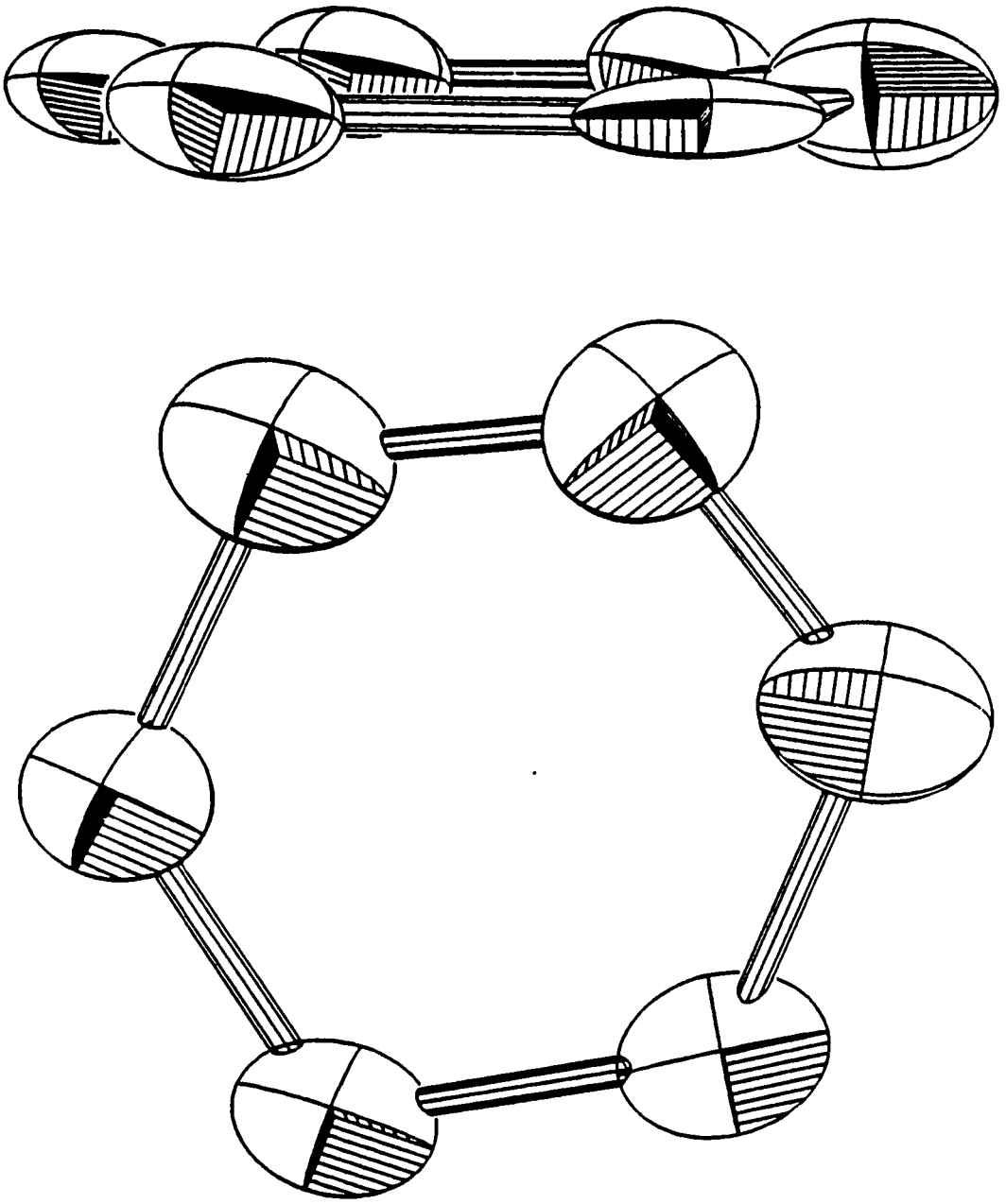

Figure III.3b. Ellipsoids representing valence orbital information. Principal axes correspond to electron occupation and have the same direction as the orbitals. Orientation identical to that of Figure III.3a

perpendicular to the molecular plane. In view of similar results obtained in the comparison of Trial 3 and Trial 1 it may be taken as a trend toward a more vibrationally-correct model. But one must also question whether this is possibly a compensation for the low p-π type orbital electron occupancies or perhaps a systematic error in the data or the weighting scheme.

Conceptually the approach taken for Trials 3 and 5 are correct. Examination of Table III.7a reveals that, for the few reflections available, the 0k0 zone has larger residuals for all trial structures. The Trial 3 value of R_w is 0.397 whereas the value of R is 0.059. This is a direct indication that the weighting scheme is faulty. This direction is also the unique direction (similar to a cylinder axis) relative to the molecule and the intensities should be largest along this reciprocal space axis. Since R and R_w are reasonably similar as a function of $\sin(\theta)/\lambda$, it is deduced that the strong reflections are underweighted in this dataset and that the vibrations perpendicular to the molecular plane are not as large as they appear. While this will have some effect on the valence occupancies of the p-π type orbitals it is uncertain as to the magnitude of this effect.

The interatomic distances and bond angles show little variation between Trials 5 and 3. From an examination of Table III.7b it is obvious that, given similar X-type parameter values, the low angle region is modeled better by

the oriented orbitals than by the spherically averaged orbitals as would be expected.

Figure III.5c is a total deformation density map (TDD) which was obtained by subtracting the spherical-atom promolecule (Trial 3) from the observed electron density. Here the bonding electron density is centered between the atoms and the lone pair density is directed radially outward from the molecule's center. There is considerable deviation from two-fold symmetry around the N2 and C2 atoms. The deformation density is also fairly pronounced.

Figure III.5d is a chemical deformation density map (CDD) which was obtained by subtracting the oriented valence orbital atom promolecule (Trial 5) from the observed electron density. The features are generally less pronounced and the chemical two-fold axis more easily seen. The non-hydrogen bond peak centers are more uniform in height and are located inside of the internuclear vectors. This may be interpreted as a type of strain induced by the formation of the sigma bonds which is approximately the same for all atoms (actually slightly lower for the two N-N bonds).

From the bond peak heights and their areas, one may estimate that the C-C bonds have the most electrons, the C-N bonds somewhat less, and the N-N bonds the least. This is in accord with theoretical calculations[42] on similar nitrogen heterobenzenes which show that the bond charge increases as one moves away from the nitrogen atoms.

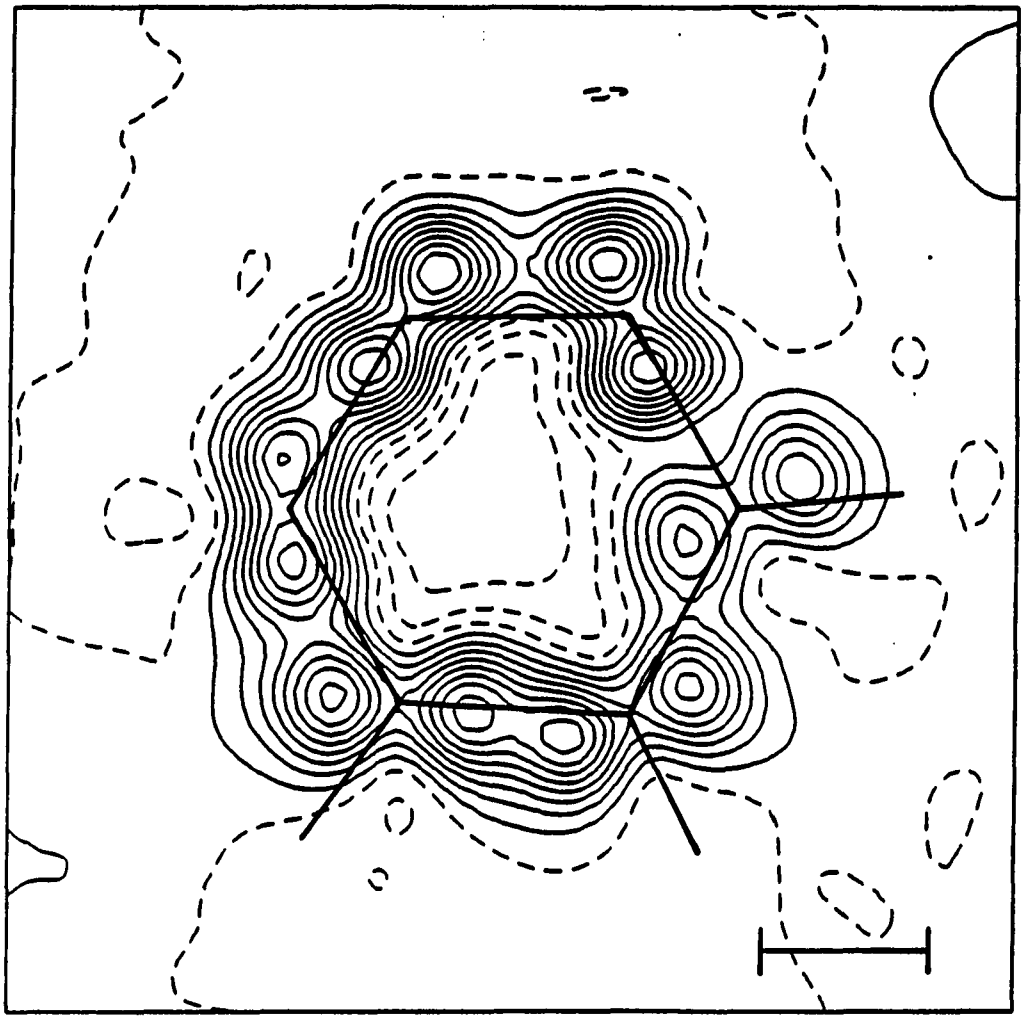

Figure III.4a. Map of the calculated ring type (type 1) p-orbitals for Trial 5 in 1,2,3-triazine. CI=0.1e$^-$/Å^3

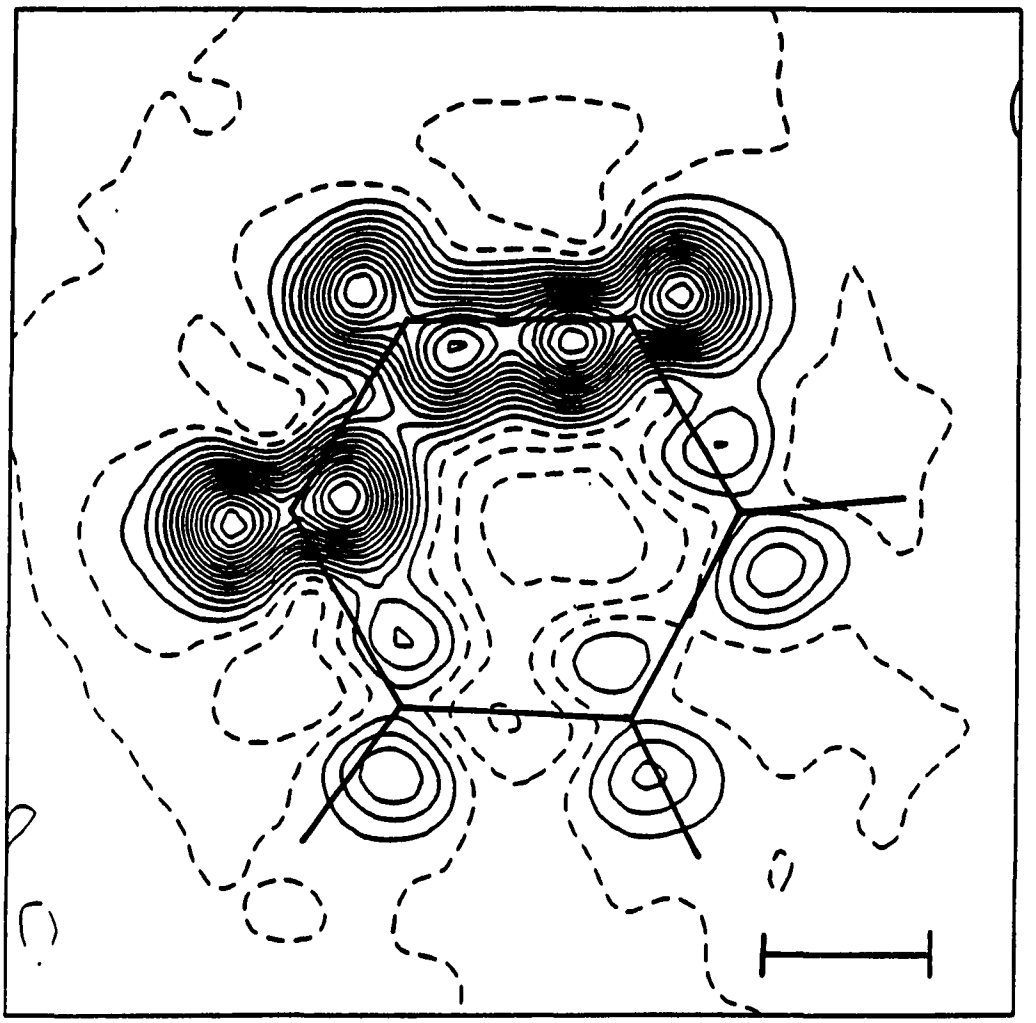

Figure III.4b. Lone pair type (type 2) orbitals. Similar to Figure III.4a

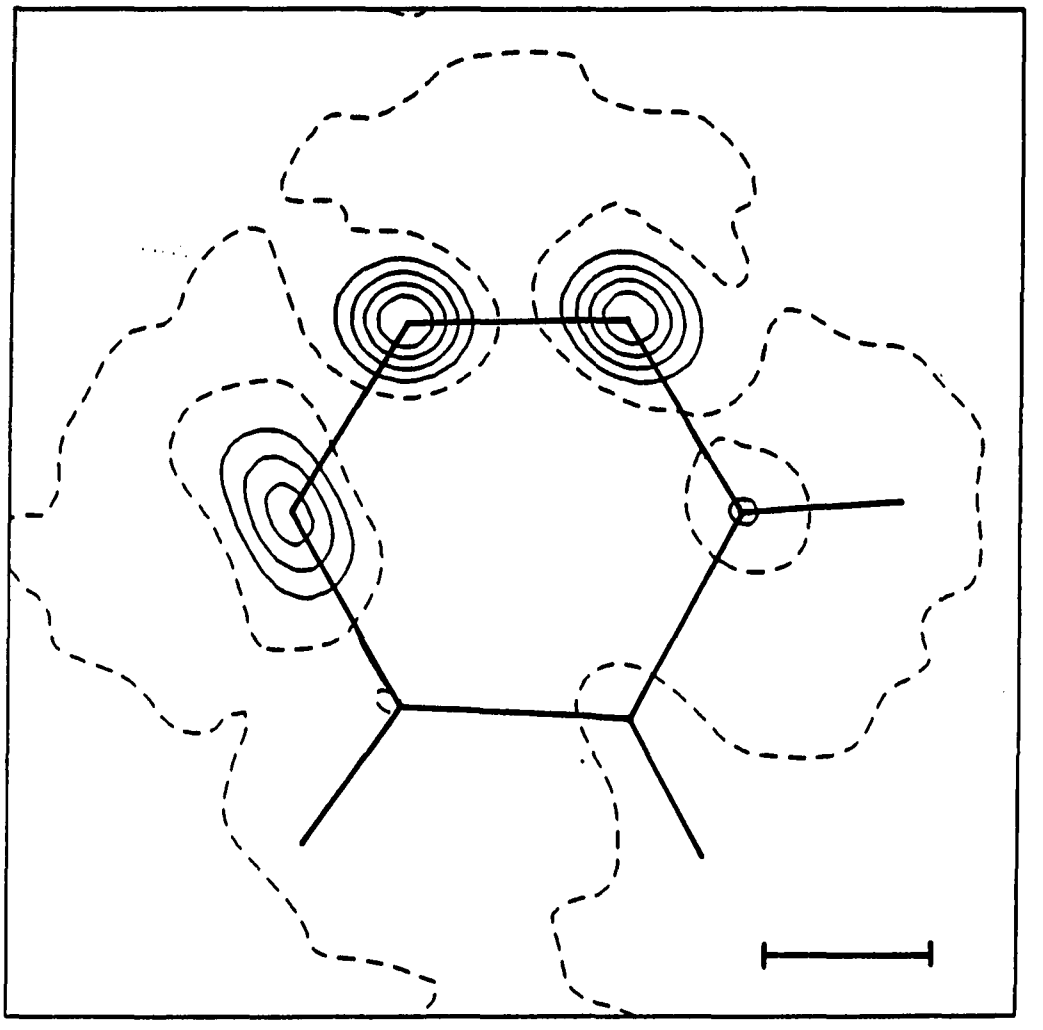

Figure III.4c. p-π type (type 3) orbitals. Similar to Figure III.4a

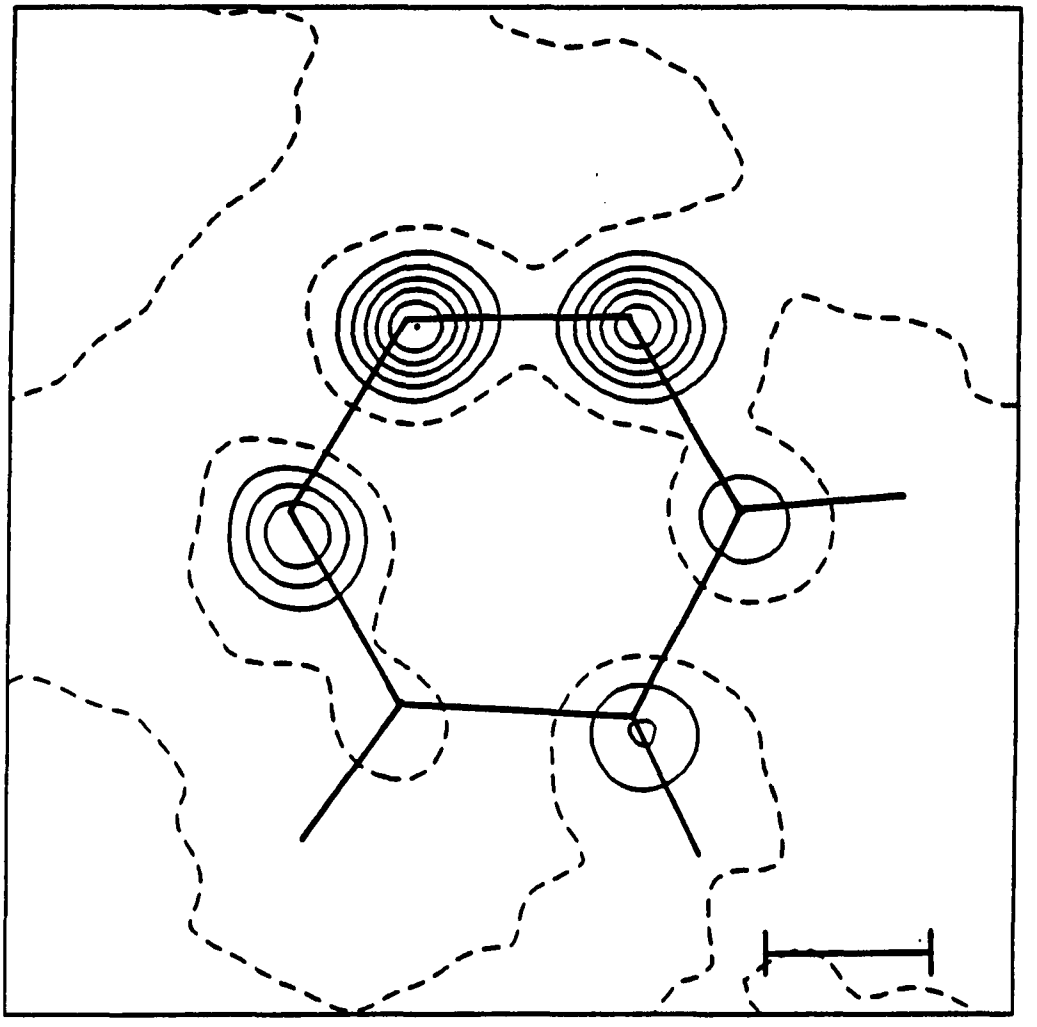

Figure III.4d. 0.4Å above the molecular plane. Similar to Figure III.4c

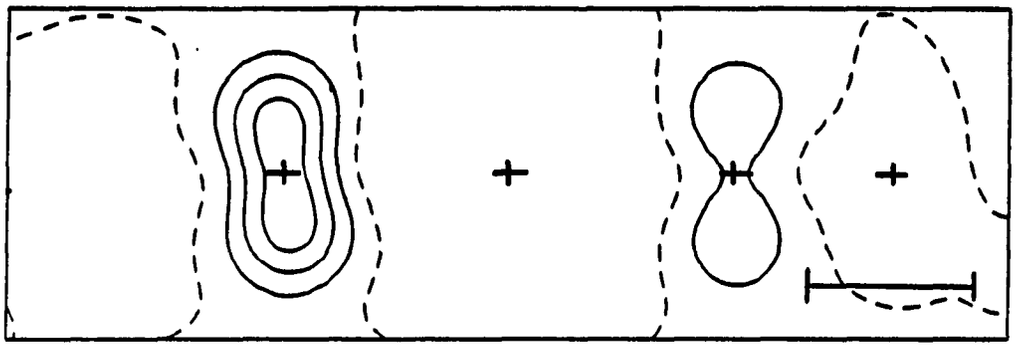

Figure III.4e. Horizontal cross-section of Figure III.4c. Crosses represent, from left to right, N1, map center, C1, and H1

Subtracting Figure III.5d from Figure III.5c yields a map (Figure III.5e) which is essentially the difference between the oriented valence density and the spherically averaged valence density. This clearly points out the regions in which the oriented orbitals do model and the spherically averaged orbitals cannot.

From Figures III.5c and 5d the argument for orienting the orbitals[18] is clearly seen. Figure III.5d is of the electron density changes which involve energy changes. The most significant features shown in Figure III.5c involves orbital orientation information which involves no energy

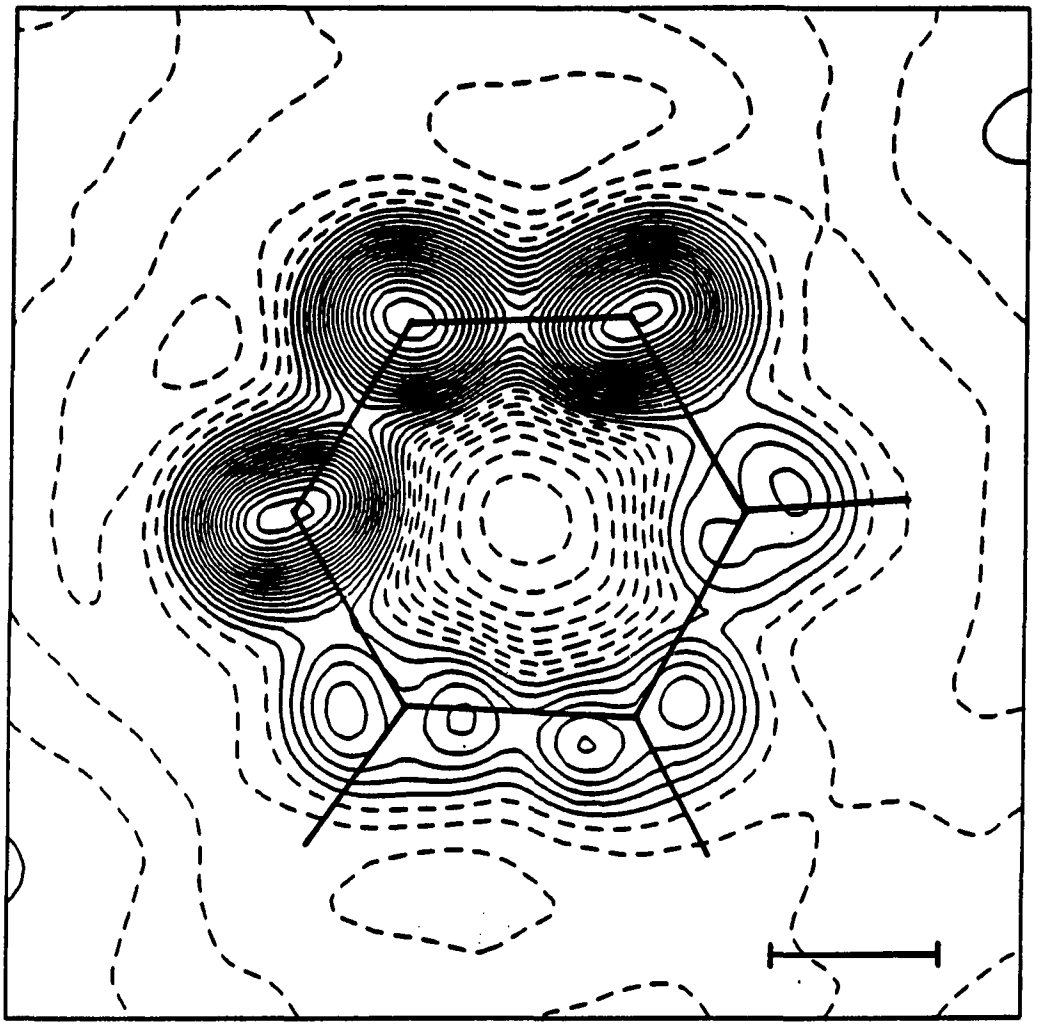

Figure III.4f. Sum of the p-orbitals. Similar to Figure III.4a

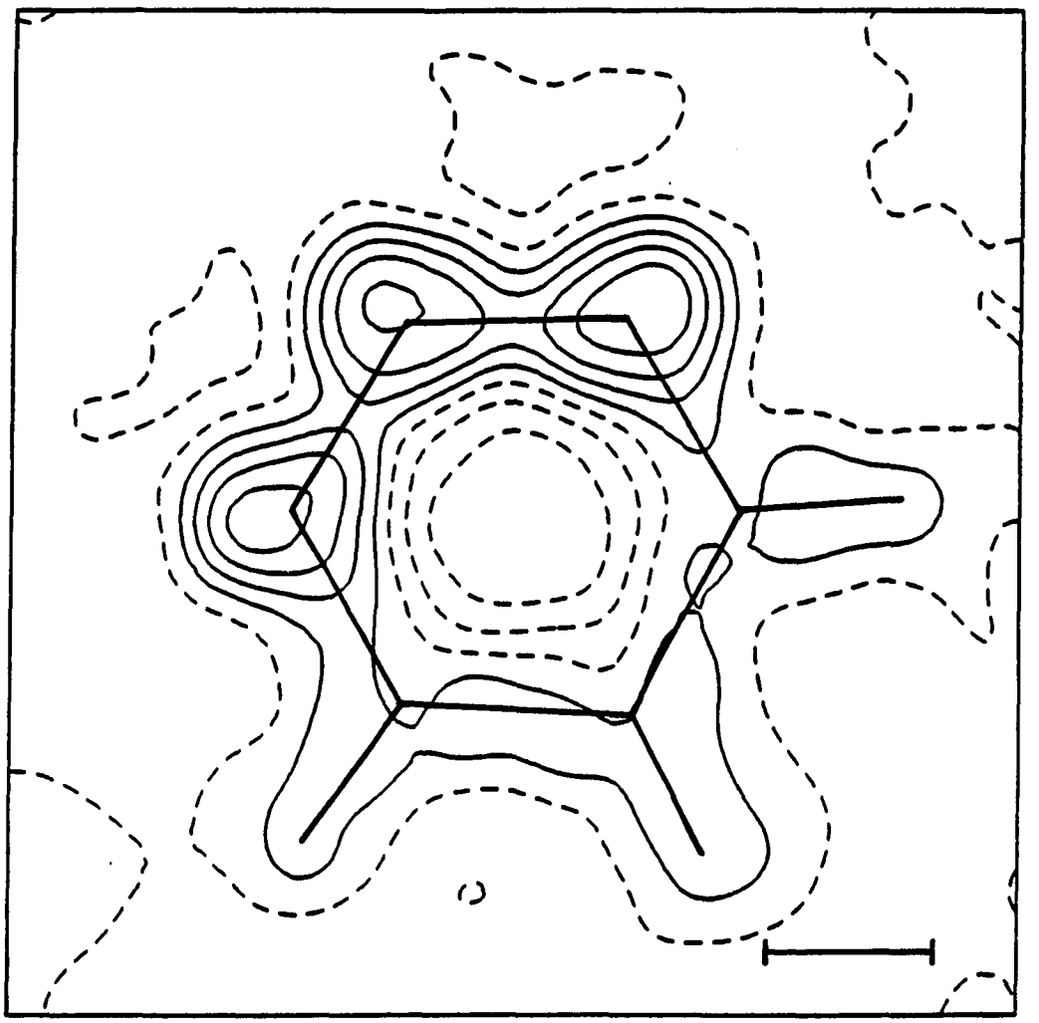

Figure III.5a. Difference density map for Trial 5. Observed density minus carbon and nitrogen 1s electrons. CI=0.5$e^-/Å^3$

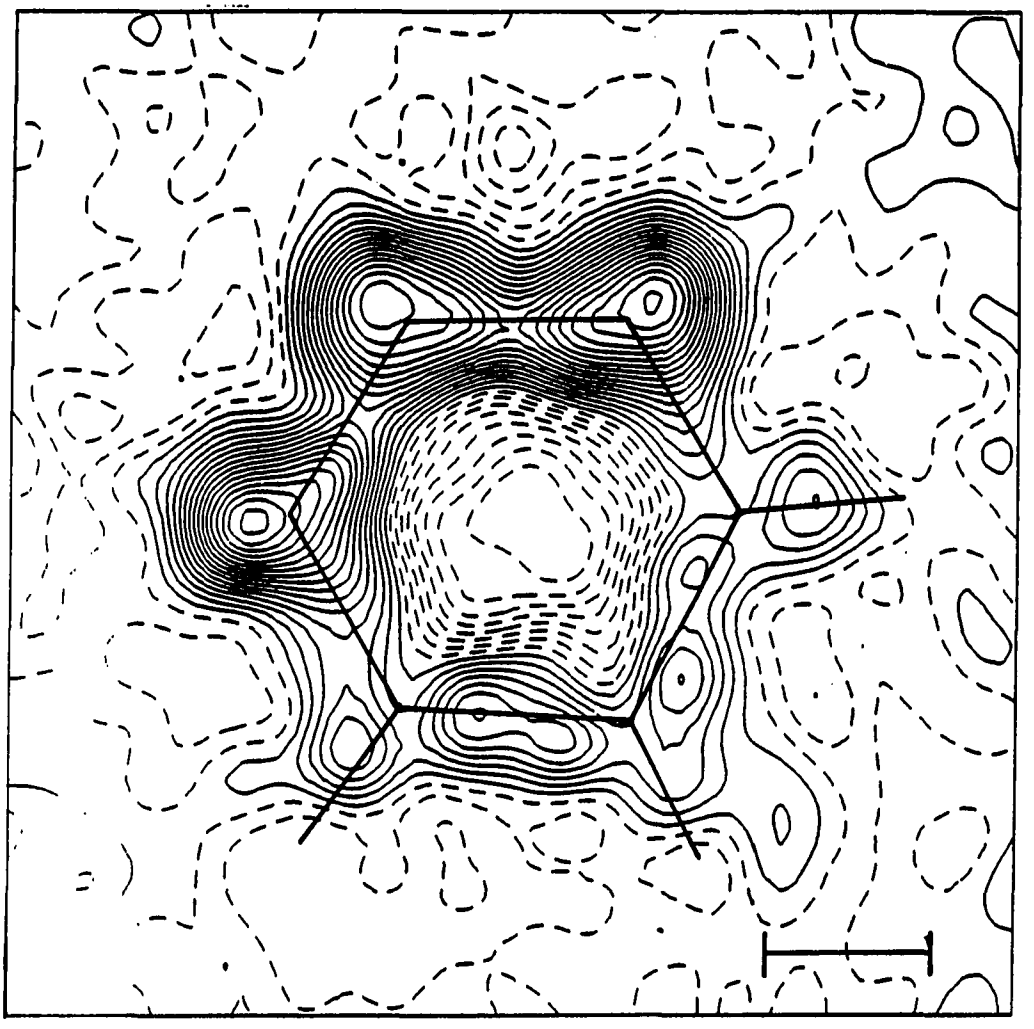

Figure III.5b. Difference density map for Trial 5. Observed density minus carbon and nitrogen 1s and 2s electrons and the hydrogen 1s electrons. CI=0.1$e^-/Å^3$

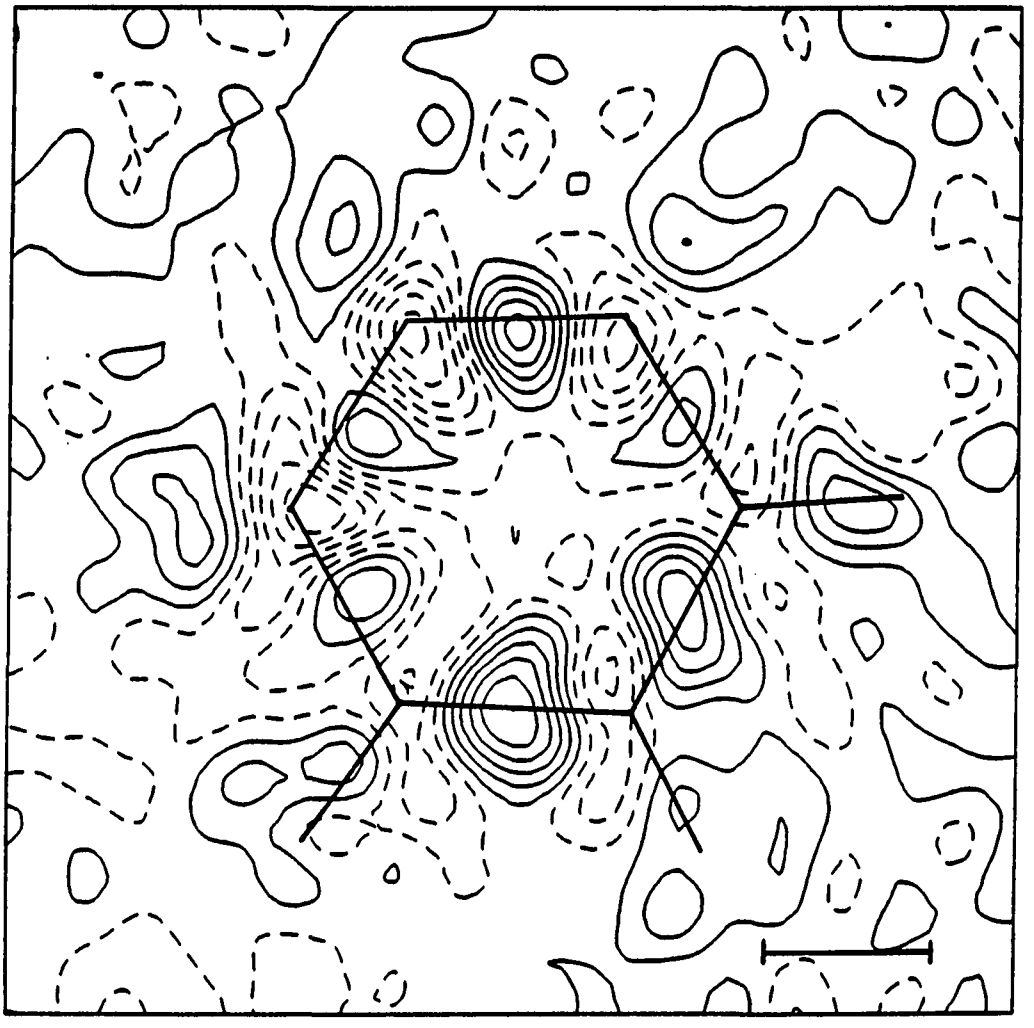

Figure III.5c. Total deformation density map for Trial 5. Observed density minus spherical-atom promolecule. CI=0.1e$^-$/Å^3

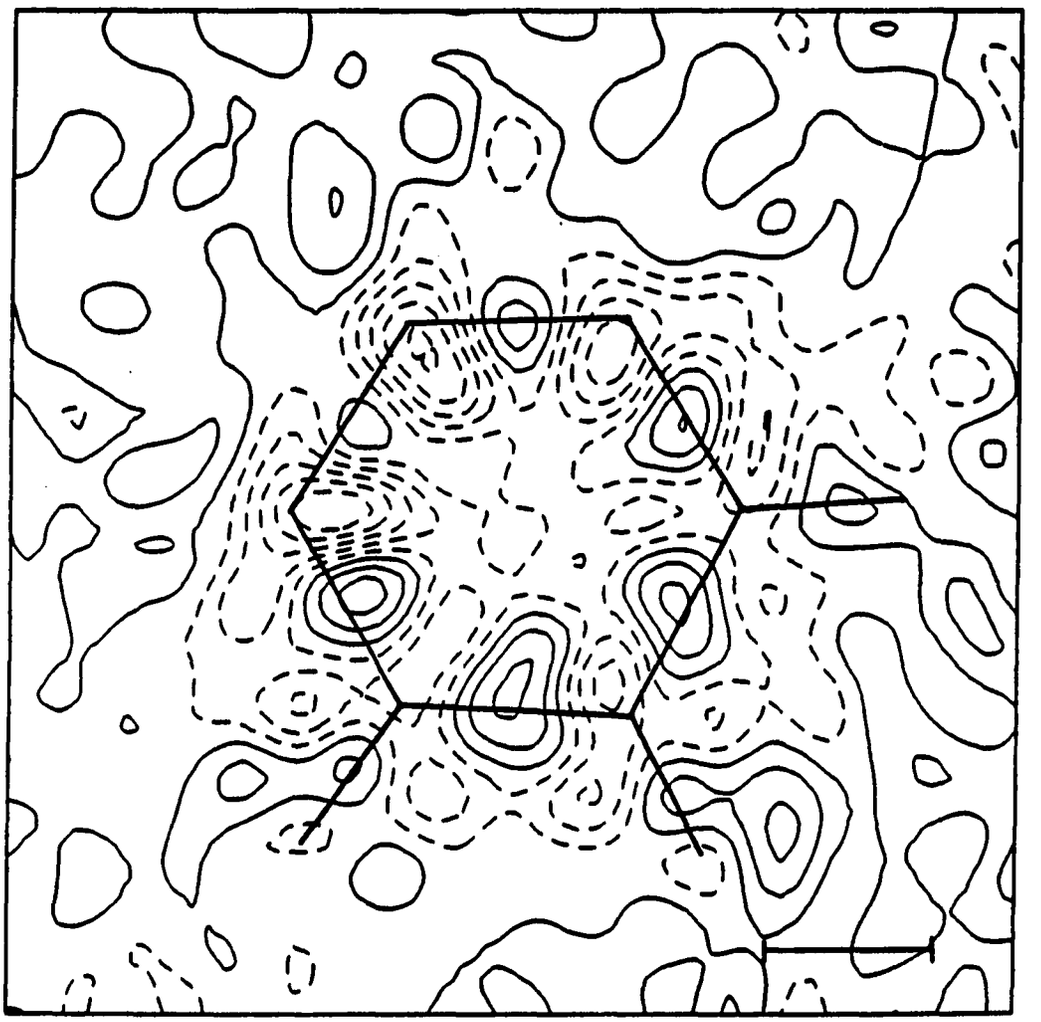

Figure III.5d. Chemical deformation density map for Trial 5. Observed density minus oriented-atom promolecule. CI=0.1e$^-$/Å^3

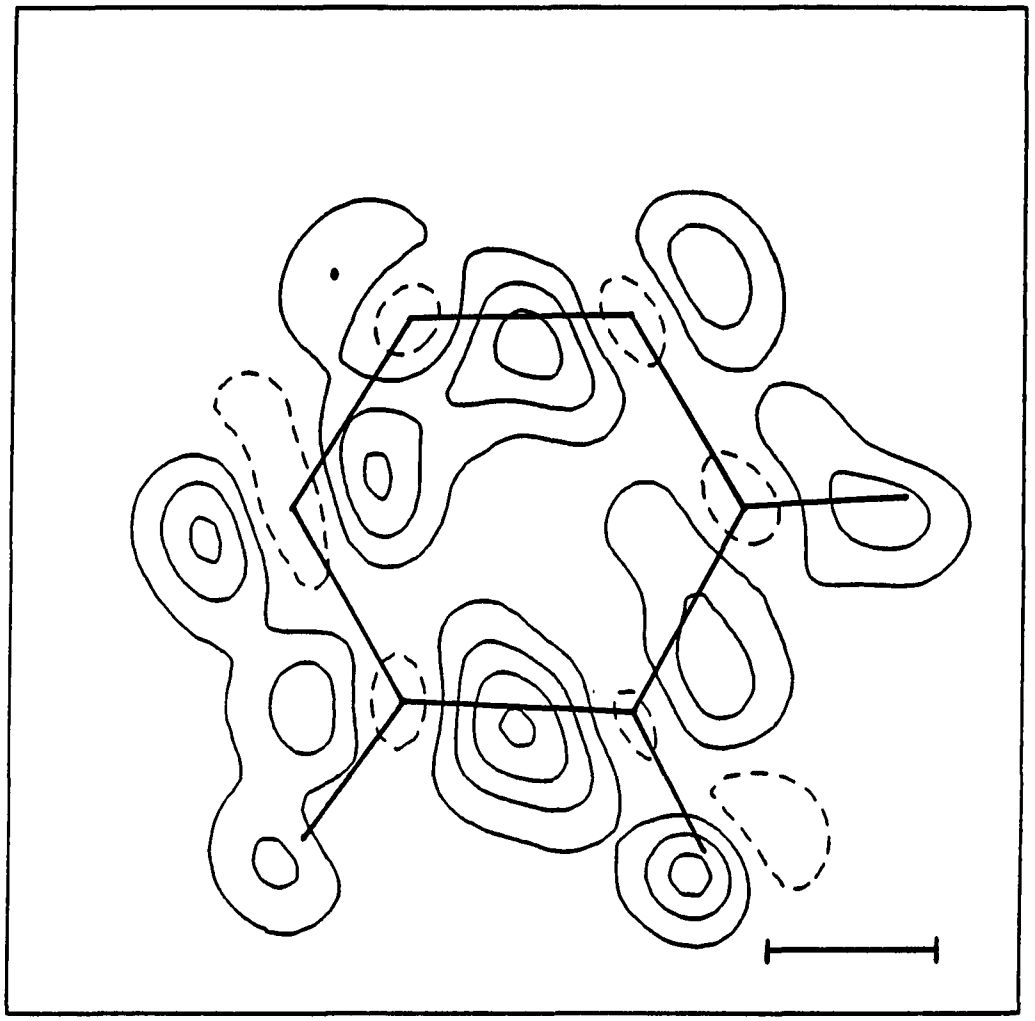

Figure III.5e. Difference between Figures III.5d and III.5c. Interpret as the electron density which is lost upon going to spherical atoms plus density changes due to atom movement

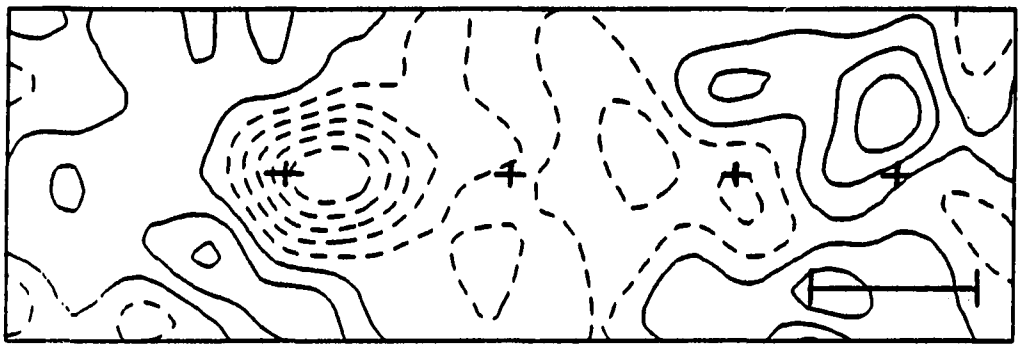

Figure III.5f. Horizontal cross-section of Figure III.4c. Crosses represent, from left to right, N1, map center, C1, and H1

change. Figure III.5c may be useful for total molecular information but does not give the insight into molecular formation (and reaction) information which is available from Figure III.5d. It is also seen, by comparing Figures III.5c and III.5d, that the electron density changes which are due to orbital orientation are twice the electron density changes which are associated with chemical changes.

By comparing the valence and deformation density shown in in Figure III.5b with the calculated valence orbitals in Figure III.4f one can see that the general features are well modeled, particularly where the peaks are at a maximum and in the regions of steep slope.

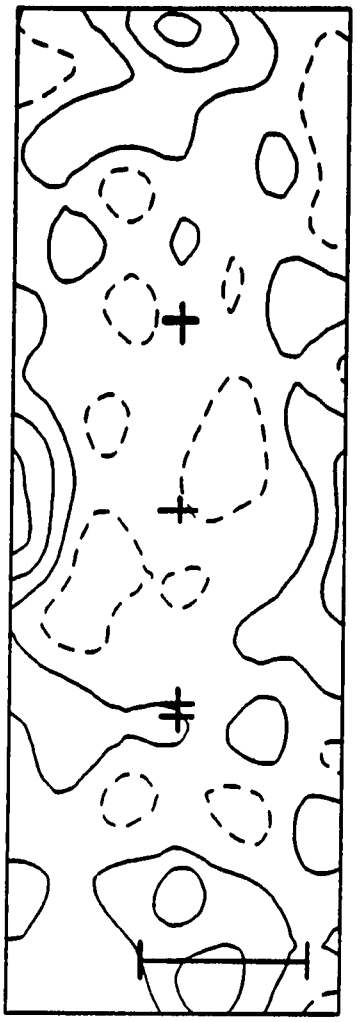

Figure III.5g. Vertical cross-section of Figure III.4c. Crosses represent the projections of, from top to bottom, N2 and N3 (indistinguishable), map center, C3, and C2

Standard and Low-Order Orbital Refinement

Given the satisfactory results from the above procedure it is of interest to attempt to obtain similar valence orbital information from a standard refinement using the total (moderate resolution) data which is available. It would also be quite useful to obtain the valence orbital information from low-order data only. Success using only low-order data would permit studies on many more compounds due to the greater number of low-order datasets which are available.

In the standard refinement (Trial 6), the X-type parameters and the Y-type parameters where refined against the entire dataset using Trial 5 as the starting point. The low-order structure (Trial 8) was obtained in an identical manner except that only data out to $\sin(\theta)/\lambda=0.6$ (a typical limit to standard datasets) were used.

The differences in the interatomic distances, atom coordinates, and rms amplitudes of vibration between Trials 5 and 6 are close to the differences between Trials 3 and 1. Analysis of these results follow the same arguments as given before. It was also of interest to see if the orbital information would be similar to that of Trial 5.

Table III.10 contains the angles between the same Y_{ia} in different structures. It is here that we see how poor the orbital orientations from Trials 6 and 8 match those from Trial 5.

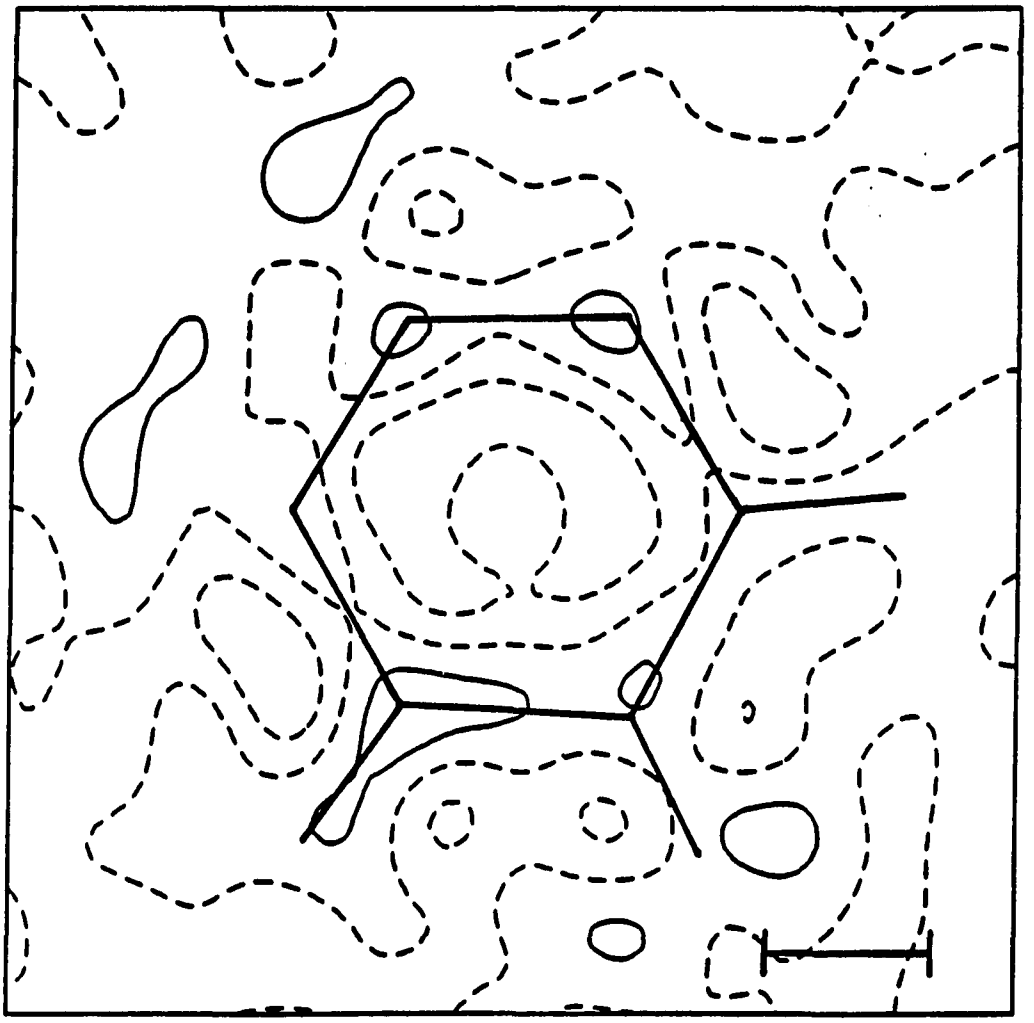

Figure III.6a. Difference density map for Trial 8. Low-order data minus promolecule. CI=0.1e$^-$/Å^3

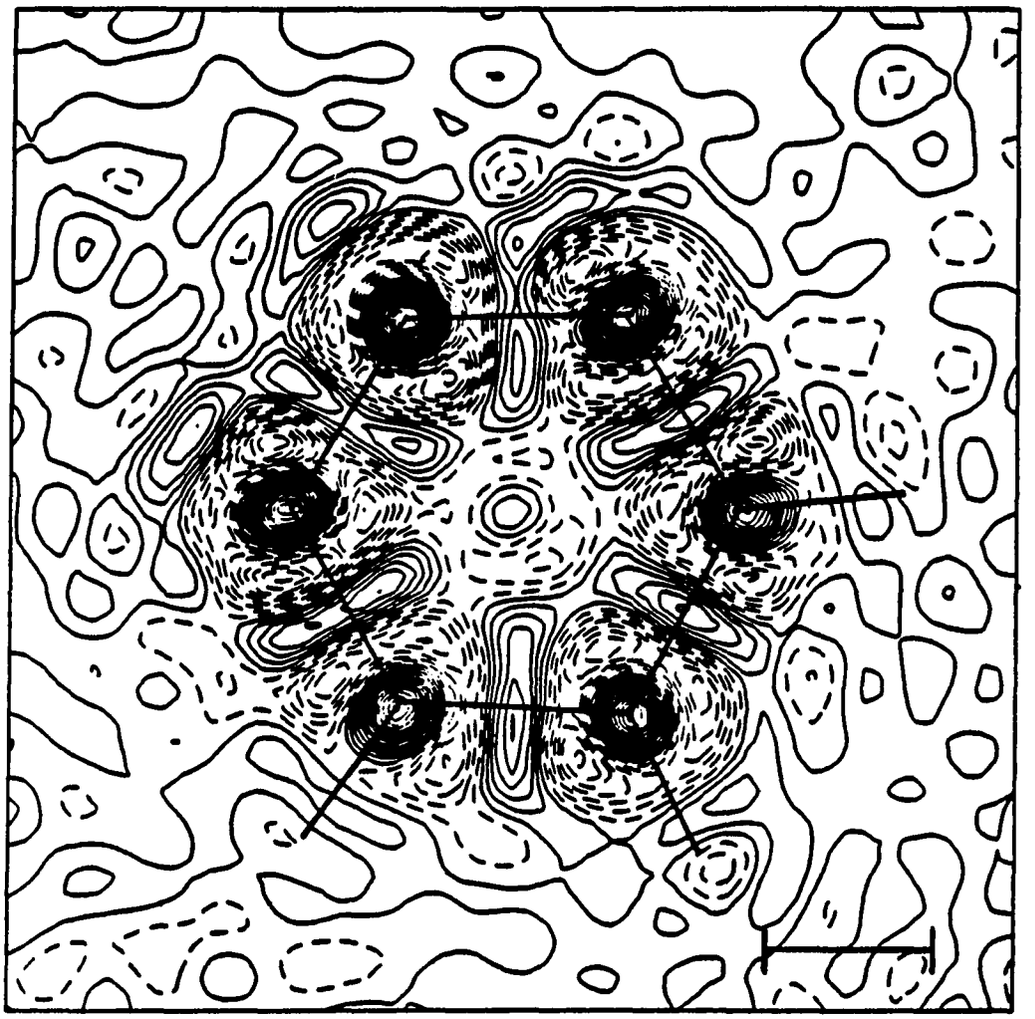

Figure III.6b. Entire data minus promolecule. Similar to Figure III.6a

It is seen that using a more accurate valence orbital model does not improve the atomic coordinates. It is concluded that using either low resolution data only or using a standard refinement on high resolution data yields incorrect results. The X-type parameters must be accurately determined before a useful orbital description can be obtained.

It is instructional to compute the difference density from Trial 8. Figure III.6a shows the difference between the low-order data and the low-order structure; it indicates that the low-order structure can model the low-order data very well. Figure III.6b is the difference between the entire dataset and the low-order model. Here we conclude that, while the low-order model fits the low-order data very well, it is an incorrect procedure which fails to accurately determine the X-type parameters. It is also proof that a low-background is not a suitable criterion for determining the data quality or the correctness of a particular promolecule.

Electron Transfer

Trial 5 is considered ultimate promolecule in that its formation involves little or no energy change. There are other chemical concepts which might be modeled which do not move the promolecule into the regime of the molecular model and may thus yield further (albeit chemical) information in

the form of the promolecule's parameters. It also follows the concept of obtaining the very best valence (non-deformation density) model which, since the data is not of high enough resolution, will allow one to obtain better X-type parameters.

By replacing the constraint that the number of electrons on each atom remains constant with the constraint that the total number of electrons in the molecule remains constant, the promolecule now embodies the concept of valence orbital electron transfer.

Trial 5 served as a starting point. By changing the constraints and alternately refining the X and Y-type parameters, the structure corresponding to Trial 9 was obtained. The net electronic charge for each atom is given in Table III.9e. These values show little change (1 to 2 standard deviations in magnitude) from the promolecule model in Trial 5. Comparisons of the parameters for Trials 5 and 9 show good agreement as would be expected.

On the basis of their electronegativities, one would predict an increase in the nitrogen atoms' net charge and a decrease in the carbon atoms' net charge. It is taken as an indicator of reasonableness that none of the atoms lost or gained a large number of electrons. On the other hand, N1 and N3 are chemically equivalent and are expected to have similar charges. Further investigations of other compounds

are necessary before the significance of these results can be properly interpreted.

Molecular Ionization

Another step towards the molecular model is to remove all constraints on the total number of electrons, allowing the valence orbitals to ionize. While this is not possible as long as one uses the incorrect procedure of fitting the scale factor to all data[43,44], it will work with this approach since the scale is more appropriately defined by the core electrons' fit to the high-order data.

Using Trial 5 as a starting point, the constraint that the number of valence electrons on each atom remain constant was removed. The X-type parameters were refined against the high-order data and the Y-type parameters were refined against the entire dataset on alternate refinement runs. Each individual orbital's occupancy behaved well, having remained in the range [0,2] without constraint. The resultant structure's (Trial 7) net atomic charges are given in Table III.9c. It is consistent from a conceptual point of view that the atoms have lost some electrons to the bonding and lone pair regions. The scale, if not accurately determined, will have the effect of adding or subtracting charge from each atom.

Discussion

For this study the data resolution was found to be lower than ideal and so a true high-order determination of the X-type parameters could not be made. Since the electron density is blurred by lowering the resolution, it is expected that the results from a higher resolution study would produce better defined results. As is seen in a comparison of Trials 5, 6, and 8, the primary effect of lowering the resolution is poorer X-type parameters. This can then have the secondary effect of causing incorrect orbital information to result.

The above argument inherently assumes, as shown in Trial 6, that the X-type parameters are obtained from a high-order refinement. Although it is an empirical relationship, it appears necessary to collect high enough resolution data in order to obtain good orbital information. The double indemnity of having only low resolution data and low accuracy parameters is amply illustrated by Trial 6 and Figures III.6.

When considering the valence electron density an interesting relationship emerges. Decreasing the temperature of a crystal during data collection causes the deformation density to sharpen and its detail to increase. As a consequence of this, the reciprocal space valence scattering functions extend out to larger values of $\sin(\theta)/\lambda$ and thus the available resolution in real space is increased. Put in another way; the more detail that exists, the more that can be seen.

The data quality in this study can be classified as moderately good. The internal agreement factor $R_{Int}(\langle I \rangle)$, a measure of random errors and other errors not based on $\sin(\theta)/\lambda$, should be at most 1 for a very good dataset intended to produce accurate quantitative results. It is difficult to check the data for systematic errors. The methods which are commonly used are based on a comparison of the observed data and the calculated data. This approach is not appropriate for the entire dataset when using a promolecule model. Only the high-order data may be properly tested and systematic errors in this range are easily compensated for by the scale and thermal parameters. There is no correct procedure of completely eliminating systematic errors from an observed dataset.

The weighting scheme used in this study was found to be less than ideal. The weights were taken as the inverse of the variance of the reflection ($\omega_k=1/\sigma^2(F)$) which are derived from the larger of $\sigma^2\langle I \rangle=\Sigma_k\ \sigma^2(I)/n^2$ or $\sigma^2\langle I \rangle=\Sigma_k\ (\langle I \rangle - I)^2/(n(n-1))$ as $\sigma^2(F)=(\sigma^2(I)+0.0004*I^2)/4I$. It is not possible to discover the source of the error without access to the original data and the algorithms for data reduction (including the absorption correction which was applied). In this case the improper weighting contributed to the thermal parameters being overly large in the direction perpendicular to the molecular plane.

The p-π (type 3) orbitals have lower occupancies compared to the other two orbital types. From a hybridization point of view one would expect sp^2 hybridization and a p-π orbital. The hybrid orbitals would be

$$h_1=1/\sqrt{3}\chi_{2s}+\sqrt{(2/3)}\chi_{2px}, \qquad \text{(III.1a)}$$

$$h_2=1/\sqrt{3}\chi_{2s}-1/\sqrt{6}\chi_{2px}+1/\sqrt{2}\chi_{2py}, \qquad \text{(III.1b)}$$

and

$$h_3=1/\sqrt{3}\chi_{2s}-1/\sqrt{6}\chi_{2px}-1/\sqrt{2}\chi_{2py}. \qquad \text{(III.1c)}$$

The total electron density is thus

$$\rho=(\chi_{1s})^2+(h_1)^2+(h_2)^2+(h_3)^2+(\chi_{2pz})^2 \qquad \text{(III.2)}$$

where there are 2 electrons in the 1s orbital, 1 in each of the hybrid orbitals, and 1 in the $2p_z$ orbital.

Using the present procedure, the 1s and 2s orbitals are considered core orbitals. Thus the direction perpendicular to the molecular plane already has roughly 2/3 of a 2s electron. The occupancy of the p_z orbital will thus be much lower than the expected value value of 1 (recall that the radial part of the 1s and 2p wavefunctions are nearly identical).

It is also true that the symmetry should be cylindrical about each atom. This is seen to be approximately true for the results obtained here by examining Figures III.3. It might be noted that the net difference between this approach and the hybridization viewpoint is that here we are lacking some of the 2s electrons. This would lead to larger than expected values for the occupancies of the p_x and p_y (types 1

and 2) orbitals.

The electron density difference maps have a ratio of deformation density peak height to bond peak height of about 0.1. This would make a high quality quantitative analysis difficult. Since the total electron density is ca. 200 times the chemical deformation density, the data need to be very accurate indeed in order to obtain good results. This is especially true for strong reflections where a relatively small percentage error will produce a very large error relative to the deformation density.

This also brings up the practice of discarding reflections which have a low signal-to-noise ratio. If the discarded reflections are not randomly distributed throughout space then a systematic effect will be seen in the deformation density.

For a molecule such as 1,2,3-triazine the reflections are strongest perpendicular to the molecular plane and thus it is most likely that these will be observed in the high $\sin(\theta)/\lambda$ region where the reflections are generally weaker, with the reflections lying in the molecular plane discarded more often.

Regardless of whether one refines on F(k) or I(k), the electron density function is derived from F(k). However the phases are unattainable directly from the observed data. The standard procedure is to transfer the phases from the model to the observed data which may then be transformed back to

real space.

In general the phases range from 0 to 2π. This adds an element of uncertainty since each has its own standard deviation. In the specific case of light-atom, centrosymmetric structures the phases may be either 0 or π, eliminating much of the uncertainty associated with the phases. It is for this reason alone that the majority of the high-accuracy studies are performed on structures which crystallize in one of the 92 centrosymmetric space groups (out of 230 possible space groups).

Since the promolecule does not accurately account for the entire molecular electron density, the phases calculated cannot be perfectly accurate. A check of the differences in phases between Trials 5 and 3 reveal that 0.4% of the reflections change phase. These reflections are generally among the weaker reflections and are dispersed evenly throughout the entire $\sin(\theta)/\lambda$ range.

One may predict that a similar finding would come from a comparison of the phases determined from Trial 5 and the true phases since the total deformation density and the chemical deformation density differ by a factor of 2.

As a test of how the phases affect the electron density maps, a difference map was calculated by transferring the phases from the promolecule without the p-orbitals to the observed data. 1.3% of the phases changed w.r.t. the phases determined by Trial 5. The resultant map (Figure III.7),

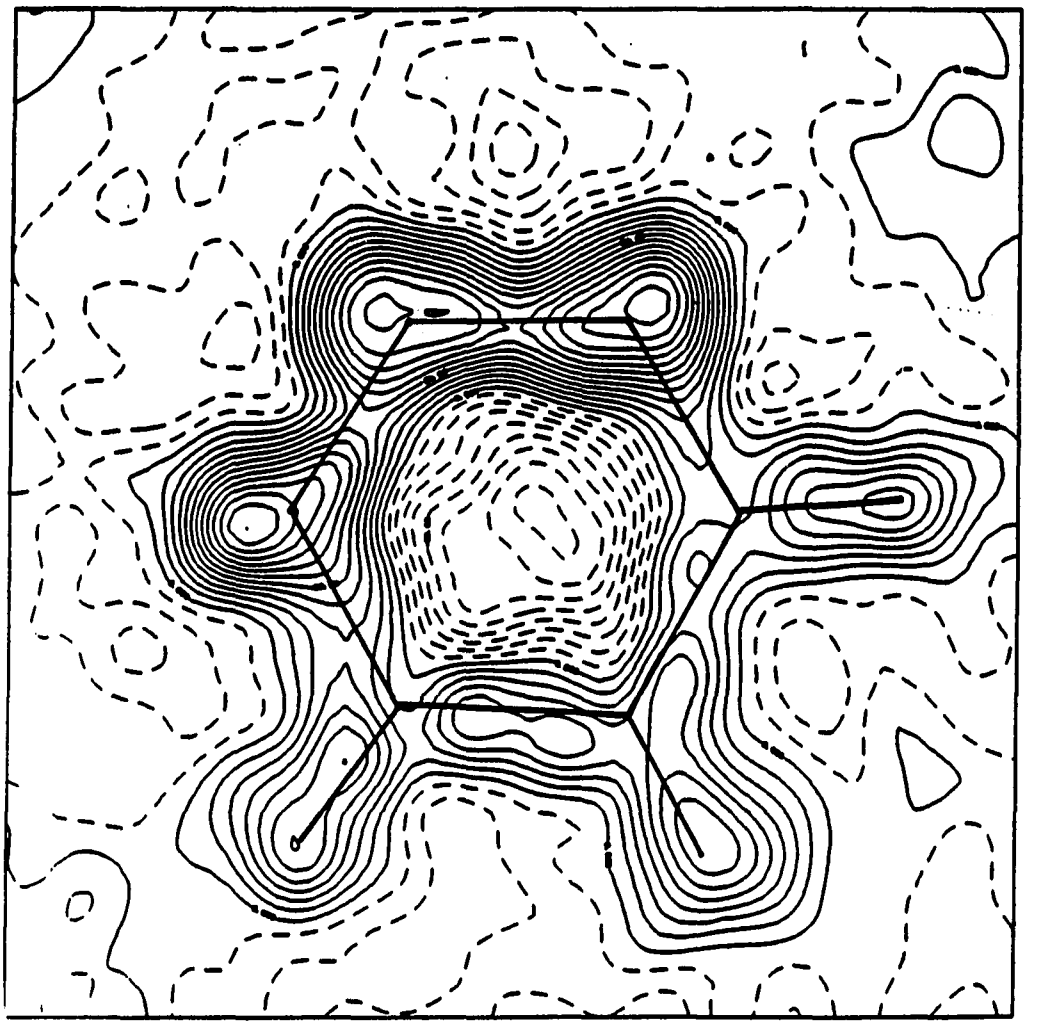

Figure III.7. Difference density map for Trial 5. Observed data with incorrect phases minus promolecule's carbon and nitrogen 1s and 2s electrons. CI=0.1e$^-$/Å^3

which can be compared to the correct map in Figure III.5b, shows differences in the peaks heights and peak shapes.

Despite the many failings of the dataset, a successful determination of the orbital orientations and their occupancies has been carried out. Figures III.4 graphically illustrates the three types of p-orbitals. The first type all have similar occupancy, approximately model the C_2 chemical symmetry, and are tangential to the ring. The second type have two distinct occupancies corresponding to the two atom types, again model the C_2 symmetry, and are radially oriented w.r.t. the ring. The third type are also split into two occupancy groups, model the C_2 symmetry, and lie perpendicular to the ring.

The three types of orbital directions model the ring sigma bonds, the lone pair and hydrogen bonds, and the p-π orbitals in a manner which follows closely our chemical intuition. The sum total of these three types of orbitals is a very good representation of the non-valence difference electron density shown in Figure III.5b which is unbiased by any valence orbital description.

That the orbitals do not follow exactly the C_2 chemical symmetry is probably a reflection of the limited resolution available in this experiment.

Conclusion

The results obtained from the study of 1,2,3-triazine are both internally consistent and consistent with our chemical intuition. The promolecule's parameters and the electron density functions yield, potentially, good qualitative information which will provide useful insights into the chemistry of molecules.

A procedure by which the oriented atom promolecule is obtained from an experimentally determined dataset has been shown to be one in which four basic steps are carried out. Obtaining the standard crystallographic promolecule model is the first step. One then determines the high-order data limit by plotting the bond (or lone pair) electron density peak heights against a $\sin(\theta)/\lambda$ maximum and determining where the curve plateaus. Next high-accuracy parameters are determined by refining the X-type parameters against the high-order data only. As a final step the Y-type parameters are refined against the entire dataset while keeping the X-type parameters fixed.

Use of high-accuracy data in obtaining high quality results is of primary importance. For a quantitative analysis it has been seen that any deviation from ideality has ramifications on the electron density. Thus if low accuracy X-type parameters are used to obtain orbital information, the results may not be meaningful. The dataset

used in this study is only of moderate quality and thus the results were not deemed to be worthy of anything more than a qualitative analysis.

CHAPTER IV. 9-TERT-BUTYLANTHRACENE

Introduction

A study of 9-tert-butylanthracene is described in this chapter. In Chapter III good quality and high resolution were determined to be two important features of the data used for a study of the orbital features of atoms. The data for 9-tert-butylanthracene are better in both respects than the data for 1,2,3-triazine.

9-tert-butylanthracene does not lend itself to a large number of studies due to its complex nature. The results presented here were obtained by following the procedure developed for the study of 1,2,3-triazine. Four trial structures are described in this chapter. The Trial 1 structure resulted from a standard crystallographic analysis. The Trial 2 structure resulted from a high-order refinement of the X-type parameters, and all data were used for the refinement of the Y-type parameters (which again include the hydrogen parameters). The high-order data cutoff was determined from the graph shown in Figure III.2. The structures in Trials 3 and 4 resulted from different electronic constraints (electron transfer and ionization, respectively) applied to the valence parameters of the carbon atoms. The X-type parameters were fixed at the values obtained from Trial 2.

The electron density functions are shown in two-

dimensional contour maps and in ORTEP-type drawings. The features of the illustrations and the refinement procedure are described in Appendix E.

Preliminary Discussion

During initial refinement the data were found to be of a higher quality than that of 1,2,3-triazine. A related compound (9-tert-butyl[Dewar]anthracene) was obtained from the same source[37,38] as these two compounds but was not studied due to its poor quality.

From Figure III.2 it is readily seen that the data have the resolution needed for a study of the orbitals. The curve plateaus well below the limit of data collection, leaving approximately 2000 pieces of high-order data for the refinement of the 163 X-type parameters.

The molecular structure is more complicated than that of 1,2,3-triazine but it presented no new difficulties during analysis. There are several different bonding situations which are, in most cases, redundant and a comparison between different bonding situations permits a check on the internal consistency of the results to be made.

A summary of the pertinent data and crystal parameters is given in Table IV.1. SCF scattering factors were used for the carbon atoms and modified HF scattering factors were used for the hydrogen atoms.

Table IV.1. Summary of the data and crystal parameters for 9-tert-butylanthracene

Chemical formula	$C_{36}H_{36}$
Crystal system	monoclinic
Space group symbol	$P2_1/c$
Lattice parameters	a=11.137(1)Å b=6.8927(8)Å β=107.680(5)° c=17.792(1)Å
Temperature of data collection	100K
Total number of reflections	42375
Number after averaging	6805
Number observed	4587 (I>0)
Internal agreement[a]	0.049
Radiation	Mo k_α (λ=0.71Å)
Sin(θ)/λ (min/max, $Å^{-1}$)	0.047/0.855

[a]Defined as $R_{Int}(<I>)=(\Sigma_k |<I>-|I|)/(\Sigma_k |<I>|)$.

Table IV.2. Summary[a] of refinement conditions for the trial structures

Trial	Refinement parameters	Electronic constrains
1	X	-
2	X,Ψ	Std
3	Ψ	Tot
4	Ψ	Ion

[a]See Table III.2 for explanation of terms used.

Table IV.3a. Atom coordinates (fractional, 10^{-4}) and isotropic thermal parameters (Å, 10^{-3}) for 9-tert-butylanthracene, Trial 1

	x	y	z	$\bar{U}^a$
C1	7600.9(4)	1612.6(7)	8121.8(3)	17
C2	8276.3(5)	764.5(8)	8821.8(3)	19
C3	9336.0(5)	-437.6(7)	8863.5(3)	17
C4	9631.9(4)	-840.1(6)	8186.7(3)	14
C5	8526.7(5)	-889.4(7)	5311.7(3)	19
C6	7661.7(6)	-576.9(9)	4589.7(3)	21
C7	6572.6(5)	560.7(8)	4543.5(3)	18
C8	6427.5(4)	1460.7(7)	5197.8(3)	15
C9	7231.1(4)	2177.1(6)	6662.5(2)	12
C10	9169.7(4)	-621.3(6)	6752.9(2)	14
C11	8906.2(4)	-57.0(6)	7440.1(2)	13
C12	7899.7(4)	1300.5(6)	7398.2(2)	12
C13	8358.9(4)	-84.6(6)	6016.1(2)	14
C14	7334.8(4)	1245.4(6)	5966.1(2)	13
C15	6505.3(4)	4134.6(6)	6605.7(3)	15
C16	7047.1(7)	5440.4(8)	7339.6(4)	25
C17	5088.0(5)	3827(1)	6480.4(5)	26
C18	6690.8(6)	5399.7(8)	5924.8(3)	20
H1	6867(34)	2369(59)	8116(21)	28(6)
H2	7988(26)	954(44)	9303(16)	18(4)
H3	9867(27)	-1067(47)	9398(17)	19(5)
H4	10311(21)	-1658(37)	8172(13)	12(3)
H5	9267(34)	-1705(61)	5368(22)	30(7)
H6	7727(29)	-1182(50)	4084(18)	21(5)
H7	5886(28)	745(49)	4006(18)	21(5)
H8	5674(19)	2097(33)	5135(12)	8(3)
H10	9856(28)	-1488(49)	6790(18)	21(5)
H61	6739(28)	6805(48)	7198(18)	20(5)
H62	7878(33)	5401(57)	7570(21)	27(6)
H63	6676(46)	5037(82)	7805(29)	42(10)
H71	4673(27)	3174(46)	6003(17)	20(5)
H72	4985(43)	3126(75)	6943(27)	39(9)
H73	4643(31)	5133(54)	6403(19)	25(6)
H81	6328(22)	6716(38)	5953(14)	13(4)
H82	7574(34)	5596(60)	6000(22)	29(7)
H83	6303(29)	4872(50)	5385(18)	22(5)

[a] $\bar{U}=(1/6\pi^2)\mathrm{Trace}\{\beta\, G^*\}$, where the form of the temperature factor is $\exp[-(k\ \beta\ k^T)/(4\pi^2)]$ for atoms with anisotropic thermal parameters. $\bar{U}$ for atoms with isotropic thermal parameters is $(1/8\pi^2)\beta$ where the form of the temperature factor is $\exp[-\beta/4\ (2\sin(\theta)/\lambda)^2]$.

Table IV.3b. Atom coordinates (fractional, 10^{-4}) and isotropic thermal parameters for atoms in 9-tert-butylanthracene, Trial 2

	x	y	z	$\bar{U}^a$
C1	7600.8(7)	1614(1)	8122.0(4)	17
C2	8276.6(8)	764(1)	8821.7(4)	20
C3	9336.0(7)	-437(1)	8863.5(4)	17
C4	9631.6(6)	-840.1(9)	8186.7(4)	15
C5	8526.5(8)	-889(1)	5311.8(4)	19
C6	7661.6(9)	-577(1)	4589.9(4)	22
C7	6572.9(8)	561(1)	4543.8(4)	19
C8	6427.6(6)	1461(1)	5197.8(4)	16
C9	7231.1(6)	2177.6(9)	6662.5(4)	13
C10	9169.4(6)	-621.6(9)	6753.0(4)	15
C11	8906.3(6)	-56.5(9)	7440.0(4)	13
C12	7900.1(6)	1300.1(9)	7397.9(4)	13
C13	8359.2(6)	-84.8(9)	6016.0(4)	14
C14	7334.7(6)	1246.0(9)	5966.0(4)	13
C15	6505.4(6)	4134.7(9)	6605.9(4)	16
C16	7046(1)	5440(1)	7339.2(6)	26
C17	5087.7(8)	3828(2)	6479.0(7)	26
C18	6692.0(9)	5400(1)	5925.1(5)	21
H1	6830(33)	2389(54)	8119(20)	27(6)
H2	7984(25)	950(41)	9305(16)	18(4)
H3	9875(27)	-1036(44)	9394(17)	20(5)
H4	10331(23)	-1661(38)	8173(15)	15(4)
H5	9310(34)	-1695(57)	5364(22)	29(6)
H6	7730(29)	-1158(48)	4086(19)	23(5)
H7	5879(27)	764(45)	3997(17)	20(4)
H8	5668(19)	2112(31)	5132(12)	9(3)
H10	9885(29)	-1503(49)	6794(19)	23(5)
H61	6745(31)	6823(51)	7191(20)	25(5)
H62	7875(33)	5398(54)	7555(20)	27(6)
H63	6675(44)	5012(75)	7795(28)	41(9)
H71	4652(28)	3140(46)	5993(18)	23(5)
H72	4989(41)	3114(68)	6950(26)	39(9)
H73	4674(33)	5006(57)	6434(21)	28(6)
H81	6319(24)	6679(39)	5949(15)	15(4)
H82	7587(35)	5632(58)	6012(22)	30(6)
H83	6331(30)	4880(50)	5402(19)	24(5)

[a] $\bar{U}=(1/6\pi^2)\mathrm{Trace}\{\beta\, G^*\}$, where the form of the temperature factor is $\exp[-(k\ \beta\ k^T)/(4\pi^2)]$ for atoms with anisotropic thermal parameters. $\bar{U}$ for atoms with isotropic thermal parameters is $(1/8\pi^2)\beta$ where the form of the temperature factor is $\exp[-\beta/4\ (2\sin(\theta)/\lambda)^2]$.

Table IV.3c. Anisotropic thermal parameters[a] (Å, 10^{-3}) for atoms in 9-tert-butylanthracene, Trial 1

	U_{11}	U_{22}	U_{33}	U_{12}	U_{13}	U_{23}
C1	15.9(1)	17.7(1)	14.9(1)	2.8(0)	1.5(2)	3.7(2)
C2	21.0(1)	20.3(2)	14.0(1)	3.0(0)	2.7(2)	3.3(2)
C3	19.6(1)	16.4(1)	13.1(1)	1.5(0)	3.4(2)	2.4(2)
C4	15.8(1)	12.6(1)	13.3(1)	1.0(0)	2.0(2)	3.3(2)
C5	21.5(1)	16.0(1)	13.9(1)	2.6(0)	-0.9(2)	4.9(2)
C6	26.0(2)	19.8(2)	12.8(1)	2.4(0)	-1.3(2)	3.2(2)
C7	20.5(1)	18.2(1)	12.5(1)	1.1(0)	0.0(2)	-1.5(2)
C8	14.5(1)	15.1(1)	13.2(1)	0.7(0)	0.5(2)	-1.6(2)
C9	10.9(1)	10.4(1)	13.3(1)	1.3(0)	-0.2(1)	0.3(1)
C10	14.4(1)	11.1(1)	13.2(1)	1.6(0)	-0.4(1)	3.0(2)
C11	12.7(1)	10.0(1)	12.5(1)	1.3(0)	0.3(1)	0.9(2)
C12	11.6(1)	11.4(1)	12.4(1)	1.4(0)	0.7(1)	0.1(1)
C13	14.6(1)	10.9(1)	12.3(1)	1.6(0)	-0.6(1)	0.3(2)
C14	12.3(1)	10.3(1)	12.5(1)	1.1(0)	0.2(1)	-0.4(1)
C15	12.7(1)	11.5(1)	17.3(1)	1.2(0)	-0.6(2)	2.5(2)
C16	32.8(2)	14.5(1)	20.2(2)	0.8(1)	-4.7(2)	4.6(2)
C17	13.8(1)	22.4(2)	36.0(2)	3.4(1)	-1.5(3)	3.2(2)
C18	25.8(2)	13.5(1)	21.0(1)	2.2(1)	6.0(2)	3.8(2)

[a] $U=(1/2\pi^2)\beta\ G^*$, where the temperature factor is of the form $\exp[-(k\ \beta\ k^T)/4\pi^2]$.

There are four trials (labeled 1 through 4) described in the remaining sections. A summary of the trial structures' refinement conditions is given in Table IV.2.

Initial Structure Refinement

The initial atomic coordinates and the data for Trial 1 were obtained from a previous study[38]. All parameters were adjusted for an optimal fit of the calculated structure factors to the experimental structure factors by means of a

Table IV.3d. Anisotropic thermal parameters[a] (Å, 10^{-3}) for atoms in 9-tert-butylanthracene, Trial 2

	U_{11}	U_{22}	U_{33}	U_{12}	U_{13}	U_{23}
C1	16.1(2)	19.5(3)	14.9(2)	2.8(1)	1.9(3)	4.6(3)
C2	21.7(3)	21.9(3)	13.8(2)	3.1(1)	2.7(3)	3.9(3)
C3	19.9(3)	17.5(2)	13.5(2)	1.5(1)	3.7(2)	3.1(3)
C4	16.3(2)	13.8(2)	13.1(2)	1.0(1)	2.0(2)	4.3(2)
C5	21.8(3)	17.1(2)	14.1(2)	2.4(1)	-0.7(2)	5.6(3)
C6	26.6(3)	21.0(3)	12.9(2)	2.4(1)	-1.4(3)	3.9(4)
C7	20.8(3)	19.5(3)	12.6(2)	1.1(1)	0.0(3)	-0.8(3)
C8	14.6(2)	16.5(2)	13.6(2)	0.7(1)	0.0(2)	-1.4(3)
C9	11.3(2)	11.5(2)	13.8(2)	1.4(1)	-0.5(2)	0.7(2)
C10	14.9(2)	12.1(2)	13.3(2)	1.5(1)	-0.4(2)	3.5(2)
C11	12.9(2)	11.3(2)	12.9(2)	1.3(1)	0.2(2)	1.4(2)
C12	11.9(2)	12.9(2)	12.3(2)	1.4(1)	1.0(2)	0.7(2)
C13	15.1(2)	12.0(2)	12.5(2)	1.5(1)	-0.7(2)	0.3(2)
C14	12.6(2)	11.7(2)	12.6(2)	1.1(1)	0.0(2)	0.1(2)
C15	13.0(2)	12.5(2)	17.7(2)	1.2(1)	-0.3(2)	2.8(2)
C16	33.1(4)	15.7(3)	20.6(3)	0.8(1)	-4.4(3)	4.7(4)
C17	14.0(3)	23.9(3)	35.5(4)	3.3(1)	-1.5(4)	2.7(3)
C18	25.6(3)	14.6(2)	21.6(3)	2.2(1)	6.5(3)	3.9(3)

[a] $U=(1/2\pi^2)\beta\ G^*$, where the temperature factor is of the form $\exp[-(k\ \beta\ k^T)/4\pi^2]$.

least squares routine using SCF scattering factors. The atomic parameters are listed in Tables IV.3. The calculated bond angles and interatomic distances are given in Tables IV.5. Tables IV.6 list the relevant quantities from the statistical analysis of the calculated structure factors' fit to the observed data.

Table IV.3e. RMS amplitudes of vibration[a] (Å) for atoms in 9-tert-butylanthracene, Trials 1 and 2

	Trial 1	Trial 2		Trial 1	Trial 2
C1	0.13	0.13	H1	0.17	0.16
C2	0.14	0.14	H2	0.13	0.13
C3	0.13	0.13	H3	0.14	0.14
C4	0.12	0.12	H4	0.11	0.12
C5	0.14	0.14	H5	0.17	0.17
C6	0.15	0.15	H6	0.15	0.15
C7	0.13	0.14	H7	0.14	0.14
C8	0.12	0.13	H8	0.09	0.09
C9	0.11	0.11	H10	0.14	0.15
C10	0.12	0.12	H61	0.14	0.16
C11	0.11	0.11	H62	0.16	0.16
C12	0.11	0.11	H63	0.21	0.20
C13	0.12	0.12	H71	0.14	0.15
C14	0.11	0.11	H72	0.20	0.20
C15	0.12	0.12	H73	0.16	0.17
C16	0.16	0.16	H81	0.11	0.12
C17	0.16	0.16	H82	0.17	0.17
C18	0.14	0.14	H83	0.15	0.15

[a]Standard deviations for the hydrogens are ca. $7*10^{-2}$.

High-Order Refinement

The high-order cutoff was obtained by plotting the maximum electron density peak height, which appeared on a difference electron density map, versus the $\sin(\theta)/\lambda$ cutoff used. A plot (see Figure III.2) reveals that the non-atomic electron density contributes very little to the x-ray data beyond $0.7Å^{-1}$. As there were sufficient data beyond $0.7Å^{-1}$ to obtain meaningful results from a least squares refinement, this was chosen as the high-order cutoff.

Table IV.4a. Trial 2 orbital parameters for 9-tert-butylanthracene

	i	λ_i	a_i[a]	b_i	c_i	Δe_i
C1	1	0.963	0.146	-0.162	0.976	0.296
C1	2	1.037	-0.204	0.960	0.190	0.371
C1	3	0.000	0.968	0.227	-0.108	-0.667
C2	1	0.836	0.178	-0.209	0.962	0.170
C2	2	1.164	0.093	0.976	0.195	0.497
C2	3	0.000	0.980	-0.055	-0.193	-0.667
C3	1	1.120	0.062	0.483	0.873	0.454
C3	2	0.808	0.035	0.874	-0.485	0.141
C3	3	0.072	0.997	-0.061	-0.037	-0.595
C4	1	0.983	-0.100	-0.741	0.664	0.317
C4	2	1.017	-0.090	0.671	0.736	0.350
C4	3	0.000	0.991	-0.013	0.134	-0.667
C5	1	0.801	-0.024	0.454	0.891	0.134
C5	2	1.132	-0.035	0.890	-0.455	0.466
C5	3	0.067	0.999	0.042	0.006	-0.600
C6	1	0.948	0.073	0.689	0.721	0.281
C6	2	1.011	0.058	0.719	-0.693	0.344
C6	3	0.041	0.996	-0.093	-0.013	-0.626
C7	1	1.022	-0.148	0.331	0.932	0.355
C7	2	0.894	0.174	0.936	-0.305	0.228
C7	3	0.084	0.974	-0.117	0.196	-0.583
C8	1	0.855	0.166	-0.385	0.908	0.189
C8	2	1.002	-0.325	0.848	0.419	0.335
C8	3	0.143	0.931	0.365	-0.015	-0.524
C9	1	0.741	0.262	-0.407	0.875	0.074
C9	2	1.104	-0.356	0.802	0.480	0.437
C9	3	0.156	0.897	0.437	-0.066	-0.511
C10	1	0.947	0.000	0.818	0.575	0.281
C10	2	0.937	0.046	0.574	-0.817	0.271
C10	3	0.115	0.999	-0.026	0.038	-0.551

[a]See text for description of vector directions.

Table IV.4a. Continued

	i	λ_i	a_i[a]	b_i	c_i	$\Delta e\bar{i}$
C11	1	0.818	0.181	0.176	0.967	0.151
C11	2	1.108	0.146	0.968	-0.204	0.441
C11	3	0.075	0.973	-0.178	-0.150	-0.592
C12	1	1.070	-0.169	-0.234	0.957	0.403
C12	2	0.930	0.257	0.927	0.272	0.264
C12	3	0.000	0.952	-0.292	0.096	-0.667
C13	1	0.961	0.104	-0.228	0.968	0.294
C13	2	0.741	-0.349	0.903	0.250	0.074
C13	3	0.298	0.931	0.364	-0.014	-0.368
C14	1	0.947	0.022	0.213	0.977	0.280
C14	2	1.033	-0.214	0.956	-0.203	0.366
C14	3	0.020	0.977	0.204	-0.067	-0.647
C15	1	0.368	-0.722	-0.679	0.130	-0.298
C15	2	0.869	0.540	-0.671	-0.508	0.202
C15	3	0.763	0.432	-0.296	0.852	0.096
C16	1	0.857	0.185	0.513	-0.838	0.190
C16	2	0.334	0.341	0.767	0.544	-0.333
C16	3	0.809	-0.922	0.386	0.033	0.143
C17	1	0.833	-0.456	-0.882	0.115	0.166
C17	2	0.998	0.889	-0.458	0.017	0.332
C17	3	0.169	0.038	0.110	0.993	-0.498
C18	1	1.026	-0.488	0.573	-0.659	0.360
C18	2	0.682	0.638	0.749	0.179	0.015
C18	3	0.291	0.596	-0.332	-0.731	-0.375

Table IV.4b. Trial 3 orbital parameters for 9-tert-butylanthracene

	i	λ_i	a_i[a]	b_i	c_i	Net[b]	Δe_i
C1	1	1.030	0.133	-0.092	0.987	0.150	0.363
C1	2	1.121	-0.197	0.973	0.117		0.454
C1	3	0.000	0.971	0.210	-0.111		-0.667
C2	1	0.844	0.183	-0.193	0.964	0.030	0.178
C2	2	1.176	0.091	0.980	0.179		0.509
C2	3	0.010	0.979	-0.055	-0.197		-0.657
C3	1	1.133	0.067	0.497	0.865	0.066	0.466
C3	2	0.826	0.034	0.865	-0.500		0.160
C3	3	0.107	0.997	-0.063	-0.041		-0.560
C4	1	1.040	-0.122	-0.493	0.861	0.127	0.374
C4	2	1.087	-0.062	0.870	0.489		0.420
C4	3	0.000	0.991	-0.006	0.137		-0.667
C5	1	0.797	-0.022	0.449	0.893	0.003	0.130
C5	2	1.138	-0.035	0.892	-0.450		0.472
C5	3	0.068	0.999	0.041	0.004		-0.599
C6	1	0.949	0.067	0.626	0.777	0.006	0.283
C6	2	1.005	0.066	0.774	-0.630		0.338
C6	3	0.052	0.996	-0.093	-0.010		-0.615
C7	1	1.047	-0.153	0.313	0.938	0.072	0.381
C7	2	0.919	0.170	0.943	-0.287		0.253
C7	3	0.105	0.974	-0.116	0.197		-0.562
C8	1	0.821	0.160	-0.364	0.918	-0.091	0.154
C8	2	0.968	-0.333	0.855	0.397		0.302
C8	3	0.120	0.929	0.369	-0.015		-0.547
C9	1	0.736	0.259	-0.401	0.879	0.002	0.070
C9	2	1.107	-0.357	0.805	0.473		0.440
C9	3	0.158	0.897	0.436	-0.065		-0.508

[a]See text for description of vector directions.

[b]Net number of electrons gained from neutral atom's number of electrons.

Table IV.4b. Continued

	i	λ_i	a_i[a]	b_i	c_i	Net	Δe_i
C10	1	0.929	0.007	0.888	0.460	-0.034	0.263
C10	2	0.925	0.048	0.459	-0.887		0.258
C10	3	0.112	0.999	-0.029	0.039		-0.555
C11	1	0.870	0.182	0.184	0.966	0.160	0.204
C11	2	1.159	0.146	0.966	-0.212		0.492
C11	3	0.131	0.972	-0.180	-0.149		-0.536
C12	1	1.099	-0.171	-0.240	0.956	0.094	0.432
C12	2	0.955	0.261	0.924	0.279		0.288
C12	3	0.040	0.950	-0.297	0.095		-0.626
C13	1	0.980	-0.099	0.221	-0.970	0.056	0.313
C13	2	0.759	-0.356	0.903	0.241		0.092
C13	3	0.318	0.929	0.369	-0.011		-0.349
C14	1	0.974	0.023	0.207	0.978	0.069	0.307
C14	2	1.051	-0.214	0.957	-0.198		0.385
C14	3	0.043	0.977	0.205	-0.067		-0.623
C15	1	0.328	-0.721	-0.681	0.131	-0.126	-0.338
C15	2	0.827	0.544	-0.673	-0.502		0.160
C15	3	0.719	0.430	-0.290	0.855		0.052
C16	1	0.821	0.173	0.522	-0.835	-0.096	0.154
C16	2	0.303	0.331	0.768	0.549		-0.364
C16	3	0.781	0.928	-0.371	-0.040		0.114
C17	1	0.738	-0.473	-0.873	0.122	-0.292	0.071
C17	2	0.897	0.880	-0.475	0.016		0.231
C17	3	0.073	0.044	0.115	0.992		-0.594
C18	1	0.955	-0.486	0.578	-0.656	-0.197	0.288
C18	2	0.619	0.641	0.745	0.183		-0.048
C18	3	0.230	0.594	-0.332	-0.733		-0.437

Table IV.4c. Trial 4 orbital parameters for 9-tert-butylanthracene

	i	λ_i	a_i[a]	b_i	c_i	Net[b]	Δe_i^-
C1	1	0.955	0.173	-0.279	0.944	-0.033	0.289
C1	2	1.012	-0.193	0.931	0.311		0.345
C1	3	0.000	0.966	0.236	-0.107		-0.667
C2	1	0.733	0.204	-0.235	0.950	-0.174	0.066
C2	2	1.094	0.088	0.971	0.221		0.427
C2	3	0.000	0.975	-0.039	-0.219		-0.667
C3	1	1.057	0.063	0.492	0.868	-0.209	0.390
C3	2	0.734	0.034	0.869	-0.494		0.068
C3	3	0.000	0.997	-0.060	-0.038		-0.667
C4	1	0.926	-0.065	-0.945	0.319	-0.102	0.259
C4	2	0.973	-0.119	0.325	0.938		0.306
C4	3	0.000	0.991	-0.023	0.133		-0.667
C5	1	0.704	-0.020	0.474	0.880	-0.262	0.038
C5	2	1.034	-0.029	0.880	-0.475		0.367
C5	3	0.000	0.999	0.035	0.004		-0.667
C6	1	0.855	0.048	0.452	0.891	-0.254	0.188
C6	2	0.892	0.086	0.887	-0.454		0.225
C6	3	0.000	0.995	-0.098	-0.004		-0.667
C7	1	0.973	-0.142	0.323	0.936	-0.192	0.307
C7	2	0.835	0.171	0.939	-0.298		0.168
C7	3	0.000	0.975	-0.117	0.188		-0.667
C8	1	0.743	0.160	-0.385	0.909	-0.339	0.076
C8	2	0.887	-0.328	0.848	0.416		0.220
C8	3	0.032	0.931	0.365	-0.009		-0.635
C9	1	0.675	0.252	-0.397	0.882	-0.198	0.009
C9	2	1.047	-0.356	0.810	0.466		0.380
C9	3	0.080	0.900	0.432	-0.063		-0.587

[a]See text for description of vector directions.

[b]Net number of electrons gained from neutral atom's number of electrons.

Table IV.4c. Continued

	i	λ_i	a_i	b_i	c_i	Net	$\Delta e\bar{i}$
C10	1	0.846	0.008	0.955	0.297	-0.316	0.180
C10	2	0.838	0.046	0.296	-0.954		0.171
C10	3	0.000	0.999	-0.021	0.041		-0.667
C11	1	0.784	0.177	0.173	0.969	-0.105	0.118
C11	2	1.082	0.141	0.970	-0.199		0.415
C11	3	0.028	0.974	-0.172	-0.148		-0.638
C12	1	1.024	-0.166	-0.225	0.960	-0.110	0.358
C12	2	0.866	0.283	0.922	0.265		0.199
C12	3	0.000	0.945	-0.315	0.090		-0.667
C13	1	0.893	-0.088	0.204	-0.975	-0.204	0.226
C13	2	0.680	-0.336	0.915	0.222		0.014
C13	3	0.223	0.938	0.347	-0.012		-0.444
C14	1	0.899	0.023	0.191	0.981	-0.141	0.233
C14	2	0.960	-0.226	0.957	-0.181		0.293
C14	3	0.000	0.974	0.217	-0.065		-0.667
C15	1	0.249	-0.729	-0.672	0.128	-0.340	-0.418
C15	2	0.760	0.544	-0.683	-0.488		0.094
C15	3	0.640	0.416	-0.287	0.863		-0.026
C16	1	0.724	0.117	0.536	-0.836	-0.392	0.057
C16	2	0.215	0.341	0.769	0.541		-0.452
C16	3	0.669	0.933	-0.348	-0.093		0.003
C17	1	0.650	-0.489	-0.865	0.110	-0.554	-0.017
C17	2	0.796	0.871	-0.490	0.014		0.130
C17	3	0.000	0.042	0.102	0.994		-0.667
C18	1	0.845	-0.486	0.580	-0.654	-0.511	0.179
C18	2	0.516	0.639	0.746	0.187		-0.151
C18	3	0.128	0.597	-0.327	-0.733		-0.539

Table IV.5a. Bond angles (°) for 9-tert-butylanthracene, Trials 1 and 2

			Trial 1	Trial 2
C2	C1	C12	122.34(4)	122.26(7)
C2	C1	H1	118(2)	117(2)
C12	C1	H1	120(2)	120(2)
C1	C2	C3	120.73(4)	120.77(7)
C1	C2	H2	119(2)	119(2)
C1	C2	H2	119(2)	119(2)
C3	C2	H2	120(2)	120(2)
C2	C3	C4	119.24(4)	119.22(7)
C2	C3	H3	121(2)	121(2)
C4	C3	H3	120(2)	119(2)
C3	C4	C11	121.30(4)	121.32(6)
C3	C4	H4	123(1)	123(1)
C11	C4	H4	115(1)	115(1)
C6	C5	C13	121.20(5)	121.23(7)
C6	C5	H5	121(2)	121(2)
C13	C5	H5	118(2)	118(2)
C5	C6	C7	119.00(4)	118.98(7)
C5	C6	H6	123(2)	124(2)
C7	C6	H6	118(2)	117(2)
C6	C7	C8	121.17(4)	121.19(7)
C6	C7	H7	120(2)	120(2)
C8	C7	H7	119(2)	119(2)
C7	C8	C14	121.99(4)	121.99(6)
C7	C8	H8	117(1)	117(1)
C14	C8	H8	121(1)	121(1)
C14	C8	H8	121(1)	121(1)
C12	C9	C14	116.54(4)	116.51(5)
C12	C9	C15	122.73(4)	122.77(6)
C14	C9	C15	120.56(4)	120.56(5)
C11	C10	C13	120.00(4)	120.02(6)
C11	C10	H10	119(2)	119(2)
C13	C10	H10	120(2)	121(2)
C4	C11	C10	119.80(4)	119.80(6)
C4	C11	C12	120.11(4)	120.12(6)
C10	C11	C12	120.09(4)	120.09(6)
C10	C11	C12	120.09(4)	120.09(6)
C1	C12	C9	123.93(4)	123.86(6)
C1	C12	C11	115.91(4)	115.93(6)
C1	C12	C11	115.91(4)	115.93(6)
C9	C12	C11	120.10(3)	120.16(5)
C5	C13	C10	119.94(4)	119.98(6)
C5	C13	C14	120.11(4)	120.10(6)

Table IV.5a. Continued

			Trial 1	Trial 2
C8	C14	C9	123.91(4)	123.93(6)
C8	C14	C13	115.92(4)	115.90(6)
C9	C14	C13	120.08(3)	120.08(5)
C9	C15	C16	112.72(4)	112.76(6)
C9	C15	C17	112.24(4)	112.26(6)
C9	C15	C18	110.26(4)	110.23(6)
C16	C15	C17	108.76(5)	108.79(8)
C16	C15	C18	102.75(4)	102.73(6)
C17	C15	C18	109.68(4)	109.63(7)
C15	C16	H61	108(2)	108(2)
C15	C16	H62	117(2)	116(2)
C15	C16	H63	111(3)	110(3)
H61	C16	H62	112(3)	111(3)
H61	C16	H63	105(3)	107(3)
H62	C16	H63	103(3)	105(3)
C15	C17	H71	113(2)	114(2)
C15	C17	H72	109(3)	108(2)
C15	C17	H72	109(3)	108(2)
C15	C17	H73	110(2)	111(2)
H71	C17	H72	111(3)	110(3)
H71	C17	H73	102(3)	104(3)
H72	C17	H73	112(3)	109(3)
C15	C18	H81	109(1)	108(1)
C15	C18	H82	110(2)	110(2)
C15	C18	H83	115(2)	115(2)
H81	C18	H82	106(3)	106(3)
H81	C18	H83	108(2)	109(2)
H82	C18	H83	108(3)	109(3)
H82	C18	H83	108(3)	109(3)

Table IV.5b. Interatomic distances (Å) for 9-tert-butylanthracene, Trials 1 and 2

		Trial 1	Trial 2			Trial 1	Trial 2
C1	H1	0.97(4)	1.01(4)	C1	C12	1.440(1)	1.442(1)
C3	H3	1.05(3)	1.04(3)	C5	H5	0.98(4)	1.01(4)
C5	C13	1.434(1)	1.433(1)	C7	H7	1.03(3)	1.05(3)
C9	C12	1.429(1)	1.429(1)	C9	C15	1.560(1)	1.560(1)
C10	C11	1.397(1)	1.396(1)	C11	C12	1.445(1)	1.444(1)
C13	C14	1.445(1)	1.446(1)	C15	C17	1.540(1)	1.540(1)
C15	C18	1.557(1)	1.557(1)	C16	H62	0.89(4)	0.89(4)
C16	H63	1.07(5)	1.06(5)	C17	H73	0.95(3)	0.93(4)
C17	H72	1.02(4)	1.01(5)	C18	H83	0.96(4)	0.96(3)
C18	H81	1.00(3)	0.98(3)	C7	C8	1.371(1)	1.371(1)
C7	C6	1.426(1)	1.425(1)	C8	H8	0.92(2)	0.93(2)
C8	C7	1.371(1)	1.371(1)	C8	C14	1.440(1)	1.439(1)
C9	C12	1.429(1)	1.429(1)	C9	C14	1.431(1)	1.431(1)
C9	C15	1.560(1)	1.560(1)	C10	H10	0.96(3)	0.99(3)
C10	C11	1.397(1)	1.396(1)	C10	C13	1.397(1)	1.397(1)
C11	C10	1.397(1)	1.396(1)	C11	C4	1.434(1)	1.434(1)
C11	C12	1.445(1)	1.444(1)	C12	C9	1.429(1)	1.429(1)
C12	C1	1.440(1)	1.442(1)	C12	C11	1.445(1)	1.444(1)
C13	C10	1.397(1)	1.397(1)	C13	C5	1.434(1)	1.433(1)

Table IV.6a. R_ω (10^{-3}) in reciprocal space zones

		ALL[a]	h00	0k0	00l	0kl	h0l	hk0
	#1[b]	4587	17	5	11	177	302	113
	#2	1713	3	1	0	49	84	32
1	#1	28	23	53	71	29	28	37
2	#1	27	20	89	54	29	26	32
2	#2	24	15	24	--	24	19	31
3	#1	27	20	87	54	29	26	32
4	#1	27	21	85	45	28	26	32

[a]ALL implies that the entire dataset was used.

[b]Number of reflections in each zone. They are dependent on $\sin(\theta)/\lambda$ and correspond to total, high-order, and low-order data respectively.

Table IV.6b. R_ω[a] (10^{-3}) in $\sin(\theta)/\lambda$ ranges

	#[b]	12	74	198	348	543	746	953	1062	651
	n	0.1	0.2	0.3	0.4	0.5	0.6	0.7	0.8	0.9
1		91	81	86	87	78	45	24	22	27
2		65	61	76	72	74	43	24	22	25
3		70	66	71	71	74	43	24	22	25
4		98	85	77	67	70	43	24	22	25

[a] R_ω is calculated for the range [n-0.1, n) where $n=\sin(\theta)/\lambda$.

[b] Number of reflections in the range [n-0.1, n).

Table IV.6c. Number of reflections with ($|E|-|F|$) in the the range $((n-1)\sigma(E), n\sigma(E)]$

n=	1	2	3	4	5	6	7	8	9	>=10
1	412	411	369	353	345	323	293	271	240	1570
2	421	429	434	376	350	328	296	271	230	1452
2[a]	106	107	117	119	91	95	116	96	88	778
3	427	421	421	400	339	316	322	266	236	1439
4	428	437	420	379	368	308	299	289	213	1446

[a] High-order data only.

Table IV.6d. Refinement results for 9-tert-butylanthracene

Trial	LSE	ERF[a]	$\sigma(\rho)$	Scale
1	621202	11.95	0.052	0.9786(4)
2[b]	357913	15.20	0.007	1.004(6)
2	563959	11.15	0.041	
3	561864	11.13	0.041	
4	558063	11.08	0.049	

[a]Values of ERF not normalized. See text for discussion.

[b]High-order data only.

Using the Trial 1 atomic parameters as initial values, the X-type parameters for Trial 2 were obtained using only the high-order data. The hydrogen atoms' parameters were refined against all the data.

Comparisons of the results for Trials 1 and 2 in Tables IV.3 show that the estimated standard deviations (esd's) are larger for the latter and that the average thermal vibrational parameters are also larger. Because this was

seen in the results for 1,2,3-triazine, we may conclude here that the spherical-atom promolecule's atoms are too large and diffuse in the valence region which, when using all the data, reduces the calculated thermal parameters. This is supported by the knowledge that some electron density has been removed from the atoms for bonding and that the electron density is generally more localized in molecules. This supports another study[45] which used a function to weight the high-order data more, thus producing results which were intermediate between a standard refinement and a high-order refinement.

The statistical information given in Tables IV.6 show that the data does not have the severe error which was encountered in the case of 1,2,3-triazine. In fact the residuals are approximately half of those obtained in Chapter III, Tables III.7. Table IV.6a does have an anomaly in the 0k0 zone reflections, but this is not in the high-order region as seen in 1,2,3-triazine. The 0k0 direction will need to be examined more closely when considering the valence orbitals since this is where the major effect will occur. We see in Table IV.6b that the error steadily decreases as we approach the high-order region which is expected since we can not hope to fit the low-order data well but insist on accurately fitting the high-order data.

There is an indication of a problem which shows up in Table IV.6c where the difference distribution ($|E|-|F|$ versus $\sigma(E)$) does not drop off in the expected fashion (as seen in

Table III.7c). It might be argued that this is due to the inability to fit the valence electron redistribution. This is ruled out however by noting that a similar distribution is seen for the high-order-only results for Trial 2.

The values of ERF and $\sigma(\rho)$ in Table IV.6d are high and low respectively. Equation (II.45) shows that $\sigma(\rho)$ is a simple function of $|E|-|F|$ and its low value agrees with the previous statistical results. The value of ERF^{46}, given in Equation (II.40), is a function of $\omega^*(|E|-|F|)^2$ and its high value can only be attributed to the weights being too large. In the future it would be wise to normalize the weights in Equation (II.40) (note that this is the only statistical analysis equation that uses weights and does not normalize their values). Using this modified ERF function, the calculated value of ERF for Trial 5 of 1,2,3-triazine becomes 1.013 and the value for Trial 2 of 9-tert-butylanthracene becomes 0.223 (the average weights are 1.788 and 2503.9, respectively). This then clears up the fault with the standard definition of the ERF and shows that the ERF is indeed lower as expected and removes the scalar dependence of the weights.

Three views of the promolecule for Trial 2 with vibrational ellipsoids are shown in Figures IV.1. The thermal ellipsoids are all close to isotropic which is an

indication of a good dataset. A close examination of the terminal methyl carbon atoms in Figure IV.1b reveals that a slight rotational disorder may be present in the tertiary-butyl group. This disorder can effect the orbital parameter determination in an adverse manner since the electron density is effectively smeared in the direction of the rotation, thereby modifying the regions of high and low slope in the density. It is these regions which were seen to be well modeled by the oriented valence shell determination in 1,2,3-triazine.

The contour maps of the observed electron density are shown in Figures IV.2. Due to the non-planarity of the molecule it was divided into sections and contoured. Note that some of the atoms lie out of the plane and will appear to have lower electron density compared to similar atoms.

It is interesting that some electron density is evident between atoms in Figures IV.2 even at this level of contouring (note that, for contrast effect, Figures IV.2b and 2e include the small additive constant from F(0,0,0) and are thus everywhere positive). No such effect was seen for 1,2,3-triazine. We also see the regions of low and high slopes in the electron density functions surrounding the atoms and may predict at this time that these will be matched by the calculated valence orbitals.

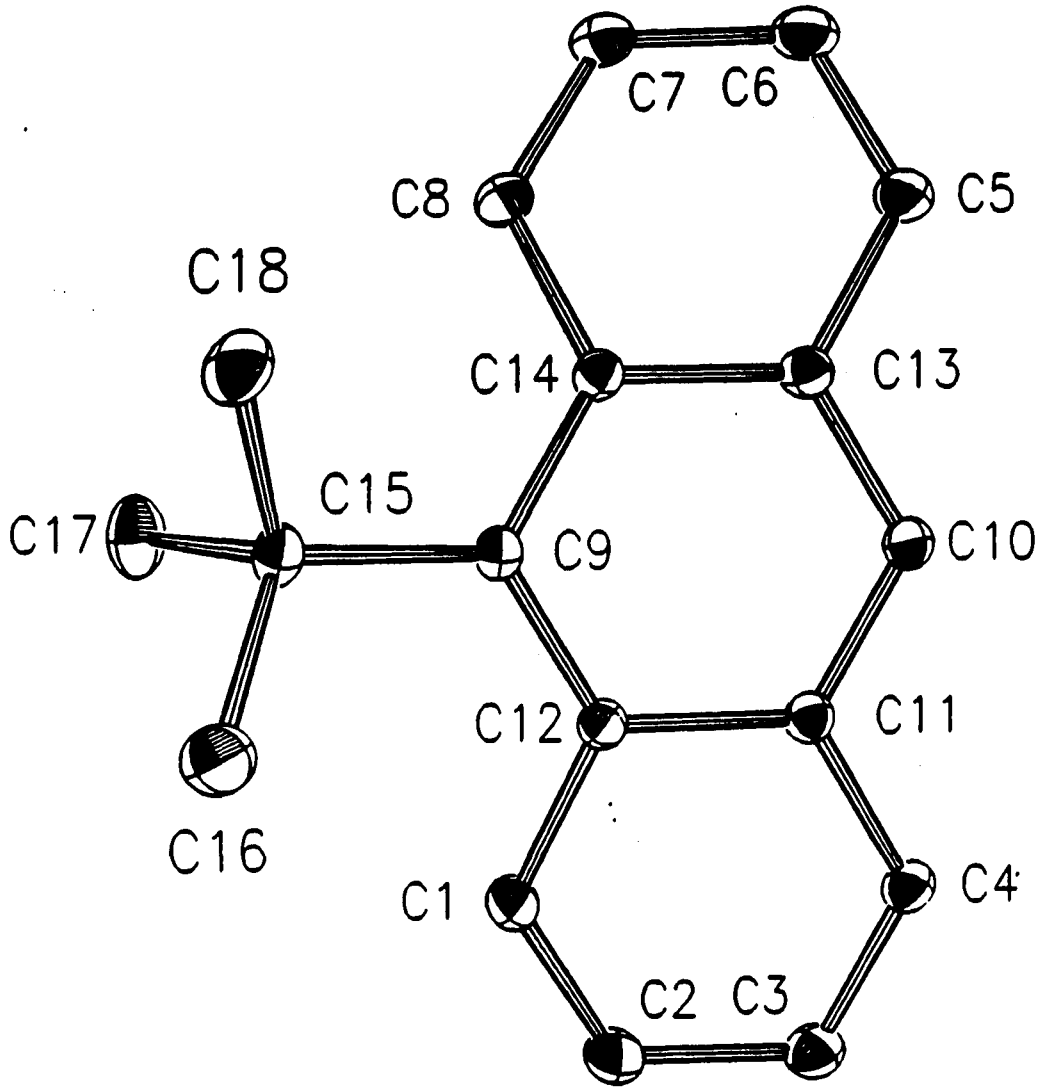

Figure IV.1a. Top view of the 9-tert-butylanthracene promolecule showing atom identifiers. Hydrogen atoms not shown for clarity

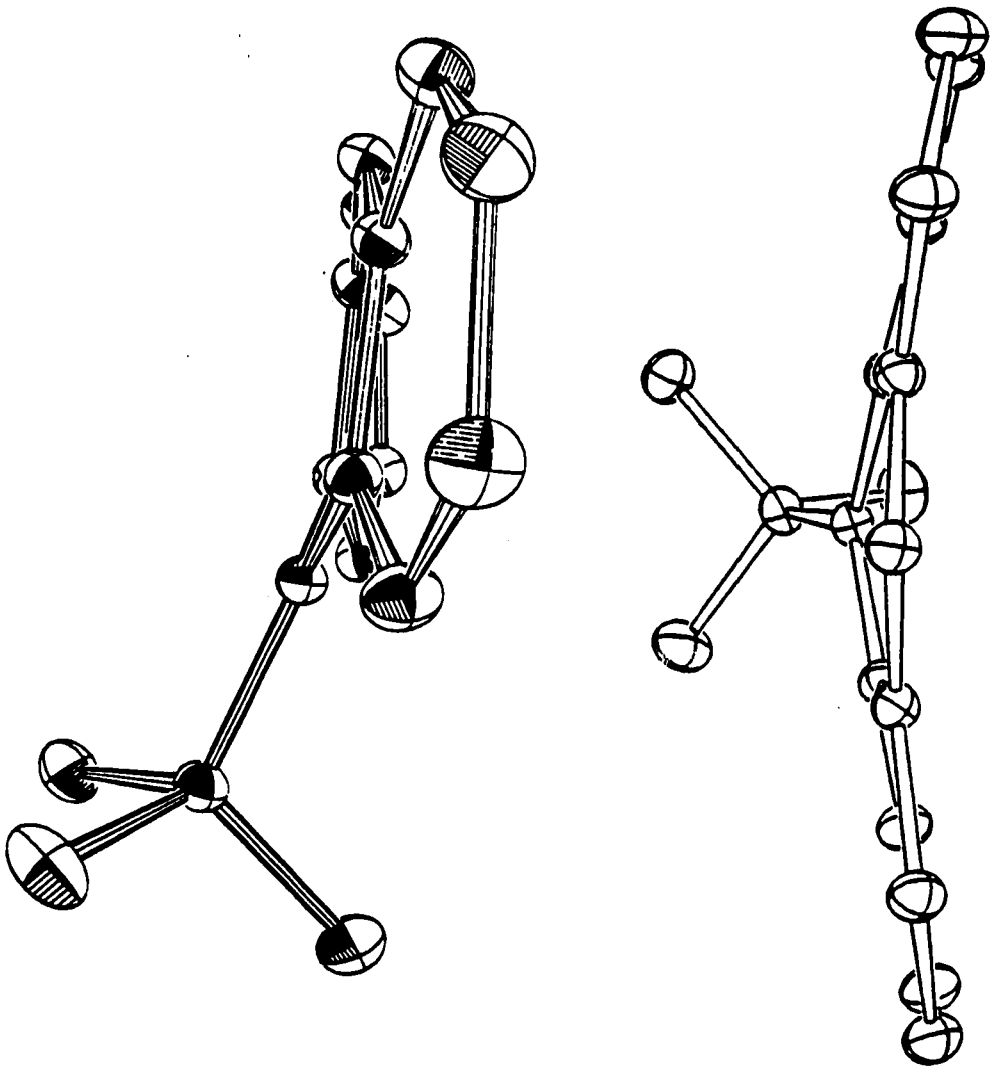

Figure IV.1b. Side (left) and front (right) views of Figure IV.1a

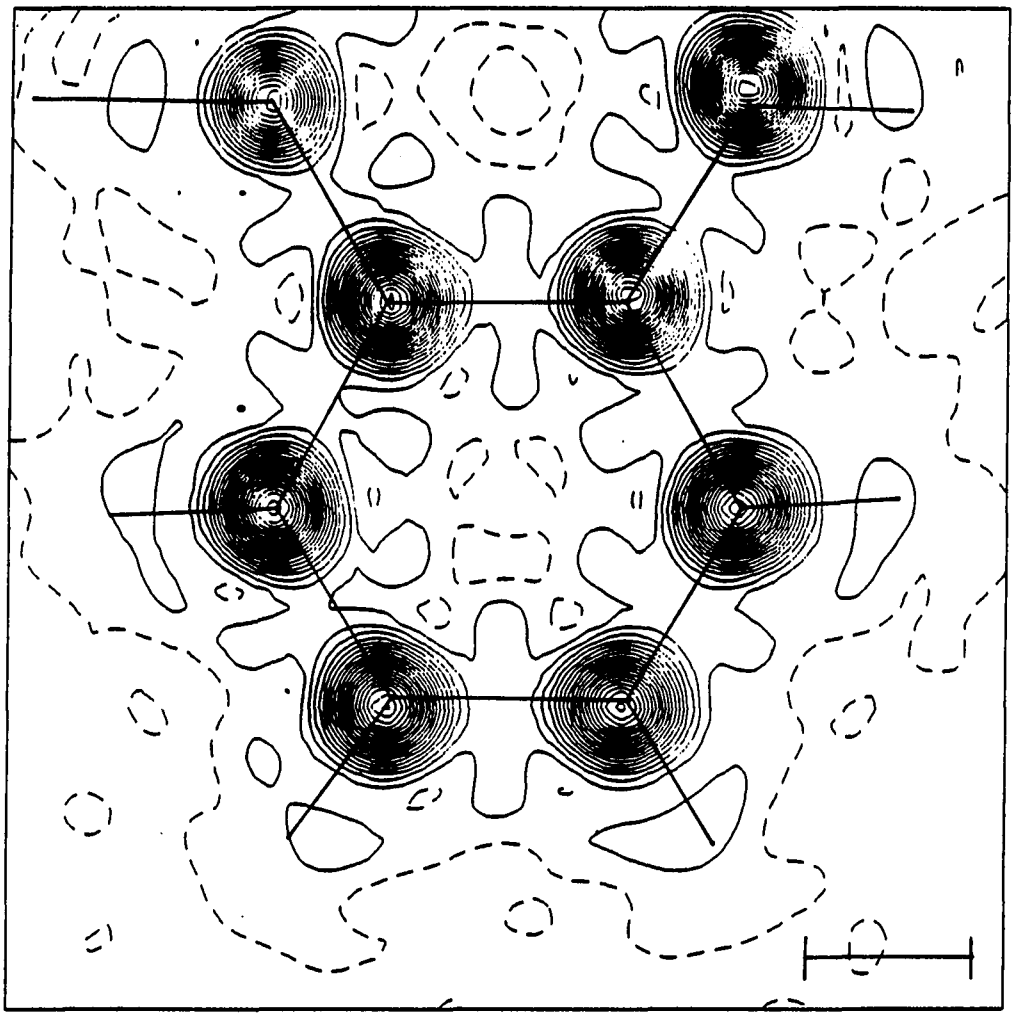

Figure IV.2a. Contour map of observed electron density for 9-tert-butylanthracene, ring containing C1 (middle left). CI=1.0e$^-$/Å^3. Small additive constant (F(0,0,0)) added for contrast to this figure and to Figure IV.2e only. See Appendix E for explanation of map features for this and all other contour maps

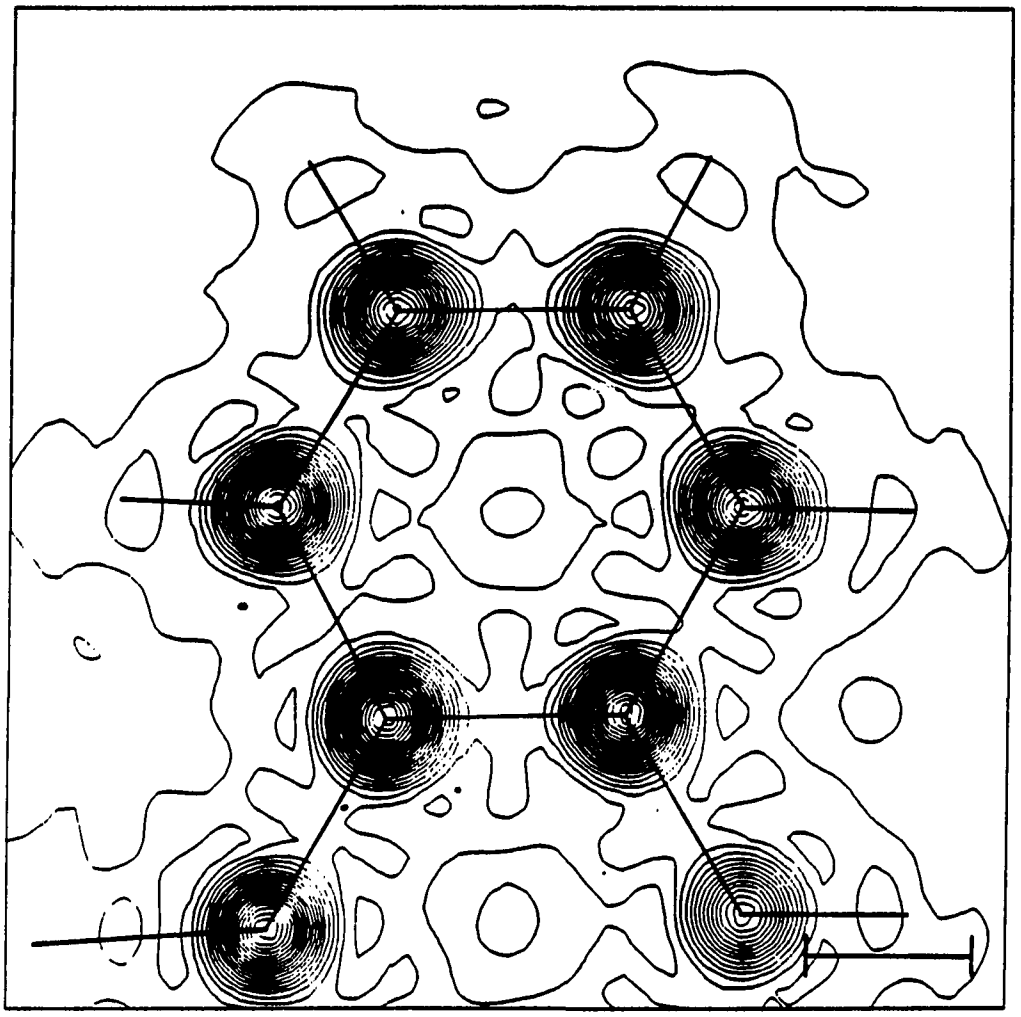

Figure IV.2b. Contour map similar to Figure IV.2a, ring containing C8 (middle left)

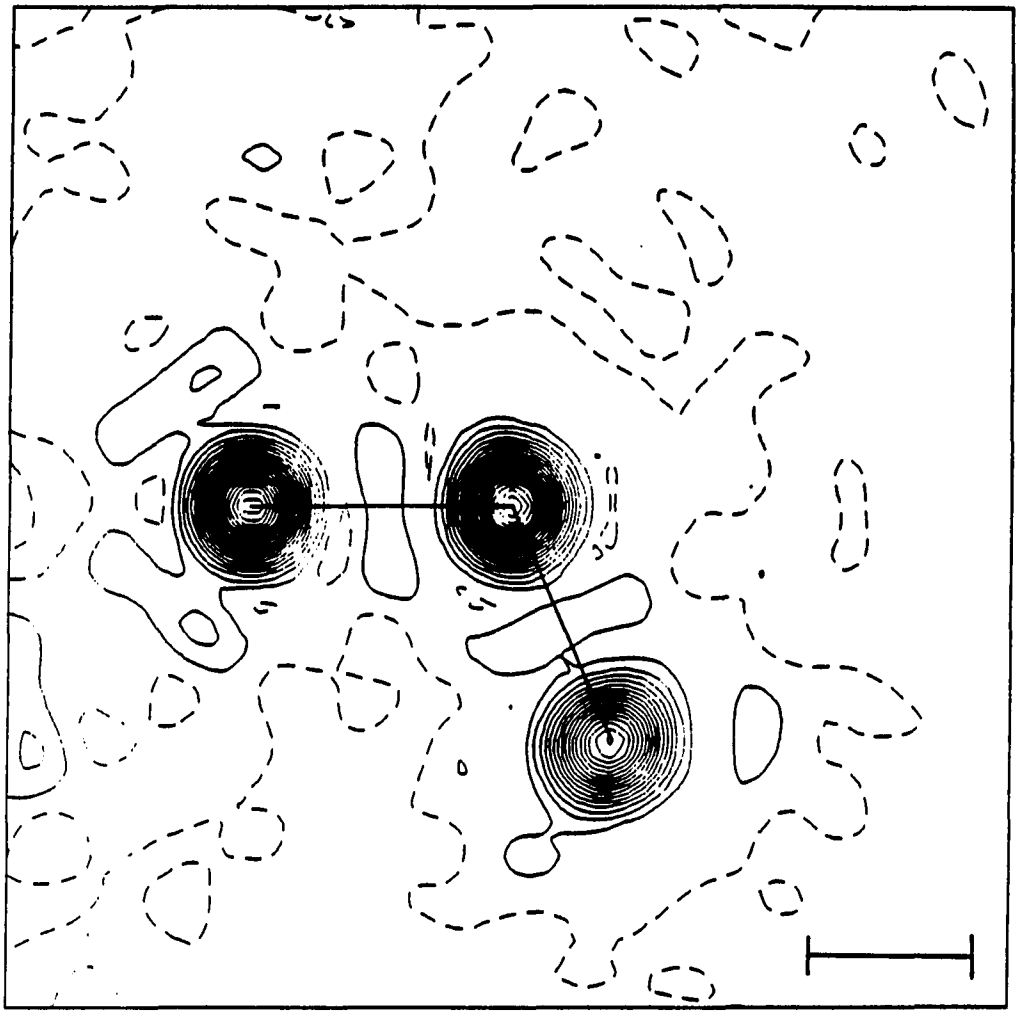

Figure IV.2c. Contour map similar to Figure IV.2a, atoms C9 (left), C15, and C16

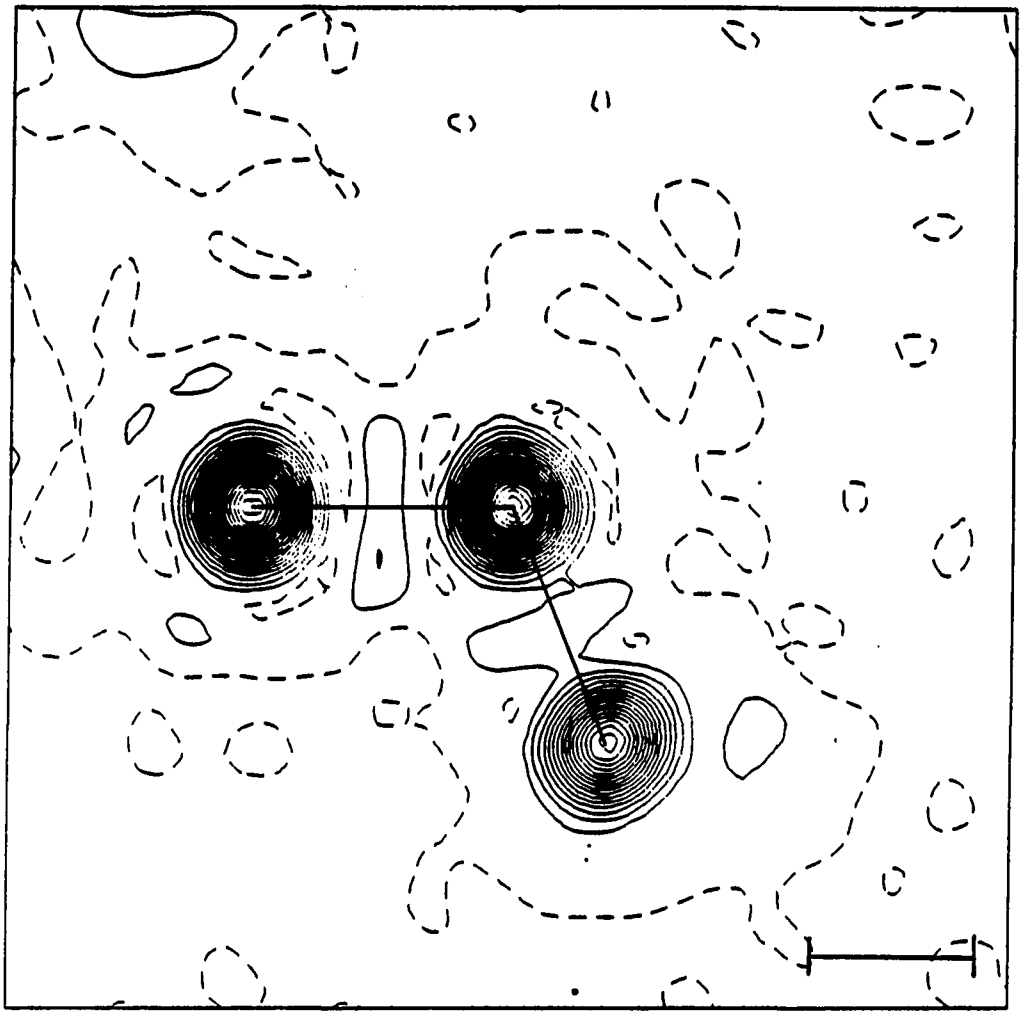

Figure IV.2d. Contour map similar to Figure IV.2a, atoms C9 (left), C15, and C17

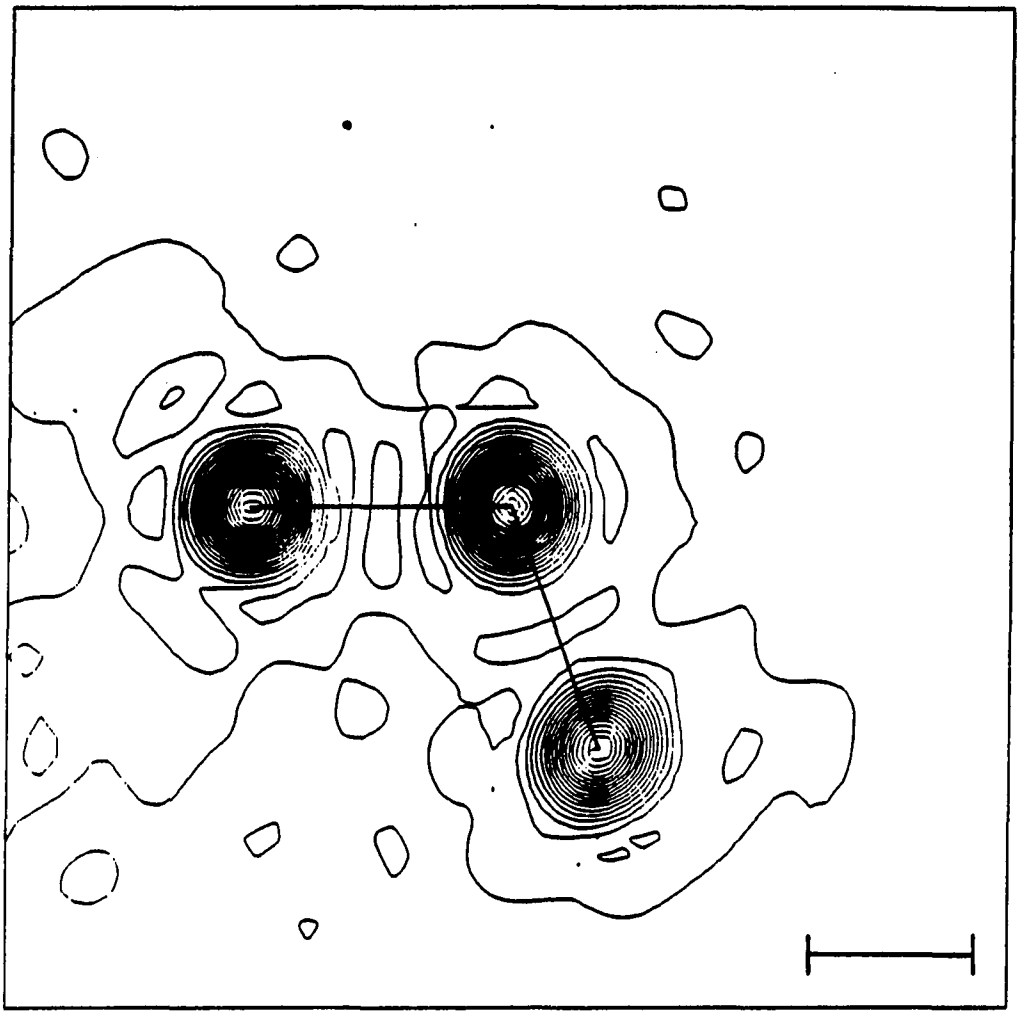

Figure IV.2e. Contour map similar to Figure IV.2a, atoms C9 (left), C15, and C18. Small constant value due to F(0,0,0) included

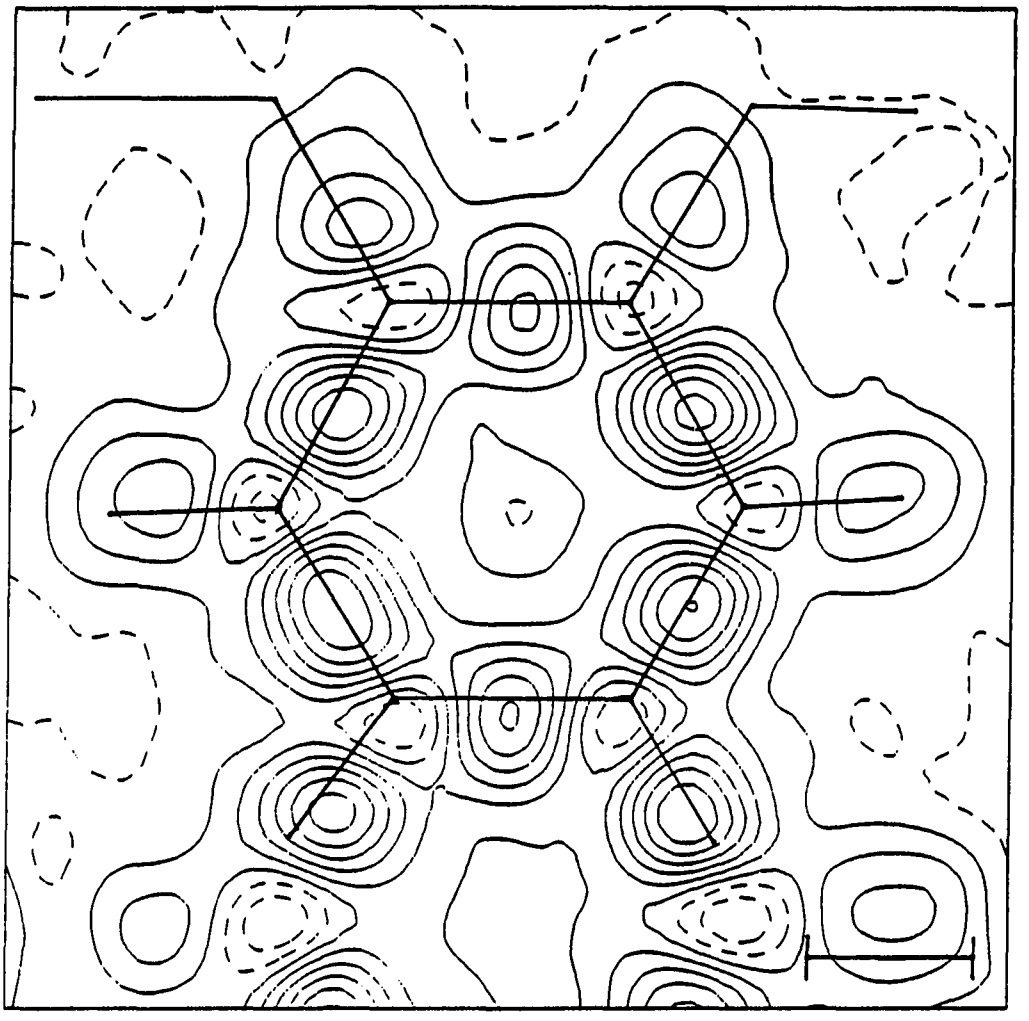

Figure IV.3a. TDD map of Trial 2 (using spherical atoms), ring containing Cl (middle left). CI=0.1$e^-/Å^3$

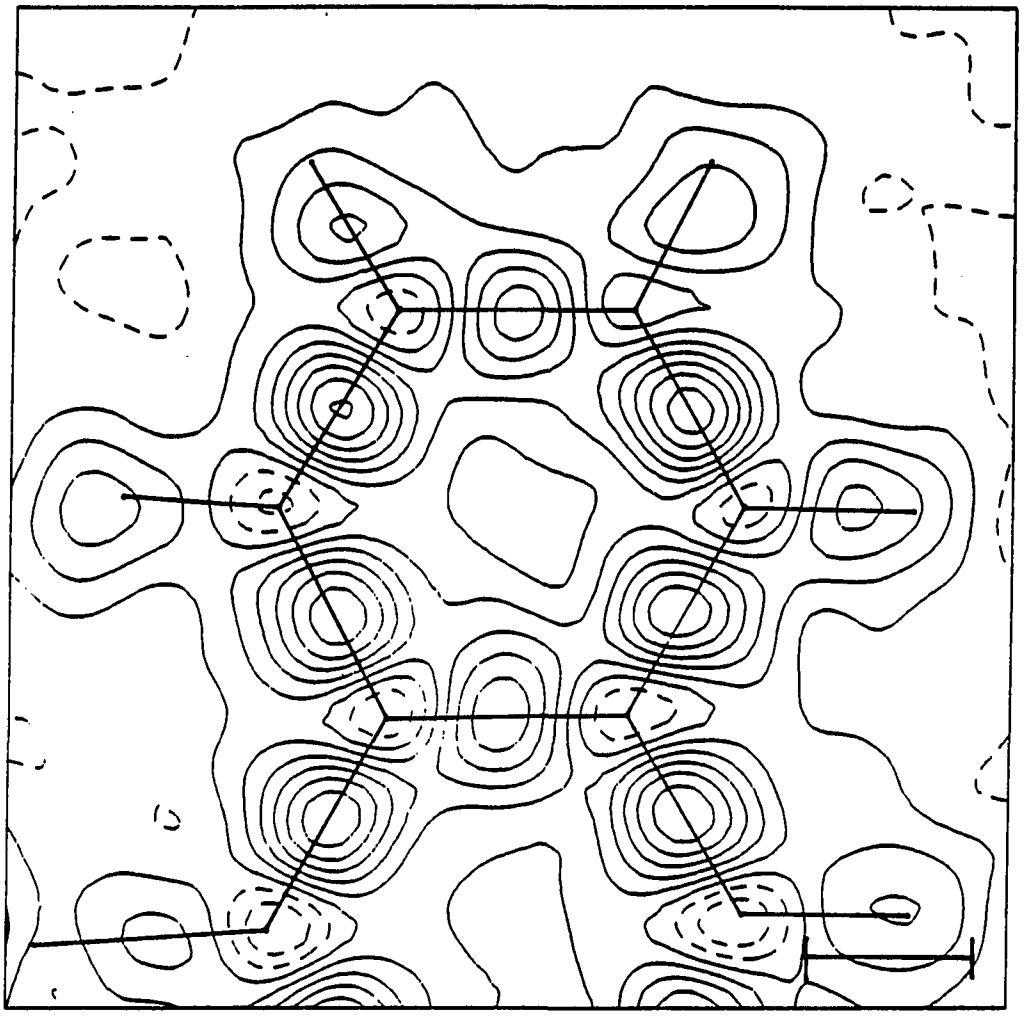

Figure IV.3b. TDD map similar to Figure IV.3a, ring containing C8 (middle left)

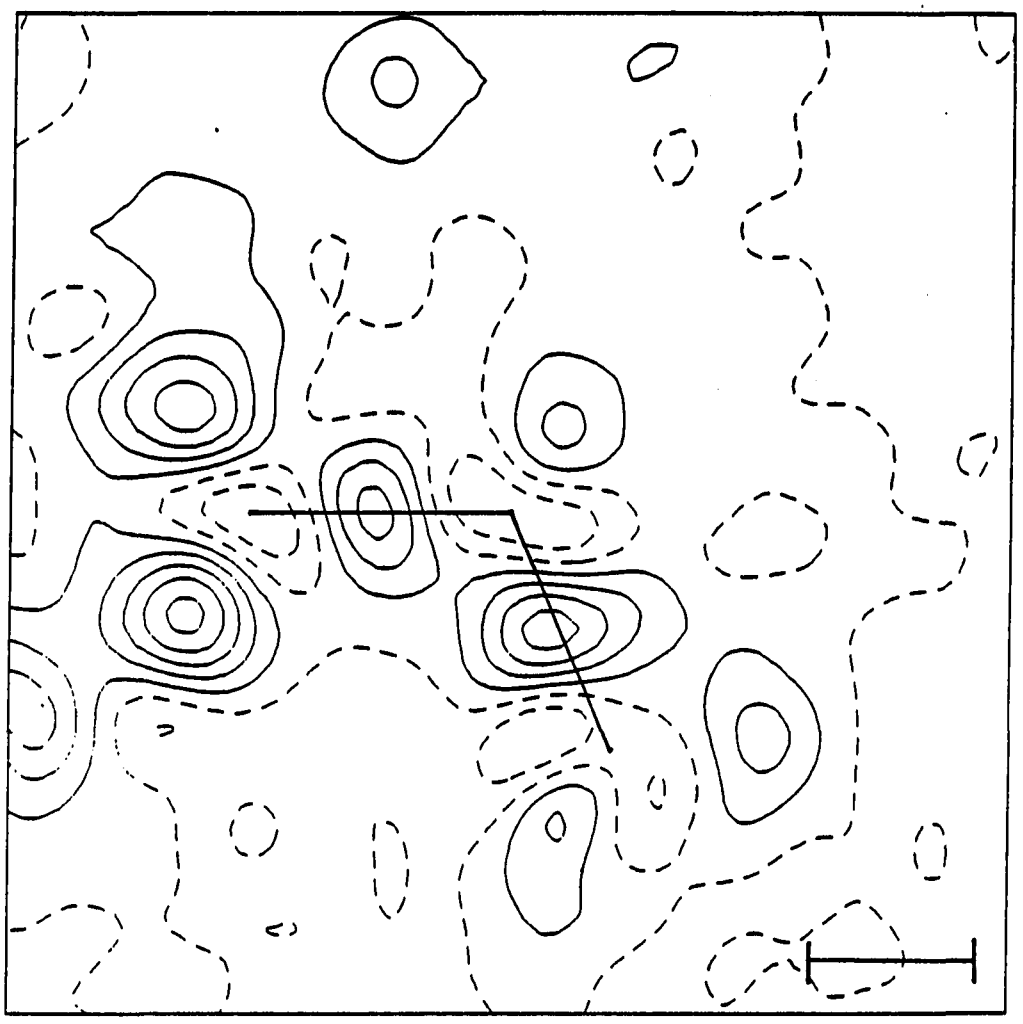

Figure IV.3c. TDD map similar to Figure IV.3a, atoms C9 (left), C15, and C16

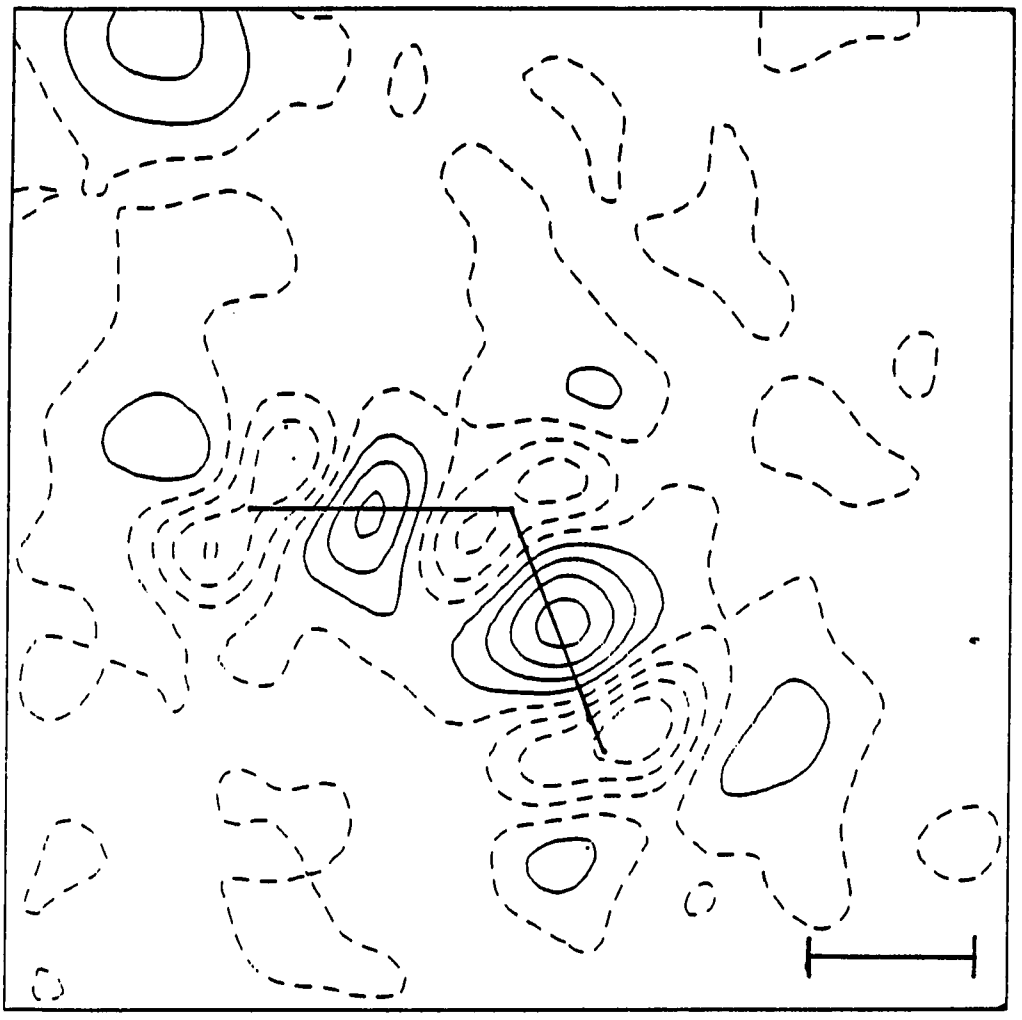

Figure IV.3d. TDD map similar to Figure IV.3a, atoms C9 (left), C15, and C17

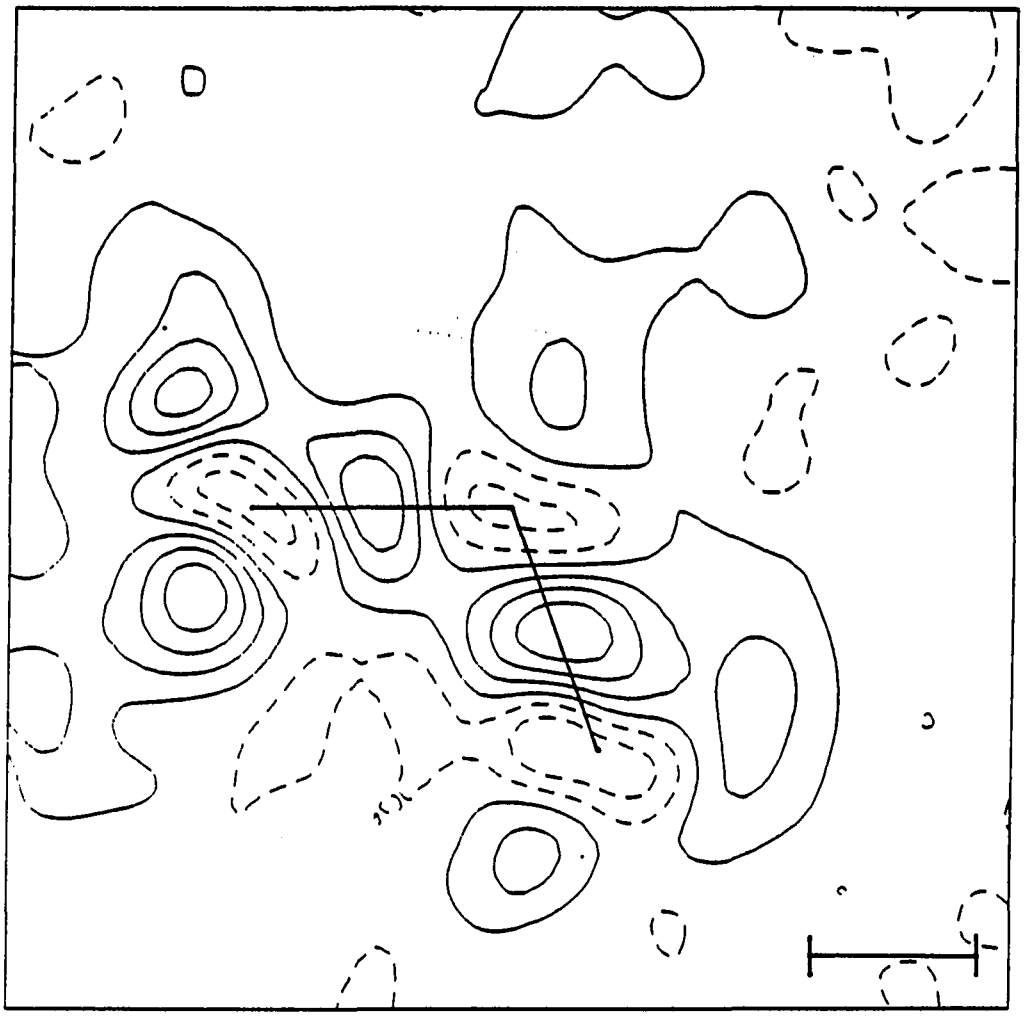

Figure IV.3e. TDD map similar to Figure IV.3a, atoms C9 (left), C15, and C18

The electron density regions around the hydrogen atom positions are seen to be relatively diffuse leading one to the conclusion that there is a large amount of freedom in the positions. The electron density in Figures IV.2d, 2e, and 2f also exhibit maxima near the bond center and depressions surrounding atoms C9 and C15. This depression can only be interpreted as being due to the Fourier truncation effect and further interpretation of the detailed electronic structure must be done using the more appropriate difference maps.

Figures IV.3 are electron density difference maps obtained by subtracting the spherical-atom promolecule from the observed electron density. These total deformation density (TDD) maps exhibit a peak height fluctuation similar to that seen in Figure II.5c for 1,2,3-triazine. The peaks are nearer to the interatomic vectors in this case and are also continuous. The peaks are more square than expected. This is an artifact cf subtracting spherical atoms. The hydrogens are again seen to be poorly accounted for by examining the residual electron density around the atomic positions.

Examining Table IV.3b we see that atoms C16, C17, and C18 have greater average thermal parameters. This coupled with the previous realization that the tertiary-butyl group may exhibit a rotational disorder prevents us from a detailed examination of this group. Note that the thermal parameters attempt to model the rotational disorder but are actually

inadequate for the purpose. The rotational disorder has not been included in the promolecule.

Valence Orbital Refinement

Three sets of orbital parameters were obtained using the X-type parameters from Trial 2. Standard electronic constraints were used in obtaining the orbital parameters for Trial 2. The electrons were allowed to transfer between valence orbitals on the atoms (keeping the molecule neutral) in Trial 3. In Trial 4 the eigenvalues were constrained only to lie in the range [0,2].

Trial 4 is an attempt to obtain a better model since some of the electrons move into the bonding regions thus lowering the number of electrons on the atoms. Although the net number of electrons in Trial 3 is lower than that of the neutral molecule, it should not be construed that the real molecule has a net charge.

The resultant orbital parameters for these three trials are listed in Tables IV.4. All of the eigenvalues in Trial 2 remained in the range of [0,2] except for eigenvalue number 3 on atoms C1, C2, C4, and C12 which tended toward negative numbers and thus were fixed at zero.

The directions a, b, and c are perpendicular, radially outward, and tangential to the three atoms consisting of the parent atom and its two neighbors for atoms C1 through C10.

The directions for atoms C11 through C14 are a) perpendicular to the parent atom and its neighbors (one of which must be C9 or C10), b) radial outward from the bond which is in common to the adjacent rings, and c) perpendicular to the aforementioned plane. For C15 b) is radially outward along the C9-C15 vector, a) is perpendicular to the plane containing C12, and c) is perpendicular to these two (in the C15-C9-C12 plane). For C16 through C18, b) is again radially outward along the interatomic vectors to C15, a) is perpendicular to the plane containing Cxx-C15-C9, and c) is perpendicular to a) and b) (in the plane).

The low values for the orbitals perpendicular to the molecular plane are presumed to be due to the extra 2s electrons in this direction as was argued in Chapter III. It is possible however that the other two orbitals are withdrawing electrons (due to the electronic constraints keeping each atom neutral) from this orbital. This argument is disproved by Trial 4 (see Table IV.4c) where the electronic constraints for the atoms and the molecule are removed. The results given in Table IV.4c show that it is more the other way around; it is the other two orbitals which are preventing these p-π type orbitals from becoming zero in nearly all the ring carbons.

Table IV.4b results from Trial 3 where only the total number of electron is constrained. Here we see that the tertiary-butyl group has lost 0.7 electrons which was picked

up by the ring system. This is in accord with our knowledge that the tertiary-butyl group is a strong electron donor when attached to a π-bound ring. How precise this conclusion is awaits testing on other structures since there are other factors involved such as the number of electrons given up to bonding.

Table IV.4c lists the results from Trial 4 in which the number of electron was not constrained. In sharp contrast to the results for Trial 3, the tertiary-butyl has a net charge of -1.8 electrons whereas the ring system has a net charge of -2.6 electrons. It is inferred that the reason for the large number of electrons lost in the rings relative to the butyl group is that they have transferred electrons into both the sigma and the π-system from the 2s and the 2p orbitals. The tertiary groups however have used only their 2p electrons in bonding to the surrounding atoms.

One should note that an error in the scale factor will have an additive effect on the net charge and on the electron density difference maps. Thus the values may be slightly high or low, depending on the quality of the fit.

As noted earlier, the tertiary-butyl group shows indications of rotational disorder. This will have the effect of lowering the number of electrons on the calculated promolecule fragment. Hence in Trial 3 the net number of electrons may not be as large if this rotational disorder were taken care of properly.

Figures IV.4 are Chemical Difference Density (CDD) maps created by subtracting the Trial 2 promolecule (complete with oriented orbitals) from the observed electron density. These maps, when compared to those of Figures IV.3, exhibit more uniform peaks heights and shapes in the bonding regions and less noise overall. The hydrogen-carbon bond peak heights are generally lower and more uniform.

The orbitals for Trial 2 are displayed in two different formats (described in Appendix E) in Figures IV.5 and IV.6. These figures show that the direction of the low occupancy orbitals are roughly perpendicular to the rings. Figure IV.5b and 6b indicate a definite tilt towards the tertiary-butyl group. As there is no systematic degree of tilt, it is assumed that the source of this effect is in the 0k0 data, perhaps an indication that the weighting or data collection scheme is faulted as was found in Chapter III. The atoms which had zero occupancy in the perpendicular orbitals were given a finite dimension to the ellipsoids so they could be drawn.

C15 of the tertiary-butyl group is more isotropic in its valence shell. That it is not completely isotropic is not unexpected since the electrophilic action of the four adjoining groups is different. If this were the sole source of its anisotropy, one would expect cylindrical symmetry along the C15-C9 bond; that this is not so is due to the systematic error noted for the ring system.

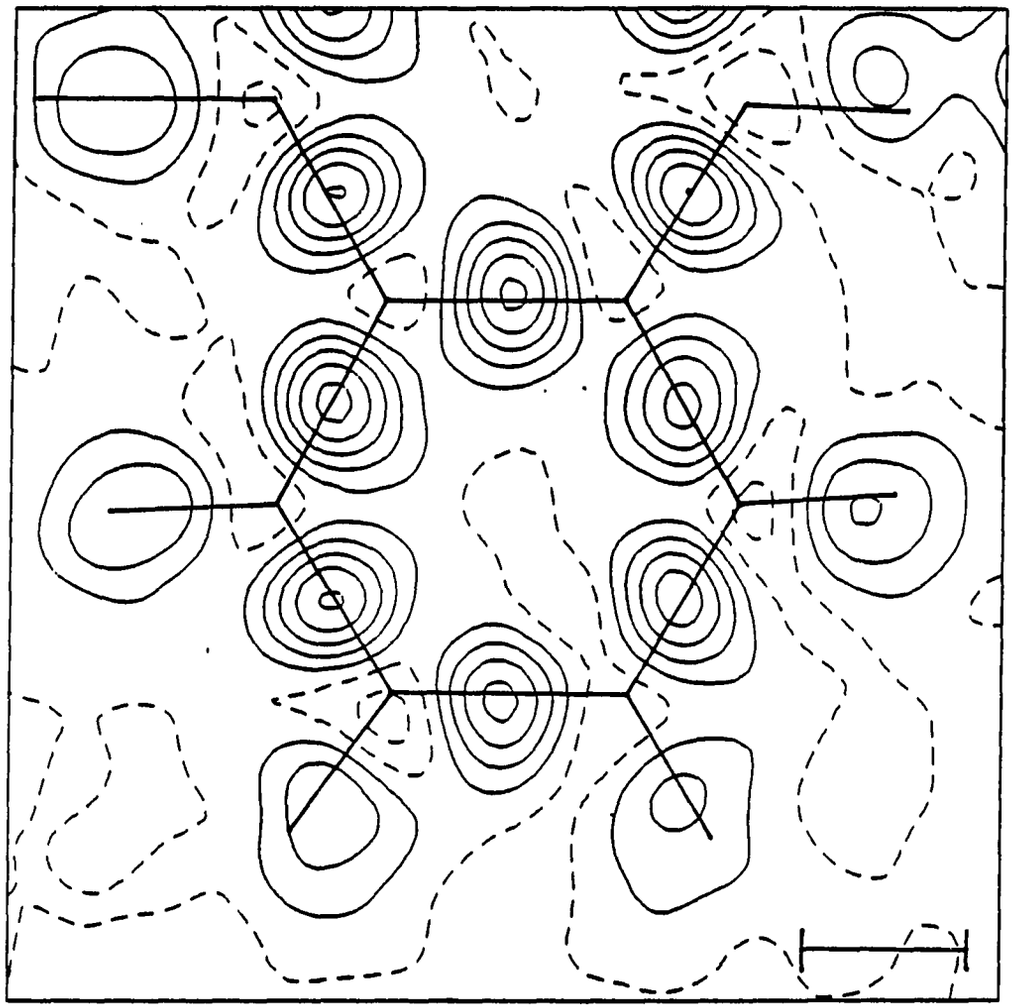

Figure IV.4a. CDD map of Trial 2_4 ring containing C1 (middle left). CI=0.1$e^-/Å^3$

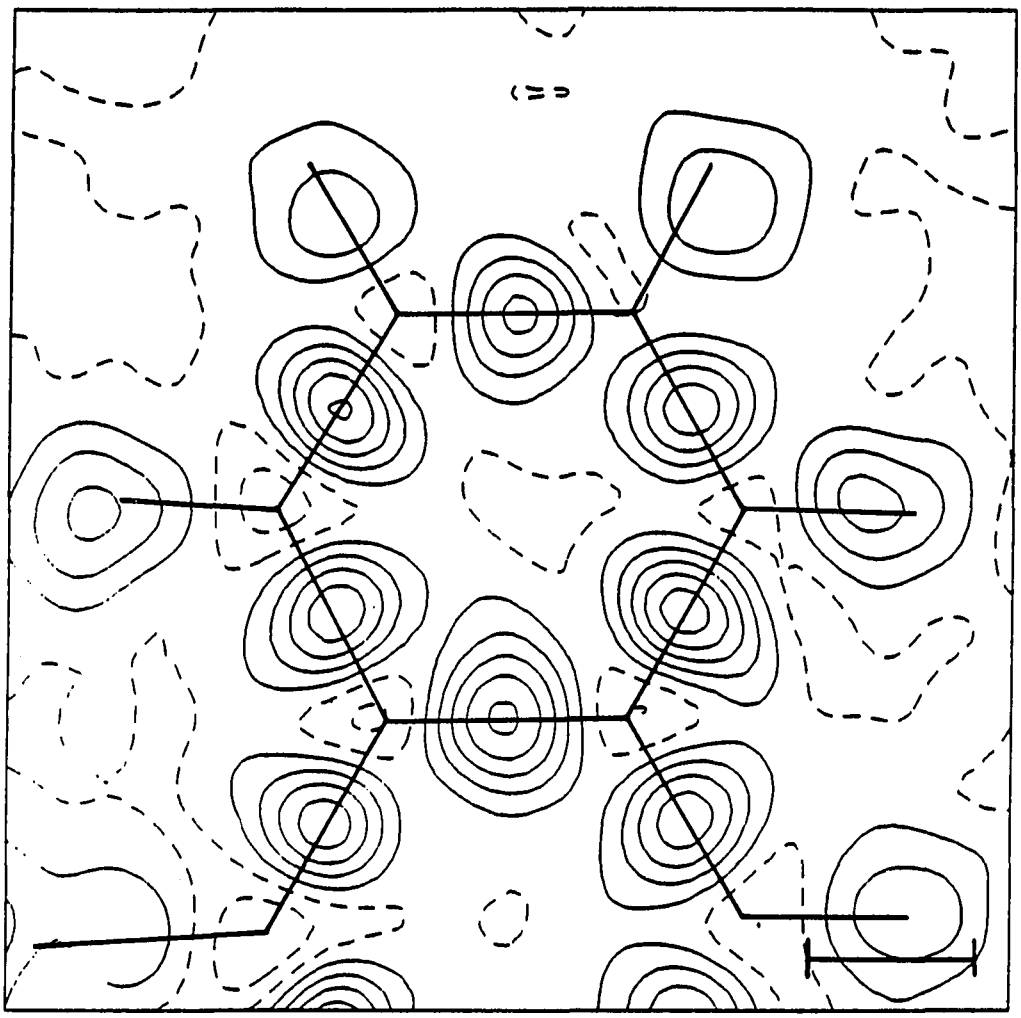

Figure IV.4b. CDD map similar to Figure IV.4a, ring containing C8 (middle left)

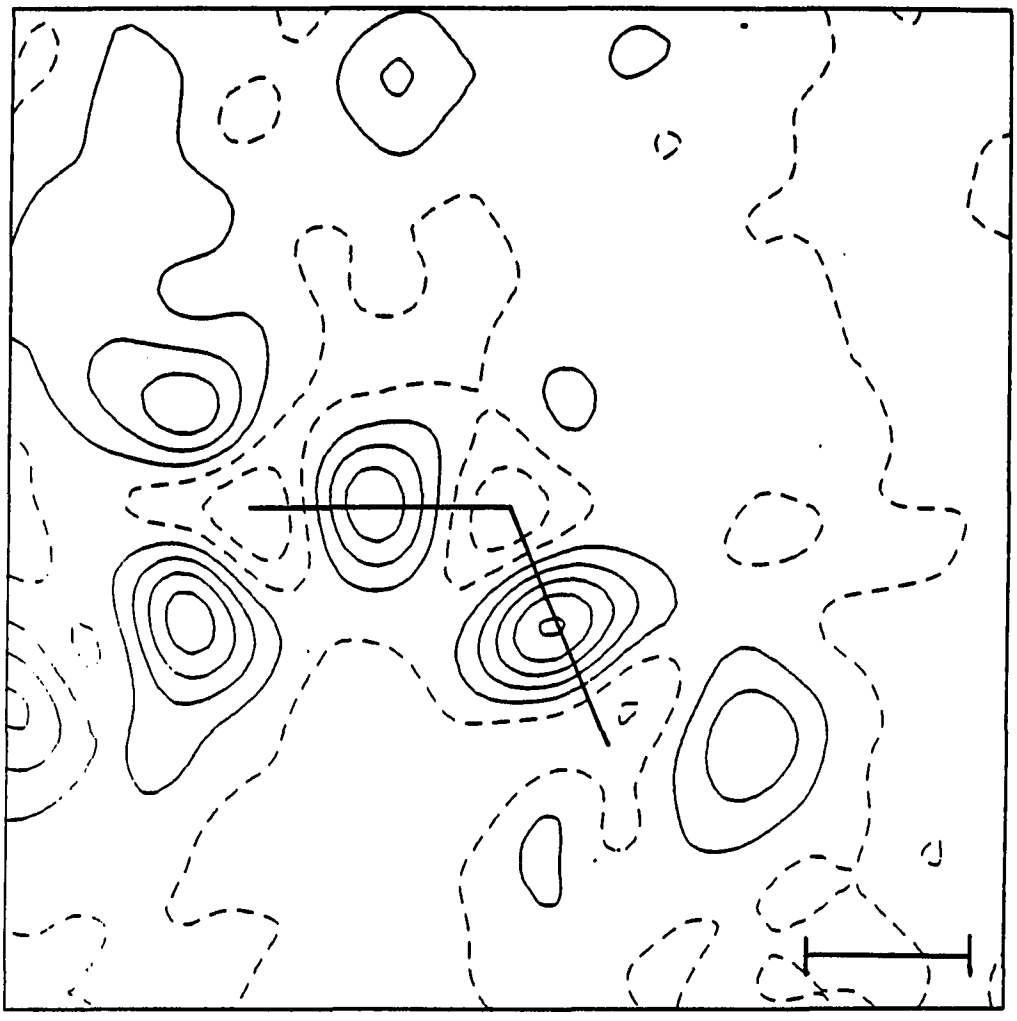

Figure IV.4c. CDD map similar to Figure IV.4a, atoms C9 (left), C15, and C16

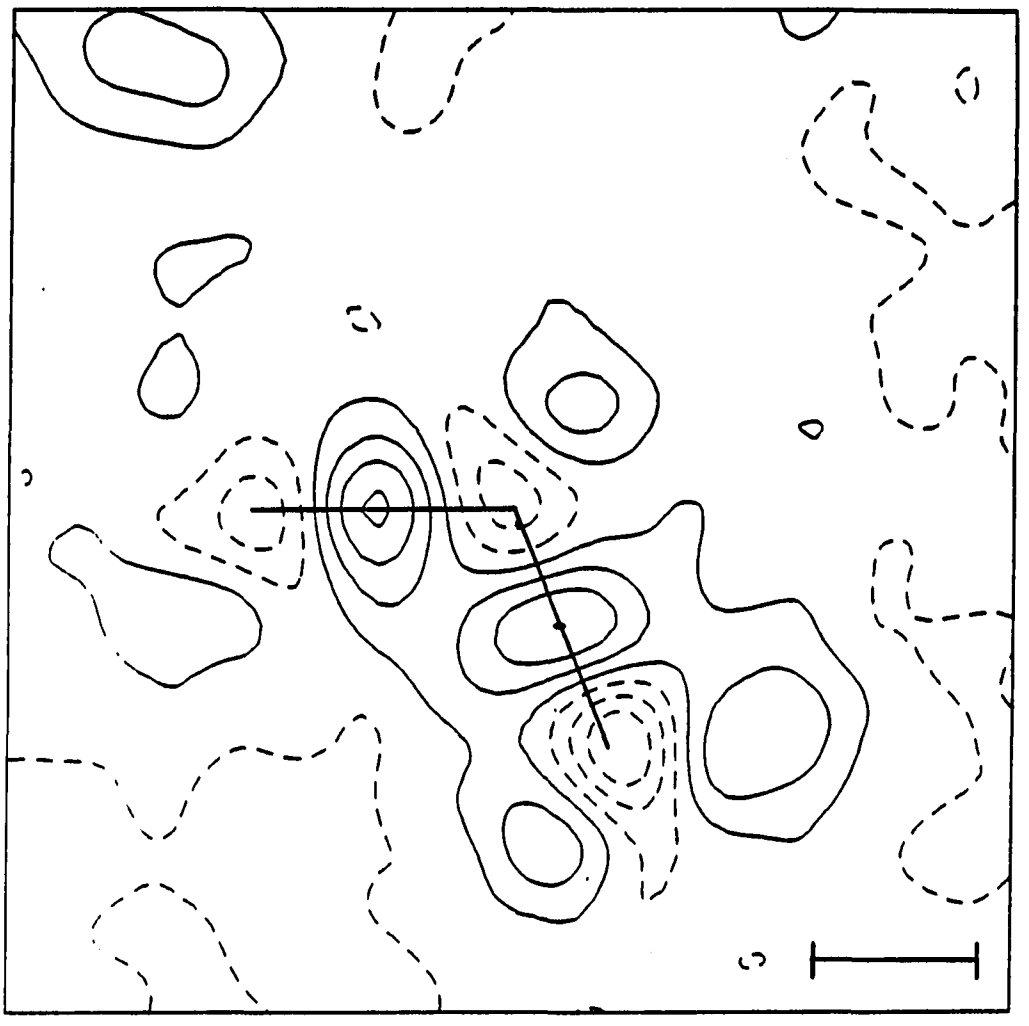

Figure IV.4d. CDD map similar to Figure IV.4a, atoms C9 (left), C15, and C17

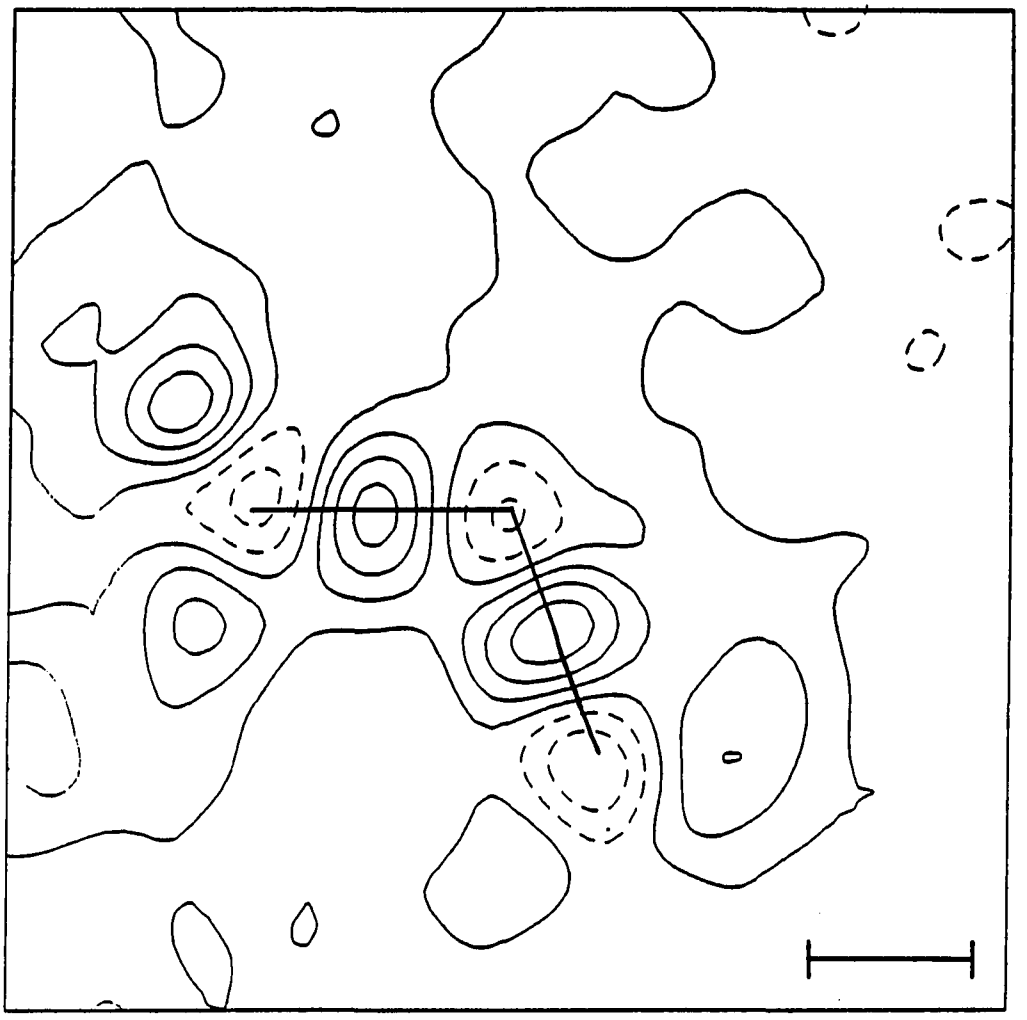

Figure IV.4e. CDD map similar to Figure IV.4a, atoms C9 (left), C15, and C18

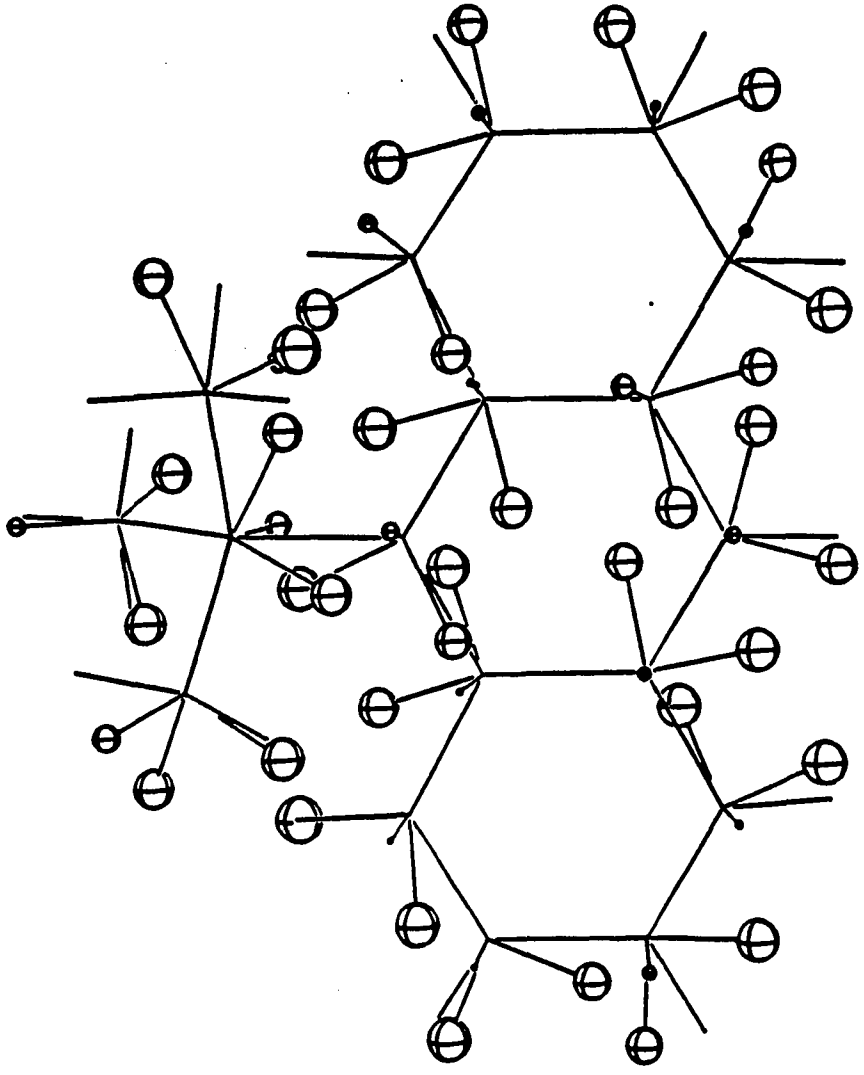

Figure IV.5a. Illustration of the orbital information from Trial 2. Pseudo-atoms placed at the ends of orbital vectors with sizes related to their electron occupancies

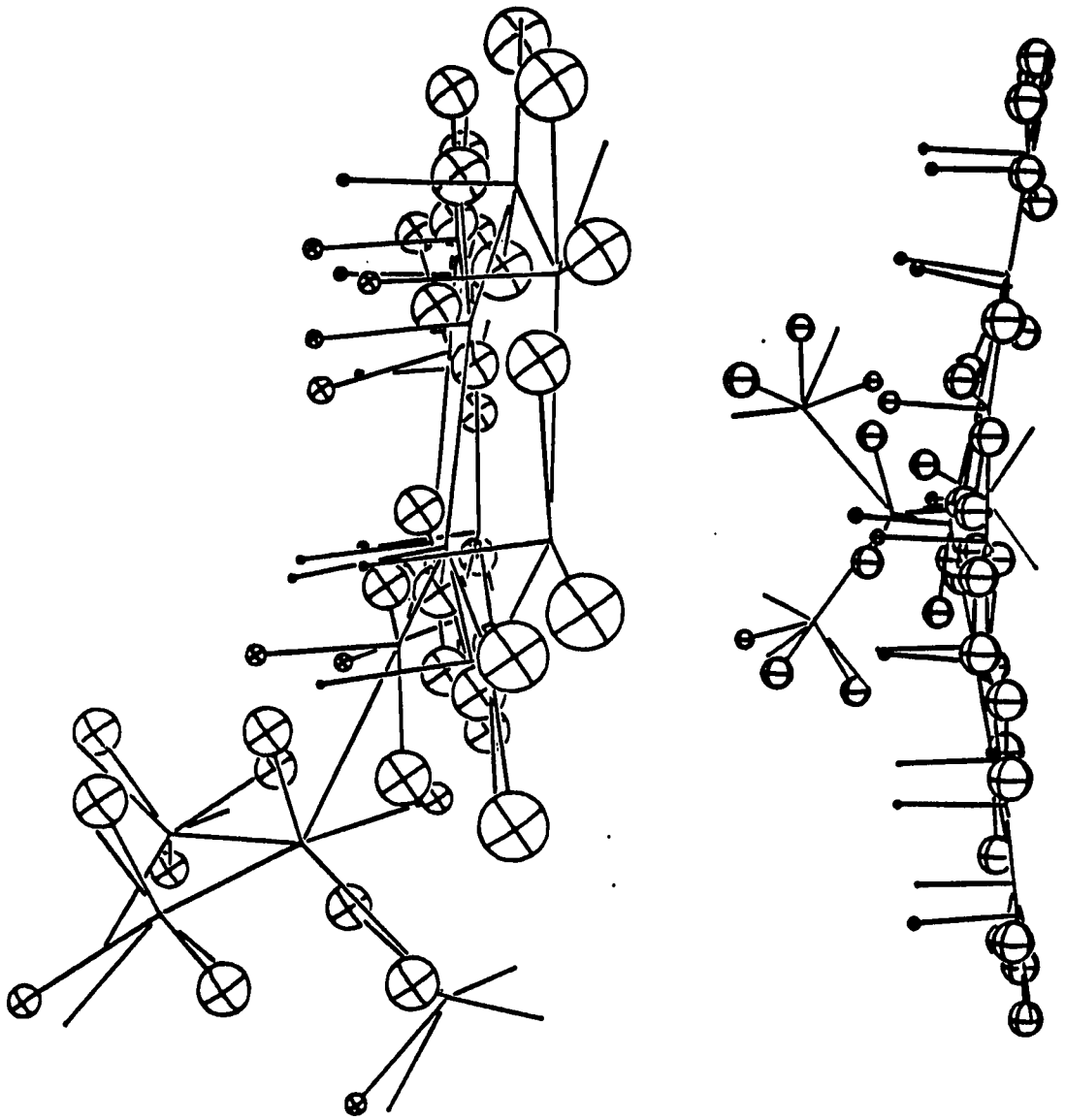

Figure IV.5b. Side and front views of Figure IV.5a

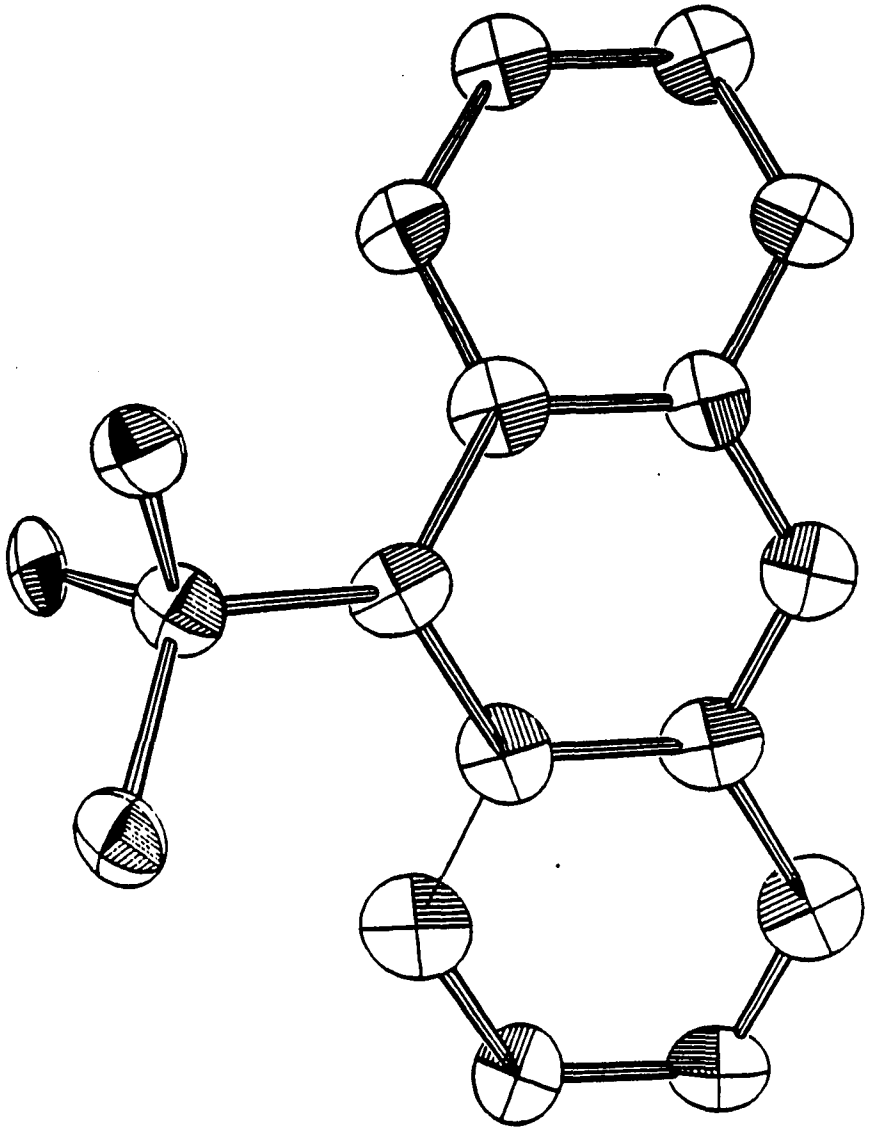

Figure IV.6a. Alternative illustration of orbital information using ellipsoids with principal axes related to electron occupancy superimposed on atomic positions. Ellipsoidal orientation is that of the orbitals

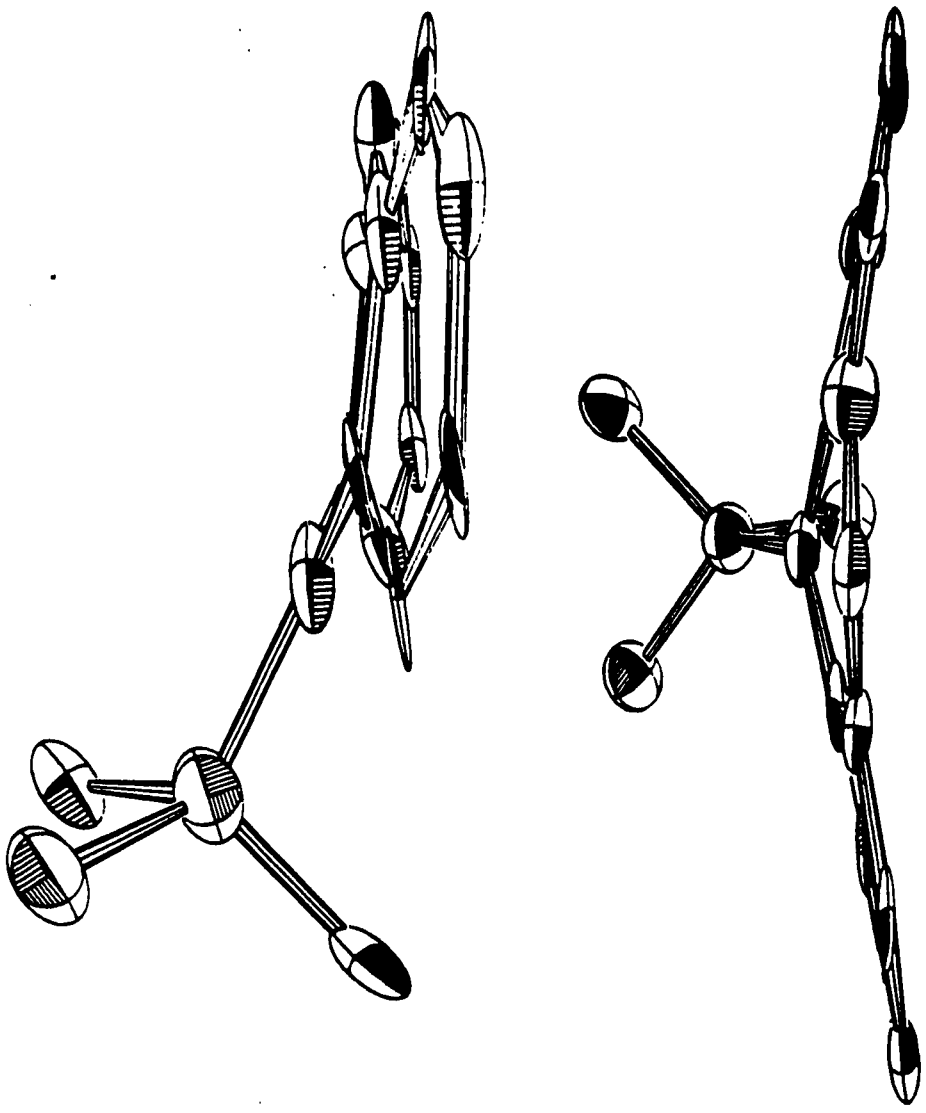

Figure IV.6b. Side and front views of Figure IV.6a

The terminal members of the tertiary group are not near what one might expect. This is assumed to be due to the same effects noted for C15 as well as the rotational disorder not being well accounted for.

Conclusion

The study of 9-tert-butylanthracene has shown that, with a better dataset, results can be obtained which are internally consistent and explainable. Towards this end it has proven useful to have a large number of similar bonding situations which may be compared with one another.

The molecule in this case is somewhat less than ideal since: 1) it has many hydrogen atoms which are not well accounted for, 2) the substituted group shows rotational disorder, and 3) there is no chemical symmetry with which to perform internal comparisons. The dataset too has every indication of being systematically biased in the low-order 0k0 reflections: similar effect was discovered in the high-order data from the same source for 1,2,3-triazine in the 0k0 direction. The effect is to tilt the orbitals such that one is directed virtually parallel to the 0k0 direction.

The differences between the TDD maps in Figures IV.4 and the CDD maps in Figures IV.5 show that the peaks in the CDD maps are more uniform and localized. The interpretation of this is that while the distribution of the TDD may not be

uniform, the electronic changes which occur upon chemical binding (as seen in the CDD maps) are. Thus while some carbon-carbon bond peaks are lower (indicating different bond strengths) in the TDD maps, the electronic changes needed to create the bonds are not different (as seen in the CDD maps).

The ring-atom orbital information shows that near cylindrical symmetry is seen perpendicular to the plane of the ring. The orbitals perpendicular to the rings have near zero occupancy, presently being explained as a compensation for the extra 2s electron contribution in this direction. The effect of the systematic error in the data on the orbital occupancies is unknown.

CHAPTER V. TETRAFLUOROTEREPHTHALONITRILE

Introduction

The study of tetrafluoroterephthalonitrile (TFT) is presented in this chapter. The data for this structure are of the highest quality and resolution available. TFT has been previously studied[14,45,47] (in other respects) which has the advantage of eliminating the need for much of the preliminary work done in the study of the structures of 1,2,3-triazine and 9-tert-butylanthracene.

The structure of TFT is relatively simple with five unique atoms per unit cell. The atoms have nearly equal atomic numbers which has the effect of allowing all atoms' parameters to be determined to equal accuracy. The lack of hydrogens is also important in this respect since they were not well determined in the other studies discussed in Chapters III and IV.

Three trial structures (1, 2, and 3) are presented in this chapter. They represent a high-order refinement of the X-type parameters (atomic positional and thermal parameters and the overall scale factor) and two of the three types electronic constraints which have been discussed in the previous two chapters. The Trial 1 structure resulted from the high-order refinement and these parameters were used for Trials 2 and 3. The Trial 2 structure resulted from a

valence shell parameter determination with the electronic constraint that each atom remains neutral. The Trial 3 structure used the no electronic constraints (i.e., the molecule was allowed to ionize). A model with the electronic constraints allowing only electron transfer was not obtained due to difficulties associated with the atoms on special positions.

The electron density functions are shown in two-dimensional contour maps and in ORTEP-type drawings. The features of the maps, drawings, and of the refinement procedure are described in Appendix E.

Preliminary Discussion

The molecule has crystallographic site symmetry of 2/m and is very nearly planar with an rms deviation from planarity of 0.004Å. The molecular site symmetry reduces the number of unique atoms from fourteen to five. Prior studies of this compound[45,47] have shown that the data are very good and comparisons with theoretical calculations are favorable[14].

Several of the atoms lie on a crystallographic symmetry element. The number of atomic positional and thermal parameters is therefore reduced in the straightforward manner

discussed in Chapter II. The orbital parameters also need to be constrained as discussed in Appendix D. This requires considerable effort in order to determine which of eight possible combinations of constraint models best describes the valence electron distribution.

This study used a high-order data cutoff of $0.85Å^{-1}$, a value which was used in a previous study[47,48]. The value of the sigma cutoff was chosen to be 0. A value of 20 has been used, but such a large value is not considered reasonable as is shown in Chapter II. A summary of the pertinent data and crystal parameters is given in Table V.1. SCF scattering factors were used for all atoms.

High-Order Refinement

The initial positions for Trial 1 were obtained from a previous study. The atomic positional and thermal parameters were refined using a $\sin(\theta)/\lambda$ cutoff of $0.85Å^{-1}$. Due to the site symmetry of atoms C2, C3, and N, the x coordinates were fixed at zero as were the U_{12} and U_{13} thermal parameters. The resultant atomic parameters are listed in Table V.3 and In Table V.4 are the interatomic distances and bond angles. Figure V.1 shows ORTEP[41] drawings of the TFT promolecule, illustrating the positional and vibrational information.

Table V.1. Summary of data and crystal parameters for TFT

Chemical formula	$C_8N_2F_4$
Crystal system	orthorhombic
Space group symbol	Cmca
Lattice parameters	a=7.6848(4)Å b=9.7350(6)Å c=9.5549(7)Å
Temperature of data collection	98K
Total number of reflections	17740
Number after averaging	2387
Number of observed	2179
Internal agreement[a]	0.016
Radiation	Mo k_α (λ=0.71Å)
Sin(θ)/λ (min/max, $Å^{-1}$)	0.098/1.151

[a]Defined as $R_{Int}(<I>)=(\Sigma_k\ |<I>-|I|)/(\Sigma_k\ |<I>|)$.

The refinement statistics are listed in Tables V.5. The atomic positional parameters are in good agreement (differences were less than 1σ) with prior studies[47]. The thermal parameters are systematically higher in this study which is to be expected since an overall temperature factor has not been included in this work.

Table V.2. Summary[a] of refinement conditions for the trial structures

Trial	Refinement parameters	Electronic constraints
1	X	-
2	Ψ	Std
3	Ψ	Ion

[a]See Table III.2 for explanation of terms used.

Table V.3. Summary of atomic parameters for TFT, Trial 1

	x[a]	y	z	RMS[b]
C1	1565.2(3)	591.2(2)	402.0(2)	0.102
C2	0	1198.2(3)	808.3(3)	0.100
C3	0	2419.9(3)	1633.3(3)	0.113
F	3060.8(3)	1152.3(2)	793.1(3)	0.124
N	0	3410.7(4)	2296.2(4)	0.139

	U_{11}[c]	U_{22}	U_{33}	U_{13}	U_{23}	U_{12}
C1	10.1(0)	9.9(1)	11.0(1)	-0.4(0)	-0.6(0)	-1.0(1)
C2	11.6(1)	8.5(1)	9.5(1)	-	-0.6(0)	-
C3	17.8(1)	9.7(1)	10.9(1)	-	-1.5(0)	-
F	11.0(1)	16.8(1)	18.2(1)	-2.1(0)	-2.2(0)	-4.6(0)
N	29.8(2)	12.5(1)	15.7(1)	-	-4.4(1)	-

[a]Fractional coordinates (10^{-4}, Å).

[b]Rms amplitudes of vibration (Å).

[c]$U=(1/2\pi^2)\ \beta\ G^*$ (10^{-3}, $Å^2$), where the temperature factor is of the form $\exp[(k\ \beta\ k^T)/(4\pi^2)]$.

Table V.4. Distances (Å) and angles (°) for Trial 1

Distance			Angle	
C1	C1	1.3839(4)	C1 C1 C2	120.45(1)
C2	C1	1.3952(3)	C1 C1 F	119.93(1)
F	C1	1.3263(3)	C2 C1 F	119.62(2)
C3	C2	1.4269(4)	C1 C2 C1	119.11(3)
N	C3	1.1539(5)	C1 C2 C3	120.45(1)
			C2 C3 N	179.75(4)

Table V.5a. R_ω (10^{-4}) in reciprocal space zones for TFT

#A[a] :	1238	2	2	3	79	28	28
#B :	2179	8	10	11	172	62	62
Trial	ALL[b]	H00	0K0	00L	0KL	H0L	HK0
1[c]	157	121	096	242	168	178	178
1	506	1035	618	922	636	552	520
2	413	729	615	936	546	488	453
3	333	439	457	540	409	372	389

[a]Number of reflections in hkl zones for high-order data (A) and all data (B).

[b]All reflections used to calculate R_ω.

[c]High-order data only.

Table V.5b. R_ω (10^{-4}) in sin(θ)/λ ranges[a] for TFT

Trial	#A[b] / #B	1	14	33	55	102	138	190	246	160 322	371 371	453 453	254 254
1[b]		100	147	197	250								
1		416	907	534	556	814	584	334	175	102	147	197	223
2		555	965	494	462	537	490	346	186	142	160	202	224
3		237	785	557	380	387	347	275	163	132	158	202	225

[a]The sin(θ)/λ ranges are [n-0.1,n) where n=0.1 to 1.2.

[b]High-order data (sin(θ)/λ ⩾ 0.85) only (A) and all data (B).

[b]High-order data were used to calculated R_ω.

Table V.5c. Number of reflections in σ(E) (10^{-4}) ranges[a] for TFT

Trial	n= 1	2	3	4	5	6	7	8	9	10	11	>11
1[b]	844	303	70	18	3							
1	1109	473	157	85	41	35	31	25	17	24	13	169
2	1067	484	161	100	59	49	27	23	23	24	20	142
3	1080	510	199	97	55	47	36	27	16	23	18	71

[a]The σ(E) ranges are defined as [(n-1)σ(E), n σ(E)). A reflection is counted if it lies in the range specified by n.

[b]Only high-order data were used in the calculation.

Valence Orbital Refinement

The valence orbital parameters must be constrained since the atoms C2, C3, and N lie on a mirror plane. As described in Appendix D, the number of variables are greatly reduced by incorporating the constraints but there are two different possible models (model A and model B) which may best describe the three atoms.

The procedure followed here was to refine all three atoms' orbital parameters first using model A and then using model B. This was followed by making eight promolecules (corresponding to the eight permutations of models A and B) and calculating the LSE for each combination. The promolecule with the lowest LSE consisted of using model A for C2 and Model B for C3 and N. The LSEs are listed in Table V.6. The promolecule was then further refined using the neutral-atom constraints to yield the orbital parameters listed in Table V.7a. The orbital information is illustrated in Figures V.2a and 2b using the technique developed in Appendix E.

The refinement of Trial 2 proceeded without great difficulty for atoms C1, C3, and N. It was difficult to determine the correct eigenvectors for atoms C2 and F due to the eigenvalues being so similar ($\lambda_1 \approx \lambda_3$ within σ for C2 and $\lambda_1 \approx \lambda_2 \approx \lambda_3$ within 3σ for F). This causes the eigenvectors to be ill-defined in the least squares determination. Generally one would constrain such parameters in order to remove

Table V.5d. Refinement results for TFT

Trial	LSE	ERF[a]	$\sigma(\rho)$	Scale
1(HO)	1560	0.3131	0.0896	8.87(2)
1	99984	2.8475	0.3325	-
2	66584	1.3304	0.3423	-
3	43343	1.0783	0.2468	-

[a]Modified ERF values as described in Chapter IV.

Table V.6. LSE for all combinations of models A and B for atoms C2, C3, and N

	C2	C3	N	LSE
Models:	A	A	A	64162
Models:	A	A	B	64163
Models:	A	B	A	64281
Models:	A	B	B	64094
Models:	B	A	A	64238
Models:	B	A	B	64113
Models:	B	B	A	64192
Models:	B	B	B	64192

Table V.7a. Orbital parameters for Trial 2

	i	λ_i	a_i[a]	b_i	c_i	Δe^-
C1	1	1.002	-0.047	0.023	-0.999	0.336
	2	0.417	0.935	0.353	-0.036	-0.250
	3	0.581	0.352	-0.935	-0.038	-0.086
C2	1	0.776	-0.152	-0.488	0.860	0.109
	2	0.467	-0.988	0.073	-0.133	-0.200
	3	0.757	-0.002	0.870	0.493	0.091
C3	1	0.406	0.709	-0.705	0.011	-0.260
	2	0.406	0.705	0.709	0.011	-0.260
	3	1.187	0.015	0.000	-1.000	0.521
F	1	1.613	-0.610	-0.780	0.139	-0.054
	2	1.655	0.713	-0.463	0.527	-0.012
	3	1.733	-0.346	0.420	0.839	0.066
N	1	0.770	0.703	-0.711	0.015	-0.230
	2	0.770	0.711	0.703	0.015	-0.230
	3	1.460	0.021	0.000	-1.000	0.460

[a]See text for explanation of orbital orientation.

Table V.7b. Orbital parameters for Trial 3

	i	λ_i	a_i[a]	b_i	c_i	Δe^-	NET[b]
C1	1	0.831	0.004	-0.013	-1.000	0.165	-0.453
	2	0.239	0.979	0.204	0.001	-0.428	
	3	0.476	0.204	-0.979	0.014	-0.190	
C2	1	0.646	-0.054	-0.493	0.869	-0.021	-0.415
	2	0.338	-0.999	0.025	-0.049	-0.329	
	3	0.602	-0.002	0.870	0.493	-0.065	
C3	1	0.318	0.709	-0.705	0.011	-0.349	-0.246
	2	0.318	0.705	0.709	0.011	-0.349	
	3	1.118	0.015	0.000	-1.000	0.452	
F	1	1.458	0.278	-0.181	0.943	-0.209	-0.512
	2	1.468	0.378	0.924	0.066	-0.199	
	3	1.563	-0.883	0.338	0.325	-0.104	
N	1	0.633	0.703	-0.711	0.004	-0.367	-0.500
	2	0.633	0.711	0.703	0.004	-0.367	
	3	1.234	0.006	0.000	-1.000	0.234	

[a]See text for explanation of orbital orientation.

[b]Net change from neutral atoms number of electrons.

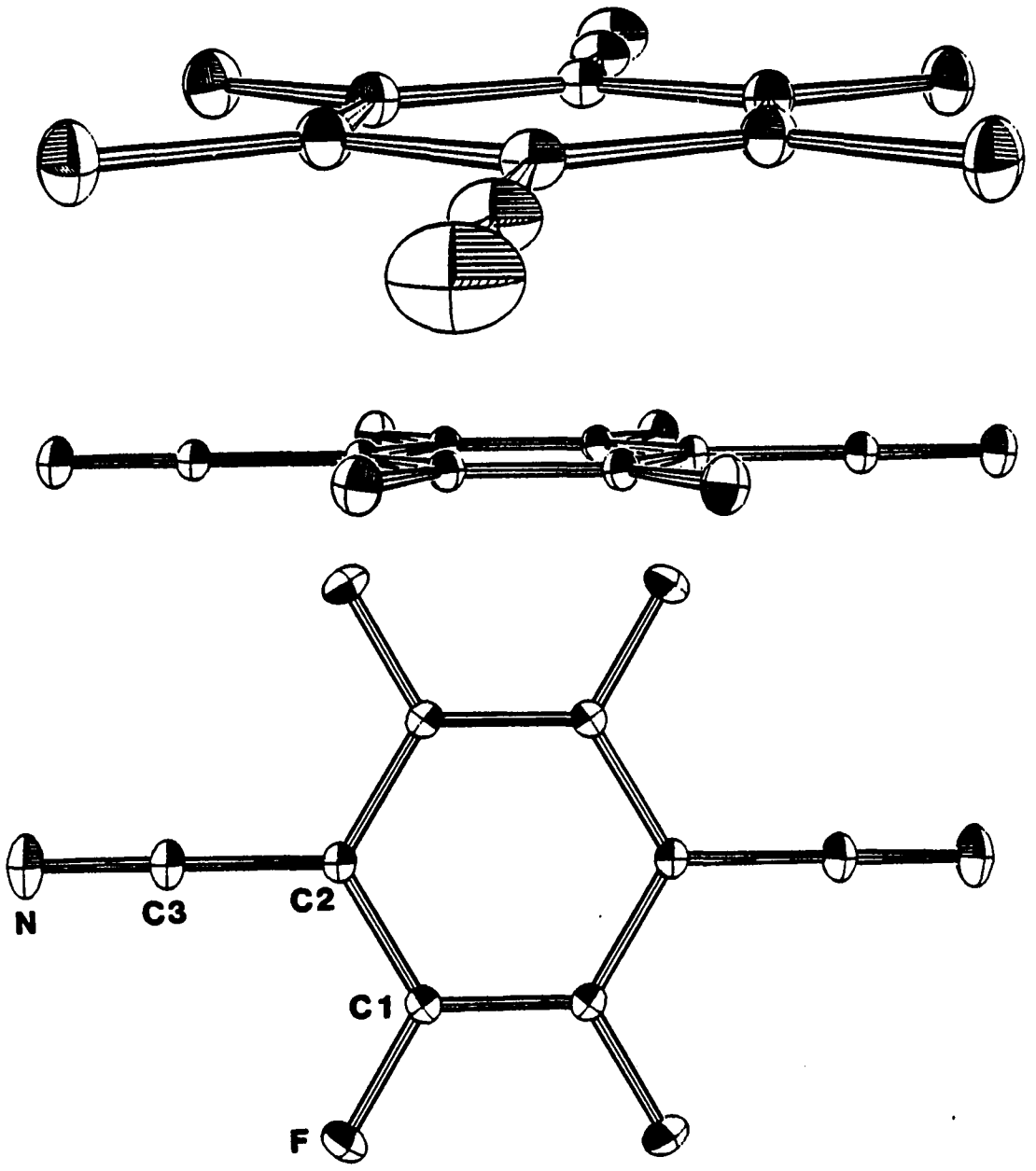

Figure V.1. Three views of the TFT promolecule showing atom identifiers. Symmetry related atoms shown for reference. Atomic vibrations represented by 50% probability ellipsoids. Mirror plane normal to ring, passing through atoms N, C3, and C2. C_2 axis normal to mirror through center of ring

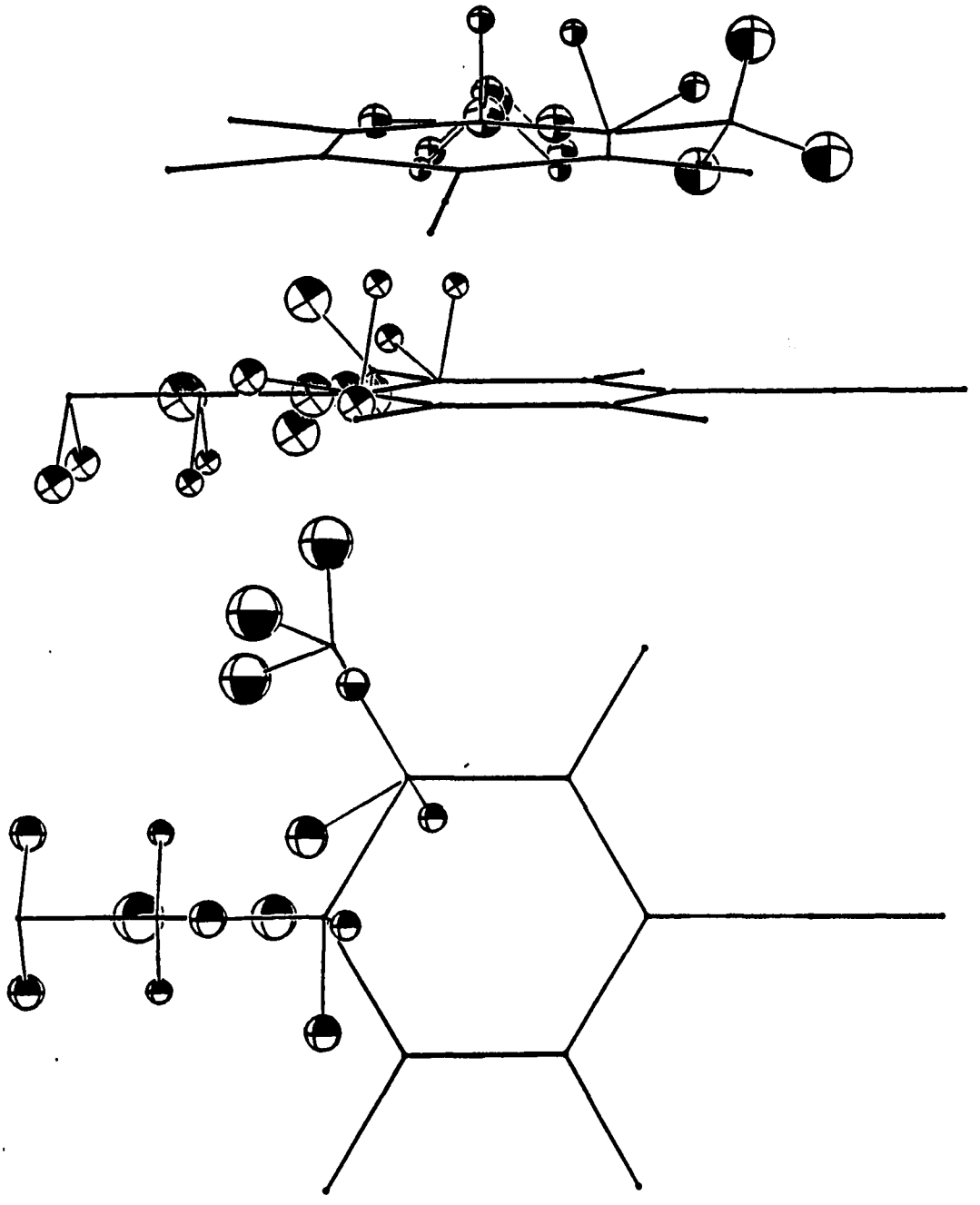

Figure V.2a. Illustrations of orbital information using pseudo-atoms at the end of the orbital direction vectors superimposed on the unique atoms of the molecule. Pseudo-atom sizes are related to orbital occupancies from Trial 2. Molecular skeleton is shown for reference

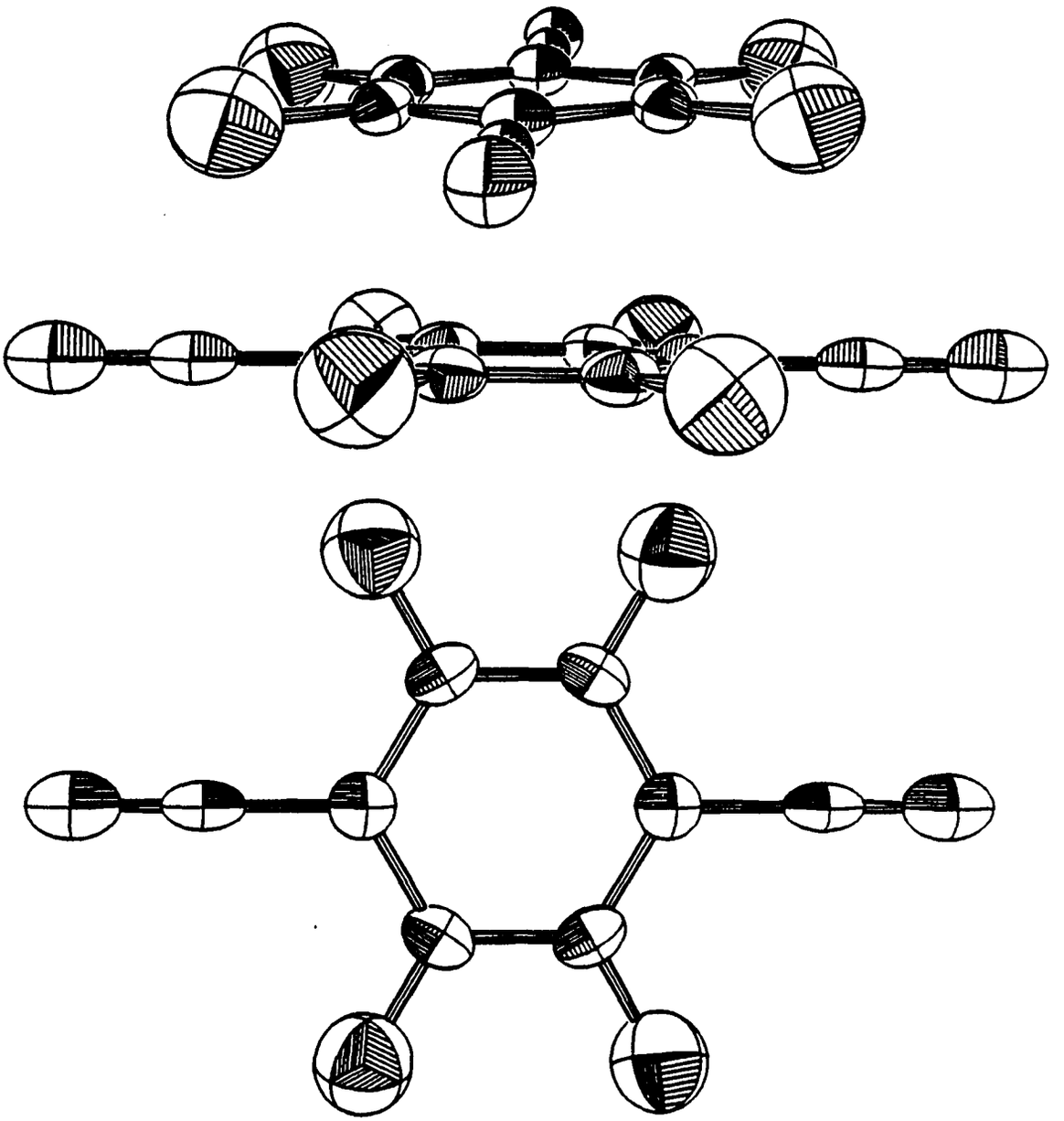

Figure V.2b. Alternate illustrations of orbital information in Trial 2. Ellipsoids with principal axial lengths related to the electron occupancies superimposed on atomic positions. Ellipsoid orientation is that of the orbitals

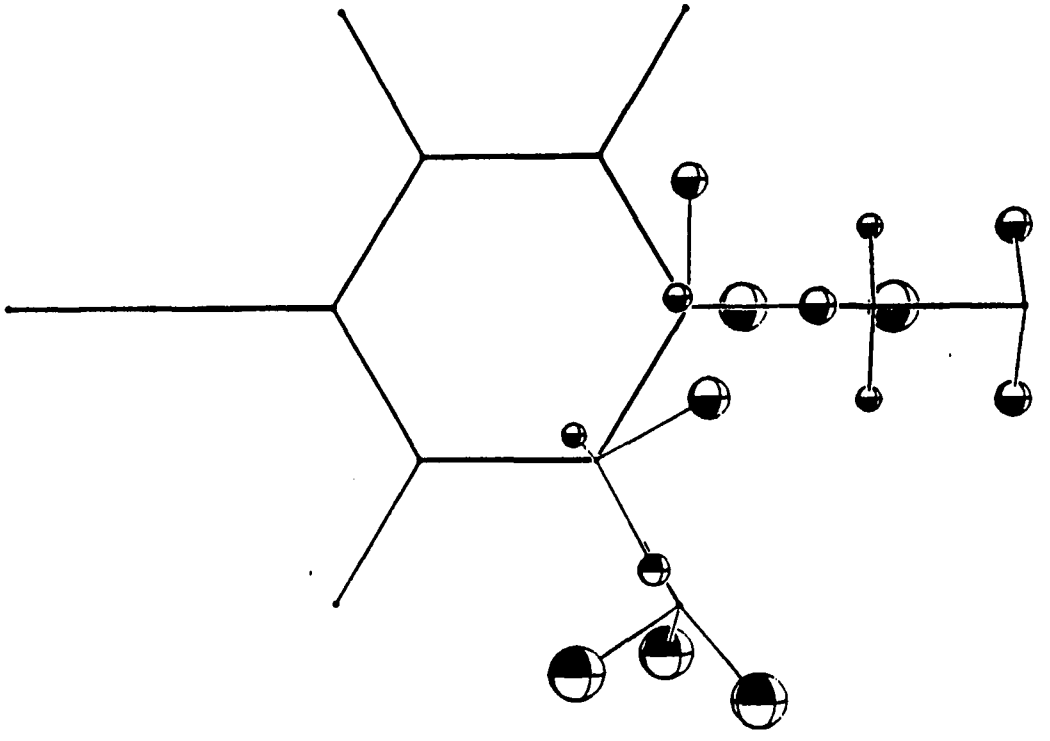

Figure V.2c. Illustration of one view of Trial 3 orbital information, similar to Figure V.2a,

the correlation.

Applying constraints to C2 is not realistic since the orientation of Y_3 is fixed perpendicular to the mirror plane and the single eigenvector parameter (theta) should be essentially independent of any relation between the two eigenvectors. For F the eigenvectors should perhaps be interrelated but this would mean setting the eigenvalues to 1.667, thus producing a spherical valence shell where the values of the eigenvector coefficients are not relevant.

In Trial 3 the electronic constraints were removed from the total number of electrons, thus allowing the molecule (and atoms) to ionize. To do this meant that the constraints on λ_3 (N_3 in Appendix D) had to be removed from the model B atoms, leaving in place the constraints that $\lambda_1=\lambda_2$ since the occupancies must still obey the site symmetry. The valence orbital refinement results are given in Table V.7b. Figure V.2c is an illustration of one view of the orbital information.

λ_1 and λ_3 are again equal (within 1.5σ) for C2 in Trial 3. The λ_3 eigenvalue (parallel to the C1-F bond) differs from λ_1 and λ_2 by 5σ producing a cylindrically symmetric valence shell ($\lambda_1\approx\lambda_2$ within σ) parallel to the bond. This dictates that λ_1 should be set equal to λ_2 and the eigenvectors constrained to reflect the local symmetry (the

degrees of freedom would be reduce from 3 to 2 in this case). Comparison of Figures V.2a and 2c show that the rotation about F is very large as one goes from Trial 2 to Trial 3. This emphasizes the fact that the orientation of F in Trial 2 is irrelevant due to the sameness of the eigenvalues.

The orientations of the a), b), and c) directions in Tables V.7 for C1 and C2 are as follows: a) is perpendicular to the benzene ring, b) is radially outward, and c) is tangential to the ring. For F, C3, and N: c) is radially outward along their bonds, b) is in the plane containing C1, C2, and the atom in question, and a) is perpendicular to b) and c). The signs of the orbital direction vectors may be changed at will.

Discussion

The valence orbital model (model B) which best describes N and C3 matches our chemical knowledge in that the triple bond is cylindrically symmetrical along the bond. It is this triple bond which also induces the net gain of electrons in orbitals parallel to the bond on both atoms in Trials 2 and 3. By now the valence orbital model (model A) which best describes C2 comes as no surprise. The valence orbitals have cylindrical symmetry normal to the molecular plane with fewer electrons in the orbital perpendicular the plane. Similar results were seen for 1,2,3-triazine and 9-tert-butylanthracene and the rationalization is the same.

The fluorine atom is quite close to being spherically symmetric in Trial 2 and cylindrically symmetric in Trial 3. C1, in contrast to prior experience, has no rotational symmetry. As shown later, this is most likely due to the differences in the C1-C1′ and C1-C2 bond density, the orbital with the highest occupancy being along the highest density (C1-C1′) bond. The lowest occupancy orbital is still normal to the molecular plane, reinforcing previous findings.

Figures V.3 are maps of the observed electron density (note that all contour maps presented in this chapter have the small constant background due to E(0,0,0) included wherever appropriate). The fragment of the molecule shown is the area surrounding the unique atoms, a mirror plane lies normal to the molecule and passes through atoms N, C3, and C2.

Figure V.3a shows the expected dominant core features as well as the triple bond. Figure V.3b is 0.4Å above the molecular plane and reveals a very intricate pattern which may be due to our inability to accurately model this region (which includes most of the π bonding) with our promolecule. This inability to model the electron density in this region can be translated into an inability to calculate the correct phases for the reflections. In Chapter II the use of incorrect phases has been shown to modify peak heights and shapes. An alternative explanation is that these are artifacts of the Fourier truncation effect described in

Appendix E and illustrated in Chapter II. The latter is not as serious as the former since such ripples will be subtracted off in the difference maps where we wish to see detailed information. Figure V.3c is a view of the N-C3-C2 axis, normal to the plane of the ring. The density shown here is nearly identical to that of Figure V.3a.

Figure V.4a is a partial difference electron density map in which the core (1s and 2s) electrons were subtracted from the observed electron density. Figure V.4b is a similar map normal to the plane of the ring. The interpretation of these maps is that they show how the valence electrons are distributed; some are still localized about the atoms and some have moved into the bonding regions. Here we see that the triple bond is very large and essentially engulfs the nitrogen atom. We also see a hexagonally curved bonding ridge around the benzene ring. This electron density lies on the inside of the atoms and is centered at the mid-points of the internuclear vectors. Although is is not clear on the maps, this ring-type electron density tapers off towards zero at the center of the benzene ring. The fluorine's valence shell is elongated towards the ring, an indication of either bonding with C1 or electrostatic distortion of its valence electron cloud.

Figure V.5 is a TDD map created by subtracting the spherical atoms in Trial 1 from the observed electron

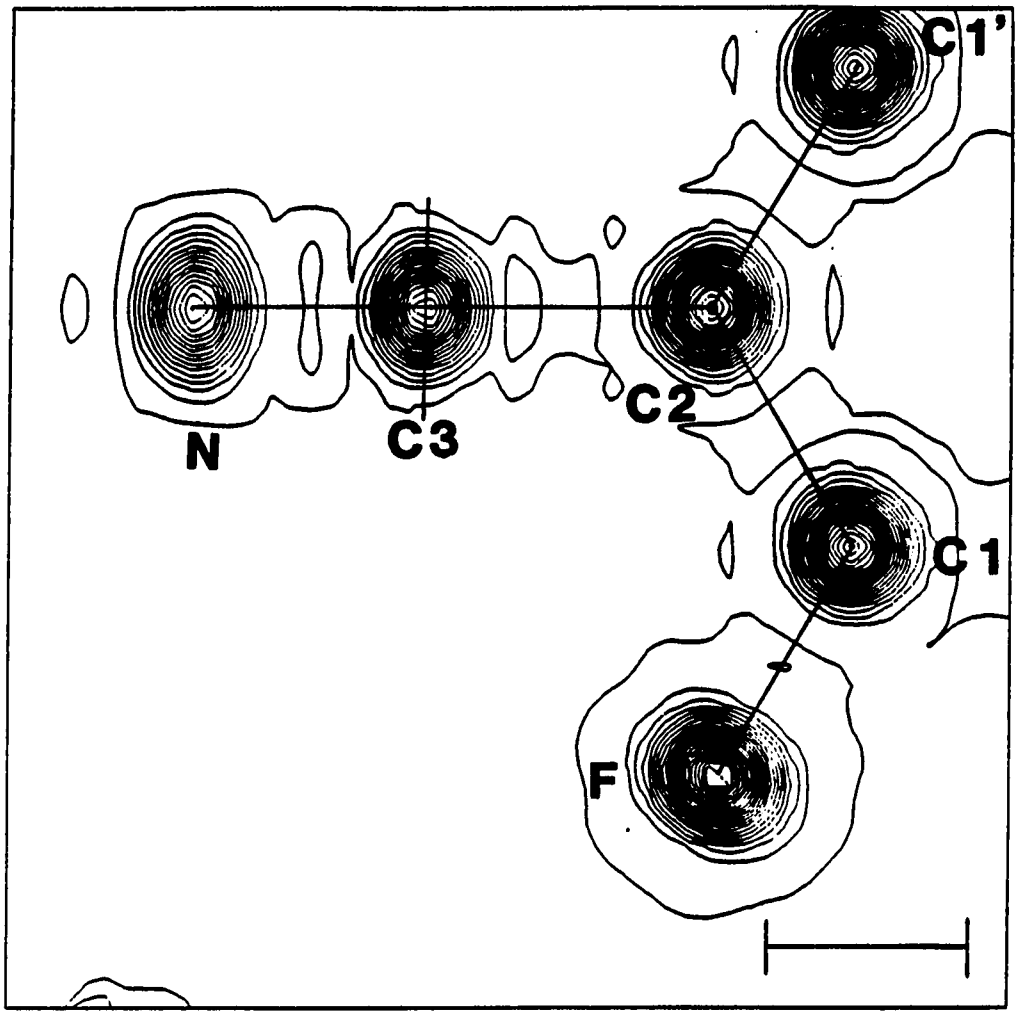

Figure V.3a. Contour map of observed electron density for TFT, CI=1.0$e^-/Å^3$. See Appendix E for explanation of map features for this and all other contour maps

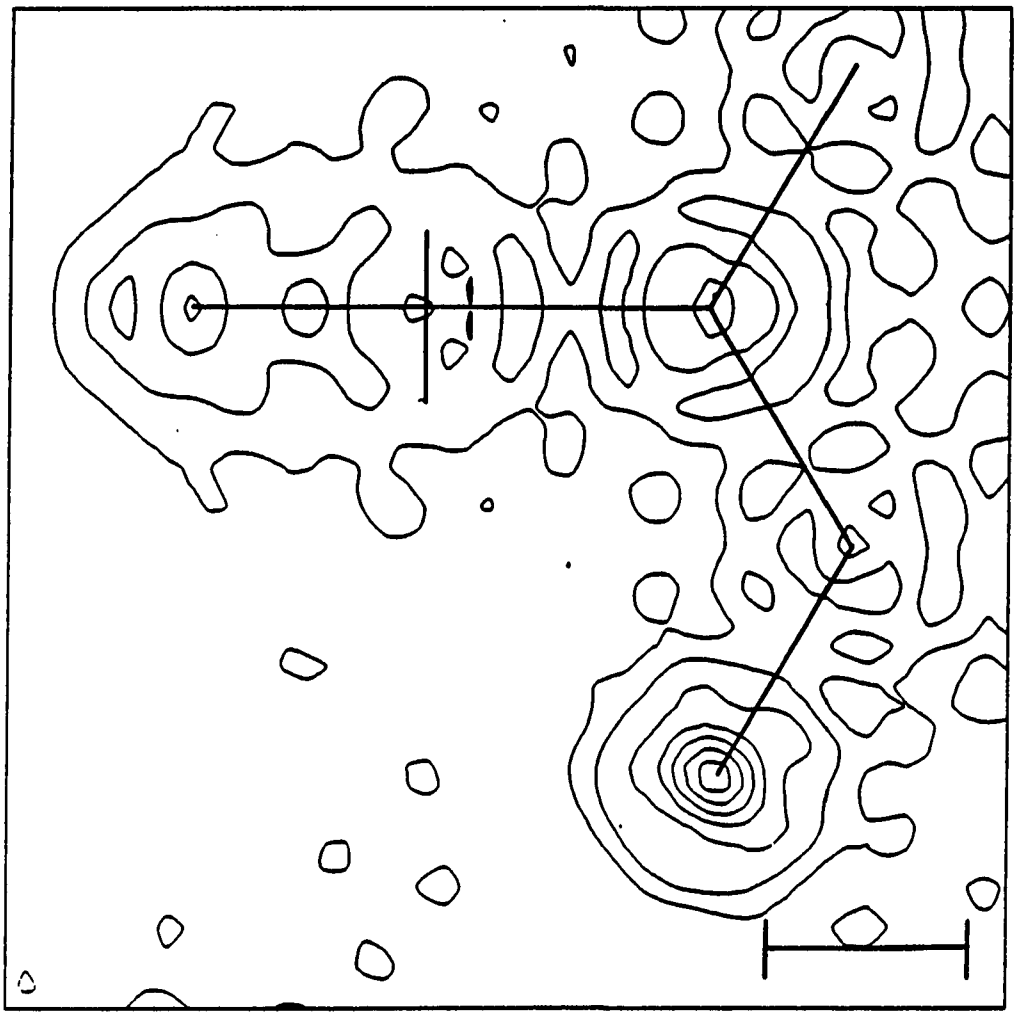

Figure V.3b. Similar to Figure V.3a. View 0.4Å above ring. CI=0.5$e^-/Å^3$

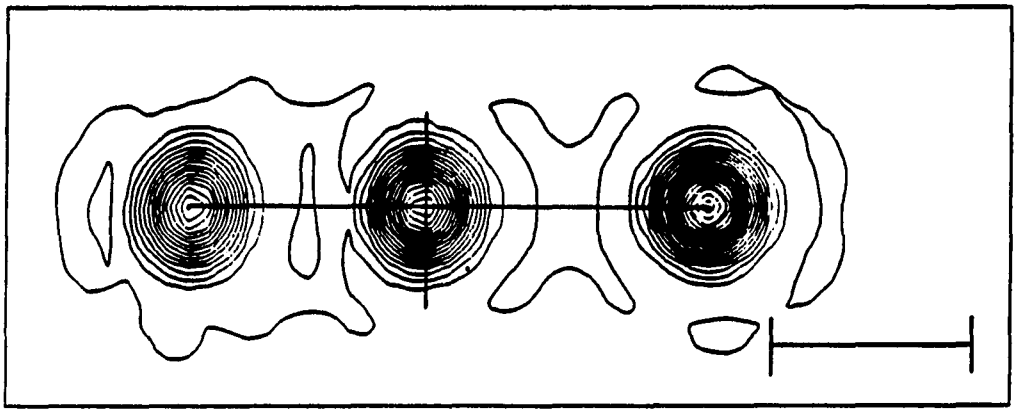

Figure V.3c. Similar to Figure V.3a. View normal to ring passing through N (left), C3, and C2. CI=1.0$e^-/Å^3$

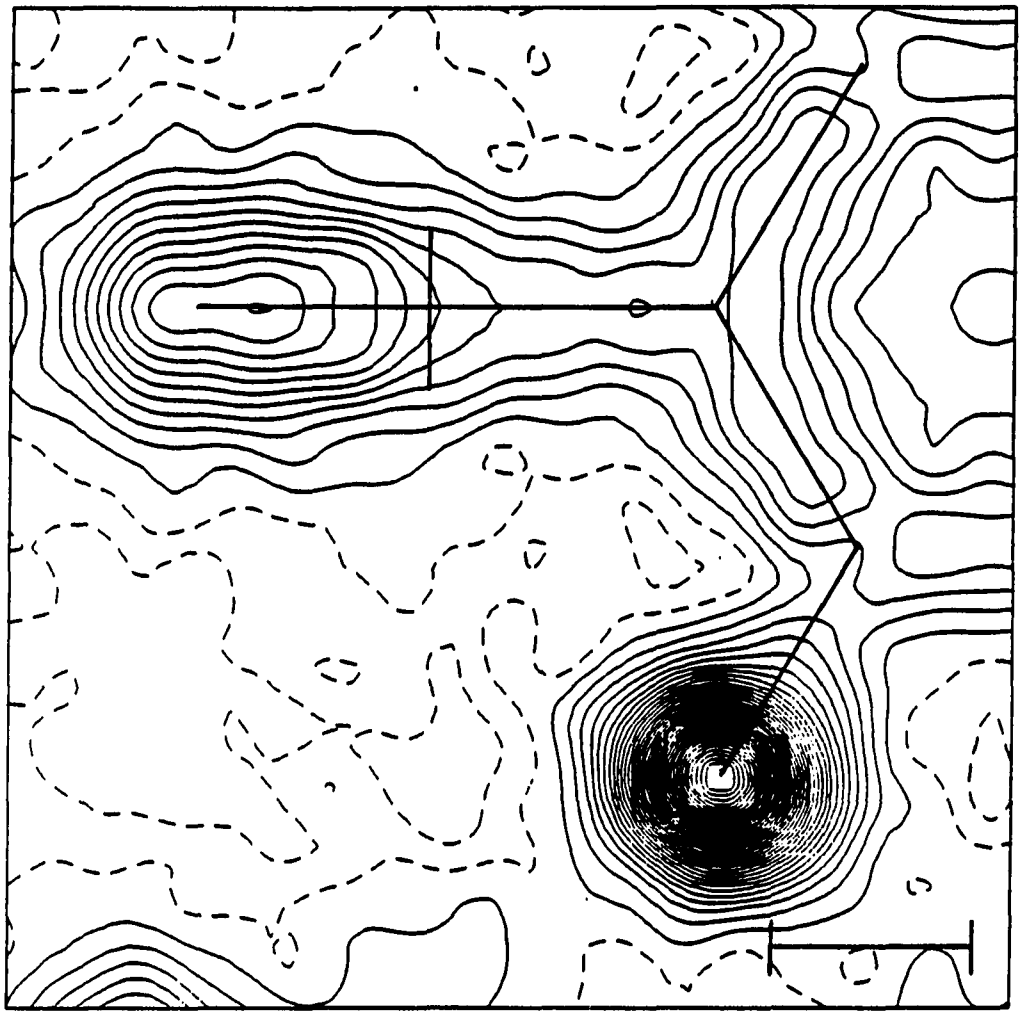

Figure V.4a. Partial difference density map. Observed density minus 1s and 2s electrons. CI=0.1e$^-$/Å^3

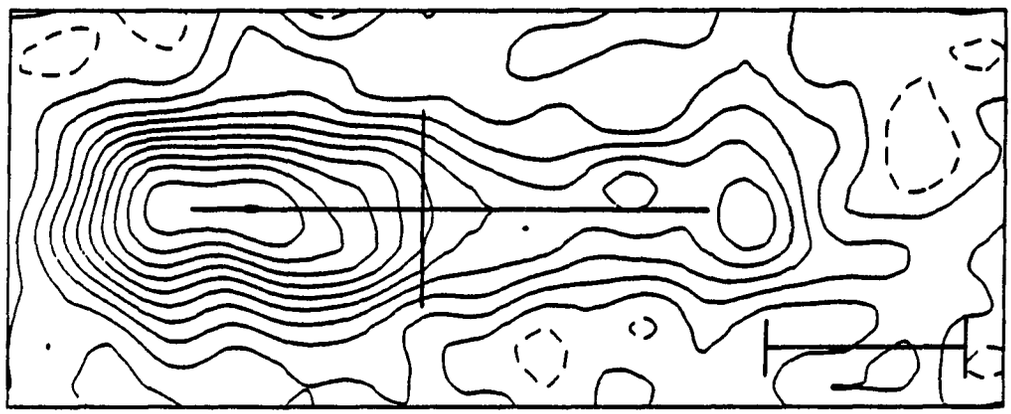

Figure V.4b. Similar to Figure V.4a. View normal to ring passing through N (left), C3, and C2. CI=0.1e$^-$/Å^3

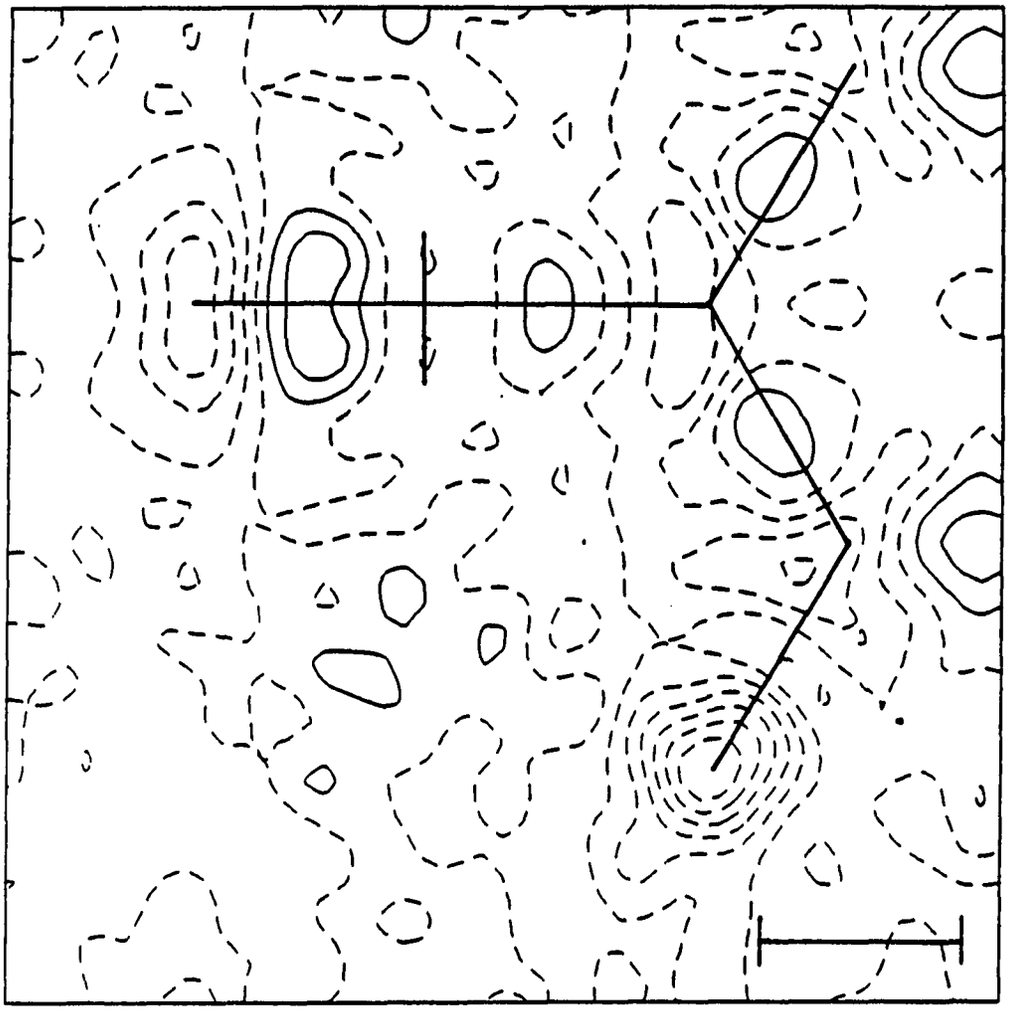

Figure V.5. TDD map using spherical atoms from Trial 1. CI=0.1e$^-$/Å^3

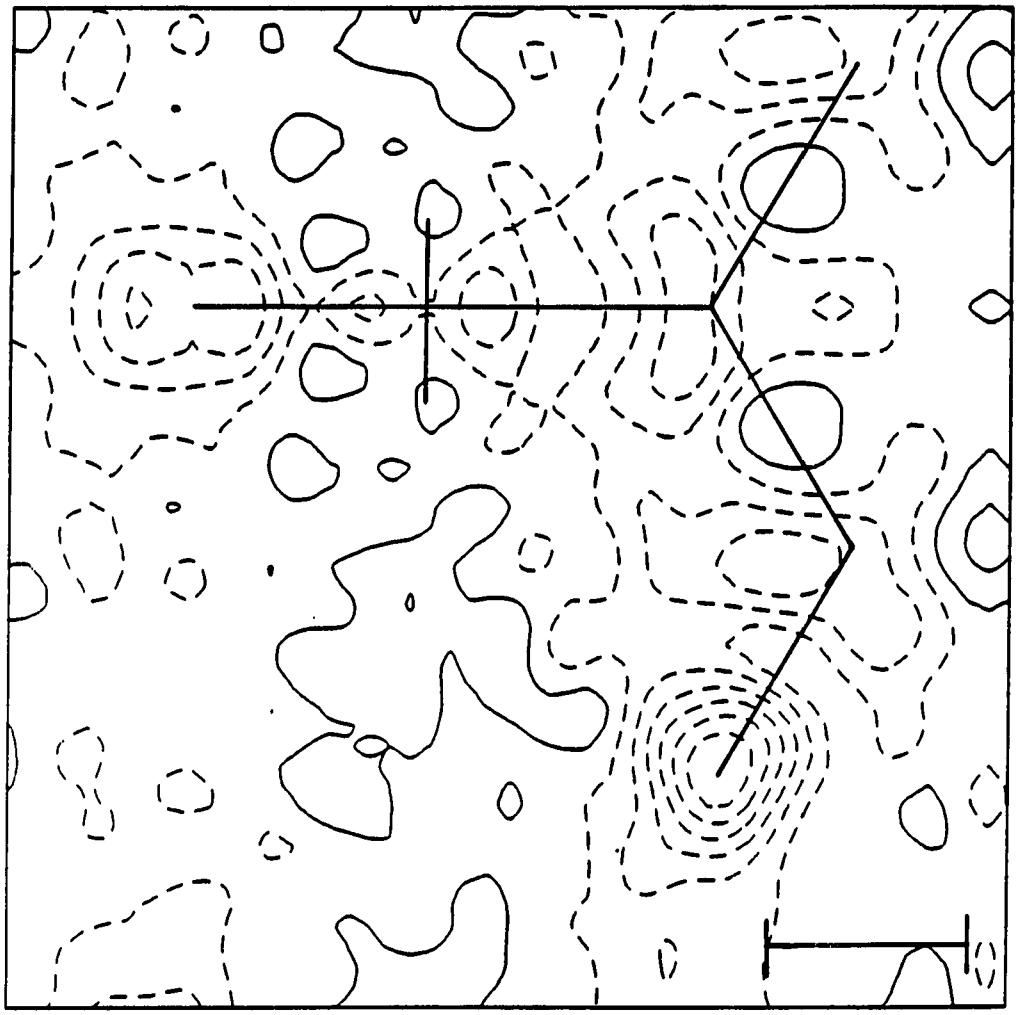

Figure V.6a. CDD map using oriented atoms from Trial 2. CI=0.1e$^-$/Å^3

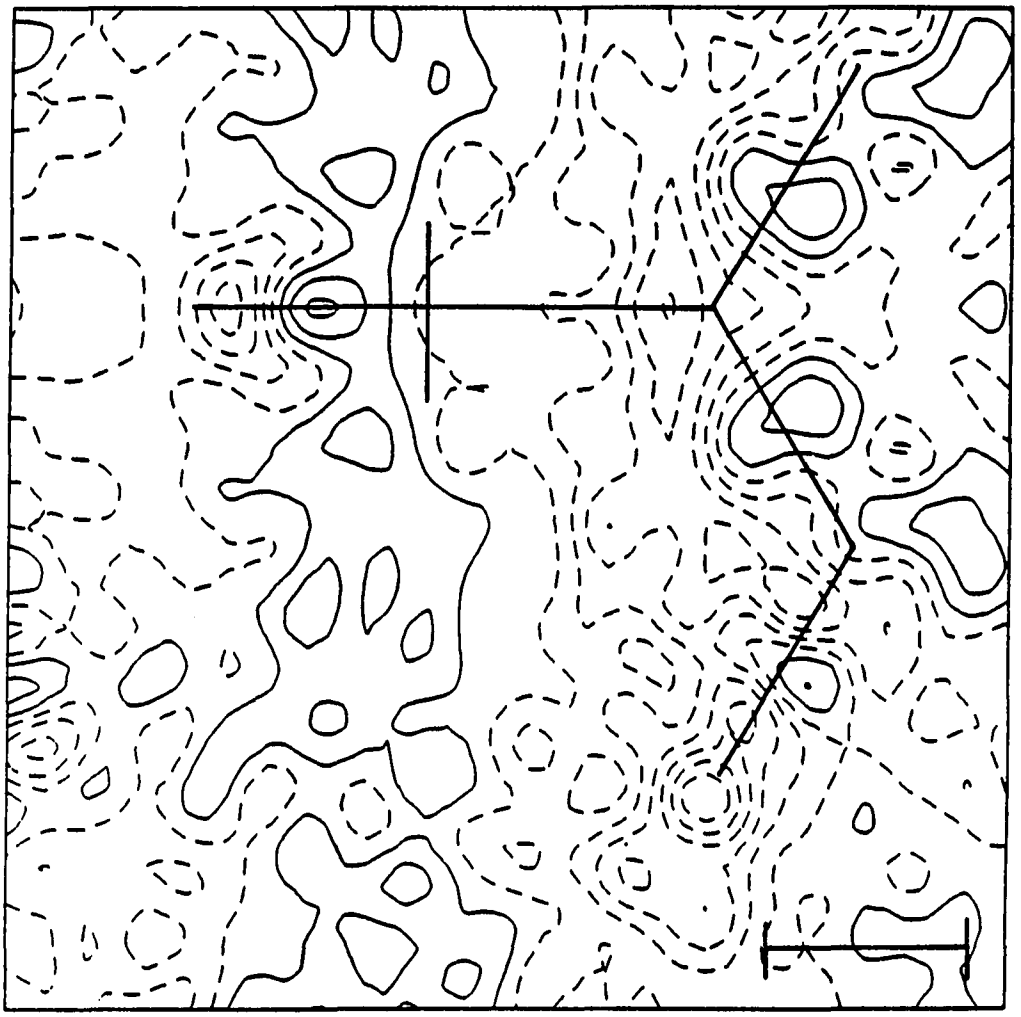

Figure V.6b. Similar to Figure V.6a. View 0.4Å above ring. CI=0.1e$^-$/Å^3

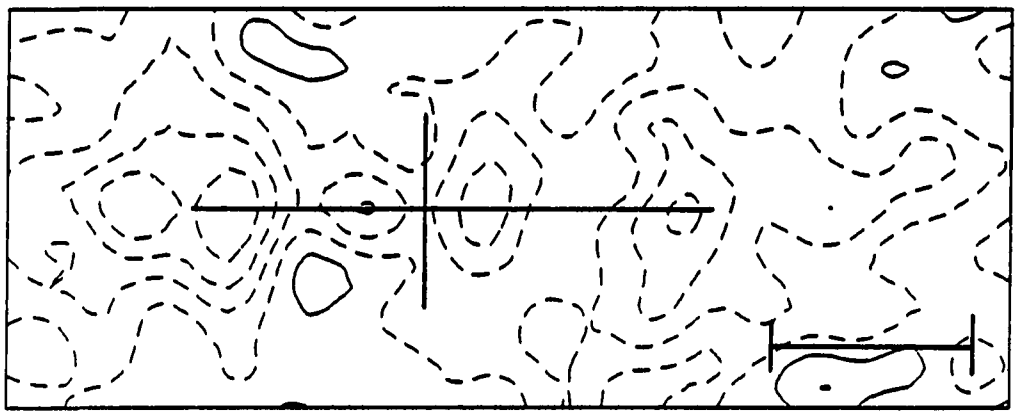

Figure V.6c. Similar to Figure V.6a. View normal to ring passing through N (left), C3, and C2. CI=0.1e$^-$/Å^3

density. Static deformation maps have been theoretically calculated[14] and the results agree qualitatively (the electron density maps calculated in this work are of the dynamic density, so called due to smearing of the electron density over space and time).

The features which are most notable are the unequal TDD peak heights of C1-C1' and C1-C2. The two-to-one ratio is in agreement with theory and corresponds to an increased bond strength[14]. This effect is also the cause of the non-cylindrical symmetry of the C1 orbitals (note that the orbital with the largest electron occupancy is along the C1-C1' bond.

The F-C1 bond exhibits a net loss of electrons from the spherical-atom promolecule. Theory predicts a build up of charge in the center of the bond and a depletion near the fluorine atom, these detailed features are not be observable due to the smearing effects present in this work. The two-to-one ratio of the N-C3 and C3-C2 bond peak heights is predicted by theory but the prediction of a build-up of electrons on the outside of the nitrogen atom is not realized.

The CDD maps created by subtracting the oriented-atom promolecule (Trial 2) from the observed electron density are shown in Figures V.6. Comparing Figures V.6a and V.5 again illustrates an improved accounting for the valence electron redistribution in the CDD maps. Figure V.6a still shows the

two-to-one C1-C1' to C1-C2 peak height ratio, but the σ bonds for N-C3 and C3-C2 have been modeled very well. The π_r (π orbitals parallel to the plane of the ring) bonding electrons are unaccounted for in the vicinity of the N-C3 bond as seen in Figure V.6a.

Figure V.6b is most illuminating since not only do we see π bonding electrons (π_p) 0.4Å above the ring in the N-C3 bond, but also above the C1-C1', C1-C2, and the F-C1 internuclear vectors. The lack of sigma-type bonding electron density in TDD maps of the F-C1 bond is a marked feature of this molecule. An examination of Figures V.4a and 6b indicate there is both sigma and π_p bonding. The lack of positive TDD density is due to the relatively excessive amount of electron density subtracted from the bond when using spherically averaged, neutral atoms.

Another feature of Figure V.6b is the N-C3 π_p orbital has a greater occupancy than does the π_r orbital. It is argued from theoretical calculations that some of the π_p should be lost due to a quinoidal-type resonance form in which the C3-C2 bond has some non-formal π_p character. Neither the C3-C2 π_p character nor the lower π_p character is found in this work.

Conclusion

The dataset is the best which has been used. The resolution extends far beyond the deformation density scattering range and absent are the errors seen in Chapters III and IV. The choice of molecule is good in that the atomic scattering powers of the atoms are nearly the same. Two features which would have improved this choice are more non-symmetry related atoms to which comparisons could be made and some type of strong intermolecular interaction which would reduce the rigid-body motion found in another study[47].

The high-order structure determination was carried out without difficulties and comparisons between this and other studies[45,47] are favorable. The main difference are in the thermal parameters which are systematically higher here owing to a lack of an overall temperature factor.

The orbital refinement was complicated by the site symmetry of the atoms N, C3 and C2. It was determined which of two possible models best described the atoms, and the results, especially for these three atoms, match our expectations. The atoms C2 and F developed some difficulty in their refinement due to the local symmetry inducing correlations amongst the eigenvectors. It was not possible to include additional constraints for most of the cases since the parameters were already constrained or since the constraints essentially consisted of fixing the atom's (F) eigenvalues to their spherical free-atom values.

Theoretical results[14] agreed well on a number of points observed in the electron density maps but the π_p bonding of F and C1 was not predicted and no evidence of the N=C3=C2 resonance structure was seen.

CHAPTER VI. SUMMARY

Review

The studies presented in this thesis have shown that it is feasible to obtain promolecule information beyond that of positional and vibrational parameters. The first step towards obtaining valence orbital information is to put aside the conventional concept that one is trying to fit the entire dataset (i.e., model all of the electron density). It is only the core information which can be truly modeled with a promolecule. A high-order parameter refinement must be completed before meaningful valence orbital information can be obtained (this is unfortunate since the very good datasets are also rare). From a high-order refinement one obtains accurate scale and atomic positional and thermal parameters.

Beyond the capabilities of the spherical-atom promolecule model, orbital information is obtained in the next stage from an oriented-atom promolecule. This information consists of eigenvalues and eigenvectors of the electron density matrix which describes the valence orbitals. The eigenvalues are simply the electronic occupation numbers for each orbital. The eigenvectors are easily understood for the p-orbitals as a rotation matrix which gives the orientation of the p-orbitals in space. Two methods of illustrating the valence p-orbital information, and how they relate to the molecule,

have been developed during the course of this research and facilitate the understanding of the results.

Concepts

The purpose behind a high-order refinement is to obtain better promolecule (X-type) parameters, something which can only be done using high-order data. This is due to the fact that the low-order data consist of: 1) core electron scattering, 2) some fraction of the non-bonded atoms' valence electrons, and 3) the remaining valence electrons which have been modified upon molecular and crystal formation. It is this third type of low-order data which we cannot model using a promolecule. The high-order data on the other hand consists of only the core electrons' contributions, and since we can model the core electron scattering very well with a promolecule, this is the only place where highly accurate parameters can be obtained. For this same reason it is only in this high-order data region where statistical analysis based on the comparison of the molecule and the promolecule can be applied.

The preceding paragraph is summarized by saying that the promolecule does not attempt to fit all of the (low-order) data. Instead we attempt to determine how much of the low-order scattering can be accounted for by a highly constrained valence orbital model. The remaining electron density is the deformation density.

Although the concepts involved in a high-order refinement have been around for a number of years[10], the techniques used in standard crystallography still are often incorrectly used. It is unfortunate that the standard practices of using an overall residual index, secondary extinction corrections, refining the scale against all data, etc., have carried over into high-order refinements.

It has been the practice in the past to assume that the changes which occur upon chemical bonding are given by the observed electron density minus a promolecule consisting of spherically averaged atoms. While this approach is informative, it is also misleading in that these are not the only due to electronic changes, but also include orientation changes which involve virtually no chemistry[18,19]. These latter changes account for approximately one half of the deformation density as seen in comparisons of TDD and CDD maps in Chapters III, IV, and V.

The net result obtained from this work is that the part of the deformation density which is due to energetic changes is separated from the information related to the orbital effects which do not include chemistry. This separation has only been possible in theory[18,19] until now.

Prerequisite Considerations

If a molecule is intended to be studied using the advanced concepts described herein, it must first have a moderate quality dataset measured in order to determine its actual suitability. It is not correct to select a molecule without first ascertaining the feasibility of obtaining useful results[39].

In Chapter III it was shown that a high-order refinement must be carried out before further information is sought. A high-order refinement requires data which extends in $\sin(\theta)/\lambda$ well beyond the point at which the deformation density contributes significantly. This dataset should also be highly accurate and free from systematic errors, conditions not met by either of the datasets described in Chapters III and IV where systematic errors had consequent effects on the orbital information obtained.

The calculated orbitals model the regions of high and low slope in the electron density function quite well. This reinforces the idea that data collection should be carried out at low temperatures in order to sharpen these features. It is just as important to carefully select a molecule with little disorder or rigid-body motion. This may be accomplished by choosing a molecule which has hydrogen bonding or using molecular packing and steric hindrance. The hydrogen atoms were not considered strongly in this work

since a method of dealing with them has not been incorporated. They are not suspected of having a serious impact on the promolecules' parameters but future work should deal with this problem, either by using more appropriate scattering factors, by using neutron diffraction data, or by calculating the optimal positions using an iterative energy minimization approach.

In order to avoid systematic errors, which are so difficult to detect, crystal preparation should be carried out carefully. Electron microscopy can give information on the crystal's quality. A spherical crystal will not suffer from anisotropic absorption effects. Thermal shocking a crystal can often improve the mosaic spread of domains within a crystal.

This work has used a number of statistical checks on the agreement between the observed and calculated structure factors. No single result is sufficient to isolate potential problems but, provided care is taken in not reading too much into the numbers, the results of the statistical tests combine to form a useful diagnostic tool. More involved analysis procedures would no doubt be beneficial in future work. One of these functions (ERF) was found in Chapter IV to be poorly defined and a new definition suggested. This function is one which utilizes all data in its calculation and thus is used in this work only for comparisons between

very similar models using identical data. The use of the standard overall residual has been dropped; there is little additional information to be gained from its use and it has been too often misused.

Refinement Considerations

Once the requirements for a dataset have been met, the structure solution follows. The first step is to obtain a rough idea of the atomic positions. Electron difference maps are then calculated with various $\sin(\theta)/\lambda$ cutoffs and the deformation density peaks heights are plotted against the $\sin(\theta)/\lambda$ cutoff limit. Some point beyond the curve plateau, which retains a significant number of reflections, is selected as the high-order data limit.

The X-type parameters (scale, non-hydrogen coordinates and thermal parameters) are accurately determined in a high-order refinement. Once the hydrogen parameters are determined using all the data, the high-order structure is finished and total deformation density (TDD) maps calculated.

Proceeding into the realm of orbital parameter refinement, one may start with a spherically symmetrical valence shell and refine all the valence orbital (Y-type) parameters simultaneously. This refinement proceeds until the parameter shifts are insignificant and thus the final, oriented-atom promolecule model is obtained. From this one

may calculate the chemical deformation density (CDD) and various functions thereof. The orbital information may also be illustrated and examined in ORTEP-type drawings.

Results

The main purpose of this work was to determine whether or not molecular information beyond that of molecular geometry could be obtained. Towards this end much of the work was centered in the area of developing a proper procedure for obtaining such information. The proof of whether or not the results are meaningful lies in both the internal consistency of the information, and in the favorable comparison of the results with theory and with chemical intuition.

The dataset for 1,2,3-triazine was known from the start to be poor in both its resolution and its quality. A systematic study of this compound did however point out many of the procedural aspects which were applied in later chapters. Its small size and simple molecular geometry proved most helpful in this respect. Other than procedural aspects, 1,2,3-triazine has shown that the regions of high and low slope in the density function can be modeled very well, and that the CDD is actually about half of the TDD.

The dataset for 9-tert-butylanthracene was of higher resolution and the molecule provided a very large number of aromatic carbons which promised a good internal comparison.

Both the dataset and the choice of molecules were found to be flawed during the latter stages of refinement however. The weights used in the weighted least squares refinement had a systematic error in the 0k0 reciprocal space direction. This error induced a tilt of all the orbitals in this direction. The tertiary-butyl group on this molecule is also suspected of being rotationally disordered which essentially smears the electron density reducing the ability to obtain good results.

9-tert-butylanthracene did provide insight into how orbitals on aromatic carbons would look using the oriented-atom promolecule. It has shown that the orbital perpendicular to the aromatic plane is of much lower occupancy relative to the orbitals in the plane of the ring. As described in Chapter IV, this is probably due to the excess 2s electrons density in the direction of the p-π orbital.

Tetrafluoroterephthalonitrile had the best dataset with respect to both resolution and accuracy. Prior high-order studies[14,47] allowed comparisons of both the parameters and the electron density maps. A comparison with theoretical calculations has shown that the qualitative results agree favorably in most respects. However there are features indicated by theory which could not be seen in the dynamic deformation maps and vice versa. A theoretical calculation of the dynamic CDD could clear up these discrepancies.

The requirement that the atoms remain in their ground-state was relaxed in this work. From a simple point of view one may apply constraints which would prevent an energy increase due to electron pairing. The constraints would result in a configuration which would be a subset of the linear combination of states which make up the ground-state. As examples, the constraints for boron and carbon would be that the electron occupation numbers remain in the range [0,1]. For nitrogen the values should be fixed at 1. For oxygen and fluorine the range is [1,2].

The results for the three compounds studied show that, for carbon, the eigenvalues nearly realize the above restrictions (maximum deviation is 0.19 electrons). The fluorine atom in TFT is within the specified range. The nitrogen atoms in both 1,2,3-triazine and TFT have a maximum deviation from 1 of 0.45 electrons. While both conform to expectations, they represent the largest deviation from the ground-state of the atoms studied so far (note that no orbital information would be available from the nitrogens if their occupation numbers were fixed to 1).

Future Work

The basic goal of this work has been to determine the feasibility of calculating valence orbital parameters. A more in-depth study remains to be carried out which this work

has made possible. A mathematical analysis of the CDD for information about the nature of chemical binding and the insights it might provide should be carried out.

The statistical analysis and correction of the data for systematic errors are also clearly deficient. In future work modified corrections for errors such as secondary extinction should be explored and better definitions of the residuals at low angles are needed; both are formidable challenges due to the relatively poorer fit in the low-order data region. It may be necessary to calculate the corrections using molecular models which do fit the entire dataset, or perhaps bonding functions which approximate the bond electron density.

Studies of other light atom molecules would provide a broader basis upon which comparisons could be made. Expansion into heavy atom molecules, such as organometallics, is mandatory for future work since it is in these many electron system where theoretical work falls short due to computational difficulties.

The concept of the oriented-atom promolecule has been expanded in this work. The promolecule's valence shells were allowed to transfer electrons and even ionize. The significance of these results await further testing as well as theoretical considerations. The promolecule which is allowed to ionize is especially intriguing since it is the best model to describe the atoms' valence orbitals which have lost electrons to the bonds.

In regards to ORALS which was written for this work, modification is needed so that refinement is carried out against I(k) instead of |E(k)| as is presently done. Further expansion of the statistical analysis routine would also be warranted. Incorporation of disorder and librational/translational rigid-body corrections are also needed to increase the accuracy of the results and enable a detailed analysis of valence orbital information without errors introduced by poor core electron modeling.

APPENDIX A. LEAST SQUARES METHODS I AND II

Method I: Minimizing $(|E|-|F|)^2$

No phase (α_k) information is used in the calculation of the normal equations. This has an advantage in the early stages of refinement when the atomic positions, which have the largest effect on the phases, are not well known and thus subject to change. This method has less of an advantage in the later stages of refinement since only the weakest (least significant) reflections are apt to show any significant change in phase. The k dependence of E(k), F(k), and α_k is dropped from all equations to simplify their appearance.

The derivation starts with the equation to be minimized

$$V=\Sigma_k\ (|E|-|F|)^2 \tag{A.1}$$

which, at the minimum, has the property

$$\partial V/(\partial \Delta v)=0 \tag{A.2a}$$

$$=2\ \Sigma_k\ (|E|-|F|)\ \partial(|E|-|F|)/\partial \Delta v \tag{A.2b}$$

where Δv is the shift in the parameter v.

Expanding the latter term in Equation (A.2b) in a first order Taylor series we see that

$$\partial(|E|-|F|)/\partial \Delta v=-\partial/\partial \Delta v\ [F'\cos(\alpha)+F''\sin(\alpha) + \Sigma_r\ [(\partial F'\cos(\alpha))/\partial r*(\partial F''\sin(\alpha))/\partial r]\ \Delta r \tag{A.3a}$$

$$=-\partial|F|/\partial v \tag{A.3b}$$

since |E| does not change with a change in parameters,

$$|F|=F'\cos(\alpha)+F''\sin(\alpha), \tag{A.4a}$$

$$\cos(\alpha)=F'/|F|, \tag{A.4b}$$

and

$$\sin(\alpha)=F''/|F|. \qquad \text{(A.4c)}$$

Thus

$$0=\Sigma_k\ (|E|-|F|)\ (-\partial|F|/\partial v) \qquad \text{(A.5a)}$$

from which, upon insertion of the Taylor series expansion into Equation (A.3a) and simplifying,

$$0=\Sigma_k\ [(|E|-|F|)-\Sigma_r\ \partial|F|/\partial r\ \Delta r]\ \partial|F|/\partial v. \qquad \text{(A.5b)}$$

Equation (A.5b) may be rewritten to yield the normal equation

$$\Sigma_k\ \Sigma_r\ \partial|F|/\partial v\ \partial|F|/\partial r\ \Delta r=\Sigma_k\ [|E|-|F|]\ \partial|F|/\partial v. \qquad \text{(A.5c)}$$

The weighted form of which is

$$\Sigma_k\ \omega_k\ \Sigma_r\ \partial|F|/\partial v\ \partial|F|/\partial r\ \Delta r= \Sigma_k\ \omega_k\ [|E|-|F|]\ \partial|F|/\partial v \qquad \text{(A.5d)}$$

and is of the form

$$\Sigma_r\ A_{v,r}\ \Delta X_r=B_v. \qquad \text{(A.5e)}$$

Since, in the normal process of computing the structure factor, phase information is already included (i.e., F is computed from the model, not |F|), the phase information must be removed from the structure factors as shown in Equation (A.4a). In practice the derivatives of F' and F'' (see Table II.4) are calculated and, using the relations in Equations (A.4), the derivatives in Equation (A.5e) are computed using

$$\partial|F|/\partial v=\partial F'/\partial v\ \cos(\alpha)+\partial F''/\partial v\ \sin(\alpha). \qquad \text{(A.6)}$$

Method II: Minimizing $(E-F)^2$

The use of this minimization procedure implies either that the exact phases are known or that the phase for each reflection will not change upon refinement. The former is difficult to realize since there are few sources of exact electron density functions for entire molecules, let alone molecules in a crystal lattice. It is easier to realize the situation where, if the phases have been calculated by fitting a molecular model to the structure factors for example, one may transfer the phases determined to another situation where the model cannot be determined so accurately. The latter argument, that the phases will not change, is actually a good approximation (n.b. nothing has been said about the accuracy of the phases) since it is usually the least significant 1% of the reflections for a centrosymmetric structure or so which change during refinement once the model is in the final stages of refinement.

This method starts with minimizing the quantity

$$V=\Sigma_k (E-F)^2 \qquad (A.7)$$

which, at the minimum, has the property

$$\partial V/\partial \Delta v=0 \qquad (A.8a)$$

$$=2 \Sigma_k \mathrm{Re}\{(E-F)\, \partial(E-F)^*/\partial \Delta v\} \qquad (A.8b)$$

where the * denotes the complex conjugate and stems from the complex nature of the structure factors.

Expanding the latter term in a first order Taylor series

expansion

$$\partial(E-F)^*/\partial\Delta v=$$

$$-\partial/\partial\Delta v\ [\ F'-i\ F''+\Sigma_k\ (\partial F'/\partial r-i\ \partial F''/\partial r)\ \Delta r \qquad \text{(A.9a)}$$

$$=-(\partial F'/\partial v-\partial F''/\partial v). \qquad \text{(A.9b)}$$

Thus

$$0=\Sigma_k\ \mathrm{Re}\{(E-F)\ (-\partial F'/\partial v+i\ \partial F''/\partial v)\} \qquad \text{(A.10a)}$$

from which, upon insertion of the Taylor series in Equation (A.9a),

$$0=\Sigma_k\ [(E'-F'-\Sigma_r\ \partial F'/\partial r\ \Delta r)(\partial F'/\partial v)$$

$$+(E''-F''-\Sigma_r\ \partial F''/\partial r\ \Delta r)(\partial F''/\partial v)] \qquad \text{(A.10b)}$$

yields the normal equation matrix

$$\Sigma_k\ \Sigma_r\ (\partial F'/\partial r*\partial F'/\partial v+\partial F''/\partial r*\partial F''/\partial v)\ \Delta r=$$

$$\Sigma_k\ [(E'-F')*\partial F'/\partial v+(E''-F'')*\partial F''/\partial v] \qquad \text{(A.10c)}$$

and is of the form $\mathbf{A}\ \mathbf{x}=\mathbf{b}$ (see Equation (A5.d)). The weighted form of the equation is

$$\Sigma_k\ \omega_k\ \Sigma_r\ (\partial F'/\partial r*\partial F'/\partial v+\partial F''/\partial r*\partial F''/\partial v)\ \Delta r=$$

$$\Sigma_k\ \omega_k\ [(E'-F')*\partial F'/\partial v+(E''-F'')*\partial F''/\partial v]. \qquad \text{(A.10d)}$$

Equation (A.10d) is essentially the simultaneous refinement on the real and imaginary parts of the structure factor which are treated as separate entities, each contributing to the parameter shifts ($\mathbf{A}'\ \mathbf{x}'=\mathbf{b}'$ and $\mathbf{A}''\ \mathbf{x}''=\mathbf{b}''$ such that $\mathbf{x}=\mathbf{x}'+\mathbf{x}''$).

APPENDIX B. $\langle j_L(k) \rangle_{ij}$

Introduction

In order to obtain meaningful and accurate results from a fit of calculated atomic orbitals to the experimental electron density one must start with accurate atomic scattering factors. The scattering factors are obtained from the Fourier transform (FT) of the atomic orbital wavefunctions ($\Psi = R_{nl}(r)\ Y_{lm}(\Omega)$). As is shown in Equation (II.13a), the radial part is transformed separate from the angular part.

Hartree-Fock wavefunctions35 were used to calculate the scattering factors used in the past in this laboratory. More accurate wavefunctions[49-52] are available and, due to the accuracy required in this research, self-consistent-field (SCF) calculated wavefunctions[49,50] were used.

The procedure to FT the radial wavefunctions has been formulated into the computer program JLK. The equations used and the details of the program are described here.

Fourier Transform of $R_{nl}(r)$

The radial wavefunctions used are of the form:

$$R_{nl}(r) = r^l \sum_k C_k\ N_l(\zeta_k)\ \exp(-\zeta_k\ r) \qquad (B.1)$$

where r is in Å, l is the orbital angular momentum quantum number, k runs over all coefficients C_k, $N_l(\zeta_k)$ are

normalization constants given by $(2\zeta_k)^{l+3/2}\ [(2l+1)!]^{1/2}$, $\zeta_k=\alpha\ \beta^k$, α and β are positive and $\beta \neq 1$.

The FT of $R_l(r)$ is given by Equation (II.10) as

$$\langle j_L(k)\rangle_{ij}=\int_0^\infty dr\ r^2\ j_L(k\ r)\ R_i(r)\ R_j(r) \qquad (B.2)$$

where i and j denote n_il_i and n_jl_j for the atom in question, L ranges from $|l_i-l_j|$ to l_i+l_j by twos, k is $\sin(\Theta)/\lambda$ in $Å^{-1}$, and $j_L(k\ r)$ are the spherical Bessel functions[23] whose functional form is:

$$j_n(x)=(-1)^n\ x^n\ [d/(x\ dx)]^n\ (\sin(x)/x) \qquad (B.3a)$$

with the recursion relation

$$j_{n+1}=(2n+1)/x\ j_n(x)-j_{n-1}(x). \qquad (B.3b)$$

Programing Aspects

For practical purposes the values of k are limited to 56 values in the range from 0 to $2Å^{-1}$. The values at k=0 are obtained by taking the integer nearest the values at $k=k_1$ (the values at k=0 are either 0 or 1).

The values of α, β, and C_k are stored for each atom in a file (COEFF) which is read by the program JLK. The integration in Equation (B.2) is carried out using a rectangular summation approach. The integration limits and intervals are read from the JLK.PAR file. The integration parameters are generally different for each atom. Each atomic scattering factor is typically calculated in three ranges of r, the results being summed.

During the integration various expectation values ($\langle r^s \rangle$, s=-2 to 2, 4, and 6) are calculated. These values and the maximum value of $R_{nl}(r)$ are useful for checking the accuracy of the integration and of the wavefunction against literature values[50-52].

The final calculation performed involves the computation of the total (spherical) scattering factor. This is done by

$$f_{sph}(k)=\Sigma_i \; n \; \langle j_0(k) \rangle_{ii} \qquad (B.4)$$

where n is the number of electrons in each orbital $n_i l_i$ (summed over m_i). The resultant values of $f_{sph}(k)$ and $\langle j_L(k) \rangle_{ij}$ for each atom are stored in a file (SF).

Due to the large number of operations involved, double precision is used throughout JLK.

Interpolation

Use of the functions require an accurate interpolation scheme which does not require a large number of operations. A reasonable balance is obtained by using Lagrange's three-point interpolation formula

$$f(x)=\frac{(x-x1)(x-x2)}{(x0-x1)(x0-x2)}*f_0+\frac{(x-x0)(x-x2)}{(x1-x0)(x1-x2)}*f_1 + \frac{(x-x0)(x-x1)}{(x2-x0)(x2-x1)}*f_2 \qquad (B.5)$$

where $x0<x<x1$.

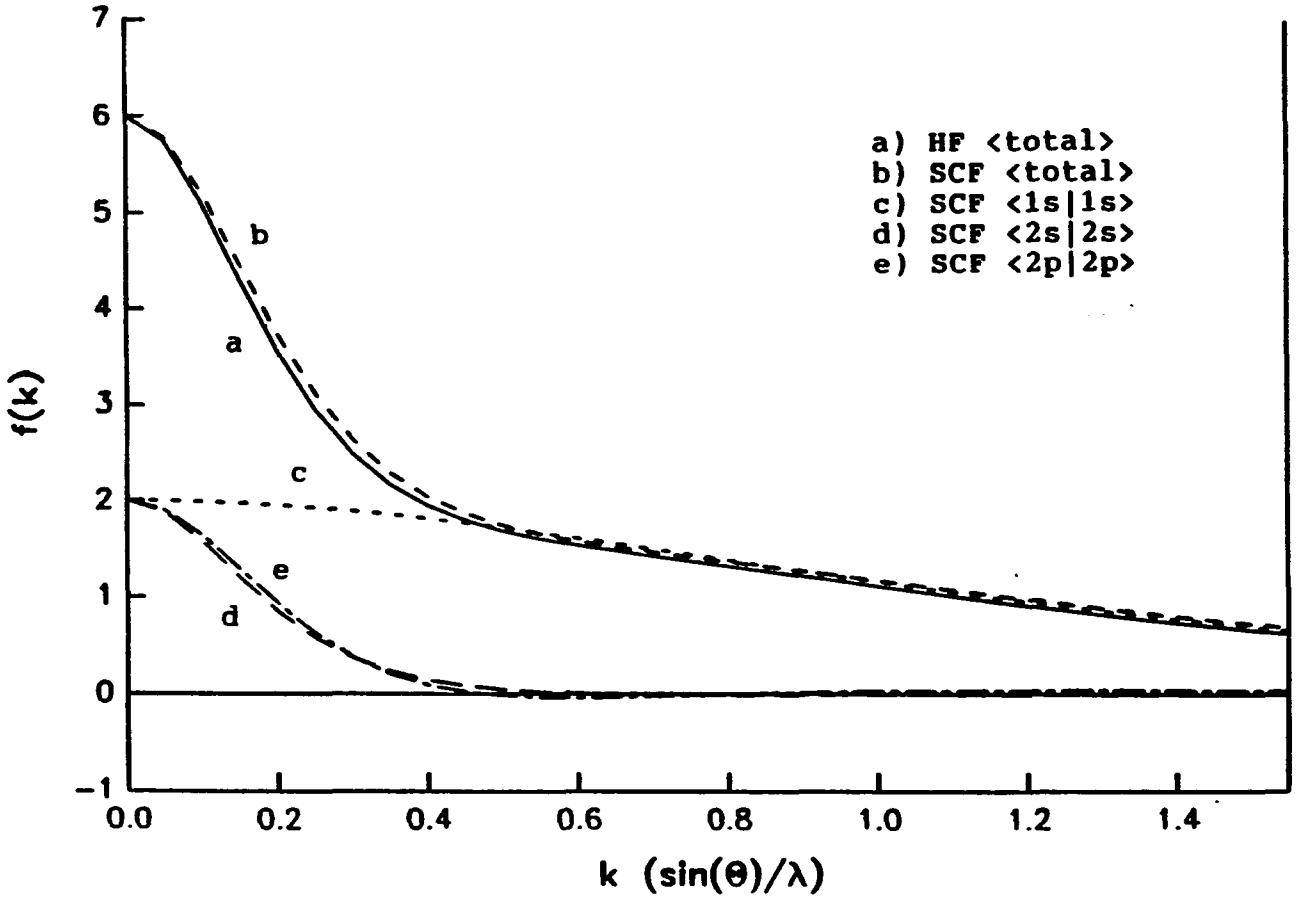

Figure B.1. Scattering factors curves for carbon

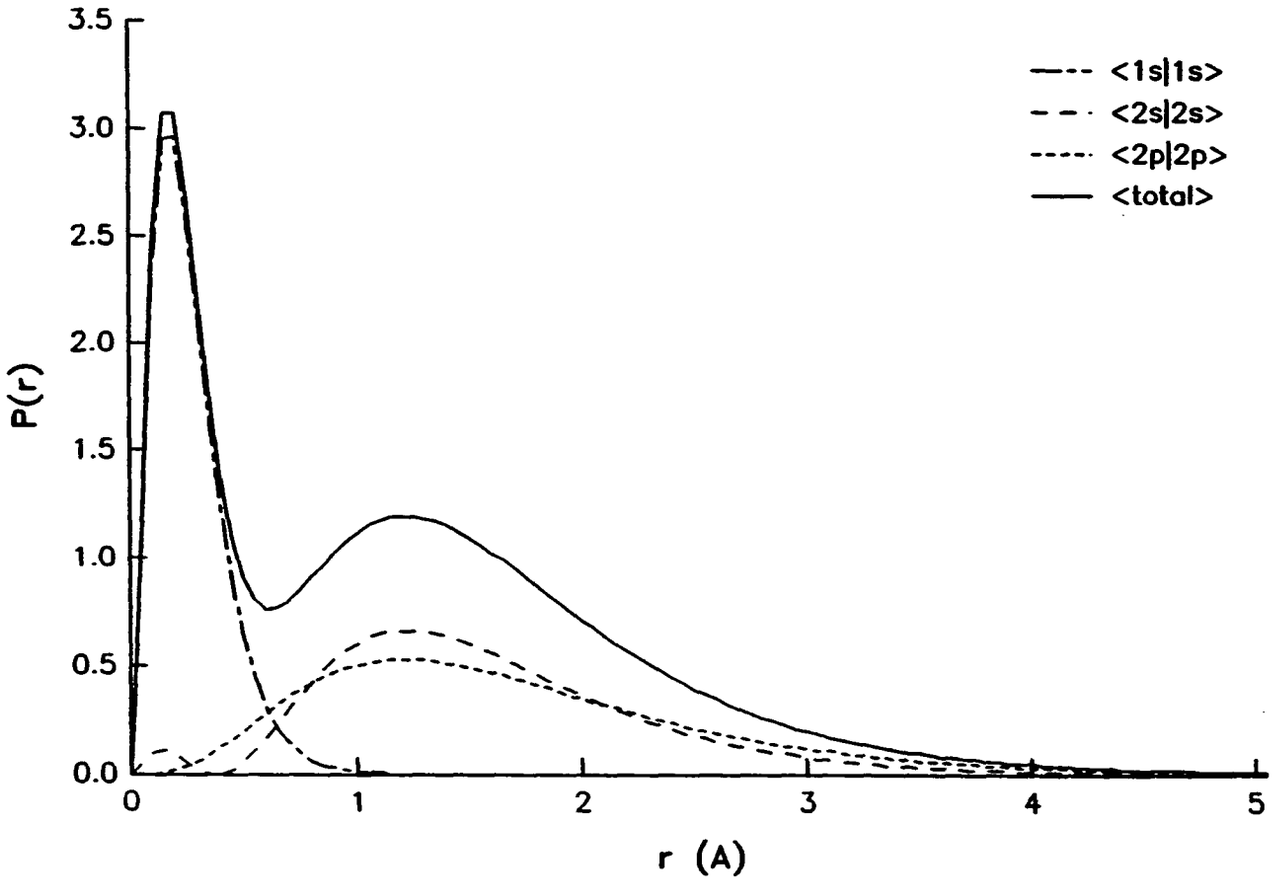

Figure B.2. Orbital electron density functions for carbon

Results and Discussion

Figure B.1 illustrates the calculated orbital scattering factor curves for carbon. For comparison the total spherical curves from the HF wavefunctions and from these calculations are also shown. Figure B.2 shows the corresponding radial electron probability functions for carbon weighted by the number of electrons. A numerical listing of the radial parts of the scattering factors for carbon are listed in Table B.2.

The curves show that the HF values cause a small underestimation of the scale factor and/or produce a temperature factor error. This is discussed in Chapter III.

Comparison of the calculated values of $\langle r^s \rangle$ with literature values show good agreement. These values are not a direct indication of the quality of the radial wavefunctions. They do, however, permit a comparison with wavefunctions which are known to be of high quality (from energy calculations). The results for carbon are shown as an example in Table B.1. The values from reference (53) are of lower quality whereas the values from reference (52) are of the highest quality available. The results from this work are not in exact agreement with those listed in reference (50) due to differences in the evaluation of Equation (B.2).

Calculation times for these curves are large. Due to the nature of the Bessel functions (steep slopes and oscillating), this is unavoidable and small integration intervals must be used.

The scattering factors for all atoms from helium to calcium have been calculated by this method. As this exhausts the present source (except for gallium and xenon), the remaining atomic wavefunctions may be obtained elsewhere[53].

Table B.1. The radial expectation values for carbon

	s	$\langle r^s \rangle^a$	$\langle r^s \rangle^b$	$\langle r^s \rangle^c$	$\langle r^s \rangle^d$
1s:	-2	65.237	65.239	65.241	
	-1	5.6644	5.6647	5.6644	5.6644
	1	0.26844	0.26842	0.26844	0.26844
	2	0.097199	0.097179	0.097200	0.097199
	4	0.024634	0.024620	0.024634	
	6	0.012176	0.012171	0.012177	
2s:	-2	3.2564	3.27051	3.25654	
	-1	0.89679	0.89887	0.89680	0.89680
	1	1.5894	1.5858	1.5894	1.5893
	2	3.0532	3.0380	3.0532	3.0521
	4	18.221	17.995	18.222	
	6	188.92	184.66	188.93	
2p:	-3	1.6903	1.6618	1.6903	1.6918
	-2	0.89199	0.87764	0.89200	
	-1	0.78351	0.77513	0.78351	0.78350
	1	1.7142	1.7425	1.7142	1.7145
	2	3.7431	3.8897	3.7431	3.7468
	4	31.795	35.143	31.795	
	6	30	591.23	489.33	

[a]This work.

[b]Reference 53.

[c]Reference 50.

[d]Reference 52.

Table B.2. Values of $\langle j_L(k) \rangle_{ij}$ for carbon

k	$f_{sph}(k)$[a]	10100[b]	20100	21101	20200	21201	21210	21212
0.00	6.000	1.000	0.000	0.000	1.000	0.000	1.000	0.000
0.01	5.991	1.000	0.000	0.003	0.998	0.034	0.998	0.001
0.02	5.964	1.000	0.000	0.006	0.992	0.067	0.990	0.004
0.03	5.919	0.999	0.000	0.008	0.982	0.100	0.978	0.009
0.04	5.858	0.999	-0.001	0.011	0.968	0.132	0.962	0.015
0.05	5.781	0.998	-0.001	0.014	0.951	0.162	0.941	0.023
0.06	5.690	0.998	-0.002	0.017	0.931	0.190	0.916	0.033
0.07	5.585	0.997	-0.002	0.020	0.907	0.216	0.889	0.043
0.08	5.469	0.996	-0.003	0.022	0.881	0.240	0.858	0.054
0.09	5.342	0.995	-0.004	0.025	0.852	0.262	0.825	0.066
0.10	5.208	0.994	-0.005	0.028	0.821	0.281	0.790	0.078
0.11	5.067	0.992	-0.006	0.030	0.788	0.297	0.753	0.091
0.12	4.921	0.991	-0.007	0.033	0.754	0.311	0.716	0.103
0.13	4.772	0.989	-0.008	0.035	0.718	0.322	0.678	0.114
0.14	4.621	0.988	-0.009	0.038	0.682	0.331	0.640	0.126
0.15	4.469	0.986	-0.011	0.040	0.646	0.337	0.603	0.136
0.16	4.318	0.984	-0.012	0.043	0.609	0.341	0.566	0.146
0.17	4.168	0.982	-0.014	0.045	0.573	0.343	0.529	0.155
0.18	4.022	0.980	-0.015	0.047	0.537	0.344	0.494	0.163
0.19	3.878	0.977	-0.017	0.049	0.501	0.342	0.460	0.170
0.20	3.739	0.975	-0.018	0.051	0.467	0.338	0.428	0.176
0.22	3.475	0.970	-0.022	0.056	0.401	0.328	0.367	0.185
0.24	3.232	0.964	-0.026	0.059	0.339	0.312	0.313	0.190
0.25	3.119	0.961	-0.028	0.061	0.310	0.304	0.288	0.192
0.26	3.012	0.958	-0.029	0.063	0.283	0.294	0.265	0.192
0.28	2.815	0.952	-0.033	0.066	0.233	0.274	0.222	0.192
0.30	2.639	0.945	-0.037	0.069	0.189	0.252	0.186	0.189
0.32	2.485	0.938	-0.041	0.072	0.150	0.230	0.154	0.184
0.34	2.349	0.930	-0.046	0.074	0.117	0.209	0.128	0.178
0.35	2.288	0.926	-0.048	0.075	0.102	0.198	0.116	0.175
0.36	2.231	0.922	-0.050	0.076	0.088	0.188	0.105	0.171
0.38	2.128	0.914	-0.054	0.078	0.065	0.168	0.085	0.163
0.40	2.039	0.905	-0.058	0.079	0.045	0.149	0.069	0.155
0.42	1.962	0.896	-0.062	0.081	0.029	0.132	0.056	0.146
0.44	1.894	0.887	-0.066	0.082	0.016	0.116	0.044	0.138
0.45	1.864	0.882	-0.068	0.082	0.010	0.108	0.039	0.134
0.46	1.836	0.878	-0.069	0.083	0.006	0.101	0.035	0.130
0.48	1.785	0.868	-0.073	0.083	-0.002	0.087	0.027	0.121

[a]These terms are the scattering factor for the spherically averaged atom and are obtained by Σ_i #e$^-$ $\langle j_0(k) \rangle_{ii}$.

[b]The five terms are n_i, l_i, n_j, l_j, and L.

Table B.2. Continued

k	$f_{sph}(k)$	10100	20100	21101	20200	21201	21210	21212
0.50	1.740	0.858	-0.077	0.083	-0.008	0.075	0.020	0.114
0.55	1.649	0.832	-0.085	0.083	-0.016	0.050	0.009	0.095
0.60	1.578	0.805	-0.091	0.082	-0.018	0.031	0.002	0.079
0.65	1.519	0.778	-0.097	0.080	-0.016	0.017	-0.002	0.066
0.70	1.466	0.749	-0.101	0.077	-0.012	0.007	-0.004	0.055
0.80	1.367	0.692	-0.107	0.070	-0.003	-0.004	-0.006	0.038
0.90	1.269	0.634	-0.108	0.063	0.006	-0.009	-0.005	0.026
1.00	1.171	0.578	-0.106	0.055	0.011	-0.010	-0.004	0.018
1.10	1.073	0.525	-0.101	0.047	0.015	-0.010	-0.003	0.013
1.20	0.977	0.475	-0.096	0.040	0.016	-0.009	-0.003	0.009
1.30	0.886	0.428	-0.089	0.034	0.017	-0.008	-0.002	0.007
1.40	0.800	0.385	-0.082	0.029	0.016	-0.007	-0.002	0.005
1.50	0.721	0.346	-0.075	0.025	0.016	-0.006	-0.001	0.004
1.60	0.649	0.311	-0.068	0.021	0.015	-0.005	-0.001	0.003
1.70	0.583	0.279	-0.061	0.018	0.013	-0.004	-0.001	0.002
1.80	0.523	0.250	-0.055	0.015	0.012	-0.004	-0.001	0.002
1.90	0.470	0.224	-0.050	0.013	0.011	-0.003	-0.001	0.001
2.00	0.422	0.201	-0.045	0.011	0.010	-0.003	0.000	0.001

APPENDIX C. EXAMPLE OF $\rho(r)$ AND $f(k)$

$\rho(r)$ and $f(k)$ for Carbon

It is interesting to examine the electron density and its Fourier transform. The general rules for understanding spherical components of $\rho_a(r)$ and their transforms are relatively simple, namely 1) a Gaussian function transforms into another Gaussian (n.b. to first order $\rho_a(r)$ is well described by a Gaussian function), 2) a sharp function transforms into a broad function, and 3) the converse of 2). These aspects of Fourier transforms are readily seen in the radial electron density functions of carbon and their transforms as shown in Figures B.1 and B.2.

Standard crystallographic practice dictates the use of spherically averaged groundstate atoms and their spherical scattering factors. The relation between real and reciprocal space is easily understood by applying the rules described above. Here however aspherical atoms are to be used. How then does the Fourier transform of the aspherical part of the electron density appear in reciprocal space?

Perhaps the easiest way to answer this question is to show an example involving the calculation of $f_{a\mu\nu}(k)$ for carbon.

By assuming that the atomic core is comprised of

$(1s^2)^2(2s^2)^2$, one may disregard these orbitals since they are directionally isotropic. The three $2p^2$ orbitals are the anisotropic components, with reciprocal space functions being $f_{2p}(k)$, and are all mutually orthogonal. Writing out these valence functions explicitly according to Equations (II.13) yields

$$\langle 21\bar{1}|21\bar{1}\rangle: \quad \langle j_0(k)\rangle_{21}\, W_0(11,11)^*Y_{00} \qquad \text{(C.1a)}$$

$$\text{and} \quad \langle j_2(k)\rangle_{21}\, [V_2(11,11)^*Y_{22}/\sqrt{2}+W_2(11,11)^*Y_{20}]$$

$$\langle 210|210\rangle: \quad \langle j_0(k)\rangle_{21}\, V_0(10,10)^*Y_{00} \qquad \text{(C.1b)}$$

$$\text{and} \quad \langle j_2(k)\rangle_{21}\, V_2(10,10)^*Y_{20}$$

$$\langle 211|211\rangle: \quad \langle j_0(k)\rangle_{21}\, W_0(11,11)^*Y_{00} \qquad \text{(C.1c)}$$

$$\text{and} \quad \langle j_2(k)\rangle_{21}\, [V_2(11,11)^*Y_{22}/(\sqrt{2})+W_2(11,11)^*Y_{20}]$$

which simplify to

$$\langle 21\bar{1}|21\bar{1}\rangle: \quad \langle j_0(k)\rangle_{21} \qquad \text{(C.2a)}$$

$$\text{and} \quad \langle j_2(k)\rangle_{21}\, [(3/2)^*(h^2-k^2)/|h|^2 + (1/2)^*(l^2-|h|^2)/|h|^2]$$

$$\langle 210|210\rangle: \quad \langle j_0(k)\rangle_{21} \qquad \text{(C.2b)}$$

$$\text{and} \quad \langle j_0(k)\rangle_{21}\, (-1/2)^*(l^2-|h|^2)/|h|^2]$$

$$\langle 211|211\rangle: \quad \langle j_0(k)\rangle_{21} \qquad \text{(C.2c)}$$

$$\text{and} \quad \langle j_2(k)\rangle_{21}\, [(-3/2)^*(h^2-k^2)/|h|^2 + (1/2)^*(l^2-|h|^2)/|h|^2].$$

The values of $\langle j_0(k)\rangle_{21}$ have only a radial dependence; thus the angular dependence is evidenced only in the latter functions for each orbital. The values of $\langle j_2(k)\rangle_{21}$ are zero at k=0, thus giving the expected result that the reciprocal

space origin has no angular dependence. As k increases so does the function $\langle j_2(k)\rangle_{21}$ until k=0.26 where it starts to decrease (as seen in Table B.2). The radial function $\langle j_0(k)\rangle_{21}$ on the other hand decreases as a function of k, the net result being a relatively greater importance of the angular orientation of the p orbitals at moderate values of k which correspond to the region of maximum electron density in the radial function $R_{21}(r)$.

The angular dependence of the reciprocal space 2p orbitals are given in the [] brackets and are quadrupolar in nature (whereas the 2p orbitals are dipolar). Plots of $Y_{11}(\Omega)$ and its transform are shown in Figures C.1 and C.2 respectively. It is seen that when k is along the lobes, the plane normal to k passes through the node and thus intercepts no electron density. The magnitude of the scattering factor is therefore less than the average and the corresponding function in reciprocal space is negative, i.e., it reduces the scattering factor in that direction.

When k is perpendicular to the lobes of the p orbital, the plane normal to k passes through the maximum electron density. This is reflected in reciprocal space by the smaller, positive lobes which cause an increase in the scattering in this direction (since the electron density is higher than the average).

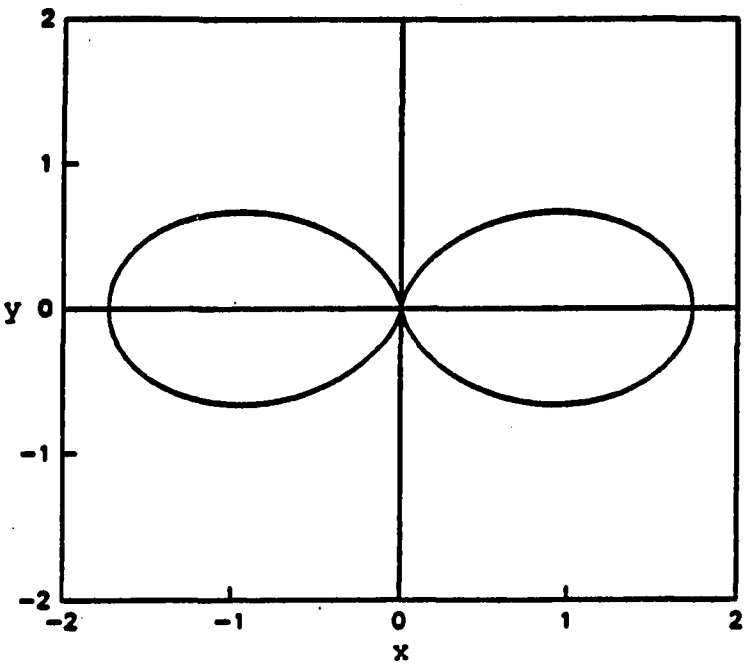

Figure C.1. Plot of $Y_{11}(\Omega)$ in xy plane

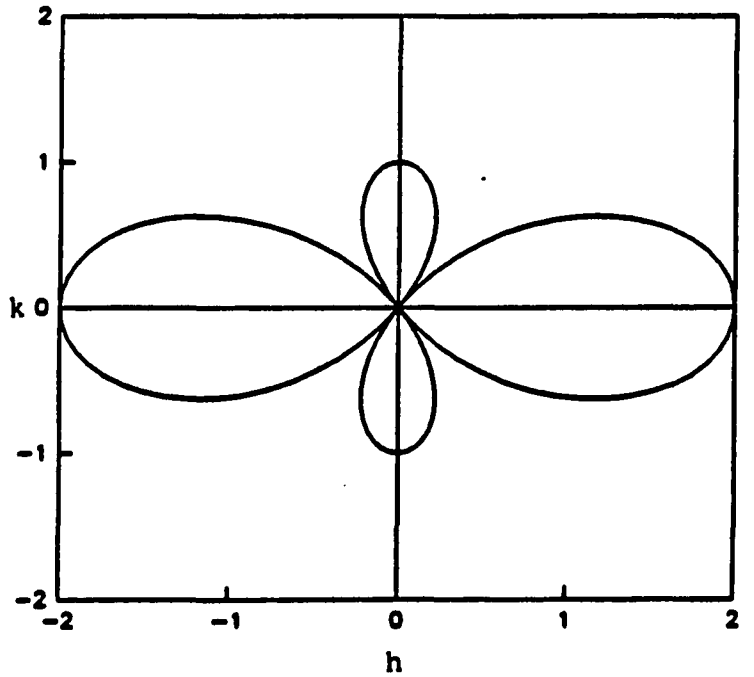

Figure C.2. Plot of $Y_{11}(\Omega_k)$ in hk plane

One final consideration is that of symmetry. It is easily argued that 1) the symmetry of the reciprocal of the orbitals each have the same symmetry as the orbitals themselves, 2) the sum over the reciprocal space functions is spherically symmetric (since the same is true in real space), and 3) that for any rotation operation ($R^3(\Omega)$) performed in real space, an identical operation ($R^3(\Omega_k)$) must be applied in reciprocal space. Both 1) and 2) are shown to be true, in this example, by examination of Equations (B.2). The third argument is easily seen by considering how the maxima and minima in the scattering factor change when the orientation of an orbital changes.

APPENDIX D. EXAMPLES OF CONSTRAINING U

Atom on a Mirror Plane

Consider an atom with a p-orbital valence shell lying on a crystallographic mirror plane perpendicular to a in an orthorhombic space group. Since the space group is orthorhombic, the Px orbital is parallel to a, Py is parallel to b, and Pz is parallel to c. This implies two possible models; model A having Ψ_3 perpendicular to the mirror plane and model B which has Ψ_3 lying in the mirror plane. There are other definitions which one could make but they reduce to these two models by permutation of the axes. By parametizing these two models we derive the constrained U matrix

A	Ψ_1	Ψ_2	Ψ_3
Py	cos(θ)	-sin(θ)	0
Pz	sin(θ)	cos(θ)	0
Px	0	0	1

(D.1a)

with no special constraints on N for model A and

B	Ψ_1	Ψ_2	Ψ_3
Py	$-\sin(\theta)/\sqrt{2}$	$-\sin(\theta)/\sqrt{2}$	cos(θ)
Pz	$\cos(\theta)/\sqrt{2}$	$\cos(\theta)/\sqrt{2}$	sin(θ)
Px	$-1/\sqrt{2}$	$1/\sqrt{2}$	0

(D.1b)

with the constraint on N that $N_1=N_2$ for model B. θ represents free rotation about the a-axis in both models.

The derivatives of each U matrix element w.r.t. θ are needed to form the normal equations matrices with θ as the adjustable parameter. The derivatives of $f_{amn}(k)$ w.r.t. U_{ij} can be shown to be related to the derivatives w.r.t. θ; viz

A	Ψ_1	Ψ_2	Ψ_3
Py	$\partial f_a/\partial U_{11}*U_{12}$	$-\partial f_a/\partial U_{12}*U_{11}$	0
Pz	$-\partial f_a/\partial U_{12}*U_{11}$	$\partial f_a/\partial U_{11}*U_{12}$	0
Px	0	0	0

(D.2a)

for model A and

B	Ψ_1	Ψ_2	Ψ_3
Py	$-\partial f_a/\partial U_{11}*U_{21}$	$-\partial f_a/\partial U_{11}*U_{21}$	$-\partial f_a/\partial U_{13}*U_{23}$
Pz	$\partial f_a/\partial U_{12}*U_{11}$	$\partial f_a/\partial U_{12}*U_{11}$	$-\partial f_a/\partial U_{23}*U_{13}$
Px	0	0	0

(D.2b)

for model B. The derivatives w.r.t. N_i are obtained in the standard fashion.

Solving the normal equations yields the shifts in θ from which a new U matrix can be formed. The "correct" model would then be that which best fits the experimental data.

Atom on a C_2 Axis

Considering an atom with a p-orbital valence shell lying on a crystallographic C_2 parallel to the a axis in an orthorhombic space group, we again derive two possible models. Model A has Ψ_3 along the symmetry axis and Model B has Ψ_3 perpendicular to the symmetry axis.

The U matrices which represent the models are identical to those in Equations (D.1). However the constraints are quite different. It can be shown that the N values for model A must have $N_1=N_2$. By considering the total electron density one can see that $N_1*\Psi_1^2+N_2*\Psi_2^2$ has cylindrical symmetry and thus the θ parameter can be set to zero. The only parameters to adjust are the occupancies for which there are two constraints (other than $0\leq N_i\leq 2$) and thus only one parameter.

Examination of model B reveals that it is identical to model B above and the procedure given there must be followed.

Atom on an Inversion Center

While the wavefunctions are not symmetric w.r.t. inversion in general, the atomic orbitals are. This implies that there are no special constraints to be considered when only inversion site symmetry exists.

Atom on Higher Site Symmetry

As the site symmetry increases, the constraints generally become increasingly more stringent. Generally there will be one or two possible models for which adjustment of the U values need be made. Other cases will have the U coefficients fixed. Each case however will have to be treated individually; when one uses d-orbitals there will be more models and also more parameters.

APPENDIX E. REFINEMENT PROCEDURES AND ILLUSTRATIONS

ORALS

All refinements described herein have been carried out using the computer program ORALS (ORiented-Atom Least Squares). Tests of the program operation have shown that the program operates correctly. Comparisons of the full matrix refinement from ALLS[54] with the standard refinement of the simplest of promolecules in ORALS have been carried out and the results are consistent.

The accuracy which is obtainable from the file structure presently used is about 10^{-4} in the residuals and 10^{-5} in the promolecule's parameters. This limitation is due to the limited precision of the numbers stored in data files and of the number of bits used in the computations. While little can be done with the observed structure factors, it would be possible to increase the precision of the promolecule's parameters by storing them in either a free- or an exponential-format. This would allow the precision for each value to be the same (as it now exists, the scale factor has 7 significant figures whereas the anisotropic thermal factors have approximately 4).

Results of the statistical analyses (see Chapter II for definitions of the quantities) and the parameter shifts are included in the diagnostic output from ORALS. The exact

definition of each of quantity which appear can be important and is therefore described below.

The "Total number of reflections" is an exact count of the number of reflections read from the HKL data file. Reflections which have a special bit set (such as if the observed intensity were less than zero) are counted as "flagged to be skipped" and no further use of the reflection is made.

Reflections which lie outside a selected $\sin(\theta)/\lambda$ range [min,max] are counted and discarded. If a reflection has $|E(h)|<\text{cutoff}*\sigma(E)$ then it too is counted and not subsequently used. Optionally, all reflections (including those which are to be discarded) are written to a new HKL file.

Of the remaining data, those reflections which are in the high-order $\sin(\theta)/\lambda$ range [HOmin,HOmax] are also counted for reference purposes. If a reflection has $|F(k)|=0$ then it is counted (and listed for the first cycle only) and discarded. The remaining reflections are used and are listed as "total number used" and include both high- and low-order data.

Next the "Number of variables" are listed for the X-type parameters (scale and all standard atomic parameters), the Ni parameters (total # of variable eigenvalues) and the Uij parameters. These are accurate representations of the total # of variables of each type at the start of the refinement

run. Note that during a least squares refinement run it is possible in special cases for a variable not to vary (such as a non-positive definite temperature factor or a non-physically meaningful eigenvalue).

It is important to realize the the number of reflections and the number of variables are the totals (i.e., they are not split into high- and low-order contributions) for a specific run (i.e., the variables will be less than or equal to the true total). For this reason the "Data/Variable ratio" and "Error of fit" may need to be calculated in the final analysis by hand.

For each refinement cycle the results of several different statistical analyses are written so that one may judge the correctness of the adjusted model. These values are calculated before the parameters are adjusted.

The residuals R, R_W, and R_I, for the reciprocal space zones and for $\sin(\theta)/\lambda$ subranges ([n-0.1,n] n=0.1,0.2,0.3,...) are calculated and written along with the number of reflections in each of these subgroups. The average values of |E(k)| and |F(k)| are written for each $\sin(\theta)/\lambda$ subrange also.

The number of reflections which have |E| in the subrange $[(n-1)\sigma(E),n\sigma(E)]$ for n=1,2,3,... are computed to permit a check for poorly fit reflections. The number of phases which change sign (for light atom, centrosymmetric structures) is

optionally listed as a function of both STOL and the sigma subranges mentioned above.

Also listed prior to each refinement cycle are the LSE, ERF, DWd, and $\sigma(\rho)$. The value of LSE is the most important and should never increase between one refinement and the next.

Each of the above values depends on the type of refinement being carried out and is coupled with the data being used. For example, if the entire data set is read but only a high-order refinement is being carried out, the LSE may not decrease. This type of caveat is true for all values, and is why the LSE and other values are often listed twice (once for the high-order data only and once for all data) in the tables of this thesis. The estimated standard deviations (esd's) for all the variables were calculated using only the data subset which was used for their refinement.

Although a refinement may be carried out on both the high- and low-order data simultaneously, convergence is not guaranteed. All results reported here use separate high- and low-order refinements.

After the final parameter refinement cycle the correlations between parameters and the estimated standard deviations are (optionally) written along with the shifts which were calculated to be applied (i.e., undamped).

If the spectral representation matrices U are refined, the empirical shifts $\Delta U = U_{new} - U_{old}$ are displayed and during the last refinement cycle the actual Δt_{amn} values with their esd's are written. If the orbital occupancies are refined then the appropriate Lagrange multipliers are written for each cycle. The undamped shifts and the (optional) esd's are written for the final cycle.

Note that all the final esd's are actually obtained for the structure before the very last set of shifts were applied. The parameter shifts should be very small near convergence and thus the esd's will change little from cycle to cycle.

Convergence Criteria

It is important to develop a feel for when a structure has reached its final, converged state, and what to do if one or more of the parameters will not converge.

For a high-order refinement of the scale and atomic positional and thermal parameters, the shift/esd ratio for all parameters in the final cycle should be less than 10^{-3}. Some structures have very low (ca. 10^{-5}) esd's and thus an alternate criteria is that the shifts should be less than 10^{-6} (10^{-6} is the smallest shift which is printed) in the last cycle. A secondary check should be that, for six refinement cycles, the signs of the shifts not change more

than twice. If this happens then the shifts should be damped.

Another problem source for the high-order refinement is high correlation between variables. Correlations which exceed about 0.75 should be handled as described in Chapter II.

The eigenvalue shifts should not oscillate and in the final refinement should have a shift/esd ratio of less than 10^{-3} (the esd's are ca. 10^{-2}). It also important that the eigenvalues do not leave the interval of [0,2]. If one eigenvalue attempts to become negative then a damping factor is automatically applied to all the eigenvalues for the atom (or to all the eigenvalues of the molecule) in question in order to maintain electroneutrality. In such a case the eigenvalue should be fixed at either 0 or 2 and the others allowed to vary. Later, it is wise to set the value slightly away from 0 or 2 (adding to or subtracting off an equal amount from the other eigenvalues) and allow it to vary again. If it still tends to leave the range [0,2] then it should truly be fixed. There have been cases where this procedure has resulted in a non-constrained value in the range of (0,2) even though, at an earlier stage, the eigenvalue attempted to leave this range.

The values of the hydrogen atoms' shifts and esd's are generally larger than for the other atoms. This is due, in

part, to the small scattering amplitude of the hydrogen atom. Therefore the refinement criteria are less stringent, the hydrogen variables being considered to have converged if their shift/esd ratio is less than 10^{-2}. It is often necessary to dampen the shifts of the hydrogen atom variables by a factor of two to speed convergence.

The Δt_{amn} components need to be small in order to maintain orthogonality of the spectral representation matrices **U**. For this reason it has become standard practice to set an upper limit to the Δt_{amn} of 0.10 in the initial stages of refinement. The limit is lowered to 0.01 in the later stages where oscillation tends to occur. If an individual Δt_{amn} is larger than the limit then all of the Δt_{amn} components for the given atom are damped. When the parameters have converged the values of Δt_{amn} are ca. 10^{-6} (their esd's are ca. 10^{-1}) and the determinant of $(I+\Delta t_{amn}/2)$ is thus ca. $1+10^{-12}$. A quick way of checking convergence is to watch the determinant from one refinement to the next. If the Δt_{amn} limit is 0.01 and a given determinant remains at approximately $1+10^{-3}$ for several cycles then the shifts are being damped severely and it is best to relax the Δt_{amn} limit back to 0.10 for a few cycles to allow **U** to become approximately correct. One should also check the empirical shifts in **U** for oscillation. If oscillation exist then the shifts should be damped.

Contour Maps

The electron density was calculated by a two-dimensional Fourier transform routine written specifically for this task. The contour maps were drawn by a program which was written as a companion to the Fourier transform program and uses the DI-3000 graphics capabilities of the VAX computer.

There are no contour values shown on the maps. However, the contour interval (CI) in $e^-/Å^3$ is given for each map in the figure title. The dimensions of the maps are in integral Å units, and measurements are facilitated by the use of a 1Å bar given on each map. The 1Å bar and the molecular (fragment) skeleton have been drawn for ease of reference. When a pertinent atom lies off the plane of the map, its position is indicated by a large cross. The negative contours on each map are dashed lines, the remaining contours are solid lines.

There are three basic types of contour maps. The first is of the observed electron density which is the Fourier transform of E(k). The second type is of the calculated (promolecule's) electron density and is the Fourier transform of F(k). The last type is of the difference between the experimental electron density and the calculated electron density. This last type is calculated by Fourier transforming E(k)-F(k). Each of these types may be for all the data or for a subset of the data. The F(k) may also be

from the entire promolecule or of some subset (e.g., the valence orbitals only). The various combinations of E(k) and F(k) permit different perspectives of the molecule to be seen. The figure titles indicate under which conditions the Fourier transform was carried out.

Each Fourier transform runs over all the reciprocal lattice points. There are two exceptions to this in that the (0,0,0) reflection and the reflections with $\sin(\theta)/\lambda$ greater than the limit of data collection are not included. The contribution of the origin reflection to electron density difference maps (E-F) is zero. For observed (E) maps it contributes only a small additive constant to the entire map. Two maps in Chapter IV and all of the maps in Chapter V have been corrected for the contribution from the origin reflection.

The exclusion of data beyond the data collection $\sin(\theta)/\lambda$ limit can have a more severe effect on the resultant electron density functions. This effect is called the Fourier truncation effect and can produce ripples in the electron density functions. Generally speaking, the more data which is excluded from the Fourier transform, the more severe the electron density ripples. It easy to see from this description that in difference electron density maps using data which extends beyond the "proper" high-order data cutoff, no ripple effect will be seen. On the other hand,

unless the $\sin(\theta)/\lambda$ cutoff is extremely high, each observed electron density map will have some ripple effects due to the large contribution by the core electrons to the high-order data.

Other Representations of the Electron Density

During the course of this work it was found that methods of displaying orbital and molecular information simultaneously were lacking. The information consists of orbital occupation and, in the case of p-orbitals, the direction of the orbitals. Towards this end, two-dimensional contour maps are not entirely satisfactory, especially for more complex molecules. It is difficult to incorporate all of the valence information in a given contour map.

Several alternative methods of showing the desired information have been devised. Two of the methods have emerged as being the most useful and utilize the molecule and ellipsoid drawing capabilities in ORTEP41.

The first method uses pseudo-atoms lying at the ends of unit vectors which point in the direction of one of the lobes of the orbitals. The pseudo-atoms are represented by spheres which have a cross-sectional area proportional to the electron occupation of that orbital.

In order to accomplish this the atomic coordinates are first orthogonalized using Equation II.27a, to obtain the

atomic coordinates in a cartesian frame of reference. The coordinates of the pseudo-atoms are then obtained by adding the coordinates of the parent atoms to the wavefunction coefficients. The final list of coordinates will consist of all atomic positions and one pseudo-atomic position for each valence orbital. The thermal parameters of the atoms are set to an isotropic value of 0.01 for clarity. The thermal parameters for the pseudo-atoms are set to the electron occupation of the corresponding orbital. This new set of atoms may be treated in a normal manner and a drawing made.

Interpretation is accomplished as suggested in the description above; the directions of the orbitals are the same as that of the pseudo-atoms and the occupancies are visually interpreted as being proportional to the area of the circles which represent the pseudo-atoms. Interpretation of any drawings done by ORTEP must always be tempered by the realization that depth queuing is used in order to enhance the visual representation. The exact relative sizes of the orbitals is therefore not always the same as the relative sizes of the orbital occupancies.

While this method does yield all the desired information, the drawings are cluttered and the symmetry of the valence electron density is not readily inferred. One might wish to note that if two p-orbitals have equal electron occupancies then their direction perpendicular to the third orbital is irrelevant.

The second method does well to overcome the disadvantages of the first with only a small consequent loss in the resolution. The second method includes all of the information included in the first method, but an entirely different format is used.

The second method again orthogonalizes the atomic coordinates using Equation (II.27a). The electron occupation numbers are then used as the magnitudes of the principal axes of an ellipsoid. By using this method it is readily seen that if two p-orbitals have equal occupation numbers then the ellipsoid cross section perpendicular to the third orbital is a circle. This argument can be extended to the case were all three orbitals have equal occupancy where the ellipsoid will be spherical.

In order to include the orbital direction information relative to the molecule, the ellipsoids are first rotated so the the principal axes are in the directions of the orbitals. This is accomplished by performing a similarity transform on the ellipsoids. The rotation matrices used are the same as that needed to bring the wavefunctions Ψ_1, Ψ_2, and Ψ_3 to the x, y and z axes respectively.

The calculation of this rotation matrix is eliminated by knowledge that the U matrix is unitary and composed of the three row vectors Ψ_i. The desired rotation matrix R performs the function R U=I. Since the U is unitary it is easily seen

that $U^T U=I$ and thus $R=U^T=U^{-1}$. The similarity transform needed to rotated the principal axes of the ellipsoids to the orbital directions is therefore $\beta=R\ N\ R^T$ where N is a diagonal matrix with the electron occupancies as its elements.

The ellipsoids are now placed at the positions given by the orthogonalized atomic coordinates and the model drawn. The resultant representation is much simpler to understand since the number of pseudo-atoms is equal to the number of atoms. The additional advantage of having the symmetry of the valence shown far outweighs the slight loss of resolution relative to the first method described.

APPENDIX F. A SELF-CONSISTENT SEMI-EMPIRICAL ABSORPTION CORRECTION TECHNIQUE

Introduction

An x-ray beam, incident upon a single crystal, is diffracted by sets of planes of electrons within the crystal. As the x-ray beam passes through the crystal, some of the intensity is transformed into other forms of energy. The intensity of the scattered x-rays are therefore dependent, on a macroscopic scale, on the amount of material through which they pass, as well as on the composition of the material.

If a crystal is rotated about the normal to a given set of planes (this is termed a ψ-scan), the variation in the intensity will depend on the path lengths of the primary and secondary beams through the crystal and thus it will reflect the shape of the crystal. Absorption therefore produces a systematic variation in the measured intensities, this systematic effect manifests itself in the molecular model used to fit the observed intensities as an increase in the calculated vibrational parameters in the direction which has the largest amount of absorption.

Numerous procedures[55] for the correction of measured intensities for absorption have been put forth. These methods may be classified as either analytic or empirical.

Analytical procedures require accurate measurements of the crystal dimensions followed by a large number of

computations to calculated the contribution of each volume element in the crystal to the total absorption. These procedures fail when the crystal not of an easily described morphology, or when glue, mother liquor, or a capillary surrounds the crystal. The measurements also need to be quite accurate.

Empirical corrections consist of two basic approaches; 1) One or more ψ-scans are measured and used to describe the various directions of the crystal, 2) the structure is refined using isotropic vibrational parameters, the observed and calculated data are then compared. And the absorption is calculated from the systematic differences as a functions of crystal direction. The former approach is often difficult to apply due to either physical limitations of the diffractometer or to low intensity of reflections at some or all orientations (ψ-values) when they are in an appropriate position. The latter approach yields somewhat dubious results due to a high correlation between the model and the calculated correction terms.

The procedure described here is an empirical correction technique which utilizes only the symmetrically equivalent data, collected during routine data collection operations, to calculate a transmittance profile which is subsequently be used for absorption correction.

Background

The standard semi-empirical methods[56,57] employ an absorption surface which is obtained by experimental ψ-scan measurements and have formed the basis of a number of absorption correction programs[58].

In this procedure the integrated intensities of a reflection near $\chi=\pm 90°$ are measured via a ψ-scan on a standard four-circle diffractometer. The normalized transmittance curve is calculated as $T(\psi)=I(\psi)/[I(\psi)]_{max}$, and these transmittance values can be placed on an absolute scale by

$$T(\psi)=T(\psi)\ \langle T(\psi)\rangle^{-1}\ \exp(-\mu\langle t\rangle) \qquad (F.1)$$

where μ is the absorption coefficient, $\langle T(\psi)\rangle$ is the average value of $T(\psi)$, and $\langle t\rangle$ is the average crystal dimension.

The primary and secondary beam directions for each reflection (collected at 2θ, ω, χ, ϕ in the $\omega=\theta$ mode) in the crystal data set are projected onto the two-dimensional representation via

$$\psi_p=\phi-\tan^{-1}[\cos(\chi)\ \tan(\theta)] \qquad (F.2a)$$

and

$$\psi_s=\phi+\tan^{-1}[\cos(\chi)\ \tan(\theta)]. \qquad (F.2b)$$

The absorption correction then takes the form

$$I°(\psi_{p,s})=I(\psi_{p,s})\ T^{-1/2}(\psi_p)\ T^{-1/2}(\psi_s) \qquad (F.3)$$

using the approximation[56] $t=(t_p+t_s)/2$.

Improved results can be obtained by use of a small step size, and by smoothing the resulting curve. One can also measure several ψ-scans at different θ values (i.e., create multiple two-dimensional representations, one for each θ range) and interpolate between the results, yielding a pseudo three-dimensional correction. An alternative method of adding a third-dimension is to use the geometric approximation $t_{(3\text{-dim})}=t_{(2\text{-dim})}/\cos(\theta)$.

This approach is relatively easy to apply and is appropriate even when the crystal is placed in a glass capillary with mother liquor or has a shape which would be difficult to describe with high precision. However, it does require that a reflection of at least moderate intensity be available at or near $\psi=90°$ and may not be feasible on, for example, a three-circle diffractometer.

Therefore an alternate procedure was devised which yields a calculated $T(\psi)$ curve(s) from the measurement of symmetry equivalent intensities in all crystal systems except triclinic. (This has the additional advantage of providing redundant data which can subsequently be averaged.)

Details of the Method

Using Equations (F.2), each absorption-corrected intensity is first written in the form of Equation (F.3).

Except for statistical fluctuations, all pairs of reflections in a symmetry equivalent group (denoted by I_g and

I_g') should be equal after application of Equation (F.3); hence

$$I_g(\psi_{p,s})\ T^{-1/2}(\psi_p)\ T^{-1/2}(\psi_s) = I_g'(\psi'_{p,s})\ T^{-1/2}(\psi'_p)\ T^{-1/2}(\psi'_s). \quad (F.4)$$

Provided the variation in μt is not large for the model in the various ψ directions, one may write

$$T^{-1/2}(\psi_p)\ T^{-1/2}(\psi_s) \simeq [T^{-1}(\psi_p)+T^{-1}(\psi_s)]/2 \quad (F.5)$$

and, carrying the approximation one step further, may rewrite Equation (F.4) as

$$I_{gi}\ T_i^{-1} = I_{gj}\ T_j^{-1} \quad (F.6)$$

where i and j denote the various combinations of the ψ values for all pairs of reflections in g.

For practical purposes, $T(\psi)$ is assumed to be adequately represented by N discrete T_i values, i=1...N (typically 18 intervals from ψ=0 to 180° are used).

N sets of linear equations are then written by selecting those symmetry equivalent groups where one reflection in each group falls in the i^{th} interval, viz:

$$I_{gi} = I_{gj}\ T_j^i, \text{ where } T_j^i = Ti/Tj. \quad (F.7)$$

Minimization of the error function in the standard least-mean-square fashion leads to the normal equation

$$\Sigma_g\ I_{gj}\ \omega_g\ I_{gi}\ T_j^i = \Sigma_g\ I_{gi}\ \omega_g\ I_{gi}, \quad (F.8)$$

the solution of which yields a transmittance curve normalized to T_i.

The solution of Equation (F.8) for each yields N curves (one for each value of T_i) which are averaged after

renormalization. Individual contributions to the average are discarded if $|\langle T_j^i \rangle - T_j^i| > Y\ \sigma\langle T_j^i \rangle$ (typically Y=6.0). The transmittance curve is placed on an absolute scale by application of Equation (F.1) and absorption correction takes the form of Equation (F.3).

The approximation given in Equation (F.5) tends to produce an overall damping in the amplitude of the calculated ψ-scan. It is possible to correct for this effect by recalculating each point in the normalized transmittance curve using the equation $T_j^{i\prime} = 4\ (T_j^i)^2\ [1+T_j^i]^{-2}$.

Application

Optimum conditions for use of this method are essentially identical to that for the normal empirical absorption correction: 1) the crystal should be mounted such that the longest crystal direction is along the phi axis, 2) μR should not be too large, 3) the crystal should possess a relatively constant cross-section, and 4) the absorption coefficient and the average crystal cross-sectional dimension should be known or be approximated; in addition at least some symmetry equivalent data must be collected.

After correction for Lorentz-polarization, decay, and spherical absorption, the data are separated into their symmetry equivalent groups and the values of ψ are calculated. Reflections are omitted if: 1) $\langle I \rangle < X\ \sigma\langle I \rangle$

where X is nominally 3.0, 2) there exists only 1 reflection in the group, or 3) if the ψ for all the reflections in the group are identical.

The transmittance curve is calculated following the procedure described in the previous section. All data are then corrected for absorption and averaged.

A θ-dependence can also be obtained, provided a sufficient amount of data exist, by dividing the data into divisions in θ and calculating separate curves for each division.

Results and Discussion

Application of this procedure to experimental data from crystal belonging to various crystal systems show improvements in the internal agreement factor (R_{Int}= Σ |F-<F>|/<F>) ranging from 7 to 35%. The results are summarized in Table F.1. A typical transmission profile is illustrated in Figure F.1.

Experience shows that, for those cases where experimental ψ-scan curves have also been measured, comparable improvements were obtained using either approach and the curves calculated by the method reported here reproduce the general features of the experimentally measured ψ-scan curves.

The curve in Figure F.1 indicates a lower sensitivity

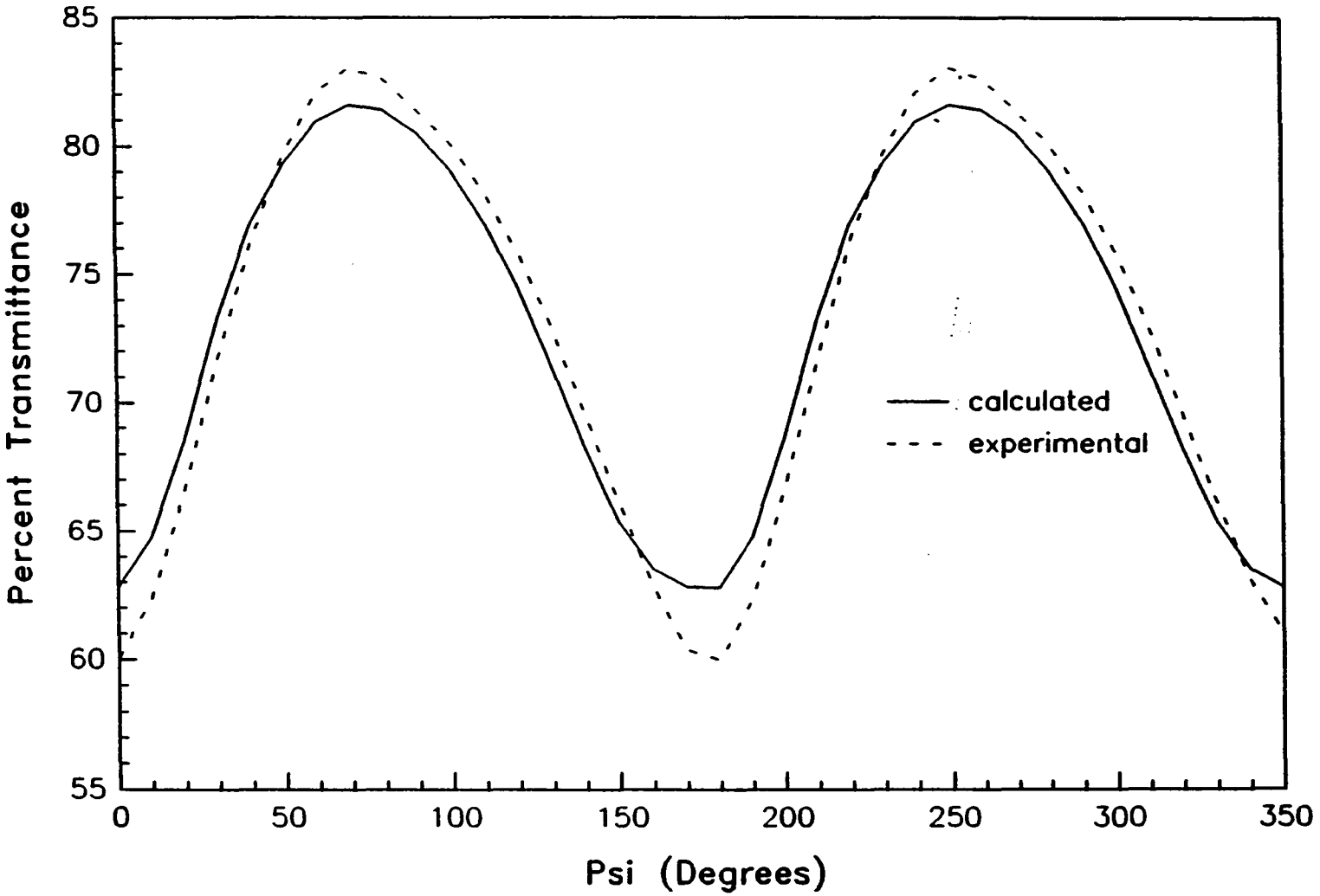

Figure F.1. Calculated and observed Ψ-scans for Compound III

Table F.1. Comparison of data averaging results using; (A) no absorption correction and (B)[a] the calculated transmittance profile

Compound[b]	Crystal System	R_{Int} (A)	R_{Int} (B)	% Improvement
I	monoclinic	4.84	4.49	7.2
II	orthorhombic	6.23	4.05	35.0
III	hexagonal	2.21	1.73	21.7
IV	rhombohedral	5.87	4.55	22.5
V	cubic	2.97	1.96	34.0

[a]All calculated curves used a maximum of ψ-ϕ=15° and were smoothed using a three-point-averaging procedure.

[b]Structural information:
I: μ(MoKα)=2.0, 2198 obsvd, 1057 avgd, Tmax/Tmin=100/84, 878 rflxns used in calculations.
II: μ(MoKα)=0.56, 1142 obsvd, 595 avgd, Tmax/Tmin=100/75, 164 rflxns used in calculations.
III: μ(MoKα)=150.0, 1506 obsvd, 197 avgd, Tmax/Tmin=82/62, 455 rflxns used in calculations, 3 calcd curves, R_{Int}(exp, 3 curves)=1.78. For these calculations the symmetry was assumed to be hexagonal; because of small distortions, the true symmetry is orthorhombic.
IV: μ(MoKα)=0.93, 3392 obsvd, 596 avgd, Tmax/Tmin=100/90, 1617 rflxns used in calculations.
V: μ(MoKα)=52.5, 804 obsvd, 177 avgd, Tmax/Tmin=46/34, 363 rflxns used in calculations, R_{Int}(exp,3 curves)=2.00.

to sharp fluctuations and an overall damping of the amplitude. These effects have two possible sources; the first is that the calculated curve represents an average over (parts of) many ψ-scan curves and the second is the approximation used in obtaining Equation (F.6).

Insight into the latter effect is gained by examination of the equations used. Examination of Equations (F.2)

reveals that, in certain regimes, it can smooth the resultant curve. In ideal cases ψ_p and ψ_s are identical; for reflections where they differ significantly, use of the approximation $t=(t_p+t_s)/2$ causes an averaging over different directions in the crystal and can cause a general damping of the profile to occur. This can, in more extreme cases of morphological asymmetry, produce shifts in the extrema of the transmittance profile. This effect is diminished when only those reflections with small values of $\tan^{-1}[\cos(\chi)\ \tan(\theta)]$ are used.

Conclusion

In general the results are very good. The calculated curves fits the major features of the experimental curves well and improvement in the internal agreement factors are noted.

The cases where this method gives unsatisfactory results are those for which the x-ray intensity data are of dubious quality and R_{Int}, with no absorption correction done, is abnormally high (above 5 to 6%). The cases where the procedure did not work are those in which not enough symmetry equivalent data were collected to perform a least-squares fit.

LITERATURE CITED

1. W. H. Bragg, Phil. Trans. (London) A215, 253 (1915).
2. P. Hohenberg and W. Kohn, Phys. Rev. B136, 864 (1964).
3. H. Hellman, Z. Phys. 85, 180 (1933).
4. R. P. Feynman, Phys. Rev. 56, 340 (1939).
5. R. W. James and G. W. Brindley, Phil. Mag. 12, No. 7, 81 (1931).
6. F. L. Hirshfeld and S. Rzotkiewicz, Mol. Phys. 27, 1319 (1974).
7. F. H. Allen, Acta Crystallogr. B42, 515 (1986).
8. R. A. Young, Acta Crystallogr. A25, 55 (1969).
9. R. McWeeney, Acta Crystallogr. 4, 513 (1951).
10. R. F. Stewart, J. Chem. Phys. 51, 4569 (1969).
11. M. Roux and R. Daudel, C. R. Helv. Seances Acad. Sci. 240, 90 (1955).
12. R. F. W. Bader and T. Nguyen-Dang, Adv. Quant. Chem. 14, 63 (1981).
13. J. P. Ritchie and S. M. Bachrach, J. Comp. Chem. 8, No. 4, 499 (1981).
14. B. Delley, Chem. Phys. 110, 329 (1986).
15. B. Dawson, Proc. Roy. Soc. A298, 264 (1969).
16. R. F. Stewart, J. Chem. Phys. 48, 4882 (1969).
17. S. Stinson, Chem. Eng. News, Feb. 17, 8 (1986).
18. W. H. E. Schwarz, P. Valtazanos, and K. Ruedenberg, Theor. Chim. Acta 68, 471 (1985).
19. W. H. E. Schwarz, L. Mensching, P. Valtazanos, and W. Von Niessen, Int. J. Quant. Chem. XXX, 439 (1986).
20. H. Lipson, in International Tables for X-ray Crystallography, Vol. II, edited by J. S. Kasper and K. Lonsdale (Kynoch, Birmingham, 1967), p. 235.

21. K. Ruedenberg, Anisotropic Atomic Electron Densities from X-ray Scattering by Crystals (to be published).

22. S. Gasiorowicz, Quantum Physics (John Wiley and Sons, New York, 1974), p. 191.

23. G. Arfken, Mathematical Methods for Physicists (Academic Press, New York, 1985), 3rd edition, p. 573.

24. M. Weissbluth, Atoms and Molecules (Academic, New York, 1978), p. 4.

25. M. Rotenberg, R. Bivins, N. Metropolis, and K. Wooten Jr., The 3j and 6j Symbols (MIT, Cambridge, 1959).

26. D. E. Sands, Vectors and Tensors in Crystallography (Addison-Wesley, London, 1982).

27. M. F. C. Ladd and R. A. Palmer, Structure Determination by X-ray Crystallography (Plenum, New York, 1978).

28. B. D. Cullity, Elements of X-ray Diffraction (Addison-Wesley, London, 1978), 2nd edition, p. 113.

29. W. J. A. M. Peterse and J. H. Palm, Acta Crystallogr. 20, 147 (1966).

30. S. I. Grossman, Calculus (Academic, New York, 1977), p. 876.

31. B. Rees, Acta Cryst, A32, 483, (1976).

32. G. H. Stout and L. H. Jensen, X-ray Structure Determination (Macmillan, New York, 1968).

33. M. A. Spackman and R. F. Stewart, in Methods and Applications in Crystallographic Computing, edited by T. Ashida and S. Hall (Oxford University, Oxford, 1984).

34. H. Neunhoeffer, M. Clausen, H-D. Voetter, H. Ohl, C. Krueger, and K. Angermund, Liebigs Ann. Chem., 1732 (1985).

35. D. T. Cromer and J. T. Waber, in International Tables for X-ray Crystallography, Vol. IV, edited by J. A. Ibers and W. C. Hamilton (Kynoch, Birmingham, 1974), p. 71.

36. R. F. Stewart, E. R. Davidson, and W. T. Simpson, J. Chem. Phys. 42, 3175 (1965).

37. K. Angermund, K. H. Claus, R. Goddard, and C. Kruger, Ang. Chem. Int. Ed. Eng. 24, No. 4, 237 (1985).

38. Appreciation is expressed to the authors in the previous reference for sharing their data, and to W. Klotzbucher for transmitting the data.

39. P. Coppens, et al., Acta Crystallogr. A40, 184 (1984).

40. P. Main, Lessigner, M. M. Woolfson, G. Germain, and J. P.Declerq, A system of Computer Programs for the Automatic Solution of Crystal Structures from X-ray Diffraction Data (University of York, York, England, 1976).

41. C. K. Johnson, OR TEP, USAEC Report No. ORNL-3794 (1965) (unpublished).

42. T. E. Peacock, The International Encyclopedia of Physical Chemistry and Chemical Physics (Pergamon, Oxford, 1972), 4, No. 2, p. 94.

43. P. Coppens, Transactions of the American Crystallographic Association (American Crystallographic Association, New York, 1972), Vol. 8, p. 93.

44. E. D. Stevens and P. Coppens, Acta Crystallogr. B36, 1864 (1980).

45. J. D. Dunitz and P. Seiler, Acta Crystallogr. B29, 589 (1973).

46. N. K. Hansen and P. Coppens, Acta Crystallogr. A34, 909 (1978).

47. P. Seiler, W. B. Schweizer, and J. D. Dunitz, Acta Crystallogr. B40, 319 (1984), and J. D. Dunitz, W. B. Schweizer, and P. Seiler, Helv. Chim. Acta 66, No. 12, 123 (1983).

48. Appreciation is expressed to the authors in the previous reference for sharing their data.

49. R. C. Raffenetti, J. Chem. Phys. 59, No. 11, 5936 (1973).

50. R. C. Raffenetti and K. Ruedenberg, Even-tempered Representations of Atomic Self-consistent Field Wavefunctions, USAEC Report No. IS-3195 (1973) (unpublished).

51. E. Clementi and C. Roetti, Atom. Data and Nucl. Data Tables 14, No. 3-4, 177 (1974).

52. C. F. Fischer, The Hartree-Fock Method for Atoms: A Numerical Approach (Wiley-Interscience, New York, 1977).

53. J. B. Mann, Atomic Structure Calculations II. Hartree-Fock Wavefunctions and Radial Expectation Values: Hydrogen to Lawrencium, USAEC Report No. LA-3691 (1968) (unpublished).

54. R. L. Lapp and R. A. Jacobson, ALLS, A Generalized Crystallographic Least Squares Program, USDOE Report No. IS-4708 (1979) (unpublished).

55. H. D. Flack, in Methods and Applications in Crystallographic Computing, edited by S. R. Hall and T. Ashida (Clarendon, Oxford, 1984), p. 41.

56. B. Kopfman and R. Huber, Acta Crystallogr. A24, 348 (1968).

57. A. C. T. North, D. C. Philips, and F. S. Mathews, Acta Crystallogr. A24, 351 (1968).

58. B. A. Karcher, Ph.D. dissertation, Iowa State University, 1981 (unpublished).

ACKNOWLEDGEMENTS

I would first like to thank my families for their support and encouragement to pursue my dreams. Special thanks go to my mother, Norma, and my wife, Taka, for the friendship we have built over the years and the times of joy and sadness we have shared.

I am grateful to Dr. Robert Jacobson for allowing me to be a part of this group and to him and the others who are and have been part of this group during my stay for exchanging ideas and information which have been the basis of my knowledge of x-ray crystallography. I am also grateful to Dr. Klaus Ruedenberg for sharing his insight into the world of atoms and molecules which has helped shaped a major portion of the work presented in this thesis.

There are many people whom I must acknowledge as a group. They are: Drs. Bruce Kelley, Karl Klose, Klaus Ruedenberg, Richard Schwarz, Terry Scott, Robert Shelton, Russell Smith, and Gerald Zweerink. Their combination of intellect and good nature is an inspiration to many; for there is far more to life than any one field of endeavor can ever encompass.

Finally I would like to dedicate this thesis to myself --- what I thought was, wasn't, and now it is.